The Dissertation Committee for Qing Xu Certifies that this is the approved version of the following dissertation:

Thermodynamics of CO_2 Loaded Aqueous Amines

Committee:

Gary T. Rochelle, Supervisor

Keith Johnston

Isaac Sanchez

Frank Seibert

Steven Bryant

Thermodynamics of CO_2 Loaded Aqueous Amines

by

Qing Xu, B.E.; M.S.E.

Dissertation

Presented to the Faculty of the Graduate School of

The University of Texas at Austin

in Partial Fulfillment

of the Requirements

for the Degree of

Doctor of Philosophy

The University of Texas at Austin

December 2011

Dedication

To my family

Acknowledgements

Firstly I would like to thank my advisor, Dr. Gary Rochelle. His guidance, encouragement, and insights for the research have inspired and helped me the most through my projects, which sometimes were not that smooth. His passion and dedication to work was very impressive to me. He was always willing to offer help and discuss the projects. Looking into my drawer, there are almost four inches of notes written by him from the weekly meeting on my specific research since year 2006 when I joined the group. Besides work, I also learned a lot from his attitude to life and to people. I feel lucky to have had him as my supervisor and I will carry the influence from him into my career in chemical engineering and into my life.

I would also like to thank the 30+ sponsors of the Luminant Carbon Management Program and the Industrial Associates Program for CO_2 Capture by Aqueous Absorption. I would have no chance to perform this research without their financial support. Thanks to their dedication to reducing the carbon dioxide emission. Specifically, thanks to Dr. Chau-Chyun Chen in Aspen Technology Inc. for his help with Aspen Plus®.

I am also grateful to the Chemical Engineering staff that has kindly supported me. Our administrative coordinator Maeve Cooney was always helpful, quick, precise, and patient. It was nice and relaxing to talk with her after spending a long time in research. I was not as good in either oral or written English in my earlier years in the US but she was very patient with that. I also want to thank Dr. Friedman for letting me use the equipment for pressure calibration, Dr. Freeman for the use of DSC, and Dr. Johnston for the use of the equilibrium cells with windows. I would like to acknowledge the help from T Stockman, Eddie Ibarra, Jim Smitherman, Butch Cunningham, Randy Rife, Patrick Danielewski, and Kevin Haynes. Their assistance in administration, processing

lab supply and equipment orders, repairing lab equipment, fixing computer problems, etc. was very effective and made my Ph.D. life easier.

I also want to express the appreciation to my excellent colleagues in the group. Marcus Hilliard, Ross Dugas, Bob Tsai, Eric Chen, Andrew Sexton, and Jason Davis joined the group before me and helped me a lot as I started. I still remember my first day in the lab when Marcus showed me how to load CO_2 into solution. And those who joined the group in similar years with me or later than me: Jorge Plaza, David Van Wagener, Sepidah Ziaii, Stephanie Freeman, Fred Closman, Xi Chen, Thu Nguyen, Stuart Cohen, Alex Voice, Peter Frailie, Chao Wang, Lynn Li, Steven Fulk, Shan Zhou, Humera Rafique, Mandana Ashouripashaki, and Omkar Namjoshi. Thank you all for the time, assistance, and companion in these years. Special thanks for the help from Peter, Jorge, and David with Aspen Plus® modeling, and experimental assistance from Steven, Alex, and Xi. I would also like to thank my undergraduate research assistants who helped me a lot with the experiments: Martin Metzner, Mychal Zipper, and Jeffrey Giordanelli. I wish you all the best in both career and life.

I am also very grateful to my friends who came into my life in Austin and shared lots of time with me: Wei X., Tuo W., Xinyu G.; my roommates Ji Z., Shao, Li J.; and many of other friends. I really appreciate the time we spent together and your understanding and support for me. I wish you all have a bright future while fulfilling your dreams.

Last but not least, I would like to thank my parents for their love and support throughout my study. I would not have come to this point without your earlier education and continuous encouragement.

Thermodynamics of CO_2 Loaded Aqueous Amines

Qing Xu, Ph.D.

The University of Texas at Austin, 2011

Supervisor: Gary T. Rochelle

Thermodynamics is important for the design of amine scrubbing CO_2 capture processes. CO_2 solubility and amine volatility in aqueous amines were measured at high temperature and pressure. A rigorous thermodynamic model was developed for MEA-CO_2-H_2O in Aspen Plus®.

CO_2 solubility at 80-190°C was obtained from total pressure measurements. Empirical models as a function of temperature and loading were developed for CO_2 solubility from 40 to 160°C in aqueous monoethanolamine (MEA), piperazine (PZ), 1-methylpiperazine (1MPZ), 2-methylpiperazine (2MPZ), PZ/2MPZ, diglycolamine® (DGA®), PZ/1MPZ/1,4-dimethylpiperazine (1,4-DMPZ), and PZ/methyldiethanolamine (MDEA). The high temperature CO_2 solubility data for MEA is comparable to literature and compatible with previous low temperature data. For MEA and PZ, amine concentration does not have obvious effects on the CO_2 solubility. The heat of CO_2 absorption derived from these models varies from 66 kJ/mol for 4 m (molal) PZ/4 m 2MPZ and to 72, 72, and 73 kJ/mol for MEA, 7 m MDEA/2 m PZ, and DGA. The heat of absorption estimated from the total pressure data does not vary significantly with temperature.

At 0-0.5 loading (α), 313-413 K, 3.5-11 m MEA (mol fraction x is 0.059-0.165), the empirical model of MEA volatility is $\ln(P_{MEA}/x_{MEA}) = 30.0-8153/T-2594\alpha^2/T$. In 7

m MEA with 0.2 and 0.5 loading, P_{MEA} is 920 and 230 Pa at 120 ℃. At 0.3-0.5 loading, the enthalpy of MEA vaporization, $-\Delta H_{vap,MEA}$, is about 70-73 kJ/mol MEA. At 0.25-0.4 loading, 313-423 K, 4.7-11.3 m PZ (x is 0.078-0.169), the empirical model of PZ volatility is $\ln(P_{PZ}/x_{PZ}) = -123+21.6\ln T+20.2\alpha-18174\alpha^2/T$. In 8 m PZ with 0.3 and 0.4 loading, P_{PZ} is 400 and 120 Pa at 120 ℃, and 2620 and 980 Pa at 150 ℃. At 0.25-0.4 loading, $-\Delta H_{vap,PZ}$ is about 85-100 kJ/mol PZ at 150 ℃ and 66-80 kJ/mol PZ at 40 ℃. $\Delta H_{vap,PZ}$ has a larger dependence on CO_2 loading than $\Delta H_{vap,MEA}$ in rich solution because of the more complex speciation/reactions in PZ at rich loading. Specific heat capacity of 8 m PZ is 3.43-3.81 J/(g·K) at 70-150°C.

Two new thermodynamic models of MEA-CO_2-H_2O were developed in Aspen Plus® starting with the Hilliard (2008) MEA model. One (Model B) includes a new species MEACOOH and it gets a better prediction than the other (Model A) for CO_2 solubility, MEA volatility, heat of absorption, and other thermodynamic results. The Model B prediction matches the experimental pK_a of MEACOOH, and the measured concentration of $MEACOO^-$/MEACOOH by NMR. In the prediction the concentration of MEACOOH is 0.1-3% in 7 m MEA at high temperature or high loading, where the heat of formation of MEACOOH has effects on P_{CO2} and CO_2 heat of absorption. Model B solved the problems of Model A by adding MEACOOH and matched the experimental data of pK_a and speciation, therefore MEACOOH may be considered an important species at high temperature or high loading. Although mostly developed from 7 m MEA data, Model B also gives a good profile for 11 m (40 wt%) MEA.

Table of Contents

List of Tables

List of Figures

Chapter 1: Introduction

This chapter introduces the application and objectives of this research. Amine based CO_2 capture is the most promising approach to reduce CO_2 emissions from coal-fired power plants. However it uses about one third of the output electricity from a power plant. New solvents and configurations have been investigated to improve the process. High temperature stripping at elevated pressure may reduce the energy cost when thermally resistant amine solvents are used. Thermodynamics is essential in the process design. Prior research in thermodynamics of CO_2 loaded amines was limited in amine types, temperature, or pressure. To better design the high temperature and pressure processes, new experiments need to be conducted to expand the temperature range to selected novel solvents, especially thermally resistant amines like piperazine and piperazine derivatives. The new data will be used in model development in Aspen Plus®.

1.1 Climate Change and CO_2 Emissions

Fossil fuel burning has increased CO_2 concentration in atmosphere over the past 200 years. The 2005 concentration of CO_2 was about 35% higher than 150 years ago. According to the US National Oceanic and Atmospheric Administration (NOAA) and the US National Aeronautics and Space Administration (NASA) data, the Earth's surface temperature has increased 1.2 to 1.4 ℉ in the past 100 years (EPA, 2007). Other aspects of climate, such as rainfall patterns, are also changing and causing weather disasters. IPCC Fourth Assessment Report – Climate Change 2007 concluded that "Most of the observed increase in global average temperature since the mid-20th century is very likely to due to the observed increase in anthropogenic greenhouse gas

generations." Researchers over the world have been investigating effective methods to manage CO_2 emissions.

Figure 1-1 shows the world CO_2 emissions in year 2007 from different sectors. The largest emission source is electricity and heat and occupies 41% of the total. The second largest source is transport, but CO_2 emission from this sector is much harder to control.

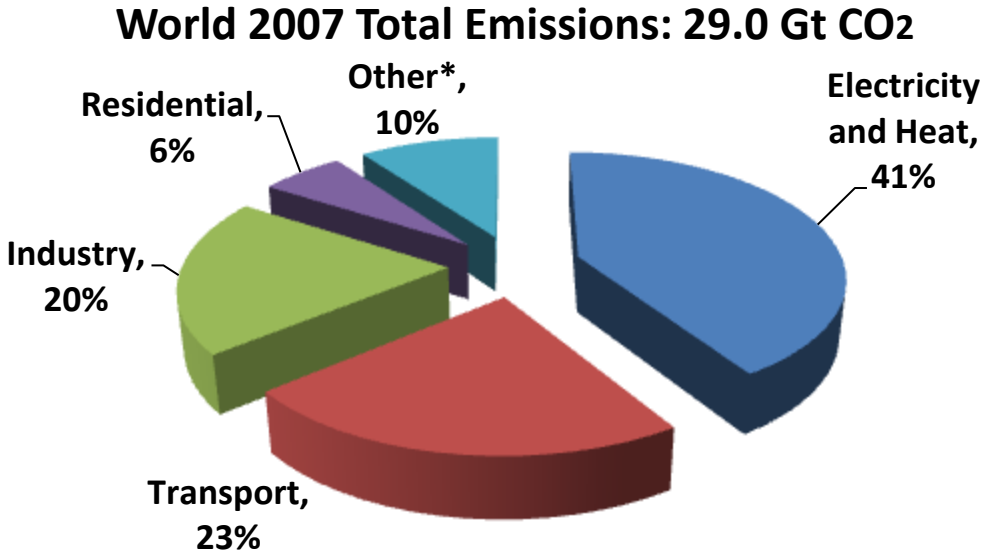

Figure 1-1: 2007 World CO_2 Emissions by Sector. **Re-plotted from Figure 11 in CO_2 emissions from fuel combustion highlights (2009 edition), International Energy Agency, 2009. *: Other includes commercial/public services, agriculture/forestry, fishing, energy industry other than electricity and heat generation, and other emissions not specified elsewhere.**

1.2 Amine Based Post Combustion CO_2 Capture

One direct approach to reduce CO_2 emissions from large stationary sources is to capture the CO_2 and store it away from atmosphere, like underground or submarine. The captured CO_2 can also be used for chemicals production as well as enhanced oil recovery (EOR). Non-biological CO_2 capture from coal fired power plants and other industry includes generally three types: pre-combustion, oxy-combustion and amine

based post combustion. Amine scrubbing has been investigated in acid gas treating processes for decades and is among the closest technology to commercialization for CO_2 capture. Aqueous monoethanolamine (MEA) solution serves as the baseline solvent to capture CO_2 from flue gas. New solvents like aqueous concentrated piperazine (PZ) are being investigated.

Figure 1-2 shows a typical amine based CO_2 capture process. The cooled flue gas at 40 ℃ with about 12% CO_2 enters the bottom of the absorber and counter-currently contacts the lean amine stream. After absorbing CO_2, aqueous amine becomes rich in CO_2 and flows out from the bottom. The temperature in the absorber is 40-70 ºC. In the cross heat exchanger the cool rich stream is heated by the hot lean stream from the stripper to above 100ºC and then the hot rich solution enters the top of the stripper. Steam is used to heat the reboiler up to 100-150 ºC to release CO_2 from the hot rich solution, and the pressure in the stripper can be elevated to 1.6-10 bar. CO_2 exits from the top of the stripper and is compressed to 150 bar for sequestration. After releasing CO_2, the hot lean solution flows out of the bottom of the stripper, cooled by the cross heat exchanger and a trim cooler, and enters the absorber. A slip stream is withdrawn from the reboiler and enters a reclaimer to remove degradation products, and the reclaimer temperature can be up to 150-180ºC.

In this process, amine solution is recycled between the absorber and stripper, the main energy input is to the reboiler and compressors.

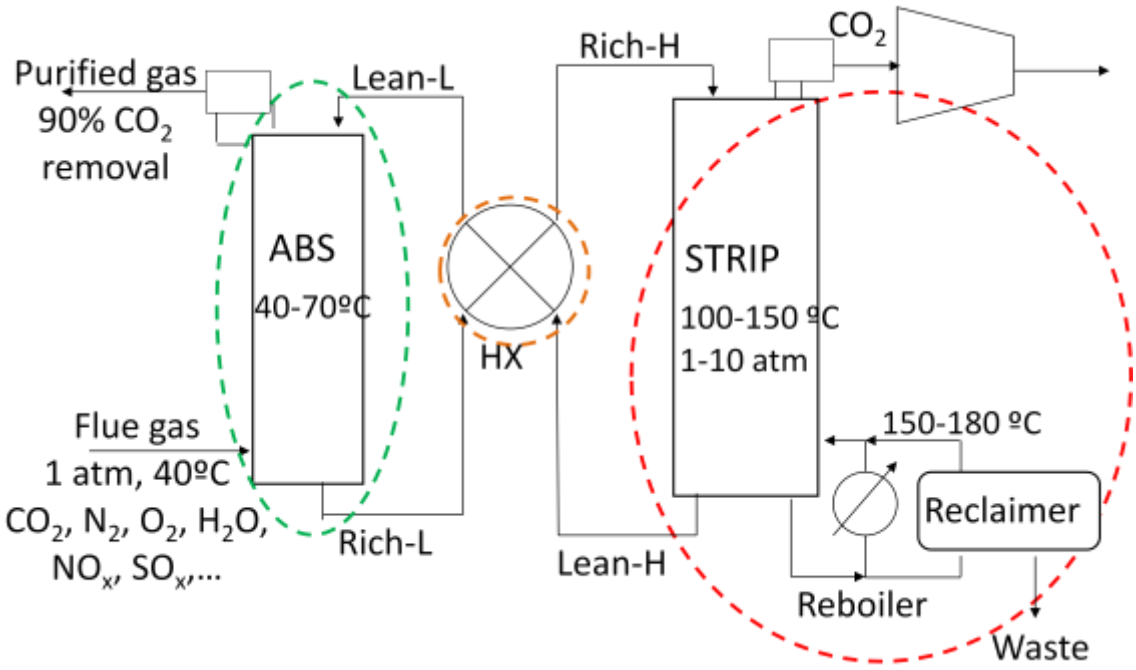

Figure 1-2: A Typical Amine Based CO_2 Capture Process

1.3 Needs for Thermodynamics and High Temperature Data

Thermodynamics is essential in the design of CO_2 capture process and researchers have been working on measuring thermal properties and building thermodynamic models of CO_2 loaded aqueous amines.

Better energy performance can be achieved by elevating the stripper temperature and pressure (Van Wagener, 2011). High temperature stripping thermally compresses CO_2 vapor before it enters the compressors. Thermal compression has a higher efficiency than mechanical compression; and less heat will be put into the heating for water vaporization because the CO_2/H_2O ratio in vapor increases as temperature increases. Some amines like MEA and ethylenediamine (EDA) are not thermally resistant and the stripper temperature cannot exceed 120ºC; but for thermally resistant amines like PZ and PZ derivatives the temperature in the stripper can be elevated to 150

ºC. For both cases high temperature thermodynamics is helpful in understanding the high temperature processes, which are in the red circle in Figure 1-2. Mid-temperature thermodynamics can be interpolated from the high temperature and low temperature data, for the design of heat exchangers in the orange circle in Figure 1-2.

Thermodynamics at greater temperature and pressure is needed for other high temperature processes. Figure 1-3 gives an example for the application in a novel stripping configuration. It was developed by Van Wagener (Rochelle et al., 2010) and shows the two stage flash stripping process. This is to replace the simple stripper configuration. After heat exchanging, the hot rich PZ solution enters the two flashes in sequence at 150 ℃. The pressure is reduced in the flashes and CO_2 is released. Then CO_2 enters different stages of the multi-stage compressor. The hot lean solution exiting the second flash goes to the heat exchanger and then goes back to the absorber. More flash stages may save more energy but the capital cost will increase. According to Van Wagener's research, 0.3 to 0.5 kJ/mol CO_2 of energy can be saved by using 2 and 3 stage flash, respectively, when 9 m MEA is used as the solvent. There are also other stripping configurations with elevated temperature and pressure saving more energy than a simple stripper, e.g., interheated column (Van Wagener, 2011).

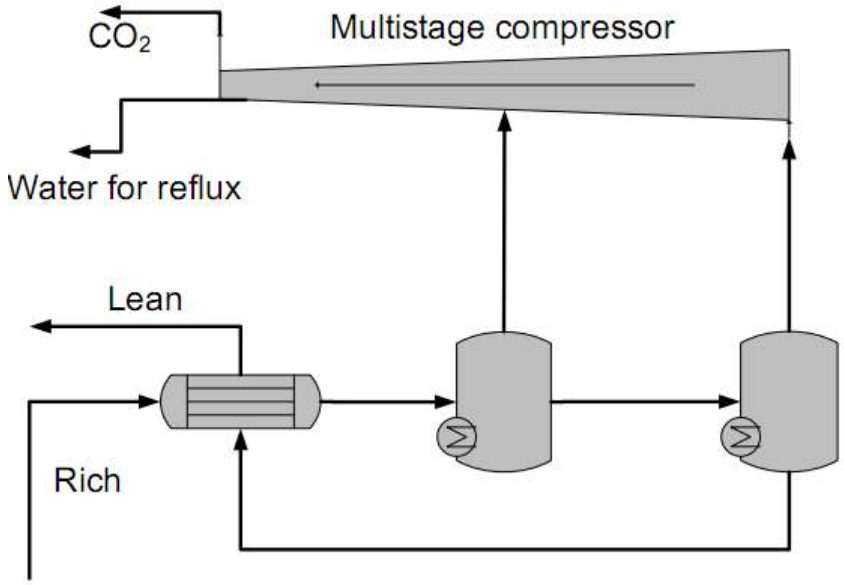

Figure 1-3: Two Stage Flash (Van Wagener, 2010[1])

Prior research in thermodynamics of CO_2 loaded amines is limited in amine types, temperature, or pressure. To better understand vapor-liquid equilibrium, heat capacity, and heat of absorption and their dependence on temperature, new experiments were conducted to expand the temperature range to selected novel solvents, especially thermally resistant amines including piperazine and piperazine derivatives.

1.4 PRIOR WORK

1.4.1 Amine Solvents

MEA has been used in acid gas treating since 1960's and is a baseline amine for CO_2 capture. It has relatively high heat of absorption, moderate reaction rate and capacity, low viscosity, low price, moderate environmentally degradability, and intensive operating experiences in industry. However it reacts with O_2 in the absorber and thermally degrades at greater than 120 ℃.

[1] Rochelle et al., 2010.

PZ has been used as a promoter for some slow amines like methyl-diethanolamine (MDEA) and 2-amino-2-methyl-1-propanol (AMP) because it accelerates the CO_2 reactions. However PZ in blends degrades faster than in aqueous PZ. Concentrated PZ is a very promising solvent because of its high capacity, fast reaction rate, negligible oxidative and thermal degradation up to 150 ℃ and moderate to high heat of absorption. The tolerance of high temperature gives the possibility of elevating regeneration temperature and pressure for better energy performance.

PZ derivatives, which include 1-methylpiperazine (1MPZ) and 2-methylpiperazine (2MPZ), are a new set of amines recently studied in Rochelle group. Preliminary results showed that PZ derivatives are also thermally resistant and react fast with CO_2 (Freeman 2011, Chen et al. 2011).

Diglycolamine (DGA®) has been used in absorbing CO_2 and H_2S from natural gas for decades. Similar to PZ, it is relatively thermally stable.

Figure 1-4 shows the structures of commonly used amines in CO_2 absorption.

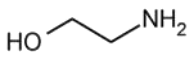

Monoethanolamine (MEA)

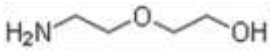

Diglycolamine® (DGA®)

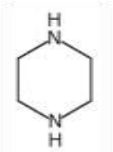

Piperazine (PZ)

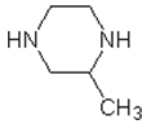

2-methylpiperazine (2MPZ)

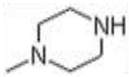

1-methylpiperazine (1MPZ)

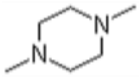

1,4-dimethylpiperazine (1,4-DMPZ)

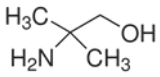

2-amino-2-methyl-1-propanol (AMP)

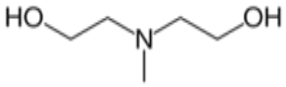

Methyldiethanolamine (MDEA)

Figure 1-4: Structure of Commonly Used Amines in CO_2 Capture

1.4.2 Vapor-liquid Equilibrium

Table 1-1 through 1-5 give a brief literature review of VLE data for unloaded and loaded aqueous amines.

Table 1-1: Summary of Literature VLE Data for MEA-H_2O

Author	Data	Pressure (kPa)	MEA (mol frac)	T (^oC)
Touhara et al. (1982)	P, T, x	0.065-5.623	0.03-0.89	25, 35
Nath and Bender (1983)	P, T, x	1.3-75	0-0.93	60, 78, 91.7
Cai et al. (1996)	P,T, x, y	66.7, 101.3	0.05-0.93	90-159
Park and Lee (1997)	P,T, x, y	101.3	0.03-0.98	100-170
Tochigi et al. (1999)	P,T, x, y	4.02-70.07	0.03-0.89	90
Hilliard (2008)	P,T, x, y	5-21	0.06-0.30	39.8-72.7
Kim et al. (2008)	P,T, x, y	6-100	0-0.56	40, 60, 80, 100

Table 1-2: Summary of Literature CO_2 Solubility in Aqueous MEA at High T/P

Author	MEA (wt%)	T (℃)	P_{CO2} (kPa)
Reed and Wood (1941)	15	100, 120, 140	138-1724
Lyudkovskaya and Leibush (1949)	3, 12, 30	25, 50, 75	254-4054
Goldman and Leibush (1959)	6, 12, 15, 30	75, 100, 120, 140	0.3-467
Jones et al. (1959)	15	40, 60, 80, 100, 120, 140	<931
Lawson and Garst (1976)	15	40, 60, 80, 100, 120, 134, 140	2.9-2786
Lee et al. (1976)	6, 15, 23, 30	25, 40, 60, 80, 100, 120	0.2-6616
Sartori et al. (1983)	3 M	40, 120	~0.3-336
Shen and Lee (1992)	15, 30	40, 60, 80, 100	1.1-2550
Murrieta-Guevara et al. (1993)	15, 30	30, 50, 100	1.5-2210
Robinson (1993)	20, 30	40, 70, 100, 120	0.003-6293
Jou et al. (1995)	30	0, 25, 40, 60, 80, 100, 120, 150	0.0012-19954
Ma'mun et al. (2005)	30	120	7-191
Aronu et al. (2011)	15,30,45,60	60, 80, 100, 120	<1060

Table 1-3: Summary of Literature VLE Data for PZ-H_2O

Author	Data	PZ (m)	T (℃)
Wilson and Wilding (1994)	P_t	0-1 (mole frac)	113, 199
Xia et al. (2003)	P_t	1.99, 3.97	120
Hilliard (2008)	T, P, x, y	0.9, 2, 2.5, 3.6, 5	40-60
Nguyen et al. (2010)	T, P, x, y	2, 5, 8, 10	40-70

Table 1-4: Summary of Literature CO_2 Solubility in Aqueous PZ

Author	PZ (m)	T (℃)	P_{CO2} (kPa)
Bishnoi et al. (2000)	0.6	40, 70	0.032-40
Perez-Salado Kamps et al. (2003)	2, 4	40-120	13.3-9560 (P_t)
Derks et al. (2005)	0.2 M, 0.6 M	25, 40, 70	0.27-111
Ermatchkov et al. (2006)	2-4.2	80, 100	0.111-77.63
Hilliard (2008)	0.9-5	40, 60	0.029-51.4
Dugas et al. (2009)	2-12	40, 60, 80, 100	0.065-39.29
Nguyen et al. (2010)	8, 10	40, 60	0.1-28.3
Kadiwala et al. (2010)	0.3 M, 1.2 M	40, 70	<7400

Table 1-5: CO_2 Solubility in DGA® in Literature

Author	DGA® (wt%)	P_{CO2} (kPa)	T (℃)
Martin et al. (1978)	60	1.6-5980	50, 100
Maddox et al. (1987)	20-60	6.8-6523	25, 40, 50, 60
Dingman et al. (1983)	65	<181	37.8, 60, 82.2

1.4.3 Specific Heat Capacity (C_p)

The specific heat capacity can be used in calculating temperature dependence of CO_2 heat of absorption and in thermodynamic modeling of the CO_2-H_2O-amine systems. Differential Scanning Calorimetry (DSC) has been used in previous research by Hilliard (2008) and Nguyen (Rochelle et al., 2009) for C_p measurement of CO_2 unloaded and loaded amine at 40-120 ℃. Tables 1-6 and 1-7 give the relative previous work on specific heat capacity measurements.

Table 1-6: Literature Summary of Specific Heat Capacity for Aqueous MEA

Author	T (°C)	Data Type	Method
Page et al. (1993)	10,25,40	unloaded	Flow microcalorimeter
Weiland et al. (1997)	25	pure, loaded, unloaded	Batch calorimeter
Chiu et al. (1999a and 1999b)	30-80	pure, unloaded	DSC
Hilliard (2008)	40-120	Pure, loaded, unloaded	DSC

Table 1-7: Literature Summary of Specific Heat Capacity for Aqueous PZ*

Author	T(°C)	Data type
Hilliard (2008)	40-120	2 m and 3.6m, unloaded
Y-R Chen et al. (2010)	30-80	x_{PZ}=0.05, 0.1, 0.15, 0.2, unloaded
Nguyen (Rochelle at al., 2009)	40-120	8-12 m, 0.21, 0.29, 0.31, 0.4 CO_2 loading

*: All used DSC method.

1.4.4 Heat of Absorption ($-\Delta H_{abs}$)

It is important to know the heat of absorption of CO_2 in aqueous amines because it effects the energy input in the reboiler, and reflects the temperature dependence of CO_2 partial pressure. In the absorber the CO_2 absorption into amine is exothermic, and in the

stripper the releasing of CO_2 is endothermic. According to the research by Kim et al. (2007), heat of absorption of CO_2 in 7m MEA increases with temperature.

There are two types of $-\Delta H_{abs}$: integral and differential. Heat of absorption obtained from CO_2 partial pressure data are referred to as differential heat of absorption. This method was used by Jou et al. (1994) for MEA solution. This method requires very accurate CO_2 partial pressure measurement and cannot get temperature dependence of ΔH_{abs}. Integral heat of absorption could be obtained from direct measurement by a calorimeter. However ΔH_{abs} from this method also has big deviations. Table 1-8 lists the summary of previous CO_2 heat of absorption measurements for aqueous MEA.

Table 1-8: Summary of CO_2 Heat of Absorption into Aqueous MEA in Literature

Author	Amine Concentration	T (°C)	P (kPa) / Loading
Mathonat et al. (1995)	30 wt% MEA	40, 80, 120	2000, 5000, 10000 kPa
Carson et al. (2000)	10, 20, 30 wt% MEA	25	Unloaded aqueous MEA
Kim et al. (2007)	30 wt% MEA	40, 80, 120	0.04-0.72 loading

1.4.5 Electrolyte-NRTL Models for MEA

The electrolyte-Nonrandom Two-Liquid (ENRTL) theory was developed by Chen et al. (1979 and 1982), then improved by Chen and Evans (1986) and Mock et al. (1986). Aspen Plus® has a built-in ENRTL model to deal with the liquid phase non-ideality, especially for aqueous or mixed solvent electrolyte systems. The model contains a Debye-Huckel term, Born-correction for mixed solvents, and the local interaction term.

In the Rochelle group, Austgen (1989) was the first to apply the ENRTL model in Aspen Plus® to the amine-H_2O-H_2S-CO_2 system. The data regression system (DRS) of Aspen Plus® was used in the rigorous thermodynamic model. After that, Posey (1996), Bishnoi (2000), Dang (2001), Freguia (2002) and Cullinane (2005) all made some contributions to the rigorous thermodynamic equilibrium/rate models. The more recent

MEA-H_2O-CO_2 model was by Hilliard (2008), and Plaza recently modified the Hilliard MEA model. The Hilliard PZ model (2008) has been modified and developed by Van Wagener, Plaza, and Frailie. The latest version is the Fawkes PZ model (Frailie et al., 2010). For amine-H_2O-CO_2 system, vapor phase non-ideality was modeled by the SRK equation of state.

With the rigorous thermodynamic models, reasonable accurate predictions should be made for the thermodynamic properties. Also the important parameters help interpreting and understanding thermal behaviors. Since the current MEA model includes limited high temperature data, the temperature dependences and the high temperature predictions are not perfect and need improvement.

1.5 RESEARCH OBJECTIVES

Thermodynamics serves as the base knowledge in the design of amine scrubbing process. CO_2 solubility, heat of CO_2 absorption, specific heat capacity and amine volatility are key thermal components to the process design. CO_2 solubility and total pressure determine how much CO_2 could be removed under certain conditions. On the other hand the heat of absorption plays an important role in the prediction of stripper energy and is critical for the process design. Specific heat capacity helps to understand the temperature dependence of heat of absorption. Amine volatility mostly involves environmental impact as well as the design of the water wash and the condenser. Investigations in amine-water systems can help to understand the more complex amine-water-CO_2 system.

There are internal connections among these factors. CO_2 partial pressure over aqueous amine is mostly determined by temperature, amine type and the CO_2 loading (mole CO_2/mol alkalinity). For a specific amine, P_{CO2} is a function of temperature and

loading. Amine volatility depends on amine structure, concentration, temperature and CO_2 loading. By taking derivatives to logarithm of the partial pressure of CO_2 or amine, more thermo parameters can be obtained:

According to Equation XVIII.9 in Lewis and Randall (1923) and Equation IV.109 in Dodge (1944), the CO_2 heat of absorption $\Delta H_{abs} = -R\frac{\partial lnP_{CO2}}{\partial(\frac{1}{T})}$. In the amine-$H_2O$ system $\Delta H_{vap,amine} = -R\frac{\partial lnP_{amine}}{\partial(\frac{1}{T})}$. R is the gas constant.

By definition, the specific heat capacity $C_p = (\frac{\partial H}{\partial T})_P$ and C_p=A+BT+CT^2+…. For the amine-water-CO_2 system, on a molar lean solution base, $\Delta H_{abs}(120℃) = \Delta H_{abs}(40℃) + \int_{120℃}^{40℃}[Cp(lean) + Cp_{CO2(g)}m_{CO2(g)}]dT + \int_{40℃}^{120℃} Cp(rich)\cdot(1 + \frac{m_{CO2(g)}}{44.01})dT$.

The primary target of this project is to quantify in aqueous MEA and PZ, how the CO_2 solubility, amine volatility and heat of absorption depend on temperature, and give theoretical explanations for these behaviors. Therefore the specific objectives of this project include:

1. Develop experimental methods for high temperature/pressure CO_2 solubility and amine volatility measurements and validate the methods by comparing with previous vapor-liquid equilibrium data of aqueous MEA.
2. Measure CO_2 solubility and amine volatility at 100-160 ℃ for aqueous MEA and PZ, and specific heat capacity up to 150 ℃ for concentrated PZ for high temperature stripping design.
3. Identify and explain the temperature dependence of CO_2 solubility and amine volatility for aqueous MEA and PZ systems.

4. Based on the vapor-liquid equilibrium and specific heat capacity data, obtain CO_2 ΔH_{abs} in aqueous MEA and PZ, as well as $\Delta H_{vap,amine}$ in aqueous MEA and PZ. Identify and explain the temperature dependence of the ΔH.
5. Improve Hilliard MEA Aspen Plus® thermodynamic model for CO_2-H_2O-MEA and test the Fawkes PZ Aspen Plus® model.
6. Screen new thermally resistant solvents by measuring CO_2 solubility at high temperature.

Chapter 2: Total Pressure and CO_2 Solubility at High Temperature and Pressure

This Chapter presents a total pressure experimental method and the measured vapor-liquid equilibrium data at 80-191 ℃. Nine amine solvents that could be used for CO_2 capture from coal-fired power plants were screened by this method: monoethanolamine (MEA), piperazine (PZ), 1-methyl-piperazine (1MPZ), 2-methyl-piperazine (2MPZ), PZ/2MPZ, PZ/1MPZ/1,4-dimethylpiperazine (1,4-DMPZ), diglycolamine® (DGA®), and two blends of PZ/methyl-diethanolamine (MDEA). CO_2 solubility was derived from the total pressure data. An empirical model was developed for each solvent to predict CO_2 partial pressure at 40-160 ℃.

The high temperature CO_2 solubility data for MEA is comparable to literature and is compatible with the previous low temperature data. For MEA and PZ, amine concentration does not have obvious effects on the CO_2 solubility. The heat of CO_2 absorption derived from these empirical models varies from 66 kJ/mol for 4 m PZ/4 m 2MPZ and to 72, 72, and 73 kJ/mol for MEA, 7 m MDEA/2 m PZ, and DGA and does not vary significantly with temperature. The measured CO_2 heat of absorption in MEA from literature is not consistent with the partial pressure CO_2 data, or with the previous measured specific heat capacity.

2.1 Review of Acid Gas Solubility Measurement at High Temperature and/or Pressure

The solubility of acid gas, such as CO_2 and H_2S, in alkanolamine solvents has been measured at high temperature and/or pressure by previous researchers. The apparatus can be sorted as static and dynamic, with or without analysis for vapor and liquid composition. In a static method the system is closed without phase circulation;

mixing is obtained by agitation or rocking. Samples of vapor and liquid can be withdrawn and analyzed after the system reaches equilibrium. If no sample is collected, mass balance and certain equations of state is needed to calculate partial pressure data. The total pressure method in this work belongs to this category.

In a dynamic method for acid gas solubility measurement, usually the vapor phase is circulated to accelerate the process to equilibrium. Therefore it is easier to collect a vapor sample in a dynamic method than in a static method.

In the acid gas-water-amine vapor-liquid equilibrium, the partial pressure of amines is very small compared with acid gas and water, and is usually ignored. At high temperature and/or pressure, the acid gas partial pressure is the main part of the total pressure. In most apparatus with sampling and analysis, the vapor stream is condensed to get rid of water and amine, and then enters the analytical instrument.

2.1.1 Static Methods without Vapor Sampling

The static method without sampling is easy to perform and requires mass balance calculation to get the solubility data. If adequate mixing can be achieved, this method can be highly productive to generate CO_2 solubility data.

Maddox et al. (1987) measured the solubility of CO_2 and H_2S in aqueous MEA, DGA®, DEA, and MDEA at 25-60 ℃. An equilibrium cell with liquid and gas charging systems was used, no sample was collected, and mixing was obtained by a shaker. The measured P_{CO2} was 4-6789 kPa.

Murrieta-Guevara et al. (1988, 1992, 1993, 1998) measured the solubility of CO_2 and H_2S in various amines at 298-373 K from 2-2730 kPa partial pressure. Gas was circulated by a magnetic pump for mixing.

Shen et al. (1992), Xu et al. (1998) and Liu et al. (1999) measured CO_2 solubility in various MEA, MDEA, MEA/MDEA, and MDEA/PZ solutions at 30-100 ℃ with P_{CO2} from 1 to 2000 kPa with an autoclave. Raoult's law was used to calculate water partial pressure, and amine partial pressure was ignored.

Derks et al. (2005) measured CO_2 solubility in 0.2 and 0.6 M PZ at 25, 40, and 70 ℃, P_{CO2} at 0.27-111.37 kPa. The equilibrium cell was agitated and sometimes liquid samples were taken.

Jenab et al. (2005, 2006) measured CO_2 solubility in the mixtures of DIPA+PZ, DIPA+MDEA, and MDEA+PZ+ Sulfolane at 30-70 ℃, 30-5000 kPa.

CO_2 solubility in a range of new solvents was measured in a double wall glass reactor by Puxty et al. (2009) at 40 ℃, 0.3-900 kPa.

Recently Aronu et al. (2011) measured the total pressure in 2.9-24.5 m CO_2 loaded aqueous MEA at 60-120 ℃ and pressure up to 1060 kPa.

Another special static method was by observation of the CO_2 releasing point from the solution through the sapphire windows. Anoufrikov et al. (2002), Kamps et al. (2003), Xia et al. (2003), and Bottger et al. (2009) used this method for P_{CO2} in aqueous PZ, MDEA, and PZ/MDEA at 313-393 K with up to 10 MPa total pressure.

2.1.2 Static Methods with Sampling and Analysis

Jones et al. (1959) measured the solubility of H_2S and CO_2 in aqueous MEA at 40-140 ℃, up to 6983 P_{CO2}. The equilibrium cell was rocked for at least 16 hr before sampling. The vapor sample was collected and analyzed by MS.

With a similar apparatus Lawson et al. (1976) measured solubility of H_2S and CO_2 in aqueous MEA and DEA at 100-300 ℉, up to 32800 mmHg P_{CO2}.

Dingman et al. (1983) measured the solubility of H_2S and CO_2 in aqueous DGA®. Total pressure was maintained at 1500 mm Hg by methane and mixing was obtained by rocking. Vapor and liquid were sampled and gas chromatography (GC) was used in analysis.

Addicks et al. (2001, 2002) measured CO_2 and methane solubility in aqueous MDEA up to 200 bar at 313 and 353 K. The vapor composition was analyzed by GC and liquid was analyzed by titration.

Huttenhuis et al. (2007) measured the solubility of H_2S and CO_2 in aqueous MDEA at 10-25℃ at 6.9-69 kPa. An equilibrium cell with agitation was used and methane used as make-up gas. After the system reached equilibrium, a small sweep stream of methane (~200 Nml/min) was routed through the reactor and the outlet was analyzed by GC.

2.1.3 Dynamic Methods

In dynamic methods for CO_2 solubility measurement, gas chromatography, infrared analyzer, and mass spectrometer have been used to analyze CO_2. Water partial pressure is usually calculated, and amine partial pressure is neglected. To maintain a relative high pressure in the system, N_2, methane, or He is usually used as the inert gas.

One series of studies used a closed system with circulation of the gas of interest by a magnetically driven piston pump. This method expanded the acid gas partial pressure to 0.001-20000 kPa and temperature can be 0-150℃. N_2 was used to maintain the total pressure P_t when P_t was less than 200 kPa. Vapor was analyzed by GC. Liquid samples were injected into NaOH solution and analyzed. Using this method, Lee et al. (1976) measured the CO_2 and H_2S solubility in aqueous MEA. Martin et al. (1978) measured the CO_2 and H_2S solubility in aqueous DGA®. Teng et al. (1989,

1990) measured the solubility of H_2S and CO_2 in aqueous AMP. Jou et al. (1982, 1994, 1995) measured solubility of H_2S and CO_2 in MDEA and CO_2 solubility in MEA and MDEA/MEA.

With a similar experimental setup, Kadiwala et al. (2010) measured CO_2 solubility in 0.3 and 1.2 M PZ at 313 and 343 K up to 7400 kPa. Liquid samples were injected into 50 wt% MEA instead of NaOH solution and then analyzed by GC. The method and experimental set-up were first standardized by comparing CO_2–water–MEA equilibrium data obtained on this set-up versus data reported in the literature by Jou et al. (1995).

Sartori et al. (1983) measured CO_2 solubility in MEA and AMP at 40-120 ℃, 0.08-300 psia P_{CO2}. An autoclave with agitation was used, and the gas mixture of CO_2 and He was sparged into the liquid and entered GC for analysis. Water balance was maintained by a pre-saturator and a condenser.

Li et al. (1994, 1995) used a similar setup as Sartori and measured CO_2 and H_2S solubility in MEA/AMP at 40-100 ℃, with acid gas partial pressure 1-200 kPa.

Mass spectrometer (MS) has been used in analyzing the vapor samples. Muhlbauer et al. (1957) measured CO_2 and H_2S solubility in aqueous MEA. Gas was analyzed by MS for CO_2, N_2, Ar, and H_2S. The sum of P_{water} and P_{amine} were measured separately and subtracted from the measured P_t. Tontiwachwuthikul et al. (1991) used similar apparatus and procedure to measure CO_2 solubility in AMP at 20-80 ℃, 1-100 kPa P_{CO2}.

Ma'mun et al. (2005) used three equilibrium cells in series, with gas circulating, and measured CO_2 solubility in aqueous MEA and MDEA. Gas phase was analyzed by Infrared analyzer for CO_2 concentration.

The total pressure method in this work is basically a static method without vapor sampling. The mixing of vapor and liquid phases was obtained by a hollow shaft with two impellers and the agitation rate can be as high as 2500 rpm. Thus adequate mixing was achieved, mass transfer was accelerated, and time to equilibrium is reduced. It is shown that this method is highly productive to generate equilibrium data for high temperature pressure CO_2-amine-water systems. The measured total pressure and calculated partial pressure of CO_2 were comparable with literature data.

2.1.4 Basic Chemistry

Figure 2-1 shows the structures of amines used in this work. Primary amines have two hydrogen atoms attached to a nitrogen atom and are generally the most alkaline. MEA and DGA are primary amines. Secondary amines have one hydrogen atom attached to a nitrogen atom, such as PZ and 2MPZ. Tertiary amines have no hydrogen atom attached to a nitrogen atom, such as MDEA and 1,4-DMPZ.

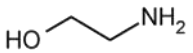

Monoethanolamine (MEA)

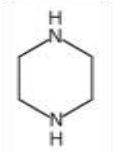

Piperazine (PZ)

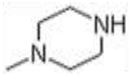

1-methylpiperazine (1MPZ)

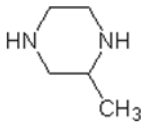

2-methylpiperazine (2MPZ)

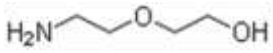

Diglycolamine® (DGA®)

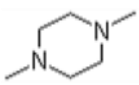

1,4-dimethylpiperazine (1,4-DMPZ)

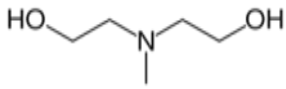

Methyldiethanolamine (MDEA)

Figure 2-1: Structure of Amines Used in This Work

The reactions between CO_2 and different types of amines are:

For primary amines:

$2RNH_2+CO_2 \leftrightarrow RNH_3^+ + RNHCOO^-$

$RNH_2+CO_2+H_2O \leftrightarrow RNH_3^+ + HCO_3^-$

For secondary amines:

$2R_2NH+CO_2 \leftrightarrow R_2NH_2^+ + R_2NCOO^-$

$R_2NH+CO_2+H_2O \leftrightarrow R_2NH_2^+ + HCO_3^-$

For tertiary amines:

$R_3N+CO_2+H_2O \leftrightarrow HCO_3^- + R_3NH^+$

R is a substituent other than a hydrogen atom.

2.2 EXPERIMENTAL METHODS

2.2.1 Apparatus

One run with aqueous MEA and three runs with aqueous PZ were conducted in the calorimeter. The autoclave was used in all the other experiments. The results do not show obvious differences between the two apparatuses.

2.2.1.1 Calorimeter

The first measurements of total pressure were performed using a 400 mL stainless steel calorimeter (by Parr Instrument) as the equilibrium cell (Figure 2-2). Pressure was measured with a Validyne® DP15 transducer (±15 kPa accuracy), calibrated by heating water and correlating the readings with known water vapor pressures from DIPPR (BYU, 1998- Provo, version 13.0). The calibration can be found in Appendix A. The voltage of the heating tape was manually controlled by a power controller to maintain selected temperature. An Omega® K type thermocouple (±1.5 ℃ accuracy) was installed inside the thermal well and an Omega® 4001A temperature controller was used as the

temperature indicator. There is an extra opening with a valve on the top of the calorimeter for venting. The calorimeter was not agitated.

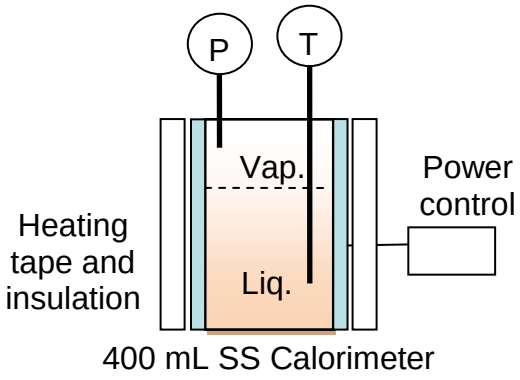

Figure 2-2: Total Pressure Measurement with a Calorimeter

2.2.1.2 Autoclave

As shown in Figure 2-3, a 500 mL stainless steel autoclave (ZipperClave®, by Autoclave Engineers) was used as the equilibrium cell for most of the measurements. Closure was effected by a resilient spring member inserted through a circumferential groove in the body and cover (Autoclave Engineers, 2009). A magnetic hollow shaft agitator (~4.60'' in length, adjustable, MAG075, MagneDrive II Series, by Autoclave Engineers) was used to get equilibrium without leaking to the atmosphere. A compressed air motor (2AM-NCC-16, by Gast®) provided agitation from 100 to 2500 rpm. The agitator circulates liquid and vapor phases. As shown in Figure 2-4, vapor entered from the top holes of the shaft and was sparged from the bottom holes of the shaft, which were under the bottom impeller (1 ¼ inch diameter). The top impeller is at about the interface of vapor and liquid to improve mixing. In some experiments, two baffle bars were placed in the autoclave for better mixing. Temperature was controlled by a Fuji Electric PXZ-4 PID temperature controller, with connection to a K-type thermocouple (±1.5 ℃ accuracy) placed inside the thermal well of the autoclave. A

pressure transducer (Druck® PTX 611, 0-30 bar absolute, ±2.4 kPa precision) was connected to a signal converter and a NI USB-6009 data logger to record data. The pressure indicator was calibrated by a dead weight pressure tester (S/N 19189/278, by Budenberg Volumetrics, INC.). The calibration can be found in Appendix A. There are extra openings with valves on the top of the autoclave for venting.

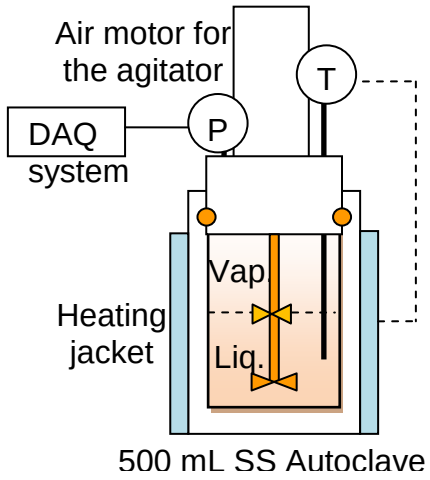

Figure 2-3: Total Pressure Measurement with an Autoclave

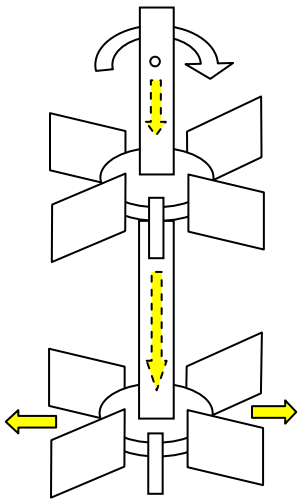

Figure 2-4: Autoclave Engineers' Patented Dispersimax™ Turbine Type Impeller with Modification. Reproduced from Autoclave Engineers Bulletin for Agitator/Mixers and modified as in the experiments. Yellow arrows are vapor flow; dashed arrows are inside the hollow shaft.

2.2.2 Solution Preparation

About 330 to 380 mL solution was prepared for each experiment. Certain amounts of amine and DDI water were weighed and combined to achieve the target molality (m). Then the mixture was stirred by a magnetic stir bar. For PZ and PZ derivatives, the mixture was heated and stirred on a hot plate to make the solid dissolve. After the solution was clear and well mixed, it was transferred into a glass gas sparging column (for PZ and PZ derivatives the column was pre-heated) on a scale. CO_2 was sparged into the solution, and the absorbed CO_2 weight was recorded. Details can be found in the Dissertations by Hilliard (2008) and Freeman (2011).

2.2.3 Procedure

Before each run, 300 to 330 mL of CO_2 loaded aqueous amine was prepared and added into the equilibrium cell. To avoid the effects of O_2, N_2 was used to purge air and then the cell was sealed. The initial pressure of N_2 and temperature were recorded. Then the cell was heated and recording of both temperatures and pressures started at around 100 ℃. After holding at temperature for at least 30 min or until the pressure did not change for 10 min, the system was assumed to be at equilibrium. The solution was heated to about 160 ℃ (or higher in selected runs) and then cooled down to 100 ℃. Data were taken during both heating and cooling processes to make the interval 10 ℃ in general. After each run the system was left overnight to cool down. Liquid samples were collected before and after each experiment at room temperature and analyzed for total inorganic carbon (CO_2) and total alkalinity (amine).

2.2.4 Analytical Methods

2.2.4.1 Total Inorganic Carbon (TIC)

The concentration of total CO_2 in solution was determined by Total Inorganic Carbon (TIC) analysis. The liquid samples collected through each run were gravimetrically diluted by a factor of 50-100, depending on the expected CO_2 concentration. About 20–30 μL diluted sample was injected into 30 wt% H_3PO_4 to release CO_2, and a continuous N_2 flow carried the CO_2 into an IR analyzer (Model 525, Horiba PIR 2000). PicoLog® software was used to record the voltage signal from the IR analyzer. In order to get a correlation curve between the voltage peak areas and carbon mass fraction, a series of calibration points were carried out at the end of each analysis by injecting known amounts of inorganic carbon standard (1000 ppm carbon, Ricca Chemical Company, Arlington, TX). Details can be found in Hilliard (2008) and Freeman (2011). The measurement precision is about 0.5-1%.

2.2.4.2 Acid Titration

The total alkalinity of each liquid sample was determined by titration using a Metrohm-Peak 835 Titrando equipped with an automatic dispenser, Metrohm-Peak 801 stirrer, and 3M KCl pH probe. 120-300X dilution of the sample was titrated with 0.1 N H_2SO_4 to pH 2.4. Details are available in Appendix A.3 of Hilliard (2008) and Appendix F of Sexton (2008). The measurement precision is about 0.5%.

2.2.5 Chemicals

Reagent chemicals were used: CO_2 (Clinical Purity, 99.5%, Matheson Tri Gas), MEA (99%, Acros Organics), anhydrous PZ (99%, Sigma-Aldrich and Acros Organics), 1-methyl-piperazine (1MPZ, 99+%, Acros Organics), 2-methyl-piperazine (2MPZ, 99%, AK Scientific), diglycolamine® (DGA®, 99%, Huntsman), Methyl-diethanolamine

(MDEA, 99%, Acros Organics), 1,4-dimethylpiperazine (1,4-DMPZ, 98.5% Acros Organics). DDI water was used for solution preparation.

2.3 CO_2 SOLUBILITY IN AMINES

The measured total pressure includes the pressure of the amine-H_2O-CO_2 system and N_2. Thus the total pressure of amine-H_2O-CO_2 is $P_t=P_{meas}-P_{N2}$, where P_{meas} is the measured pressure and P_{N2} is the N_2 partial pressure; N_2 was assumed to be an ideal gas so $P_{N_2} = P_{N_2,0} \cdot \frac{T(K)}{T_0(K)}$. 0 stands for the initial condition.

The partial pressure of CO_2 was estimated by subtracting an estimate of the water partial pressure from the total pressure.

$$P_{CO_2} = P_t - P_{H_2O} - P_{amine} = P_t - P^*_{H_2O} \cdot x_{H_2O} - P^*_{amine} \cdot x_{amine} \quad (2\text{-}1)$$

P_{H2O} and P_{amine}: partial pressure of water and amine.

P^*_{H2O} and P^*_{amine}: pressure of pure water and pure amine at T.

The mole fractions in solution were represented as $x_{H2O}+x_{amine}=1$, assuming there is water and total amine but no free CO_2. P_{amine} was assumed to be negligible except for MEA. Pure H_2O and MEA pressure was obtained from DIPPR (1998-Provo, BYU).

Liquid analysis gives the total CO_2 loading at room temperature. At low to medium temperature, CO_2 loading $\alpha = \frac{n_{T,CO_2}}{n_{T,alkalinity}}$. At temperature above 100°C, liquid loadings were corrected by the estimated amount of CO_2 in the vapor.

$$\alpha = \frac{n_{T,CO_2} - n_{V,CO_2}}{n_{T,alkalinity}}$$
$$n_{V,CO_2} = \frac{P_{CO_2} V_{vap}}{RT} \quad (2\text{-}2)$$

Where $n_{T,\ CO2}$ and $n_{V,\ CO2}$ are the total CO_2 (mol) and CO_2 in vapor (mol), respectively. $n_{T,\ alkalinity}$ is the total alkalinity (mol).

2.3.1 Benchmark – CO_2 Solubility in MEA

Figure 2-5 shows a favorable comparison of the MEA data in this work with data by Jou et al. (1995), Dugas et al. (2009), and Ma'mun et al. (2005). The lines are predicted by the empirical model from this work, which will be presented in the next section. Figure 2-6 shows a comparison of total pressure data in this work with data by Aronu et al. (2011).

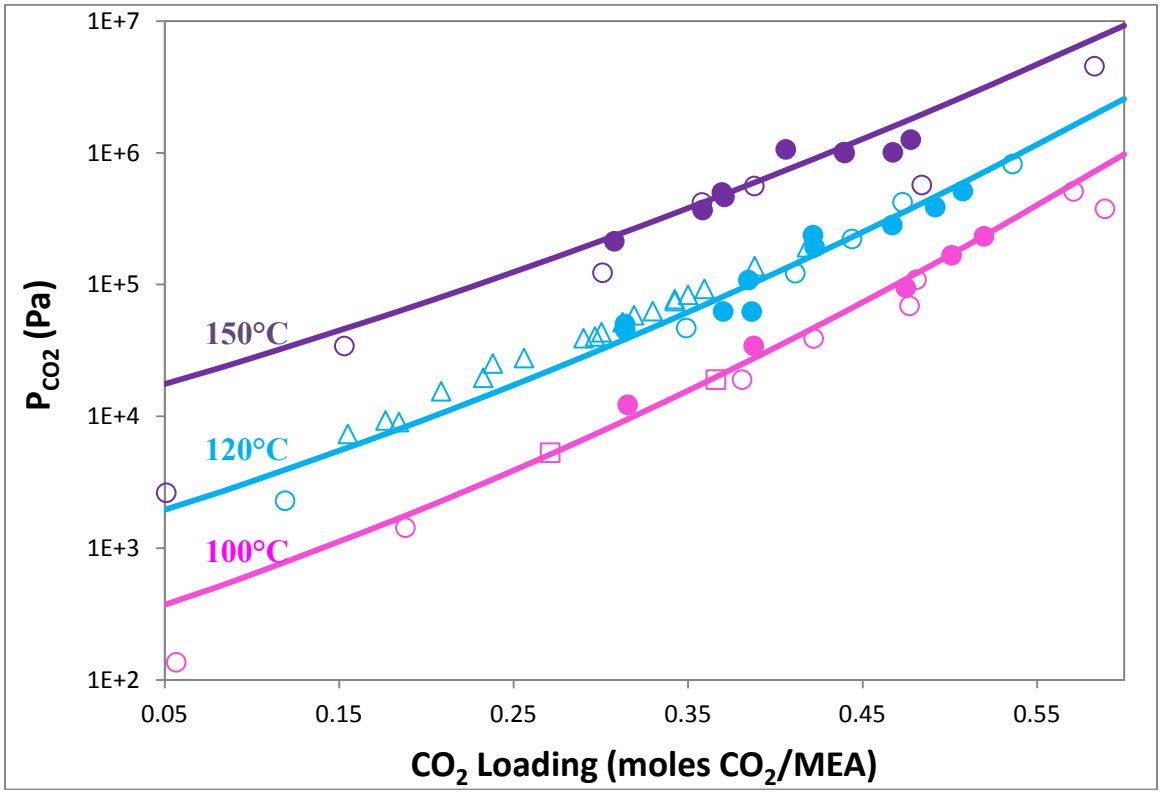

Figure 2-5: Comparison of CO_2 Solubility in 7 m MEA at 100, 120 and 150°C. ●: This work; ○: Jou et al. (1995); □: Dugas et al. (2009); Δ: Ma'mun et al. (2005); Lines: empirical model, 7 m MEA.

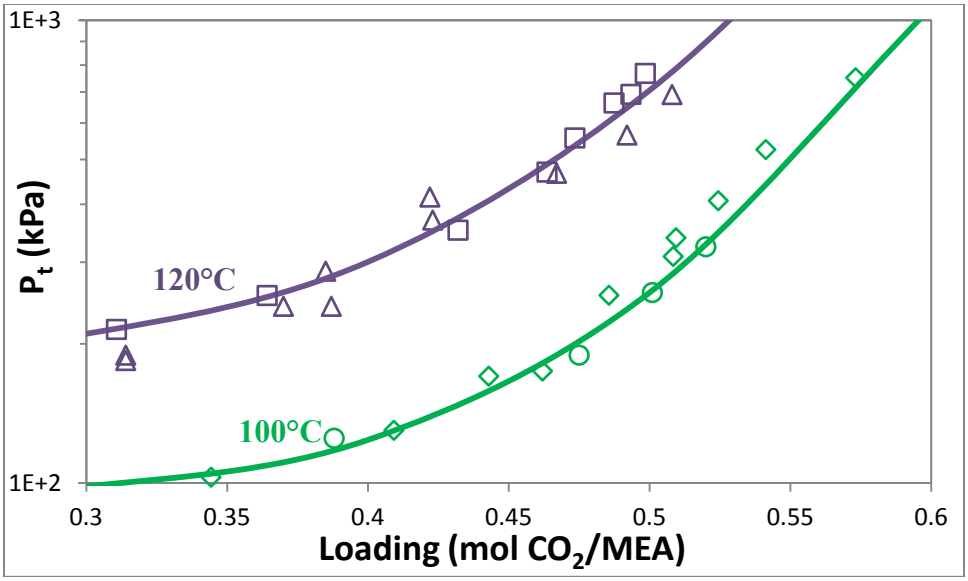

Figure 2-6: Comparison of Total Pressure in 7 m MEA. **○: 100°C this work; ◊: 100°C Aronu et al. (2011); Δ: 120°C this work; □: 120°C Aronu et al. (2011); lines: empirical model.**

2.3.2 CO_2 Solubility in Amines

Tables 2-1 to 2-9 present all the data from this work for MEA, PZ, 1MPZ, 2MPZ, PZ/2MPZ, DGA, PZ/1MPZ/1,4-2MPZ, 7 m/2 m MDEA/PZ, and 5 m/5 m MDEA/PZ. Loading is reported as mol CO_2/equivalent alkalinity. Amine concentration is given as molality (m, gmol/kg water).

Table 2-1: Measured Total Pressure and Calculated CO_2 Solubility in MEA

MEA	T	Loading	P_{CO2}	P_t	MEA	T	Loading	P_{CO2}	P_t
m	℃		kPa	kPa	m	℃		kPa	kPa
6.97*	110	0.424	138	266	6.86	120.4	0.314	50	189
6.97*	110	0.424	123	251	6.86	121.8	0.314	45	184
6.97*	120	0.422	237	415	6.86	129.9	0.313	77	220
6.97*	120	0.423	192	370	6.86	131.9	0.313	73	217
6.97*	130	0.419	352	594	6.86	141.4	0.311	131	279
6.97*	130	0.421	292	535	6.86	142.3	0.31	145	293
6.97*	140	0.414	613	937	6.86	150.2	0.308	213	366
6.97*	140	0.417	464	788	6.86	152	0.307	236	390

MEA	T	Loading	P_{CO2}	P_t	MEA	T	Loading	P_{CO2}	P_t
m	℃		kPa	kPa	m	℃		kPa	kPa
6.97*	150	0.406	1062	1490	6.86	159	0.303	332	490
6.86	101	0.475	95	189	6.87	100	0.501	167	258
6.86	111	0.472	171	303	6.87	120	0.492	387	565
6.86	121	0.467	283	467	6.87	140	0.477	764	1089
6.86	130	0.461	448	691	6.87	150	0.467	1008	1437
6.86	139	0.45	716	1032	6.85	100	0.52	233	324
6.86	140	0.452	683	1008	6.85	120	0.508	512	691
6.86	149	0.44	997	1414	6.85	140	0.489	964	1289
6.86	150	0.439	1012	1440	6.85	150	0.478	1259	1688
6.86	160	0.424	1427	1984	6.85	160	0.464	1626	2184
6.86	161	0.424	1442	2013	6.87	120	0.37	63	241
6.86	166	0.42	1568	2216	6.87	140	0.364	217	542
6.82	100	0.388	34	125	6.87	150	0.358	368	797
6.82	110	0.387	61	190	6.87	160	0.351	569	1126
6.82	120	0.387	62	241	10.39	100	0.411	40	127
6.82	120	0.385	108	287	10.39	110	0.410	98	220
6.82	129	0.382	176	412	10.39	120	0.407	176	346
6.82	131	0.383	153	403	10.39	130	0.403	316	547
6.82	140	0.378	289	614	10.39	140	0.397	515	825
6.82	140	0.377	308	633	10.39	150	0.389	801	1210
6.82	150	0.371	463	892	10.39	160	0.379	1189	1720
6.82	150	0.369	500	929	10.60	100	0.520	321	407
6.82	160	0.361	724	1281	10.60	110	0.516	477	599
6.82	160	0.361	732	1289	10.60	120	0.509	703	872
6.82	170	0.348	1090	1805	10.60	130	0.501	996	1226
6.82	170	0.35	1051	1766	10.60	140	0.489	1417	1726
6.86	109	0.314	36	169	10.60	150	0.477	1859	2267
6.86	111.3	0.315	22	157	10.60	160	0.462	2435	2964
6.86	101.1	0.315	12	143					

*: conducted with the calorimeter apparatus.

Table 2-2: Measured Total Pressure and Calculated CO_2 Solubility in PZ

PZ	T	Loading	P_{CO2}	P_t	PZ	T	Loading	P_{CO2}	P_t
m	℃		kPa	kPa	m	℃		kPa	kPa
7.78*	110	0.312	125	251	7.93	161	0.337	1816	2369
7.78*	110	0.312	125	251	7.93	163	0.334	1934	2516
7.78*	120	0.311	211	385	7.86	110.1	0.252	14	140
7.78*	120	0.311	211	385	7.86	118.5	0.251	28	193
7.78*	130	0.311	268	505	7.86	129.9	0.251	59	295
7.78*	130	0.310	343	579	7.86	131.1	0.250	100	344
7.78*	140	0.308	517	833	7.86	140.9	0.249	124	449
7.78*	140	0.308	546	863	7.86	141.1	0.248	166	492
7.78*	150	0.304	894	1311	7.86	149.5	0.247	252	663
7.78*	150	0.305	864	1281	7.86	151.5	0.247	237	670
7.78*	160	0.301	1247	1788	7.86	159.8	0.244	417	955
7.43*	100	0.311	79	168	7.86	163.4	0.243	447	1036
7.43*	110	0.311	41	167	7.86	171.9	0.239	664	1388
7.43*	110	0.310	115	242	7.86	173.2	0.237	749	1497
7.43*	119	0.310	146	315	7.86	180.5	0.234	957	1844
7.43*	120	0.310	95	270	7.86	182.9	0.231	1093	2030
7.43*	130	0.308	285	522	7.86	191.8	0.224	1482	2623
7.43*	130	0.309	195	433	8.00	100	0.448	711	800
7.43*	140	0.306	531	849	8.00	100.6	0.451	596	686
7.43*	140	0.307	427	745	8.00	110	0.444	881	1006
7.43*	150	0.302	877	1296	8.00	112.2	0.444	891	1026
7.43*	150	0.304	653	1072	8.00	117.8	0.440	1067	1228
7.43*	160	0.298	1317	1861	8.00	120	0.438	1175	1348
7.43*	160	0.301	974	1518	8.00	128.3	0.433	1423	1647
7.43*	169	0.297	1374	2054	8.00	129.4	0.431	1507	1738
7.43*	170	0.291	1954	2651	8.00	140.5	0.424	1901	2221
7.43*	180	0.281	3006	3888	8.00	140.6	0.423	1928	2248
7.93*	120	0.328	116	290	8.00	146.7	0.418	2203	2583
7.93*	125	0.328	124	327	4.93	100.6	0.292	20	115
7.93*	130	0.327	229	465	4.93	108.9	0.291	31	157
7.93*	139	0.325	441	748	4.93	110.6	0.291	40	174
7.93*	140	0.325	440	756	4.93	120	0.290	60	242
7.93*	149	0.321	780	1184	4.93	130	0.289	105	353
7.93*	150	0.321	777	1193	4.93	138.9	0.287	152	473
7.93*	160	0.317	1238	1778	4.93	140	0.286	176	507

PZ	T	Loading	P_{CO2}	P_t	PZ	T	Loading	P_{CO2}	P_t
m	℃		kPa	kPa	m	℃		kPa	kPa
7.93*	161	0.318	1181	1737	4.93	150	0.283	273	709
7.93*	167	0.311	1831	2473	4.93	150	0.283	295	732
7.92	100	0.306	20	109	4.93	159.4	0.278	447	1005
7.92	110	0.306	37	162	4.93	160.6	0.277	457	1032
7.92	120	0.304	89	262	4.93	169.4	0.271	665	1381
7.92	130	0.303	135	371	4.93	170	0.269	711	1436
7.92	130	0.303	156	392	4.93	180	0.261	991	1909
7.92	140	0.301	256	571	4.93	180.6	0.260	1035	1967
7.92	140	0.300	291	607	4.93	191.1	0.248	1436	2615
7.92	150	0.297	460	876	4.96	100	0.372	76	169
7.92	150	0.296	510	926	4.96	100.6	0.371	103	198
7.92	160	0.292	723	1263	4.96	109.4	0.370	140	268
7.92	160	0.289	849	1389	4.96	110	0.369	170	301
7.92	170	0.283	1160	1852	4.96	120	0.367	243	425
7.92	170	0.282	1251	1943	4.96	120.6	0.366	272	458
7.92	174	0.278	1421	2183	4.96	130	0.363	388	636
7.94	81	0.422	94	137	4.96	130.6	0.362	415	667
7.94	82	0.421	126	171	4.96	140	0.358	578	909
7.94	89	0.421	151	210	4.96	140	0.357	607	938
7.94	90	0.419	197	258	4.96	148.3	0.352	823	1240
7.94	94	0.419	200	271	4.96	150	0.351	835	1271
7.94	100	0.417	322	410	4.96	160	0.344	1149	1715
7.94	101	0.418	277	369	4.96	160.6	0.342	1194	1769
7.94	110	0.413	478	604	4.96	170	0.334	1538	2264
7.94	111	0.414	447	576	4.96	170.6	0.333	1580	2317
7.94	120	0.410	623	797	4.96	175	0.329	1775	2593
7.94	120	0.409	682	856	7.92	100	0.416	301	390
7.94	130	0.404	898	1134	7.92	110	0.413	471	597
7.94	130	0.403	945	1181	7.92	120	0.408	679	853
7.94	139	0.398	1228	1534	7.92	130	0.402	971	1207
7.94	140	0.397	1243	1558	7.92	140	0.395	1302	1618
7.94	146	0.393	1452	1825	7.92	150	0.387	1709	2125
7.94	150	0.389	1646	2062	7.92	160	0.378	2192	2732
7.94	150	0.389	1639	2055	7.80	120	0.300	64	238
7.94	157	0.384	1911	2411	7.80	140	0.297	220	537
7.75	100	0.373	174	263	7.80	150	0.294	374	791

PZ	T	Loading	P_{CO2}	P_t	PZ	T	Loading	P_{CO2}	P_t
m	℃		kPa	kPa	m	℃		kPa	kPa
7.75	110	0.371	281	407	7.80	160	0.289	602	1142
7.75	110	0.367	419	545	7.93	100	0.357	86	174
7.75	120	0.367	444	618	7.93	120	0.352	270	443
7.75	120	0.364	577	751	7.93	130	0.349	433	669
7.75	130	0.359	798	1034	7.93	140	0.344	668	984
7.75	134	0.361	723	989	7.93	150	0.338	980	1396
7.75	140	0.357	913	1229	7.93	160	0.330	1358	1898
7.75	140	0.353	1085	1401	9.69	100	0.302	25	111
7.75	150	0.345	1505	1922	9.69	110	0.301	59	181
7.75	151	0.347	1415	1844	9.69	120	0.300	112	280
7.75	160	0.337	1919	2460	9.69	130	0.299	203	432
7.75	160	0.337	1892	2433	9.69	140	0.296	354	661
7.93	110	0.368	223	348	9.69	150	0.292	585	989
7.93	119	0.365	390	558	9.69	160	0.287	918	1443
7.93	121	0.367	304	483	9.92	100	0.379	209	297
7.93	129	0.360	609	838	9.92	110	0.376	367	492
7.93	137	0.357	760	1050	9.92	120	0.372	567	741
7.93	139	0.354	901	1208	9.92	130	0.367	840	1075
7.93	146	0.350	1106	1479	9.92	140	0.362	1167	1482
7.93	150	0.346	1316	1731	9.92	150	0.355	1588	2003
7.93	152	0.345	1369	1807	9.92	160	0.347	2065	2603

*: conducted with the calorimeter apparatus.

Table 2-3: Measured Total Pressure and Calculated CO_2 Solubility in 1MPZ

1MPZ	T	Loading	P_{CO2}	P_t	1MPZ	T	Loading	P_{CO2}	P_t
m	℃		kPa	kPa	m	℃		kPa	kPa
7.76	120	0.192	225	399	7.66	100	0.246	244	333
7.76	130	0.188	381	617	7.66	120	0.238	630	804
7.76	140	0.183	616	932	7.66	130	0.232	917	1154
7.76	150	0.178	903	1320	7.66	140	0.224	1289	1606
7.76	160	0.170	1282	1823	7.66	150	0.215	1744	2161
					7.66	160	0.205	2272	2814

Table 2-4: Measured Total Pressure and Calculated CO_2 Solubility in 2MPZ

2MPZ	T	Loading	P_{CO2}	P_t	2MPZ	T	Loading	P_{CO2}	P_t
m	℃		kPa	kPa	m	℃		kPa	kPa
7.61	120	0.279	145	319	6.69	160	0.340	2269	2819
7.61	130	0.276	262	499	7.41	100	0.392	306	398
7.61	140	0.272	449	766	7.41	110	0.387	519	648
7.61	150	0.266	715	1133	7.41	120	0.380	792	971
7.61	160	0.258	1126	1668	7.41	130	0.372	1129	1372
6.69	120	0.379	571	748	7.41	140	0.362	1594	1919
6.69	130	0.372	859	1100	7.41	150	0.350	2118	2547
6.69	140	0.363	1247	1569	7.41	160	0.337	2751	3307
6.69	150	0.353	1709	2133					

Table 2-5: Measured Total Pressure and Calculated CO_2 Solubility in PZ/2MPZ*

PZ+2MPZ	T	Loading	P_{CO2}	P_t	PZ+2MPZ	T	Loading	P_{CO2}	P_t
m	℃		kPa	kPa	m	℃		kPa	kPa
7.63	120	0.306	142	316	7.86	100	0.397	227	315
7.63	130	0.303	252	489	7.86	120	0.389	576	750
7.63	140	0.300	427	744	7.86	130	0.384	837	1073
7.63	150	0.295	673	1091	7.86	140	0.376	1201	1517
7.63	160	0.288	1011	1554	7.86	150	0.369	1585	2001
					7.86	160	0.359	2084	2624

*: PZ/2MPZ mol ratio ≈ 1:1.

Table 2-6: Measured Total Pressure and Calculated CO_2 Solubility in DGA

DGA	T	Loading	P_{CO2}	P_t	DGA	T	Loading	P_{CO2}	P_t
m	℃		kPa	kPa	m	℃		kPa	kPa
9.55	120	0.402	252	421	9.6	100	0.488	356	442
9.55	130	0.396	417	647	9.6	120	0.473	732	901
9.55	140	0.387	662	970	9.6	130	0.463	990	1220
9.55	150	0.375	975	1380	9.6	140	0.450	1329	1637
9.55	160	0.361	1359	1885	9.6	150	0.437	1699	2104
					9.6	160	0.421	2150	2676

Table 2-7: Measured Total Pressure and Calculated CO_2 Solubility in PZ/1MPZ/1,4-DMPZ

Amine*	T	Loading	P_{CO2}	P_t	Amine*	T	Loading	P_{CO2}	P_t
m	℃		kPa	kPa	m	℃		kPa	kPa
7.57	100	0.320	276	365	7.57	160	0.269	2771	3314
7.57	110	0.316	455	581	7.92	120	0.240	165	338
7.57	120	0.310	702	876	7.92	130	0.237	276	513
7.57	130	0.303	1036	1274	7.92	140	0.234	466	782
7.57	140	0.294	1497	1814	7.92	150	0.228	742	1158
7.57	150	0.283	2052	2470	7.92	160	0.221	1129	1669

*: Amine concentration is the total of PZ, 1MPZ, and 1,4-DMPZ and the mol ratio is about 3.75:3.75:0.5.

Table 2-8: Measured Total Pressure and Calculated CO_2 Solubility in 7 m MDEA / 2 m PZ

Amine*	T	Loading	P_{CO2}	P_t	Amine*	T	Loading	P_{CO2}	P_t
m	℃		kPa	kPa	m	℃		kPa	kPa
10.51	110	0.133	78	202	10.49	140	0.205	1376	1688
10.51	120	0.132	136	307	10.49	150	0.193	1866	2278
10.51	130	0.129	226	460	10.49	160	0.177	2477	3011
10.51	140	0.125	355	668	10.71	100	0.234	189	276
10.51	150	0.119	553	964	10.71	110	0.229	346	470
10.51	160	0.113	787	1321	10.71	120	0.223	527	698
10.49	100	0.236	253	341	10.71	130	0.214	827	1060
10.49	110	0.232	411	535	10.71	140	0.203	1181	1492
10.49	120	0.225	634	806	10.71	150	0.191	1609	2019
10.49	130	0.216	962	1196	10.71	160	0.178	2054	2587

*: Amine concentration is the total alkalinity of MDEA and PZ and the mol ratio of MDEA/PZ is about 7:2.

Table 2-9: Measured Total Pressure and Calculated CO_2 Solubility in 5 m MDEA / 5 m PZ

Amine*	T	Loading	P_{CO2}	P_t	Amine*	T	Loading	P_{CO2}	P_t
m	℃		kPa	kPa	m	℃		kPa	kPa
14.43	110	0.221	98	220	14.61	100	0.277	111	197
14.43	120	0.219	173	342	14.61	110	0.275	204	326
14.43	130	0.216	298	528	14.61	120	0.271	350	519
14.43	140	0.212	489	796	14.61	130	0.266	567	797
14.43	150	0.206	760	1165	14.61	140	0.259	901	1208
14.43	160	0.197	1144	1670	14.61	150	0.250	1289	1693
					14.61	160	0.240	1776	2301

*: Amine concentration is the total alkalinity of MDEA and PZ and the mol ratio of MDEA/PZ is about 5:5.

Empirical models were regressed based on the data in this work and selected literature for each amine. The models for MEA, PZ, 1MPZ, 2MPZ, DGA have been reported (Xu et al., 2011) and some of them are updated in this paper, and new models for the rest of the amines are regressed from the new data.

Table 2-10 lists the correlated parameters, coefficient of determination (R^2) for the empirical models, and the literature that provided additional data for the regression.

Table 2-10: Empirical Correlation of CO_2 Partial Pressure (P_{CO2}, Pa) with Loading (α, gmol CO_2/equiv. alkalinity) and T (K). $\ln P_{CO_2}(\mathrm{Pa}) = a + b\frac{1}{T} + c\alpha + d\alpha^2 + e\frac{\alpha}{T} + f\frac{\alpha^2}{T}$

	MEA	PZ	1MPZ	2MPZ	PZ/2MPZ
a	38.6±0.4	35.3±0.3	34.0±0.1	39.9±0.8	40.1±0.8
b	-12379±139	-11054±120	-9923±50	-12469±267	-12807±266
c	NF**	NF**	NF**	-21.6±2.6	-21.3±2.4
d	-16.0±2.5	-18.9±2.7	NF**	NF**	NF**
e	3556±231	4958±347	7555±107	13990±905	14114±837
f	8702±932	10163±1085	NF**	NF**	NF**
R^2	0.994	0.993	0.999	0.999	0.999
Literature*	Jou et al. 1995; Hilliard 2008; Dugas 2008; Ma'mun 2005; Aronu 2011.	Hilliard 2008; Dugas 2008; Ermatchkov 2006; Nguyen 2010; Kamps 2003.	Chen 2011	Chen 2011	Chen 2011

	DGA	PZ/1MPZ/1,4-DMPZ	7 m MDEA/2 m PZ	5 m MDEA/5 m PZ	
a	49.2 ±2.3	34.5 ±0.1	31.2 ±0.2	36.1 ±0.2	
b	-15066 ±761	-10629 ±54	-8701 ±58	-11199 ±173	
c	-42.8 ±6.2	NF**	23.0 ±1.1	NF**	
d	26.0 ±4.2	NF**	-18.8 ±3.5	-29.1 ±4.3	
e	14174 ±1814	7578 ±120	NF**	10551 ±772	
f	NF**	NF**	NF**	NF**	
R^2	0.998	1.000	0.999	1.000	
Literature*	Chen 2010	Rochelle 2010	Chen 2010	Chen 2010	

*: "et al." is neglected to save space in this table.

**: NF – not fit. It means the coefficient was not important in improving the regression, so it was excluded in the final regression and its value is 0.

Figures 2-7 through 2-15 show the temperature and loading dependence of CO_2 solubility in the screened solvents, respectively.

In Figure 2-7 the MEA data is compared with Aspen® model prediction by Hilliard (2008). The Hilliard model is good for 60-120 ℃ within 0.2-0.5 loading. At higher than 140 ℃, it over predicts the CO_2 partial pressure.

In Figure 2-8 the PZ data is compared with the PZ Aspen® Fawkes model prediction by Frailie et al. (2010). The Fawkes model predicts well for 40-160 ℃ with 0.2-0.45 loading. At higher than 0.45 loading, there is no experimental data and the model prediction is higher than the empirical correlation.

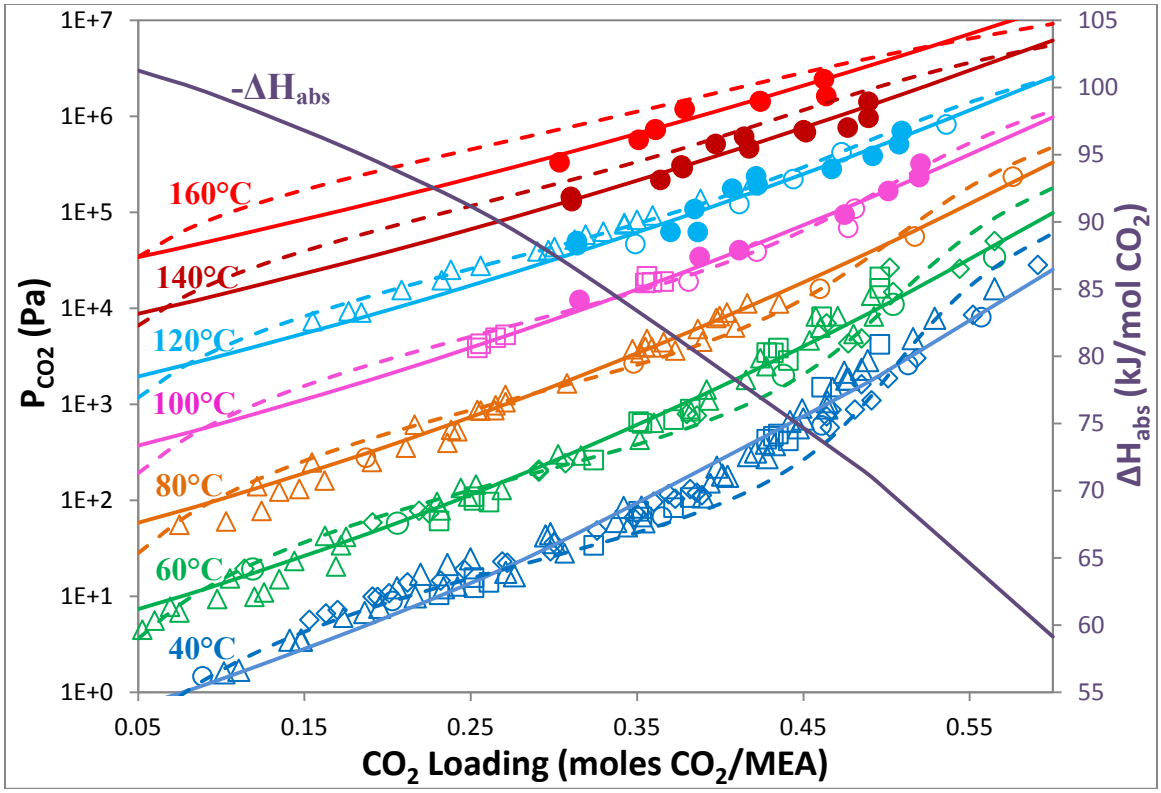

Figure 2-7: CO_2 Solubility in 2.9-24.6 m MEA. ●: this work; ○: Jou et al. (1995); □: Dugas et al. (2008); ◊: Hilliard (2008); Δ: Ma'mun et al. (2005); solid lines: empirical model; dashed lines: Aspen® Hilliard Model (2008) for 7 m MEA.

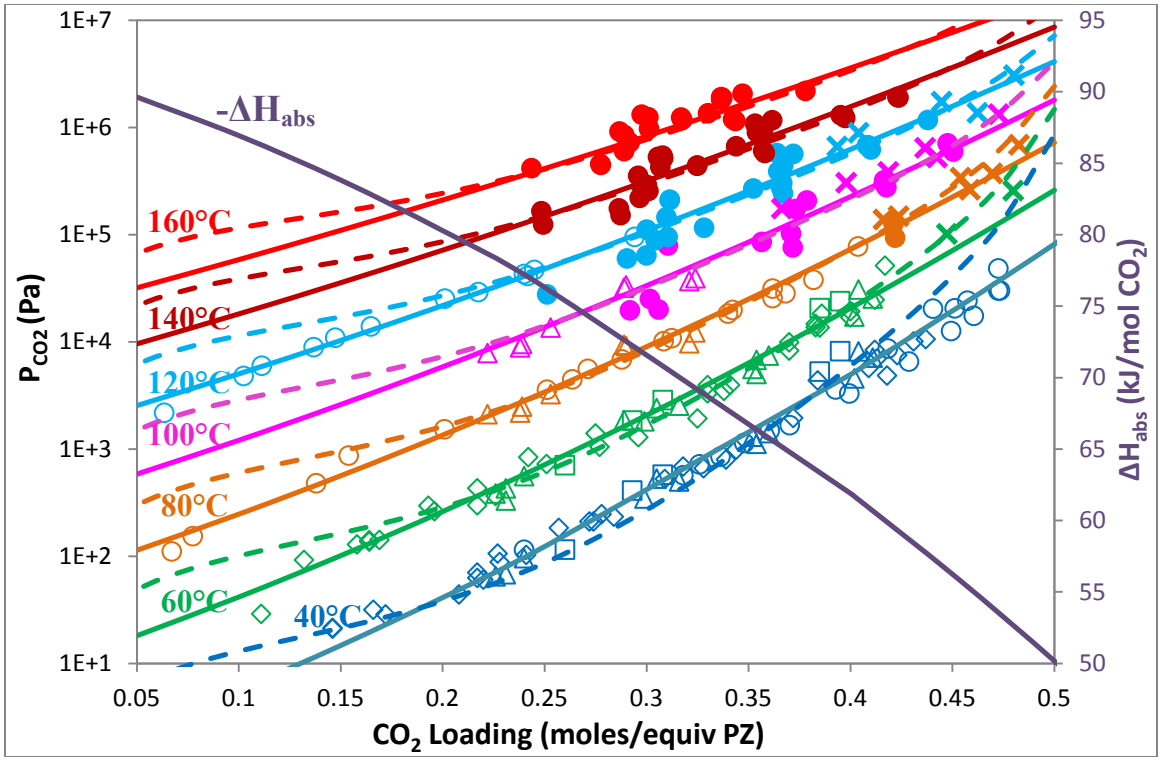

Figure 2-8: CO_2 Solubility in 0.9-12 m PZ. **●: this work; ○: Ermatchkov et al. (2006); □: Nguyen et al. (2010); ◊: Hilliard (2008); Δ: Dugas et al. (2008); X: Kamps et al. (2003); solid lines: empirical model; dashed lines: Aspen® Fawkes Model (Frailie et al., 2010) for 8 m PZ**

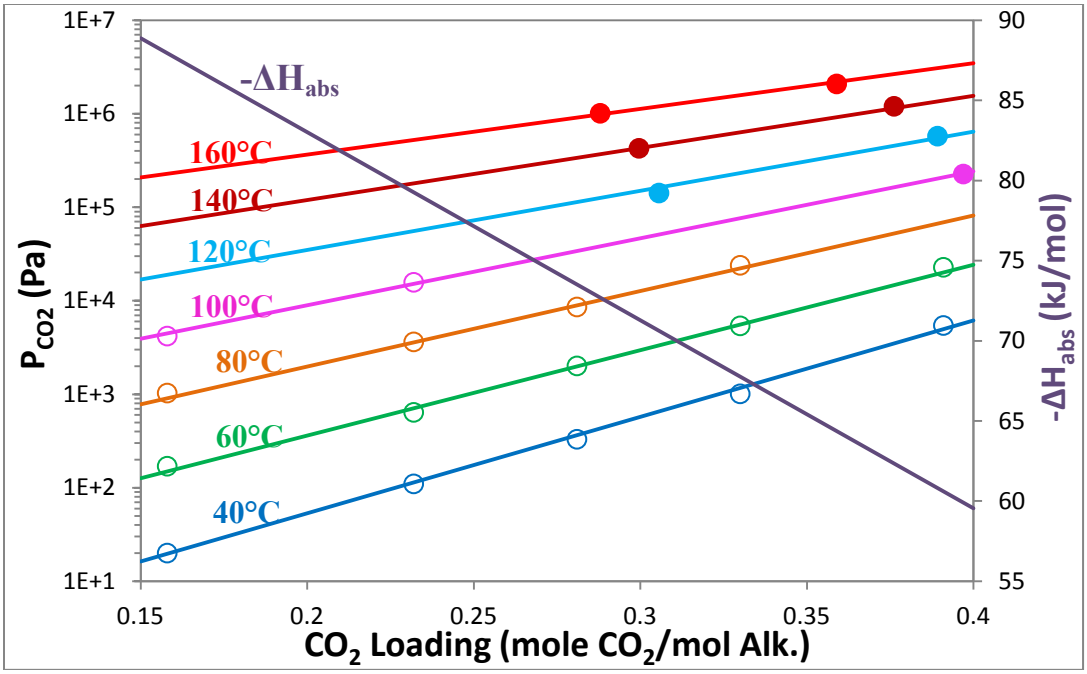

Figure 2-9: CO_2 Solubility in 4 m PZ/4 m 2MPZ. ●: this work; ○: Chen et al., 2011; solid lines: empirical model.

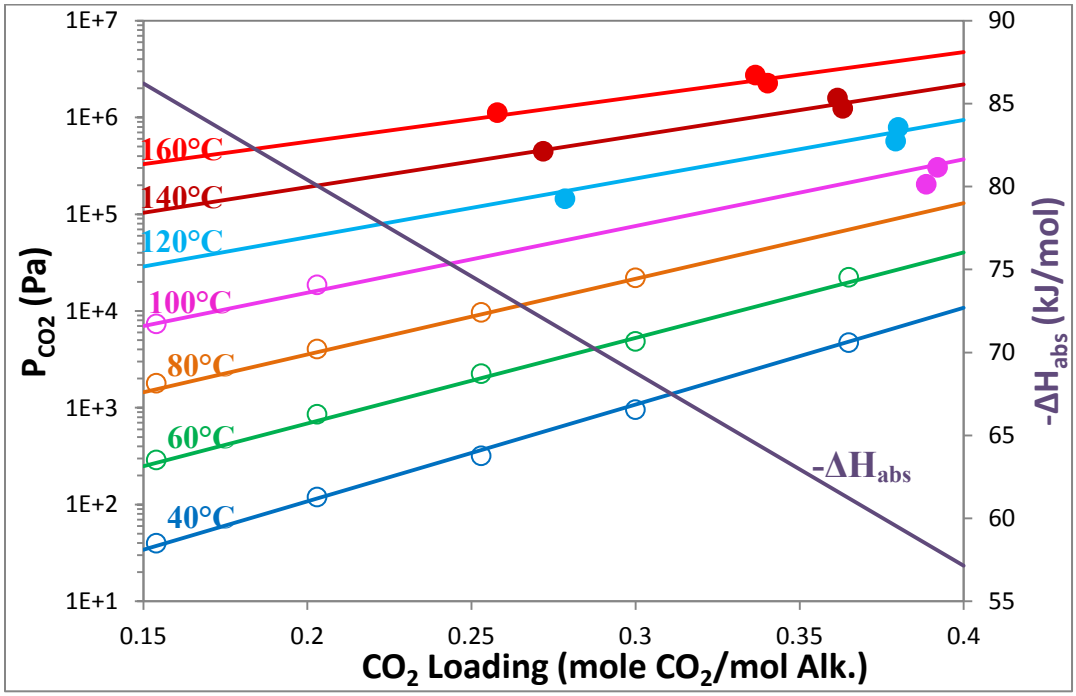

Figure 2-10: CO_2 Solubility in 8 m 2MPZ. ●: this work; ○: Chen et al., 2011; solid lines: empirical model.

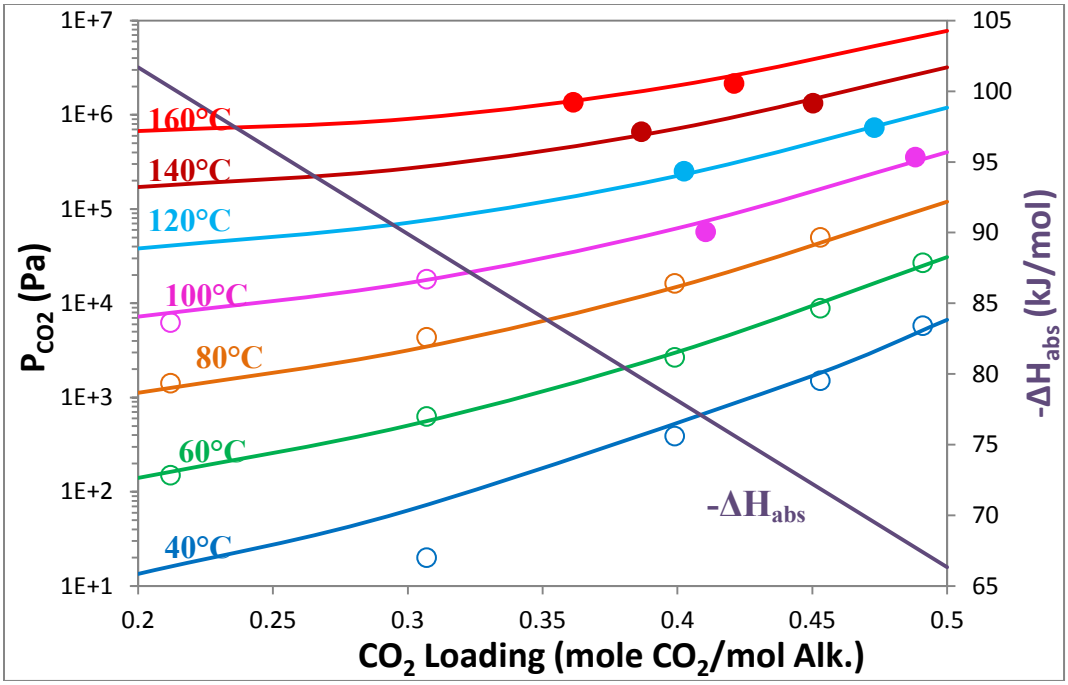

Figure 2-11: CO_2 Solubility in 10 m DGA. ●: this work; ○: Chen et al., 2010; solid lines: empirical model.

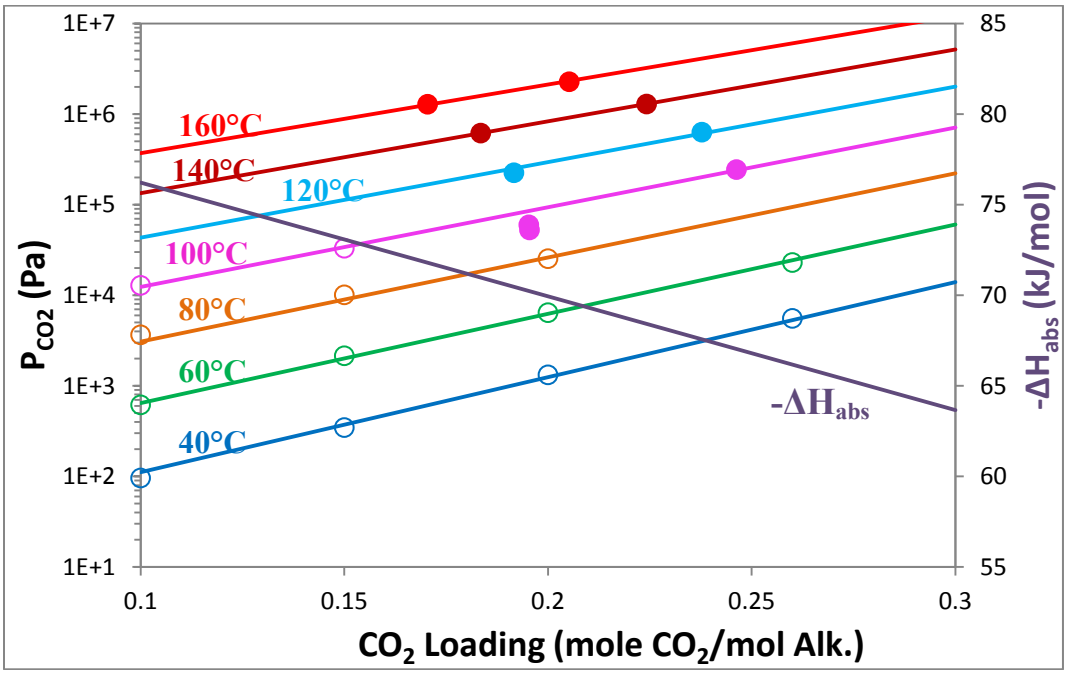

Figure 2-12: CO_2 Solubility in 8 m 1MPZ. ●: this work; ○: Chen et al., 2011; solid lines: empirical model.

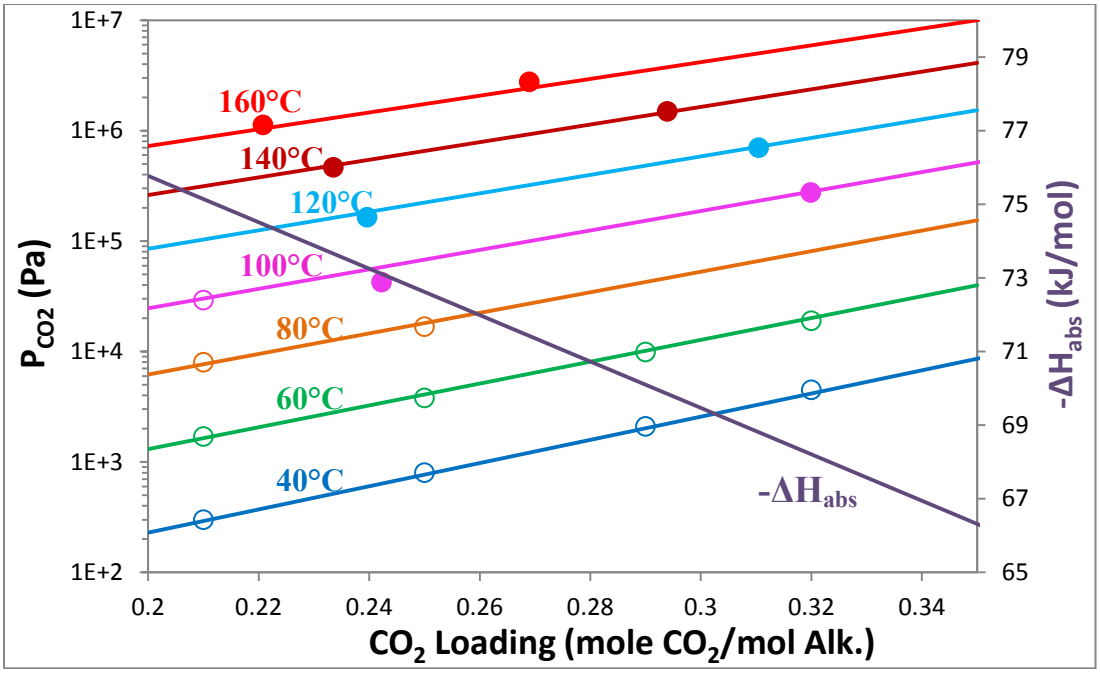

Figure 2-13: CO_2 Solubility in 3.75/3.75/0.5 m PZ/1MPZ/1,4-DMPZ. ●: this work; ○: Rochelle et al., 2010; solid lines: empirical model.

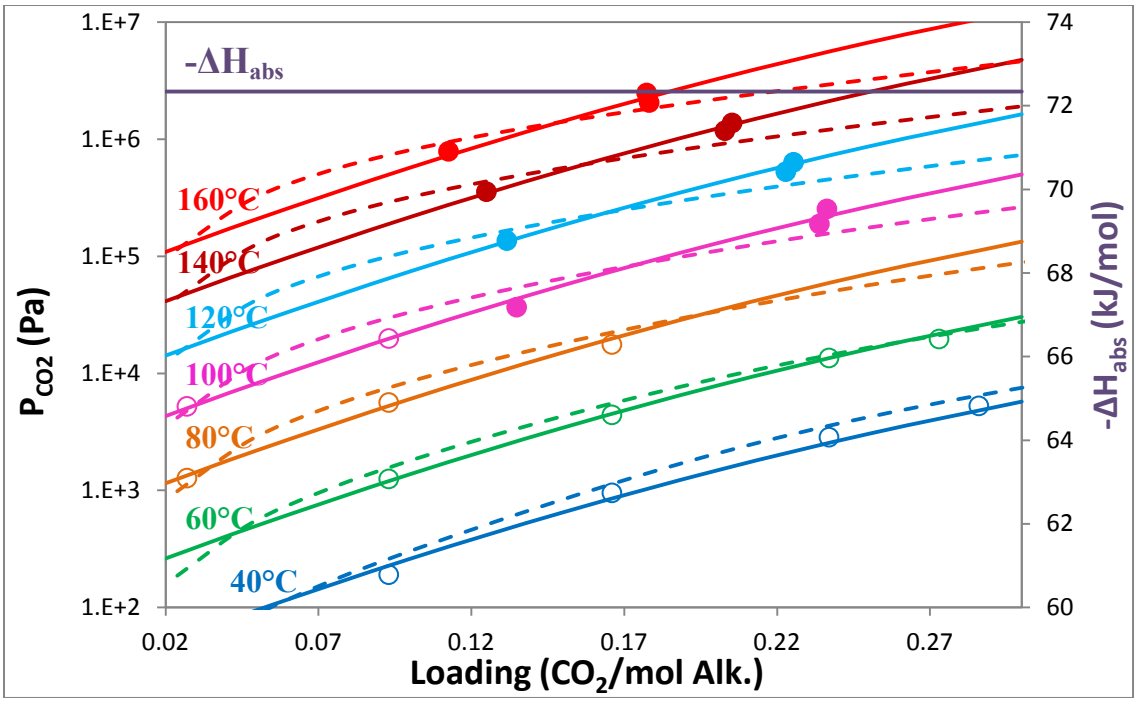

Figure 2-14: CO_2 Solubility in 7 m MDEA/2 m PZ. ●: this work; ○: Chen et al. 2010; solid lines: empirical model; dashed lines: Aspen® Fawkes Model (Frailie et al., 2010)

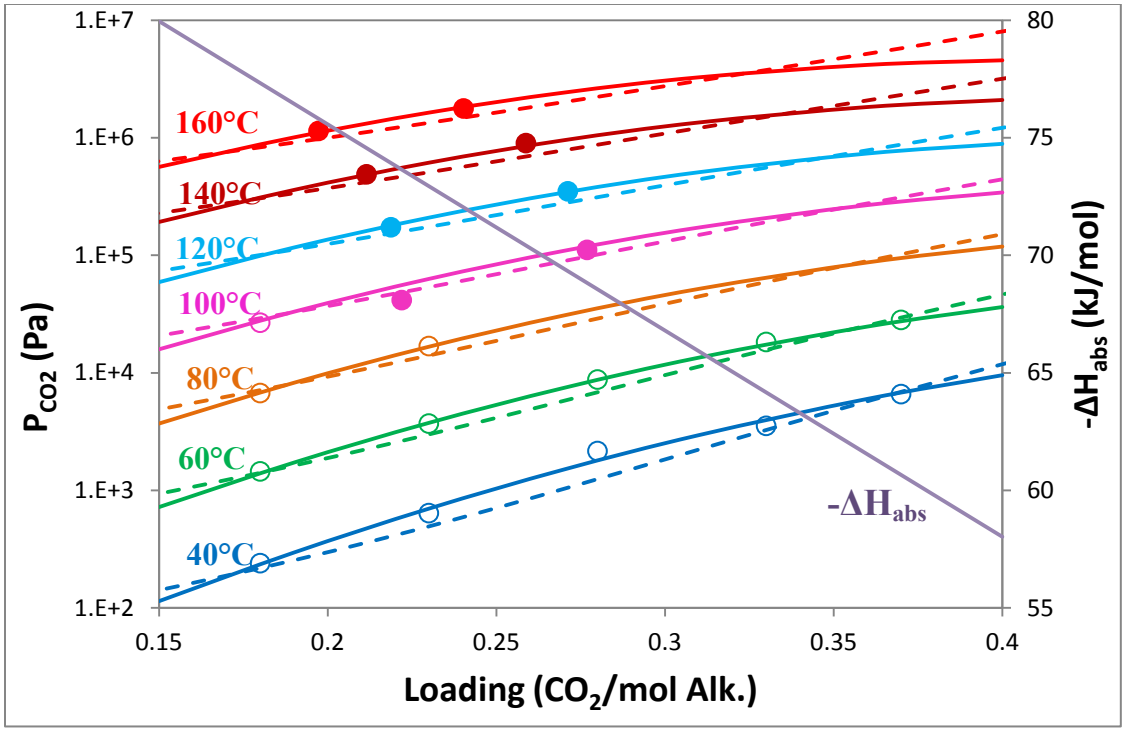

Figure 2-15: CO_2 Solubility in 5 m MDEA/5 m PZ. ●: this work; ○: Chen et al., 2010; solid lines: empirical model; dashed lines: Aspen® Fawkes Model (Frailie et al., 2010)

2.3.3 Error Analysis

Errors generally came from the measurements of temperature, pressure, liquid analysis of CO_2 and amine, CO_2 partial pressure calculation, and the correction of the CO_2 loading in liquid. Table 2-11 lists the estimated error from the experiment.

Table 2-11: Estimated Error from the Total Pressure Experiments

Error Source	Value range	Estimated Error
Measured pressure: P_{meas}	200-3,000 kPa	2.4 kPa
$P_t = P_{meas}-P_{N2}$	200-3,000 kPa	4.8 kPa
T measurement	80-190 °C	1 °F (0.6 °C)
Alkalinity from titration	5-10 mol/kg sol.	1%

Error Source	Value range	Estimated Error
CO_2 wt% from TIC	6-15 wt%	2%
P_{CO2} calculation	100-2,500 kPa	10%
Correction of CO_2 loading in liquid	0.25-0.55	0.005
Total error in P_{CO2}	-	15%
Total error in CO_2 loading	-	0.01

Figure 2-16 gives an example in aqueous PZ that most of P_{CO2} data fall within the ±25% deviation curves from the empirical model prediction.

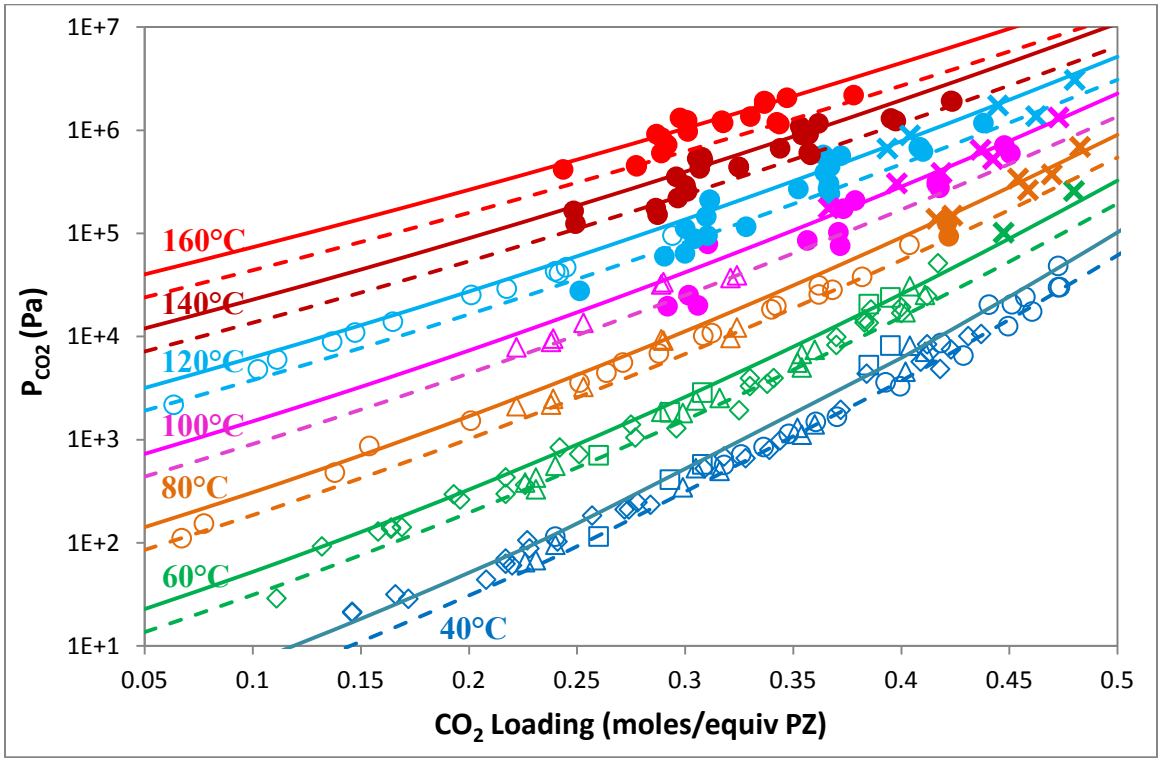

Figure 2-16: CO_2 Solubility in 0.9-12 m PZ – Deviation from the Empirical Model.
●: this work; ○: Ermatchkov et al. (2006); □: Nguyen et al. (2010); ◊: Hilliard (2008); Δ: Dugas et al. (2008); X: Kamps et al. (2003); solid lines: +25% from empirical model – 8 m PZ; dashed lines: -25% from empirical model - 8 m PZ

2.3.4 Total Pressure in CO_2 Loaded Aqueous Amines

Total pressure can be calculated using the empirical models of P_{CO2}. From DIPPR (1998-Provo, BYU), pure water vapor pressure can be expressed as:

$$P^*_{H2O}(Pa) = \exp\left(A + \frac{B}{T(K)} + ClnT(K) + DT(K)^E\right) \quad (2\text{-}3)$$

Where A=73.649, B= -7258.2, C= -7.3037, D=4.1653E-6, E=2.

Pure amine pressure P^*_{amine} is neglected except for MEA.

$$P^*_{MEA}(Pa) = \exp\left(A' + \frac{B'}{T(K)} + C'lnT(K) + D'T(K)^{E'}\right) \quad (2\text{-}4)$$

Where A'=92.624, B'= -10367, C'= -9.4699, D'=1.9E-18, E'=6.

$$x_{H2O} = \frac{\text{mol of } H_2O}{\text{mol of amine} + \text{mol of } H_2O} \quad (2\text{-}5)$$

$$x_{amine} = \frac{\text{mol of amine}}{\text{mol of amine} + \text{mol of } H_2O} \quad (2\text{-}6)$$

Therefore

$$P_t = P_{CO2} + P_{H2O} + P_{amine} = P_{CO2} + P^*_{H_2O} \cdot x_{H_2O} + P^*_{amine} \cdot x_{amine} \quad (2\text{-}7)$$

Substitute the empirical model of P_{CO2} and Equation (2-3) through (2-6) into Equation (2-7) and yield the total pressure P_t.

Figures 2-17 and 2-18(a) are the total pressure in 7 m MEA and 8 m PZ, respectively. The model prediction fits the data well. For the reading convenience in practice, Figure 2-18(a) is enlarged in Figure 2-18(b).

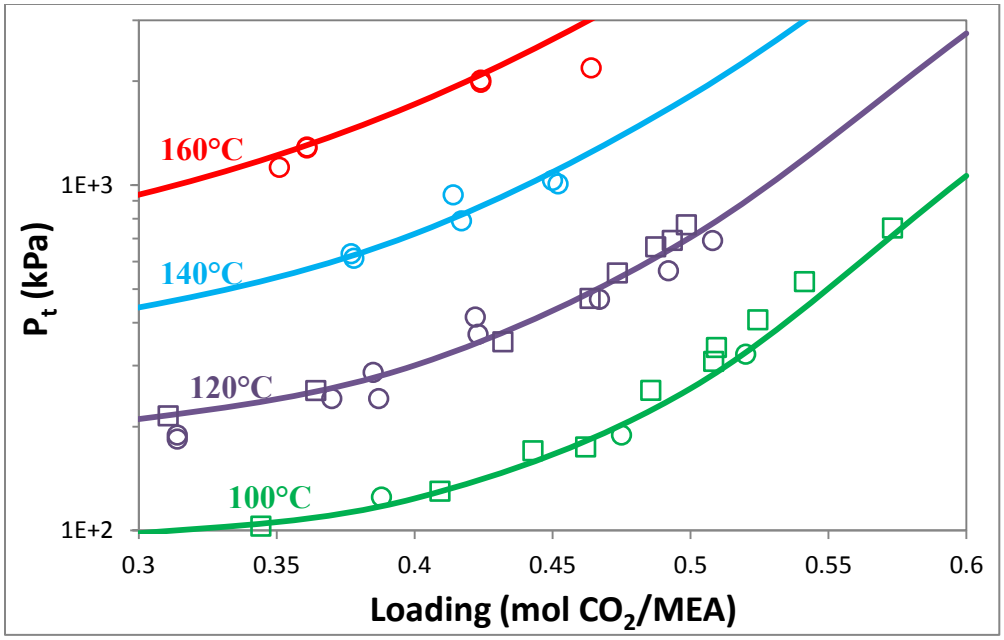

Figure 2-17: Comparison of Total Pressure in 7 m MEA. ○: this work; □: Aronu et al. (2011); lines: Equation (2-7).

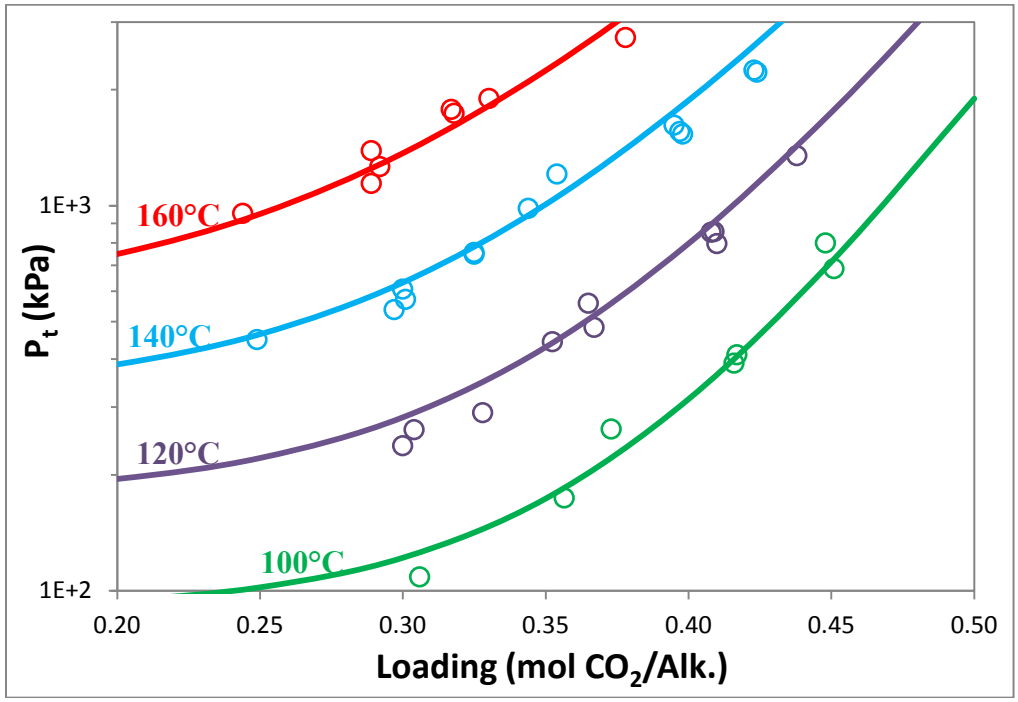

Figure 2-18 (a): Comparison of Total Pressure in 8 m PZ. ○: this work, experimental data; lines: Equation (2-7).

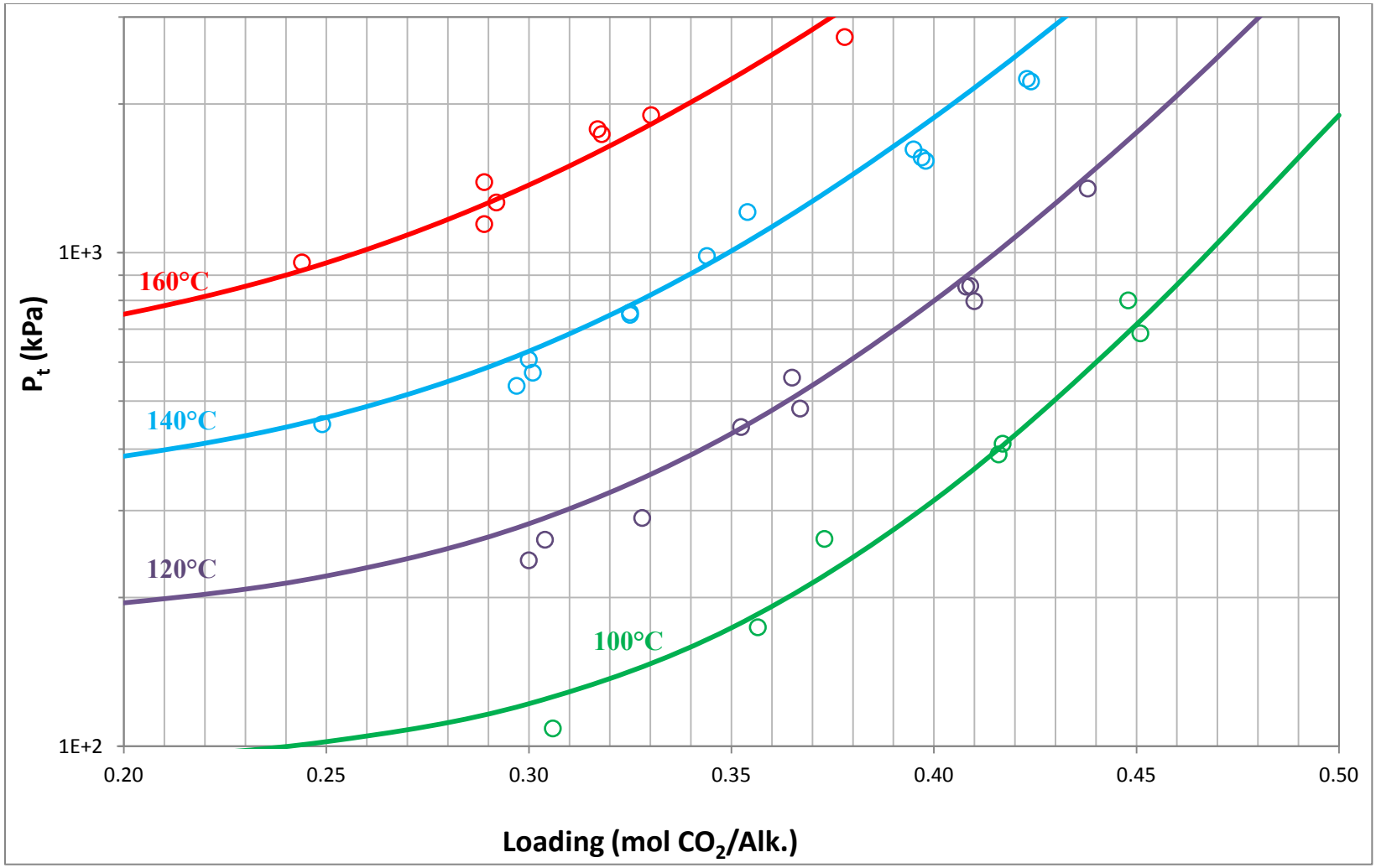

Figure 2-18 (b): Comparison of Total Pressure in 8 m PZ. ○: this work, experimental data; lines: Equation (2-7).

2.3.5 Heat of Absorption of CO_2 in Aqueous Amines

2.3.5.1 Apparent Differential Heat of Absorption

Equation XVIII.9 in Lewis and Randall (1923) and Equation IV.109 in Dodge (1944) relate the fugacity with the heat of absorption of a solution constituent.

$$\left(\frac{\partial ln f_1}{\partial T}\right)_{P,N} = \frac{H_1^* - \bar{H}_1}{RT^2}$$ Equation (XVIII.9), Lewis and Randall (1923)

Where f_1 is the fugacity of the constituent 1, $H_1^* - \bar{H}_1$ is the heat absorbed per mol when a small quantity of the constituent X_1 evaporates from the solution into a vacuum.

$$\frac{\partial ln \bar{f}_i}{\partial T} = -\frac{\bar{H}_i - \bar{H}_i^o}{RT^2}$$ Equation (IV.109), Dodge (1944)

Where $\bar{f}_i$ is the fugacity of the constituent i, $-(\bar{H}_i - \bar{H}_i^o)$ is the heat absorbed per mol when a small quantity of the constituent X_i evaporates from the solution into a vacuum.

Applying the derivation to CO_2 loaded aqueous amines, the equilibrium is $CO_2(g) \leftrightarrow CO_2(aq)$. i refers to CO_2 and:

$\bar{G}_i$: partial molar Gibbs free energy; G_i^o: Gibbs free energy at standard state; $\bar{f}_i$: fugacity; f_i^o: fugacity at standard state; S_i^o: entropy at standard state; $\bar{S}_i$: partial molar entropy; $\bar{H}_i$: partial molar enthalpy; H_i^o: enthalpy at standard state.

By the definition of fugacity, between the two states CO_2(g) and CO_2(aq),

$$\bar{G}_i - G_i^o = RTln\frac{\bar{f}_i}{f_i^o} \quad (2\text{-}8)$$

Take derivatives on both sides with respect to T,

$$\left(\frac{\partial \bar{G}_i}{\partial T}\right)_{p,x} - \left(\frac{\partial G_i^o}{\partial T}\right)_{p,x} = Rln\frac{\bar{f}_i}{f_i^o} + RT\left(\frac{\partial ln\bar{f}_i}{\partial T}\right)_{p,x} - RT\left(\frac{\partial ln f_i^o}{\partial T}\right)_{p,x} \quad (2\text{-}9)$$

f_i^o does not change with T, and from (2-8), $Rln\frac{\bar{f}_i}{f_i^o} = \frac{\bar{G}_i - G_i^o}{T}$, thus

$$\left(\frac{\partial \bar{G}_i}{\partial T}\right)_{p,x} - \left(\frac{\partial G_i^o}{\partial T}\right)_{p,x} = \frac{\bar{G}_i}{T} - \frac{G_i^o}{T} + RT\left(\frac{\partial ln\bar{f}_i}{\partial T}\right)_{p,x} \quad (2\text{-}10)$$

Then apply $\left(\frac{\partial G_i^o}{\partial T}\right)_{p,x} = -S_i^o = -\frac{H_i^o - G_i^o}{T}$, $\left(\frac{\partial \bar{G}_i}{\partial T}\right)_{p,x} = -\bar{S}_i = -\frac{\bar{H}_i - \bar{G}_i}{T}$ to (2-10)

and get

$$\left(\frac{\partial ln\bar{f}_i}{\partial T}\right)_{p,x} = -\frac{\bar{H}_i - \bar{H}_i^o}{RT^2} \quad (2\text{-}11)$$

Assume $\bar{f}_i = P_i$, then $\left(\frac{\partial lnP_i}{\partial T}\right)_{p,x} = -\frac{\bar{H}_i - \bar{H}_i^o}{RT^2} = -\frac{-\Delta H_{abs}}{RT^2}$,

$$-\Delta H_{abs} = R\left(\frac{\partial lnP_{CO_2(g)}}{\partial \frac{1}{T}}\right)_{P,x} \quad (2\text{-}12)$$

This should be used under constant total pressure and loading. According to Figure 2 in De Koeijer et al. (2004), at constant loading and temperature, P_{CO2} increases 2-3% when the total P increases from 1 to 25 bar. In this work P_t and P_{CO2} are within 0-30 bar range, so the effect of P_t on P_{CO2} was neglected.

For CO_2, the critical pressure P_c = 7.38 MPa and the critical temperature T_c = 304.3 K, therefore at 160 ℃ and 25 bar, the compressibility factor of CO_2: $Z_{CO2} \approx 0.98$. Thus for most experimental data points $Z_{CO2} \geq 0.98$. The assumption $f_{CO2} \approx P_{CO2}$ can be made in this work.

According to Equation (2-12), correlations of $-\Delta H_{abs}$ were derived from the empirical models of P_{CO2}. Table 2-12 gives $-\Delta H_{abs}$, lean and rich CO_2 loading, and CO_2 capacity derived from the empirical models. Within the precision of these measurements and estimates, the heat of CO_2 absorption is independent of temperature and amine concentration, but varies with CO_2 loading. The statistics of the empirical regression suggest that the heat of absorption is determined with a confidence interval of 0.5 to 9 kJ/mol.

Table 2-12: Heat of CO_2 Absorption and CO_2 Capacity

Solvent (m)	ΔH_{abs} (J/mol CO_2)	$-\Delta H_{abs}$ kJ/mol CO_2 [1]	CO_2 loading [2] (mol/mol alkalinity)			CO_2 Capacity [3] (mol/kg amine+H_2O)
			Lean	Mid	rich	
2.9–24.6 MEA	$-R(-12379+3556\alpha+8702\alpha^2)$	72±2	0.434	0.483	0.535	0.50 [4]
0.9–12 PZ	$-R(-11054+4958\alpha+10163\alpha^2)$	67±2	0.310	0.354	0.400	0.85 [5]
7.7–8 1MPZ	$-R(-9923+7555\alpha)$	69.4±0.5	0.162	0.208	0.258	0.85
6.7–8 2MPZ	$-R(-12469+13990\alpha)$	67±3	0.267	0.314	0.367	0.89
4/4 PZ/2MPZ	$-R(-12998+14684\alpha)$	66±3	0.294	0.341	0.391	0.89
9.6–10 DGA	$-R(-15066+14174\alpha)$	73±9	0.400	0.445	0.490	0.44
3.75/3.75/0.5 PZ/1MPZ/1,4-DMPZ	$-R(-10629+7578\alpha)$	70.9±0.5	0.232	0.278	0.328	0.87
7/2 MDEA/PZ	72.3	72.3±0.5	0.135	0.201	0.288	0.84
5/5 MDEA/PZ	$-R(-11199+10551\alpha)$	69±2	0.214	0.270	0.346	0.98

1: The heat of absorption of CO_2 at mid-loading. 2: The loadings where P_{CO2} is 0.5, 1.5, and 5 kPa at 40 ℃ corresponds to lean, mid-, and rich loading, calculated from the empirical models. 3: moles of CO_2/kg (water+amine). 4: 7 m MEA. 5: 8 m PZ.

2.3.5.2 Carnot Cycle Derivation

Equation (2-12) can also be derived from the following process. As shown in Figure 2-19, (1+m_{CO2}(gram)/1000) kg of CO_2 loaded rich amine solution was chosen as the system. The equilibrium CO_2 partial pressure at T and T+dT are $P^*(T)$ and $P^*(T+dT)$, respectively. In step 1 the rich amine solution reversibly releases m_{CO2} g of CO_2 gas and absorbs $-\Delta H_{abs}(T)\cdot {}^{m_{CO2}}/_{44.01}$ kJ heat; the m_{CO2} g of CO_2 is at equilibrium pressure, $P^*(T)$. In step 2, the m_{CO2} g CO_2 was compressed reversibly to $P^*(T+dT)$, and the lean solution and CO_2 gas are heated to T+dT. In this step the system (1 kg lean solution + m_{CO2} g CO_2 gas) absorbs heat to increase temperature, and extra work dW is put into the system for isothermal and reversible compression. In step 3, the CO_2 gas at $P^*(T+dT)$ is absorbed into the amine solution, and releases heat of $-\Delta H_{abs}(T+dT)\cdot {}^{m_{CO2}}/_{44.01}$ kJ. In step 4 the temperature of the rich amine is reduced from T+dT to T to the initial state.

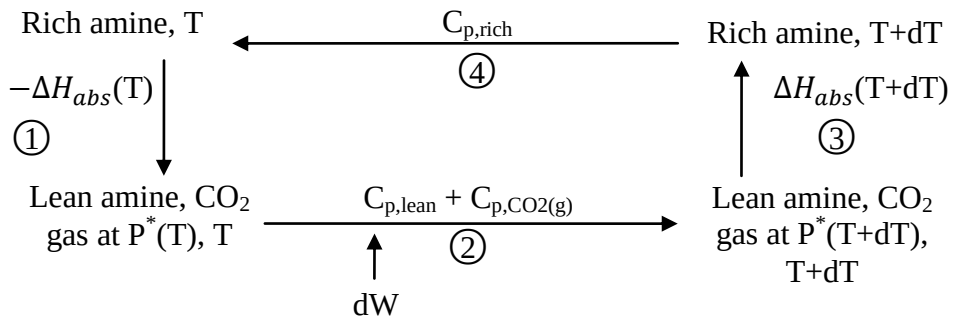

Figure 2-19: Illustration of Temperature Dependence of CO_2 Solubility and Heat of Absorption

In order to correlate enthalpy change in step 1 and 3 with the work dW in step 2, equivalent work of the cycle is calculated. The equivalent work is the largest work that can be withdrawn from heat dQ from a heat reservoir at T and can be calculated from Carnot Cycle. Assume the reference temperature is T_0, the efficiency is: $(T-T_0)/T$. Therefore, in step 1 and 3, equivalent work is $m_{CO2}/44.01 \cdot \Delta H_{abs}(T)\ (T-T_0)/T$ and $m_{CO2}/44.01 \cdot \Delta H_{abs}(T+dT)\ (T+dT-T_0)/(T+dT)$, respectively.

dW is the isothermal and reversible work to the CO_2 gas, assuming this CO_2 is an ideal gas, thus

$$dW = \frac{m_{CO2}}{44.01} RTln\frac{P^*(T+dT)}{P^*(T)} = \frac{m_{CO2}}{44.01} RTln\frac{P+dP}{P} = \frac{m_{CO2}}{44.01} RT[ln(P+dP) - lnP] = \frac{m_{CO2}}{44.01} RTdlnP \quad (2\text{-}13)$$

The heat input in step 2 and 4 are for the heating of lean solution, rich solution, and CO_2 gas. Therefore

$$Q_2 - Q_4 = (C_{p,lean}(\frac{kJ}{kg} \cdot K) \cdot 1kg + \frac{m_{CO2}\ g}{44.01g/mol} \cdot C_{p,CO2}kJ/mol)dT - C_{p,rich}(\frac{kJ}{kg} \cdot K) \cdot \left(1kg + \frac{m_{CO2}\ g}{1000g/kg}\right)dT$$

Because $C_{p,lean} \cdot 1 + \frac{m_{CO2}}{44.01} \cdot C_{p,CO2} - C_{p,rich} \cdot \left(1 + \frac{m_{CO2}}{1000}\right) \approx 0$

Thus for the cycle in Figure 2-19, the equivalent work equation is:

$$-\Delta H_{abs}(T)\cdot\frac{m_{CO2}}{44.01}\cdot\frac{T-T_0}{T}=dW-\Delta H_{abs}(T+dT)\cdot\frac{m_{CO2}}{44.01}\cdot\frac{T+dT-T_0}{T+dT} \quad (2\text{-}14)$$

dT is very small, so $\Delta H_{abs}(T)\approx\Delta H_{abs}(T+dT)$ and $T\approx T+dT$. And substitute Equation (2-13) into (2-14):

$$-\Delta H_{abs}(T)\cdot\frac{m_{CO2}}{44.01}\cdot\frac{T-T_0}{T}=\frac{m_{CO2}}{44.01}RTdlnP-\Delta H_{abs}(T)\cdot\frac{m_{CO2}}{44.01}\cdot\frac{T+dT-T_0}{T}$$

$$-\Delta H_{abs}(T)\cdot\frac{T-T_0}{T}=RTdlnP-\Delta H_{abs}(T)\cdot\frac{T+dT-T_0}{T}$$

$$\frac{\Delta H_{abs}(T)}{R}\cdot\frac{dT}{T^2}=dlnP$$

$$-\frac{\Delta H_{abs}(T)}{R}/d\left(\frac{1}{T}\right)=dlnP$$

$$-\frac{\Delta H_{abs}(T)}{R}=\frac{dlnP}{d\left(\frac{1}{T}\right)}$$

Where P is P_{CO2}.

This agrees with Equation (2-12), and the assumption made here is $f_{CO2}=P_{CO2}$ and $Q_2=Q_4$, which is reasonable when P is not very large, and dT is very small.

2.3.5.3 Inconsistency of the Measured Heat of Absorption and P_{CO2}

ΔH_{abs} by this method is the differential heat of absorption. Because of the accuracy of CO_2 partial pressure measurements, the empirical correlations show no temperature dependence of ΔH_{abs}. Figure 2-20 compares $-\Delta H_{abs}$ from the MEA empirical model and measured $-\Delta H_{abs}$ by Kim et al. (2007). The empirical model generally predicts the data, but the empirical equation does not represent the temperature dependence of the Kim data.

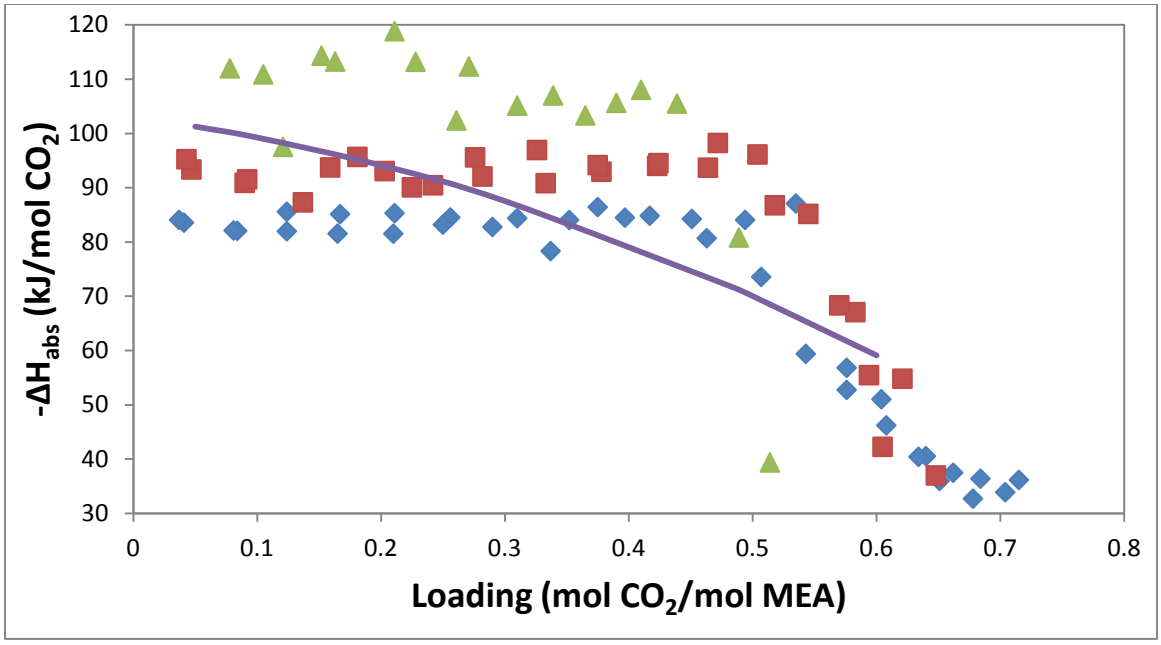

Figure 2-20: Comparison of Heat of Absorption of CO_2 in MEA. **Data points: Kim et al. (2007), ◊: 40°C, □: 80°C, Δ: 120°C; solid lines: empirical model from this work.**

To better compare measured $-\Delta H_{abs}$ from Kim et al. (2007) and the P_{CO2} data from this work, the literature $-\Delta H_{abs}$ was regressed to get a piecewise function as in Equation (2-15). Figure 2-21 shows a fit of the empirical model. A few outliers in the data were not used in the regression.

$$\begin{cases} -\Delta H_{abs} = -13.67 + 0.308T & (\alpha \leq 0.46) \\ -\Delta H_{abs} = -127.13 + 246.65\alpha + 1.02T - 1.54\alpha T & (0.46 \leq \alpha \leq 0.66) \\ -\Delta H_{abs} = 35.66 & (\alpha \geq 0.66) \end{cases} \quad (2\text{-}15)$$

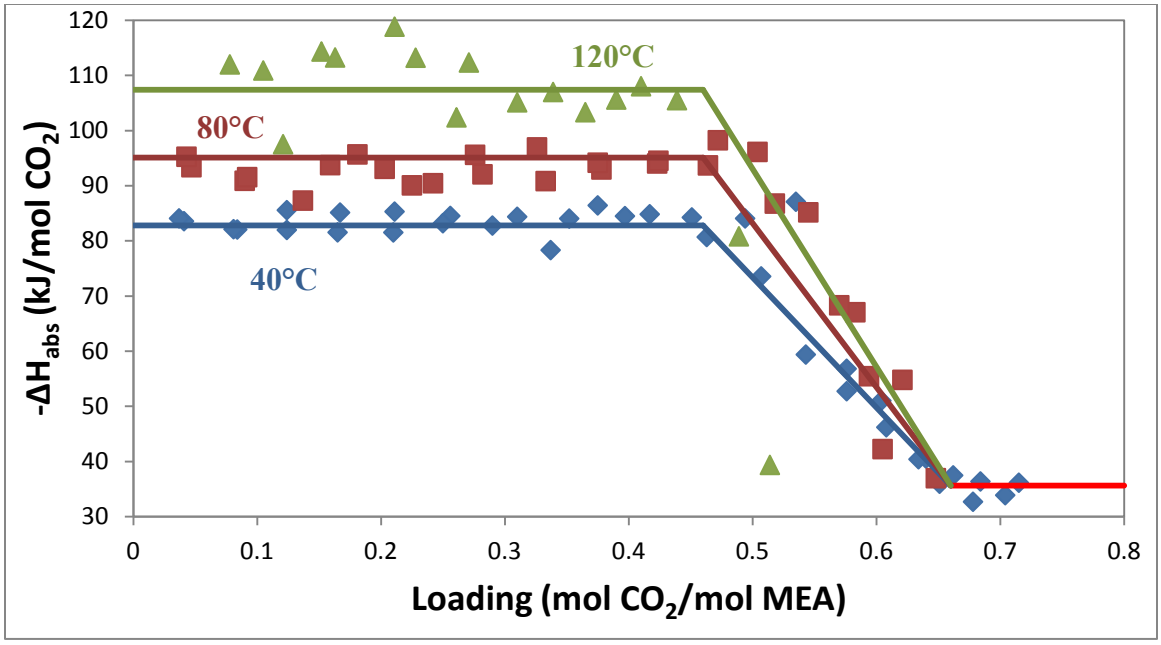

Figure 2-21: Empirical Model of Heat of Absorption of CO_2 in 7 m MEA. **Data points: Kim et al. (2007), ◊: 40°C, □: 80°C, Δ: 120°C; solid lines: empirical model Equation (2-15).**

Then Equation (2-15) was integrated to get P_{CO2}. The literature $-\Delta H_{abs}$ is at 40-120 ℃, thus P_{CO2} at 80 ℃ was chosen as the reference to calculate P_{CO2} at other temperature. The empirical model of P_{CO2} in MEA from this work was used to get P_{CO2} at 80 ℃. Figure 2-22 shows a comparison of the prediction from this integration and the experimental data by Kim et al. (2007). At 40 ℃, 80 ℃, and 120 ℃ lean loading, the model matches the data well, at 120 ℃ rich loading and at 160 ℃, the model over-predicts the data. This illustrates that the measured heat of absorption at high temperature in Kim et al. (2007) is higher than expected values from P_{CO2} measurements in this work.

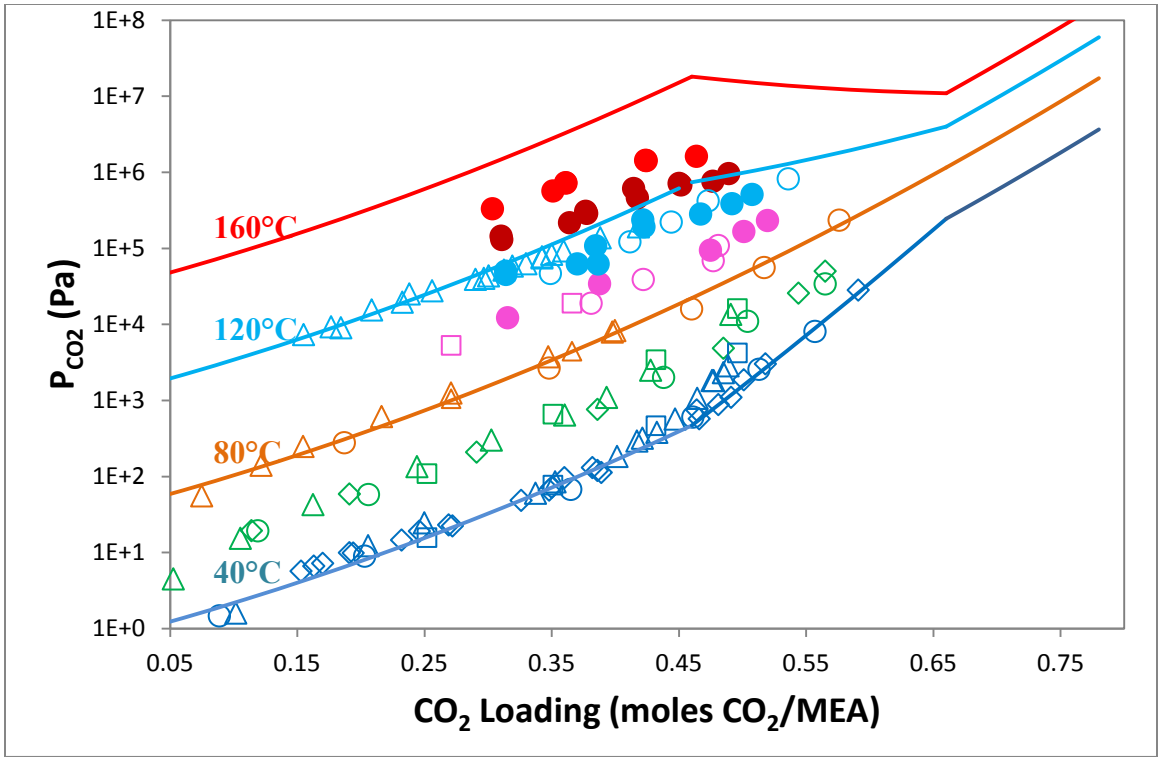

Figure 2-22: CO_2 Solubility in 7 m MEA. **●: this work; ○: Jou et al. (1995); □: Dugas et al. (2008); ◊: Hilliard (2008); Δ: Ma'mun et al. (2005); lines: Equation (2-15) integrated with the P_{CO2} empirical model.**

2.3.5.4 Inconsistency of the Measured Heat of Absorption and Specific Heat capacity

To further compare the data consistency, measured specific heat capacity was used to get the temperature dependence of $-\Delta H_{abs}$. Absorption of CO_2 at different temperature can be related with several steps shown in Figure 2-23. The dependence of C_p and ΔH_{abs} on pressure is ignored. In step 1 and 3, CO_2 is absorbed into lean amine at T_1 and T_2, respectively. C_p is the specific heat capacity. For amine solution, $C_p \approx C_v$ and can be measured by differential scanning calorimetry (DSC).

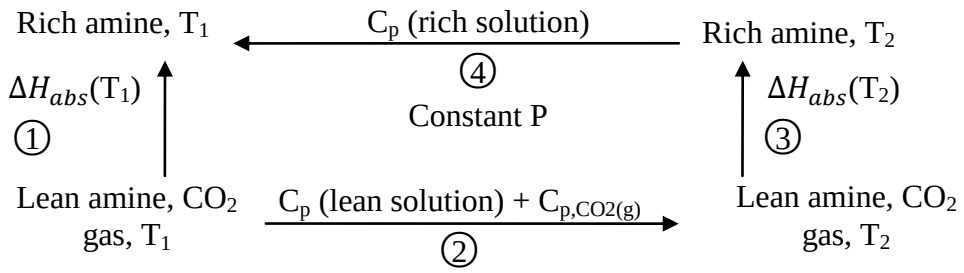

Figure 2-23: Illustration CO_2 Heat of Absorption at Different Temperature

On 1kg lean solution base, when a small amount (m_{CO2} gram) of CO_2 gas is absorbed:

$$\Delta H_{abs}(T_1)\cdot\frac{m_{CO2(g)}}{44.01}=\Delta H_{abs}(T_2)\cdot\frac{m_{CO2(g)}}{44.01}+Q_2+Q_4=\Delta H_{abs}(T_2)\cdot\frac{m_{CO2(g)}}{44.01}+\int_{T_1}^{T_2}\left[Cp(lean)+\frac{Cp_{CO2(g)}m_{CO2(g)}}{44.01}\right]dT+\int_{T_2}^{T_1}Cp(rich)\cdot(1+\frac{m_{CO2(g)}}{1000})dT \quad (2\text{-}16)$$

Using the specific heat capacity data of 7 m CO_2 loaded MEA from Hilliard (2008), a simple correlation of C_p was developed:

$$C_{p,soln}=(2.68\pm0.02)+(0.00286\pm0.00004)T+(-0.605\pm0.007)\alpha \ \text{(kJ/kg K)} \quad (2\text{-}17)$$

Where T is temperature in K, α is CO_2 loading. Figure 2-24 shows a favorable fitting of the data and Equation (2-17).

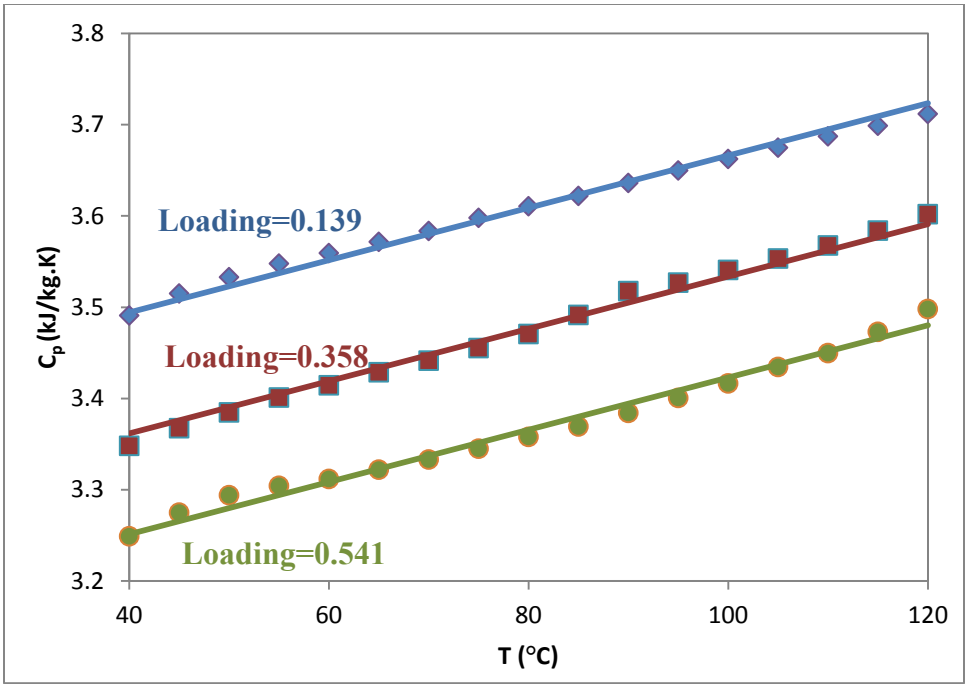

Figure 2-24: Specific Heat Capacity of 7 m MEA. **Points: Hilliard (2008) experimental data. Lines: from Equation (2-17)**

Using the C_p of CO_2 gas from DIPPR database (1998-Provo, BYU), a simple equation was correlated:

$$C_p(CO_2, g) = (0.0253 \pm 0.0005) + (4.11E-5 \pm 1.2E-6)T \quad \text{(kJ/mol K)} \qquad (2\text{-}18)$$

$-\Delta H_{abs}$ at 80 ℃ from Equation (2-15) was used as the reference state to calculate $-\Delta H_{abs}$ at other temperature and Equation (2-17) and (2-18) are used in the integration.

A calculation example of the integration is given here:

Example: at the loading of 0.35, $-\Delta H_{abs}$ at 80 ℃ from Equation (2-15), which represents Kim's experimental data, is 95.1 kJ/mol CO_2. Assume m_{CO2}=0.01 g, according to Equation (2-16):

$$-\Delta H_{abs}(120℃) = -\Delta H_{abs}(80℃) + (Q_2 + Q_4) \cdot \frac{44.01}{m_{CO2(g)}}$$

$$= 95.1 + \frac{44.01}{0.01} \cdot \int_{353.15}^{393.15} \left[Cp(lean) + \frac{Cp_{CO2(g)} 0.01}{44.01}\right] dT + \frac{44.01}{0.01} \cdot \int_{393.15}^{353.15} Cp(rich) \cdot (1 + \frac{0.01}{1000}) dT$$

According to Eq. (2-17) and (2-18),

$$Cp(lean) = 2.68 + 0.00286T - 0.605 \cdot 0.35 = 2.46825 + 0.00286T$$

$$Cp(rich) = 2.68 + 0.00286T - 0.605 \cdot \left[0.35 + \frac{0.01/44.01}{\frac{1000 \cdot 7}{1000 + 7 \cdot 61.08 + 7 \cdot 0.35 \cdot 44.01}}\right]$$

= 2.46822+0.00286T

$$Cp_{CO2(g)} = 0.0253 + 4.11E - 5T$$

Therefore,

$-\Delta H_{abs}(120℃) = 95.1 + \int_{353.15}^{393.15}[(2.46825 + 0.00286T) \cdot 4401 + 0.0253 +$

4.11E−5T−1.00001(2.46822+0.00286T)·4401dT

$= 95.1 + \int_{353.15}^{393.15}(0.0487 - (8.48E - 5)T)dT = 95.1 + 0.7 = 95.8$ (kJ/mol)

Table 2-13 compares the calculated -ΔH_{abs} from Equation (2-15) and (2-16) at the loading of 0.35. Figure 2-25 shows a comparison of -ΔH_{abs} from Equation (2-15) and (2-16) over 0-0.72 loading. The temperature dependence of calculated -ΔH_{abs} is very small compared with the measured data. Therefore, the measured -ΔH_{abs} by Kim et al. (2007) is not consistent with the measured C_p either.

If -ΔH_{abs}(40 ℃)=82.8 kJ/mol CO_2 from Equation (2-15) is used as the reference, and Equation (2-16) is used to calculate the temperature dependence of -ΔH_{abs}, the -ΔH_{abs} at 80 ℃ is about 83.6 kJ/mol CO_2 and agrees well with the -ΔH_{abs} from the P_{CO2} empirical model.

Table 2-13: Comparison of $-\Delta H_{abs}$ in 7 m MEA

	$-\Delta H_{abs}$ (kJ/mol CO_2), ldg=0.35		
	40 ℃	**80 ℃**	**120 ℃**
By Eq. (2-15)	82.8	95.1	107.4
By Eq. (2-16)	94.3	95.1	95.8
Empirical model from P_{CO2}	83.7±2		

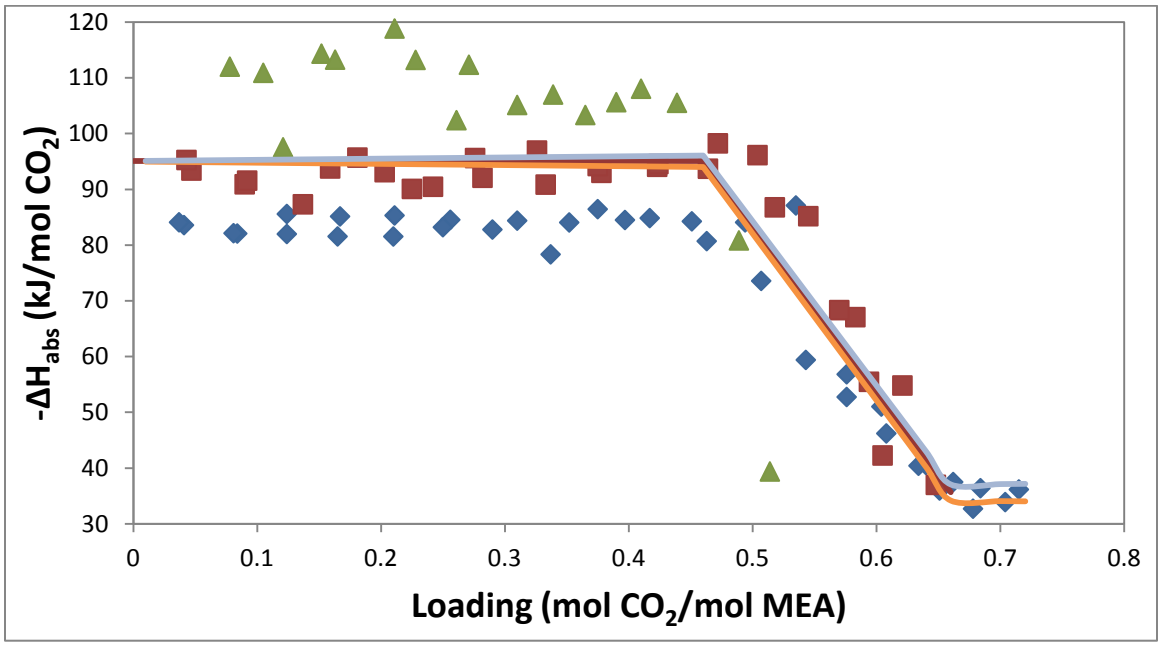

Figure 2-25: Heat of Absorption of CO_2 in 7 m MEA, Comparison of Equation (2-16) and Measured Data. **Data points: Kim et al. (2007), ◊: 40°C, □: 80°C, Δ: 120 ℃; solid lines: prediction by Equation (2-16).**

2.4 Conclusions and Recommendations

CO_2 solubility data was obtained using total pressure measurements. Empirical models as a function of temperature and loading were developed for CO_2 solubility from 40 to 191°C in aqueous MEA, PZ, 1MPZ, 2MPZ, PZ/2MPZ, DGA, PZ/1MPZ/1,4-DMPZ, and PZ/MDEA. The high temperature CO_2 solubility data for MEA is comparable to that by Jou et al. (1995) and Ma'mun et al. (2005). The high temperature data is also compatible with previous low temperature data.

For MEA and PZ, amine concentration does not have obvious effects on the CO_2 solubility.

The heat of CO_2 absorption derived from these models varies from 66 kJ/mol for 4 m PZ/4 m 2MPZ and to 72, 72, and 73 kJ/mol for MEA, 7 m MDEA/2 m PZ, and DGA.

The heat of absorption estimated from the total pressure data does not vary significantly with temperature. The temperature dependence of the heat of CO_2 absorption in MEA measured by Kim et al. (2007) is not consistent with either the measured total pressure or the measured specific heat capacity.

Chapter 3: High Temperature Amine Volatility and Specific Heat Capacity

This Chapter presents a high temperature experimental method for vapor-liquid equilibrium (VLE) of CO_2 loaded aqueous amines. It is a single vapor pass dynamic VLE apparatus with online gas sampling and analysis by FTIR. Monoethanolamine (MEA) volatility in MEA-H_2O from this work is comparable with literature data. MEA volatility in 7 molal (m, gmol/kg H_2O) MEA-CO_2-H_2O and piperazine (PZ) volatility in 5-11 m PZ-CO_2-H_2O were measured at 120 to 150 ℃, 0.24 to 0.49 CO_2 loading. At 0-0.5 loading (α), 313-413 K, 3.5-11 m MEA (mol fraction x is 0.059-0.165), MEA volatility can be expressed by $\ln(P_{MEA}/x_{MEA}) = 30.0\text{-}8153/T\text{-}2594\alpha^2/T$. At 0.25-0.4 loading, 313-423 K, 4.7-11.3 m PZ (x is 0.078-0.169), PZ volatility can be expressed by $\ln(P_{PZ}/x_{PZ}) = -123+21.6\ln T+20.2\alpha-18174\alpha^2/T$. The enthalpy of vaporization $\Delta H_{vap,MEA}$ and $\Delta H_{vap,PZ}$ have a strong dependence on speciation and free amine concentration in the solution. $\Delta H_{vap,PZ}$ has a larger dependence on CO_2 loading than $\Delta H_{vap,MEA}$ in rich solution because of the more complex speciation/reactions in PZ at rich loading.

The temperature of the DSC specific heat capacity method was extended to 150 ℃ and C_p of 8 m PZ was measured as 3.43-3.81 J/(g·K) at 70-150°C.

3. 1 Review of High T Vapor-liquid Equilibrium Measurements of Aqueous MEA and PZ

3.1.1 Amine-water

The vapor-liquid equilibrium of MEA-H_2O and PZ-H_2O has been studied. Experimental data includes total pressure and amine volatility. For the application to CO_2 capture, amine volatility is needed to estimate the amine in the purified flue gas from the absorber or the condenser of the stripper.

Total pressure measurements are usually performed in a static equilibrium cell. Touhara et al. (1982) studied the total pressure of MEA-H_2O with 0-100% MEA at 25 and 35 ℃ and the total pressure was from 0.065 to 5.623 kPa. Nath and Bender (1983) measured the total pressure of MEA-H_2O with 0-100% MEA at 60, 78, and 91.7 ℃ and the total pressure was from 1.3 to 84.7 kPa. These data can be used in thermodynamic modeling of MEA-CO_2-H_2O.

The most used method for MEA volatility measurement has been an ebulliometer or a similar equilibrium cell. After the system reaches equilibrium, vapor condensate and liquid samples are collected and analyzed by GC or titration. Cai et al. (1996) measured the binary isobaric equilibrium of MEA-H_2O at 101.33 kPa and 66.66 kPa with 0-100% MEA using a modified Rose-Williams still. Park and Lee (1997) measured VLE of MEA-H_2O with 0-100% MEA at 100-170 ℃. Tochigi et al. (1999) measured VLE of MEA-H_2O with 0-100% MEA at 90 ℃ using a modified Rogalski-Malanoski equilibrium still. Kim et al. (2008) used an ebulliometer to measure the VLE of MEA-H_2O at 40-100 ℃ with 0-56% MEA. Chemetron Corporation and Texaco Chemical had MEA volatility data for 10, 20, and 30 wt% MEA at 10-71 ℃ and the curves can be found in Figure 3-20 of *Gas Purification* (Kohl et al. 1997). Hilliard (2008) measured MEA volatility at 40-73 ℃ with 6-30 wt% MEA, using a special FTIR method with vapor phase circulation.

Most of the data above at high temperature are for high MEA concentration except in the work of Kim et al. (2008) and Hilliard (2008).

Less work has been done on PZ-H_2O vapor-liquid equilibrium. Wilson and Wilding (1994) measured total pressure of 0-100% PZ at 113 and 199 ℃. Xia et al. (1997) measured total pressure of 1.99 and 3.97 m PZ at 120 ℃. Hilliard (2008) and

Nguyen et al. (2010) measured PZ volatility in 0.9-10 m PZ at 40-70 ℃ with the same FTIR method as used in MEA-H_2O.

3.1.2 CO_2-amine-water

CO_2 loaded amines have lower amine volatility and higher total pressure than the unloaded amines. Therefore it is more difficult to measure the amine volatility in CO_2 loaded aqueous amines, especially at high temperature and pressure. Hilliard (2008) and Nguyen (2010) measured amine volatility at 40-60 ℃ in CO_2 loaded MEA and PZ using the same FTIR method as used in amine-water systems.

At high temperature, because of the high total pressure and the pressure limit of the FTIR analyzer (1-1.5 atm), vapor circulation between FTIR and the equilibrium cell becomes hard to achieve and new methods need to be developed.

Therefore in this work, a single vapor pass vapor-liquid equilibrium apparatus was set up. Vapor flowed continuously through the solution; the outlet vapor sample was depressurized and analyzed by an FTIR analyzer. MEA-H_2O vapor-liquid equilibrium was measured and compared with literature to validate the method.

3.2 Experimental Methods

3.2.1 Chemicals

Reagent chemicals were used: CO_2 (Clinical Purity, 99.5%, Matheson Tri Gas), MEA (99%, Acros Organics), anhydrous PZ (99%, Acros Organics). DDI water was used for solution preparation. Oil bath fluid: DC 200 fluid 50 CS (Dow Corning).

3.2.2 Solution Preparation

About 550 to 800 mL solution was prepared for each experiment. Amine and DDI water were weighed and combined to achieve the target molality (m). Then the

mixture was agitated by a magnetic stir bar. For PZ, the mixture was heated and stirred on a hot plate to make PZ dissolve. After the solution was clear and well mixed, it was transferred into a glass gas sparging column (for PZ the column was pre-heated) on a scale. CO_2 was sparged into the solution, and the absorbed CO_2 weight was recorded. Details can be found in the Dissertations by Hilliard (2008) and Freeman (2011).

3.2.3 Apparatus

Figure 3-1 shows the dynamic vapor-liquid equilibrium apparatus with a single vapor pass. Two 200 mL (i.d=1.5 in, depth=7 in) and one 600 mL (i.d=2.5 in, depth=8 in) stainless steel vessels (4752 and N4764-T-SS, Parr Instrument Co.) were used as equilibrium cells in series. Each cell has a split ring closure, and the maximum working pressure and temperature are 200 bar and 350 ℃. All of the vessels were submerged in an oil bath (EX-35, Thermo Fisher Scientific) for temperature control. For some experimental runs, one 200 mL and one 600 mL equilibrium cells were used. Data from these runs are presented with superscripts in the results section. Details of the equilibrium cells and the oil bath can be found in Appendix B.1 and B.2.

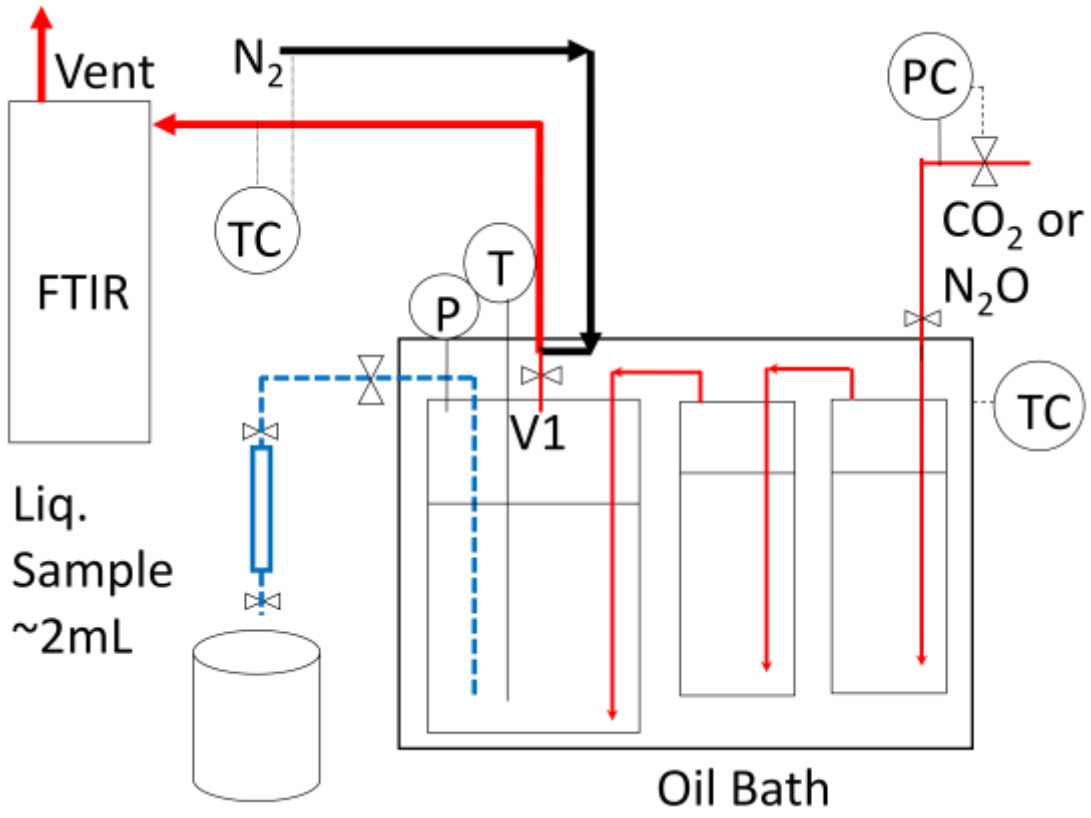

Figure 3-1: Single Vapor Pass VLE Apparatus with an Oil Bath. **Solid red line: vapor pass; dashed blue line: liquid sample pass**

The temperature of the 600 mL cell was measured by a K-type thermocouple and read by an HH506RA data logger from Omega® with 0.1 ℃ precision and the error is within ±0.6°C. A pressure transducer (Druck® PTX 611, 0–30 bar absolute) was connected to an in-house signal converter and data logger NI USB 6009. LabView® SignalExpress® software was used for data recording. The pressure data acquisition system was calibrated by a dead weight pressure tester (S/N 19189/278, by Budenberg Volumetrics, Inc.). The total pressure measurement error is ±2.4 kPa. Calibrations of the pressure transducer and the thermocouple and other details can be found in the Appendix B.3 and B.4.

3.2.4 Procedure

About 170, 170, and 450 mL of the solution was placed into the three cells, respectively. To avoid oxidative degradation, N_2 was used to purge air and then the cells were sealed and submerged under the oil.

In some experimental runs a different volume of solution was used. Figure 3-2 shows the evolution of the HTPVLE apparatus with the oil bath. By sequentially increasing mass transfer the results indicate that adequate mass transfer was achieved with two cells and high liquid level for MEA-H_2O, three cells and high liquid level for MEA-CO_2-H_2O, and two cells and mid liquid level for PZ-CO_2-H_2O.

Figure 3-2: Evolution of HTPVLE Apparatus with Oil Bath

After the temperature stabilized at the target value, the CO_2 feed valve was opened and CO_2 entered the cells. The vapor lines were made of 1/8 inch stainless steel tubes and no special spargers were used. The CO_2 feeding point was less than 0.5 in from the bottom of each cell. CO_2 feed pressure was controlled by the regulator at the cylinder.

After the temperature and pressure stabilized again, a vapor stream was continuously withdrawn from the top of the third cell, with a Swagelok® metering valve (SS-SS4-SL) for flow rate control. This vapor sample stream was 50-250 mL/min at standard pressure and was diluted by about 1.5 SLPM N_2. The N_2 flow and the stream after dilution were maintained at 180 ℃ by a 7 ft heated Teflon® line with temperature control and power supply to the Gasmet™ portable sampling system. The diluted stream was analyzed continuously by an FTIR analyzer (Gasmet™ DX-4000) with

Calcmet® software. The Swagelok® metering valve (SS-SS4-SL) was adjusted to get measurable concentrations in the FTIR.

The FTIR has a 10 meter gas sampling cell held at 180 ℃ with a working pressure of 1-2 bar. It was previously calibrated for measurements of CO_2, N_2O, MEA, PZ, and H_2O. The calibration was performed using a Gasmet calibrator with a syringe pump, a manual needle valve, and a stainless steel injection chamber. The calibration has been described previously in Goff (2005), Hilliard (2008), and Nguyen et al. (2010). Goff (2005) estimated relative expanded uncertainty in the vapor phase concentration to be ±2%. In this work, a few calibration points of MEA and PZ were checked to make sure the calibration sets were still good to use.

After the concentrations in the FTIR were stable, the vapor feeding and sampling valves were closed. The liquid sampling valves were opened quickly to let about 25–50 mL high pressure liquid flush through the 1/8 in stainless steel line, and then closed to trap about 2 mL liquid in the sample bomb. Liquid samples were then cooled to room temperature and analyzed. A cooling pack with frozen materials was applied to the liquid sampling line to reduce flashing when the sampled solution had high CO_2 loading.

For the benchmark experiments to measure MEA volatility in MEA-H_2O, N_2O instead of CO_2 was fed into unloaded aqueous MEA. The temperature for benchmark experiments was 80–140 ℃ with a 10 ℃ interval. The total pressure was controlled at 2 to 4.5 bar. No liquid sample was taken during the experiment, because MEA concentration was almost constant through a run. The reported MEA concentration at each temperature is based on samples before and after each run.

Details of solution charging, starting up, finishing, and cleaning procedures can be found in Appendix B.5.

3.2.5 Liquid Phase Analysis

3.2.5.1 CO_2 Concentration

The concentration of total CO_2 in solution was determined by Total Inorganic Carbon (TIC) analysis. The liquid samples collected through each run were gravimetrically diluted by a factor of 50-100, depending on the expected CO_2 concentration. About 20–30 μL diluted sample was injected into 30 wt% H_3PO_4 in the TIC column to release CO_2, and a continuous N_2 flow carried the CO_2 into an IR analyzer (Model 525, Horiba PIR 2000). PicoLog® software was used to record the voltage signal from the IR analyzer. In order to get a correlation curve between the voltage peak areas and carbon mass fraction, a series of calibration points were carried out at the end of each analysis by injecting known amounts of inorganic carbon standard (1000 ppm carbon, Ricca Chemical Company, Arlington, TX). Details can be found in Hilliard (2008) and Freeman (2011).

3.2.5.2 Amine Concentration

The total alkalinity of each liquid sample was determined by titration using a Metrohm-Peak 835 Titrando equipped with an automatic dispenser, Metrohm-Peak 801 stirrer, and 3 M KCl pH probe. 120-300X dilution of the sample was titrated with 0.1 N H_2SO_4 to pH 2.4. Details are available in Appendix A.3 of Hilliard (2008) and Appendix F of Sexton (2008).

3.2.6 Partial Pressure Calculation

The vapor compositions in the diluted stream were analyzed by FTIR and these were converted into concentrations in the vapor phase inside the equilibrium cell:

$$y_i = \frac{y'_i}{y'_{H_2O} + y'_{amine} + y'_{CO_2} + y'_{N_2O}} \tag{3-1}$$

y_i - mole fraction of component i in vapor

y'_i - mole fraction of component i in diluted gas.

i is water, amine, CO_2 or N_2O.

The partial pressure of each component was calculated from concentrations and total pressure using Equation 3-2:

$$P_i = P_t \cdot y_i \tag{3-2}$$

P_t - total pressure, Pa.

P_i - partial pressure of i, Pa.

i is water, amine, CO_2 or N_2O.

3.3 RESULTS

3.3.1 Benchmark – MEA Volatility in MEA-H_2O

Table 3-1 gives results for MEA volatility in MEA-H_2O.

Table 3-1: MEA Volatility in MEA-H_2O at High Temperature

2 eq. cells, high liq. level*					3 eq. cells, high liq. level				
T	**MEA**	**P_{MEA}**	**P_{H2O}**	**P_t**	**T**	**MEA**	**P_{MEA}**	**P_{H2O}**	**P_t**
℃	**m**	**Pa**	**kPa**	**kPa**	**℃**	**m**	**Pa**	**kPa**	**kPa**
99.4	6.91	434	95	95	80.5	6.89	153	44	44
120.2	6.94	1305	183	184	100.4	6.88	437	93	93
120.2	6.97	1345	207	208	120.3	6.87	1421	202	203
130.1	7.00	2085	261	263	130.1	6.86	2090	272	274
					140.2	6.86	2914	362	365

*: 2 equilibrium cells were used; filled with 170 and 450 mL solution, respectively.

Figure 3-3 compares normalized MEA volatility in 3.5-11 m MEA-H_2O from this work and literature. The literature data are comparable to these results. Hilliard's data (2008) at low temperature (<45 ℃) are not consistent with other literature and give a different slope. Simulated MEA volatility by the Hilliard Aspen Plus® MEA Model (2008) generally predicts the data from this work.

Normalized MEA volatility did not undergo any obvious change when a third cell was added with a high liquid level. Therefore we can conclude that adequate mass transfer has been obtained with two equilibrium cells, with high liquid level, for the MEA-H_2O system.

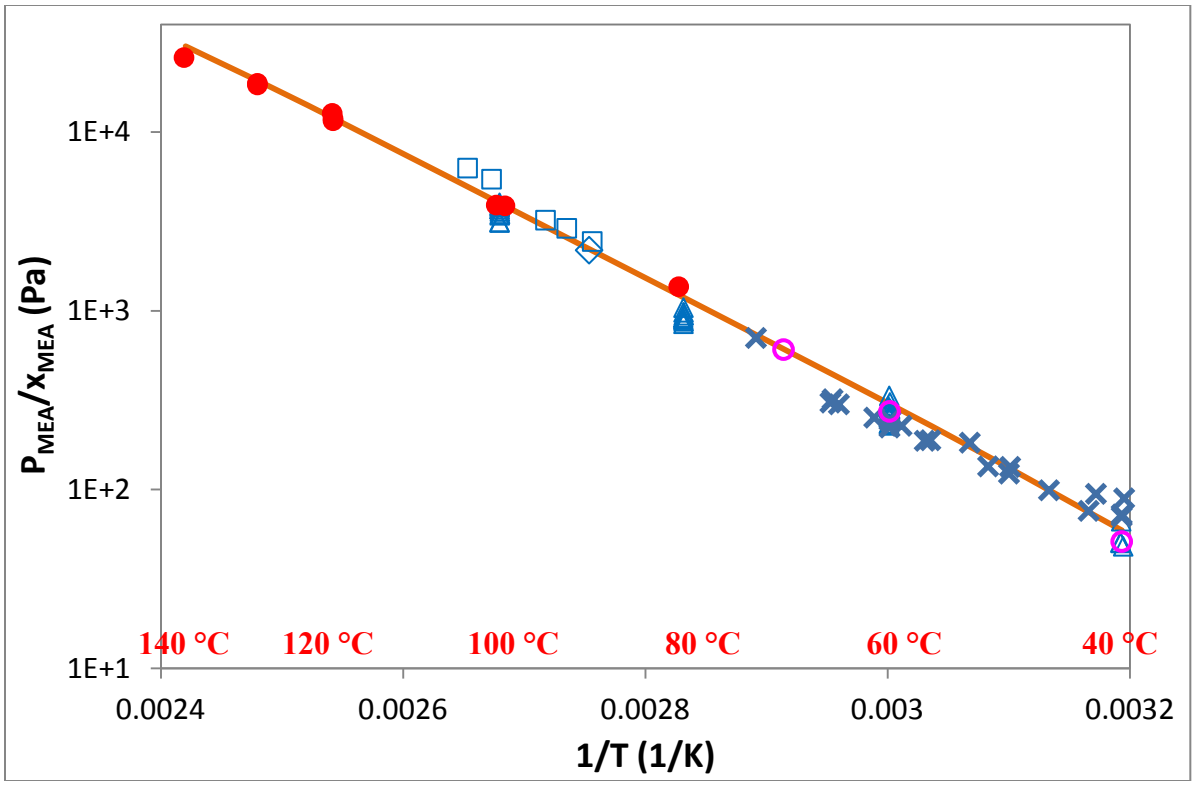

Figure 3-3: Comparison of Normalized MEA Volatility in 3.5-11 m MEA-H_2O. □: Cai et al. (1996); ○: Figure 3-20, *Gas Purification* (Kohl et al., 1997); ◊: Tochigi et al. (1999); Δ: Kim et al. (2008); X: Hilliard (2008); ●: this work; line: Aspen Plus® Hilliard Model - 7 m MEA (2008); $x_{MEA} = \frac{\text{mol of MEA}}{\text{mol of MEA+mol of } H_2O}$.

Figures 3-4 and 3-5 presented the ratio of measured P_{MEA} to simulated P_{MEA} using the Hilliard Aspen Plus® MEA model (2008). Figure 3-4 shows that the low temperature Hilliard's data below 45°C are further off the model. At low temperature (<55°C), Hilliard's measured P_{MEA} is larger than simulated P_{MEA}, while above 55 ℃,

Hilliard's measured P_{MEA} is smaller than simulated P_{MEA}. Most of Kim's data are smaller than the simulated P_{MEA} and some of the 60 ℃ data are further off. Data from the other literature and from this work are predicted by the model. Figure 3-5 shows that one series of Kim's data, which is at 60°C by comparing with Figure 3-4, has a trend to decrease as MEA concentration increases. For data from the other literature and this work, there is no obvious error associated with MEA concentration, when MEA varies from 3.5 to 11 m.

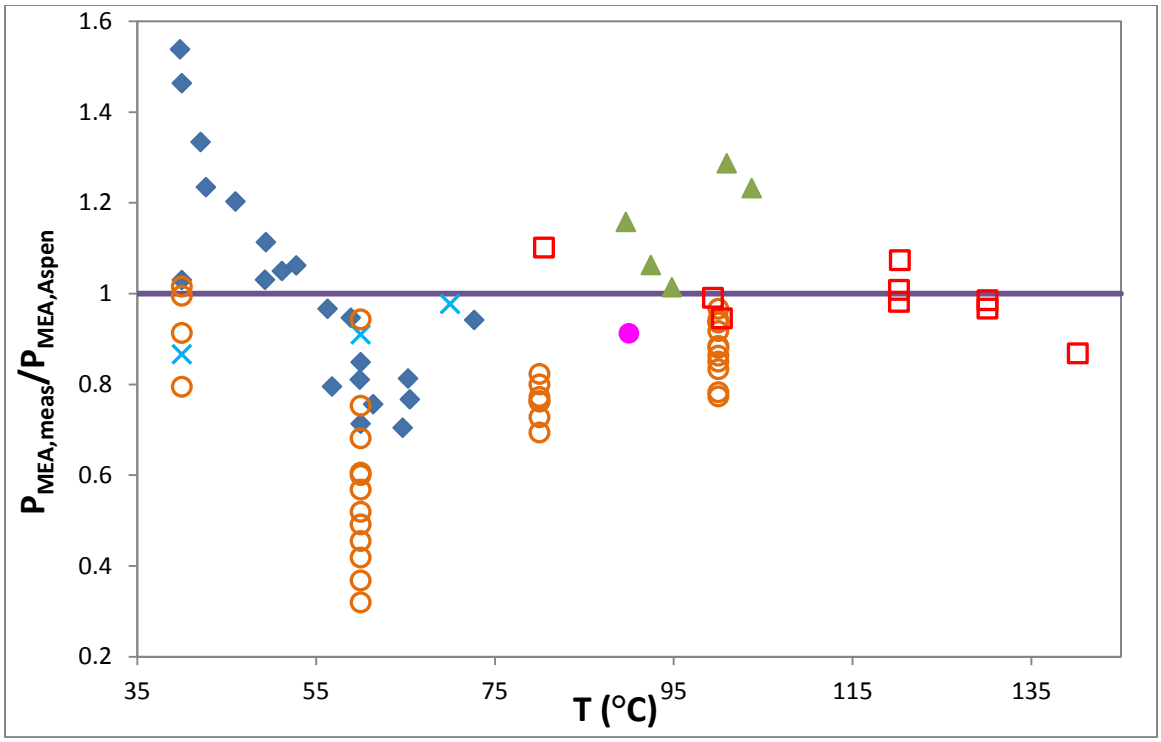

Figure 3-4: Temperature Dependence of $P_{MEA,meas}/P_{MEA,Aspen}$ in 3.5-11 m MEA.
$P_{MEA,meas}$ are experimental data and $P_{MEA,Aspen}$ are by Hilliard Aspen Plus® MEA model; ▲: Cai et al. (1996); X: Figure 3-20, *Gas Purification* (Kohl et al., 1997); ●: Tochigi et al. (1999); ○: Kim et al. (2008); ♦: Hilliard (2008); □: this work.

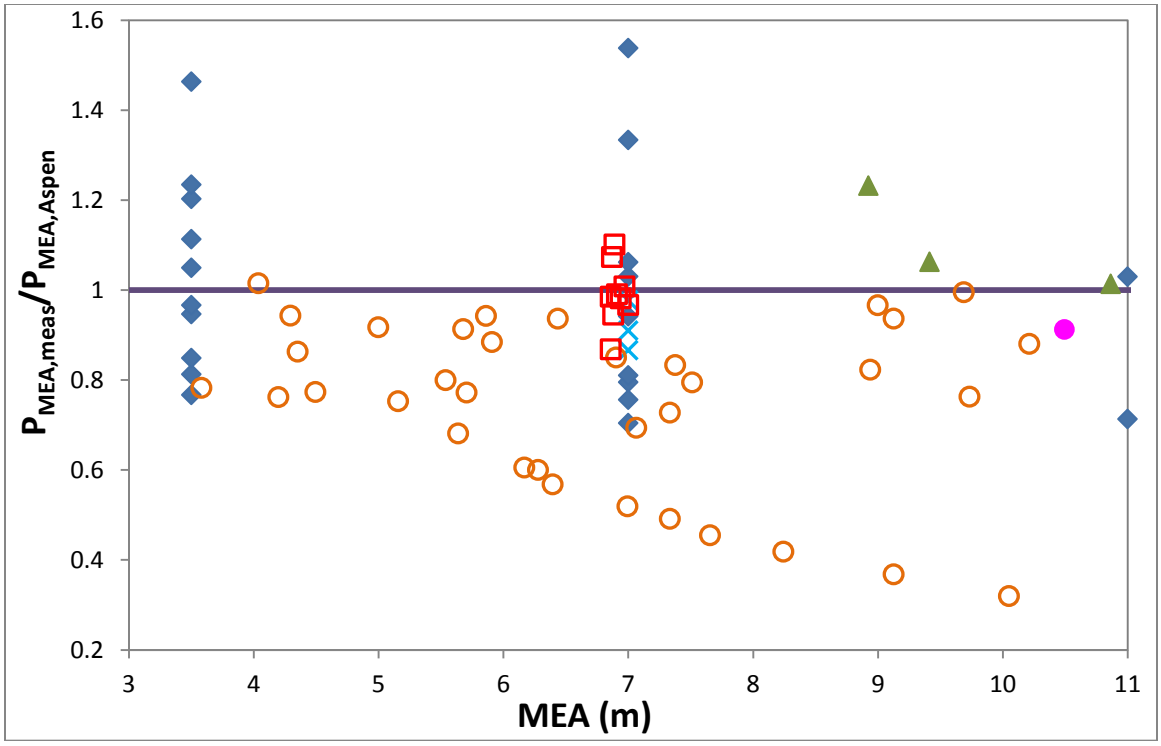

Figure 3-5: MEA Concentration Dependence of $P_{MEA,meas}/P_{MEA,Aspen}$ in MEA-H_2O, 40-140°C. **$P_{MEA,meas}$ are experimental data and $P_{MEA,Aspen}$ are by Hilliard Aspen Plus® MEA model; ▲: Cai et al. (1996); X: Figure 3-20, *Gas Purification* (Kohl et al., 1997); ●: Tochigi et al. (1999); ○: Kim et al. (2008); ♦: Hilliard (2008); □: this work.**

Figure 3-6 gives MEA volatility in 7 m solution. New data at 80 to 140 ℃ are comparable with literature data and are predicted by the Aspen Plus® Hilliard MEA Model (2008). Hilliard's data at 40 to 45°C are not consistent.

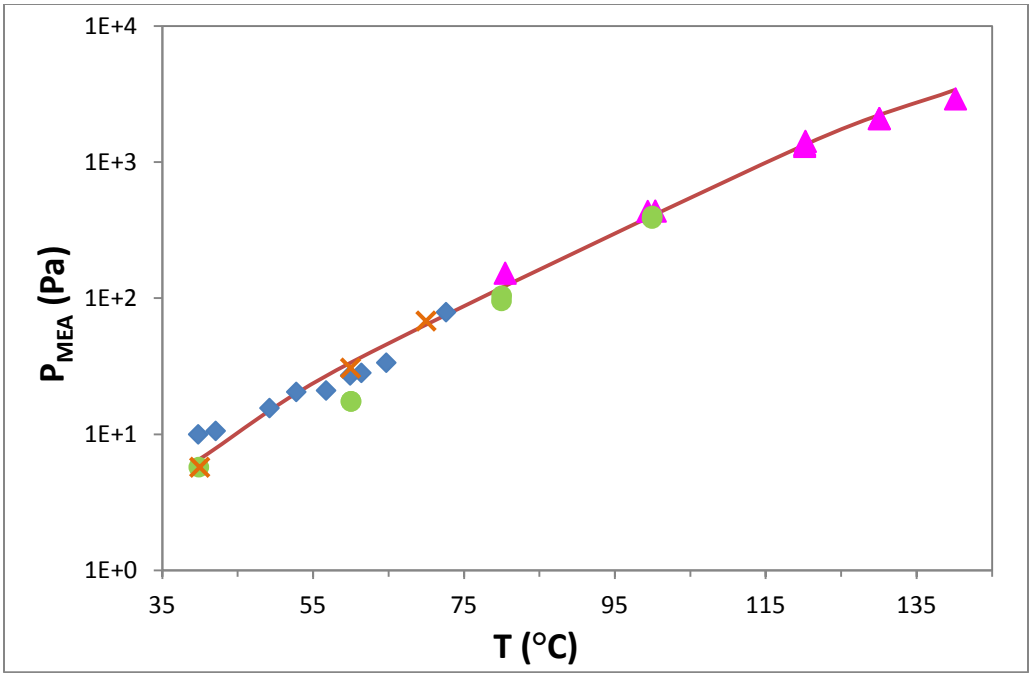

Figure 3-6: MEA Volatility in 7 m MEA. **X: Figure 3-20, Gas Purification (Kohl et al., 1997); ♦: Hilliard (2008); ●: Kim et al. (2008); ▲: this work; line: Aspen Plus® Hilliard Model – 7 m MEA (2008)**

3.3.2 MEA Volatility in MEA-CO_2-H_2O

Table 3-2 gives MEA volatility in CO_2 loaded MEA. Experiments were conducted with various CO_2 loading at 120 and 140 ℃. P_{MEA} and P_{CO2} are from vapor phase measurement. CO_2 loading (mol/mol MEA) was calculated from the empirical model of P_{CO2} in Chapter 2 (Table 2-10) using the measured T and P_{CO2}. The loading from liquid analysis was not used because of the non-systematic error with it. The analyzed loading is different from the calculated loading using the CO_2 partial pressure empirical models, and the difference does not depend on CO_2 loading or temperature. Higher pressure may result in a bigger difference, but this trend is not obvious either. This error probably comes from liquid sampling, where the pressure decreased fast from about 2-25 atm to 1 atm. Therefore, the liquid tended to flash when it flushed through the sampling line, and the composition of the liquid sample trapped in the bomb may be

different from that of the liquid phase in the equilibrium cell. Attaching a frozen pad to the liquid sampling line helped to reduce the flash, however, since the flow rate of liquid sampling was large, some of CO_2 still flashed out of the liquid. MEA concentration reported in Table 3-2 was from liquid phase analysis, assuming the flashing of MEA and water is much less than that of CO_2, making small changes in the MEA concentration.

Table 3-2: MEA Volatility in MEA-CO_2-H_2O

T	MEA	Loading*	P_{MEA}	P_{CO2}	P_{H2O}	P_t
℃	m		Pa	kPa	kPa	kPa
119.9	6.90	0.324	573	43	155	199
119.9	6.87	0.351	642	62	167	230
120.3	6.82	0.489	223	454	180	634
139.9	6.81	0.222	1627	49	326	376
140.0	6.63	0.367	1389	263	314	578
139.9	6.57	0.469	718	969	316	1286
140.3	6.86	0.467	795	966	317	1283
140.2	6.90	0.389	1110	352	324	677
120.4	7.00	0.361	610	73	169	243

*: CO_2 loading (mol/mol MEA) was calculated from the empirical model of P_{CO2} in Chapter 2 (Table 2-1) using the measured T and P_{CO2}.

The MEA volatility from this work in MEA-H_2O and MEA-CO_2-H_2O is regressed along with 50-73°C data from Hilliard (2008). Hilliard's data at lower temperature (<50 ℃) were not included because they are not consistent with other literature. Equation 3-3 is the empirical model.

$$\ln\left(\frac{P_{MEA}}{x_{MEA}}\right) = (30.0 \pm 0.3) + (-8153 \pm 96)\frac{1}{T} + (-2594 \pm 81)\frac{\alpha^2}{T} \qquad (3\text{-}3)$$

$$R^2 = 0.994$$

Using this correlation, for 7 m MEA with 0.2 and 0.5 CO_2 loading, the partial pressure of MEA is 923 and 231 Pa at 120 ℃, and 2552 and 683 Pa at 140 ℃.

Figure 3-7 compares normalized MEA volatility from this work and Hilliard data (2008) at 40 and 60 ℃. The volatility decreases with CO_2 loading, because amine reacts with CO_2 and there is less free amine in the solution as the loading increases. The Hilliard Aspen Plus® model (2008) over-predicts high temperature data at high CO_2 loading. The empirical model of Equation 3-3 fairly predicts the 60-140 ℃ data. The 40^o data from Hilliard were not regressed and are not represented by the empirical model. They do not seem to be consistent with the other data. Figure 3-8 gives the same data sets as in Figure 3-7, but uses P_{CO2} as the horizontal axis instead of CO_2 loading.

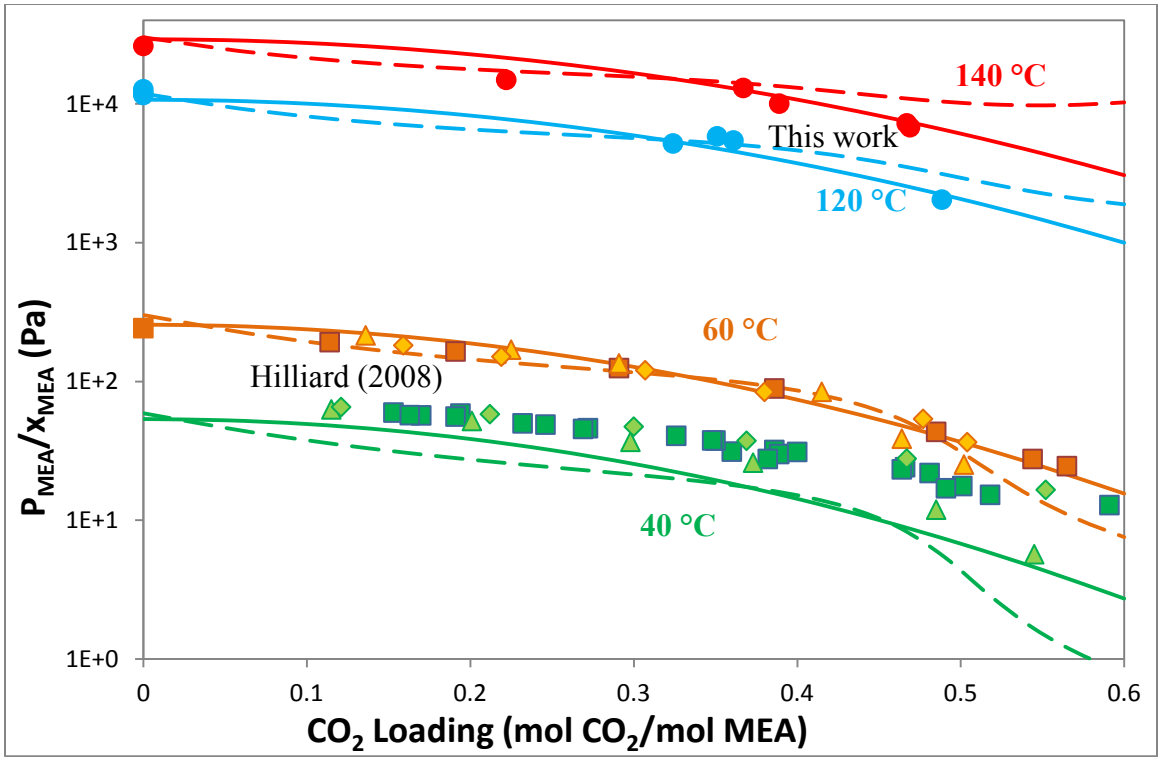

Figure 3-7: Comparison of Normalized MEA Volatility in 3.5-11 m MEA. Hilliard (2008) MEA: ♦ 3.5 m, ■ 7 m, ▲ 11 m; ●: this work; solid lines: empirical model of Eq. 3-3; dashed lines: Aspen Plus® Hilliard Model – 7 m MEA (2008). $x_{MEA} = \frac{\text{mol of total MEA}}{\text{mol of total MEA + mol of } H_2O}$.

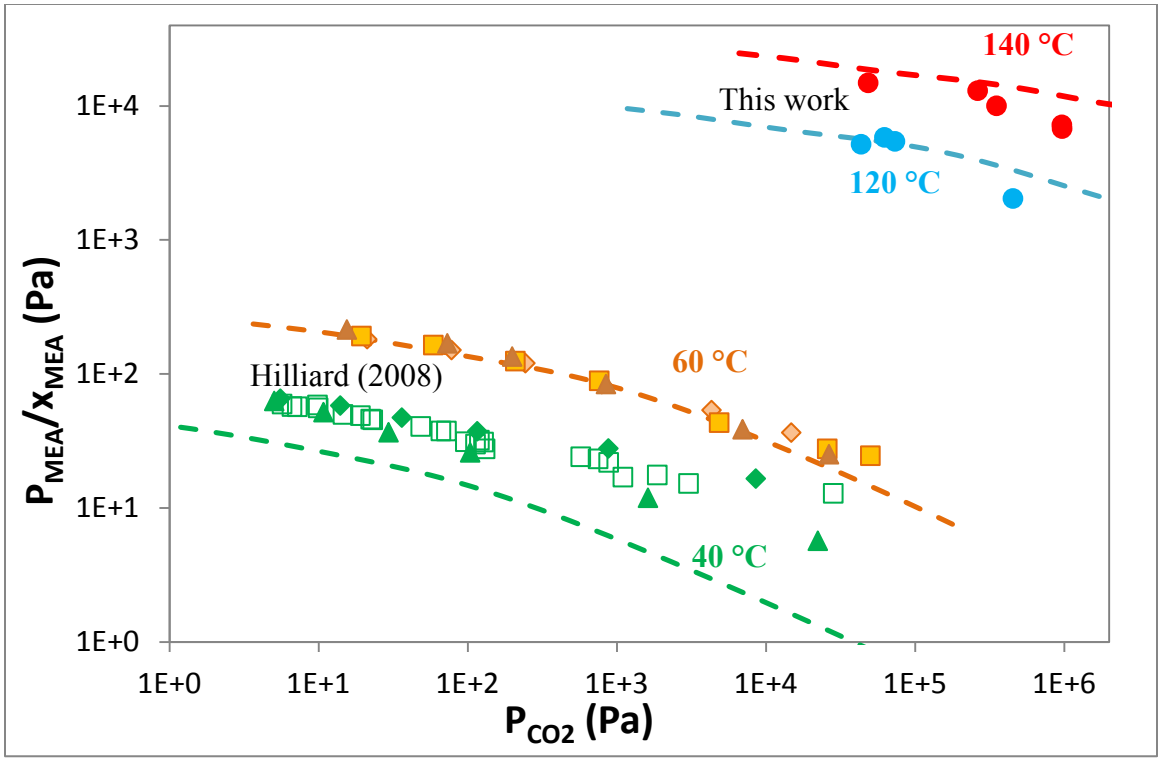

Figure 3-8: Comparison of Normalized MEA Volatility in 3.5-11 m MEA (2).
Hilliard (2008) MEA: ♦ 3.5 m, □ 7 m, ▲ 11 m; ●: this work; dashed lines: Aspen Plus® Hilliard Model – 7 m MEA (2008). $x_{MEA} = \frac{\text{mol of total MEA}}{\text{mol of total MEA + mol of } H_2O}$.

3.3.3 PZ Volatility in PZ-CO_2-H_2O

Table 3-3 gives PZ volatility in CO_2 loaded PZ. Experiments were conducted with various CO_2 loading at 120 and 150 ℃. P_{PZ} and P_{CO2} are from vapor phase measurement. As in the MEA-CO_2-H_2O system, CO_2 loading (mol/equiv. PZ) was calculated from the P_{CO2} and T with the empirical model, the equation in Table 2-10 in Chapter 2.

Table 3-3: PZ Volatility in PZ-CO_2-H_2O

T	PZ	Loading ***	P_{PZ}	P_{CO2}	P_{H2O}	P_t	T	PZ	Loading ***	P_{PZ}	P_{CO2}	P_{H2O}	P_t
℃	m		Pa	kPa	kPa	kPa	℃	m		Pa	kPa	kPa	kPa
120.0	7.74	0.391*	106	535	161	696	149.4	8.29	0.267*	2851	309	395	707
119.5	8.17	0.291*	482	91	166	257	149.8	5.91	0.391*	840	2051	493	2545
119.8	8.08	0.391*	191	528	163	691	149.7	6.11	0.239*	2078	212	419	633
118.6	8.70	0.302*	523	104	154	259	149.0	6.11	0.258*	2042	268	406	675
120.1	6.14	0.391*	130	530	178	708	149.8	4.73	0.389*	615	2004	519	2523
119.6	6.48	0.289*	338	89	170	259	149.7	4.91	0.243*	1742	223	428	653
120.1	4.89	0.391*	67	532	183	715	150.0	9.54	0.392*	1261	2112	443	2557
119.8	5.08	0.280*	232	77	179	256	149.4	10.21	0.259*	4533	275	403	683
120.4	9.86	0.397*	139	599	159	759	149.0	10.75	0.398**	1623	2234	444	2679
120.6	10.40	0.396**	142	599	158	757	148.6	11.30	0.273**	4720	324	356	685
119.3	10.65	0.305**	554	113	150	264	149.0	7.50	0.320	1730	667	381	1049
120.2	7.81	0.385	169	485	160	645	149.0	7.69	0.305	1820	533	372	907
120.3	8.02	0.327	228	174	171	344	149.2	7.80	0.278	2859	363	382	748
120.4	7.72	0.392	80	552	156	709	149.0	7.83	0.253	3617	250	363	617
120.0	7.69	0.325	176	166	158	325	149.9	7.65	0.393	1188	2140	452	2593
149.7	8.22	0.391*	1269	2064	478	2543	149.8	7.75	0.369	1459	1452	417	1871
149.5	8.76	0.261*	3139	287	397	687	149.8	7.86	0.295	2879	474	367	844
149.9	7.66	0.390*	1164	2033	474	2508	149.5	7.92	0.249	3397	242	377	623

*: 2 equilibrium cells were used, filled with 100 and 300 mL solution; **: 2 equilibrium cells were used, filled with 170 and 450 mL solution; ***: loading = mol CO_2/equivalent PZ, estimated from T and P_{CO2} using the equation in Table 2-1 in Chapter 2.

The PZ volatility from this work was regressed along with 40-65℃ data by Nguyen et al. (2010). Equation 3-4 is the empirical model.

$$\ln(\frac{P_{PZ}}{x_{PZ}}) = (-123 \pm 3) + (21.6 \pm 0.6)\ln T + (20.2 \pm 3.5)\alpha + (-18174 \pm 1933)\frac{\alpha^2}{T} \quad (3\text{-}4)$$

$$R^2 = 0.996$$

Using this correlation, for 8 m PZ with 0.3 and 0.4 CO_2 loading, P_{PZ} is 398 and 119 Pa at 120℃, and 2622 and 982 Pa at 150℃.

Figure 3-9 compares normalized PZ volatility from this work and Nguyen et al. data (2010) at 40 and 60℃. The volatility decreases with CO_2 loading, because amine

reacts with CO_2 and there is less free amine in the solution as the loading increases. The empirical model of Equation 3-4 and Aspen Plus® Fawkes Model (Frailie et al., 2010) fairly predict 40-150 ℃ data. Figure 3-10 gives the same data sets as in Figure 3-9, but uses P_{CO2} as the horizontal axis instead of CO_2 loading.

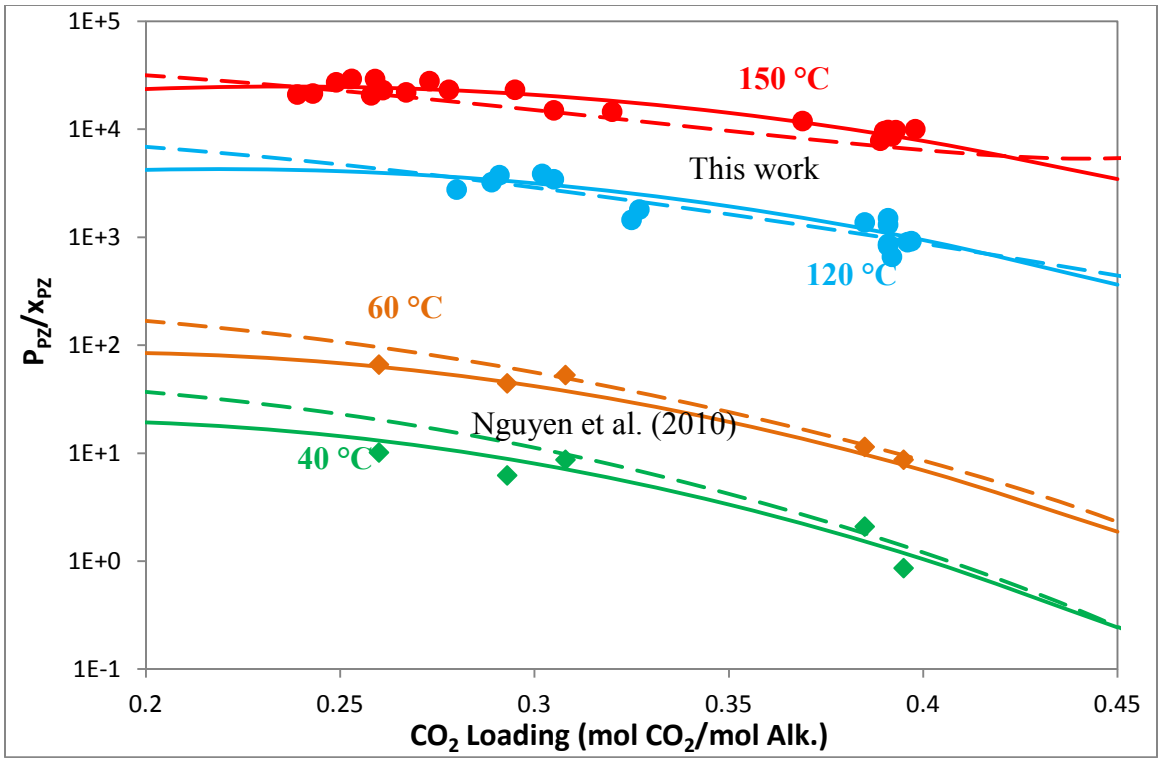

Figure 3-9: Comparison of Normalized PZ Volatility in CO_2 loaded 4.7-11.3 m PZ.
♦ Nguyen et al. (2010); ●: this work; solid lines: empirical model of Eq. 3-4; dashed lines: Aspen Plus® Fawkes Model – 8 m PZ (Frailie et al., 2010).
$$x_{PZ} = \frac{\text{mol of total PZ}}{\text{mol of total PZ + mol of } H_2O}.$$

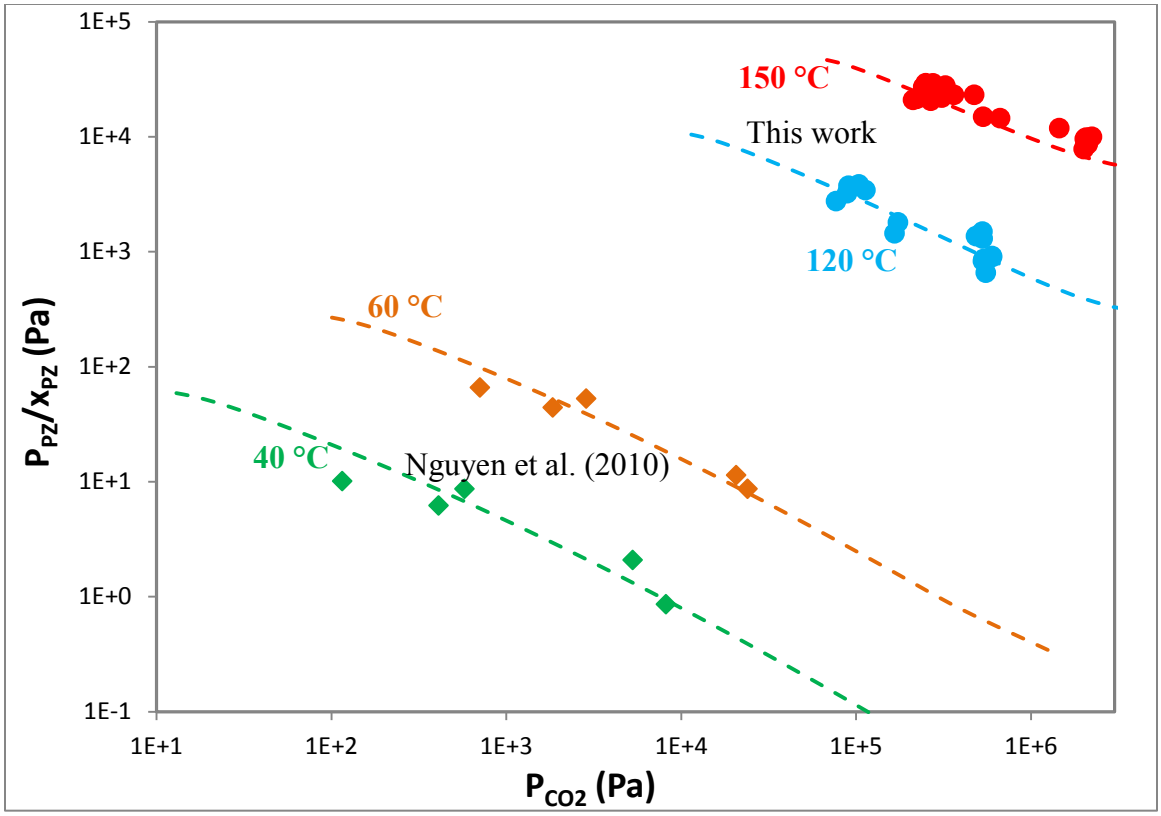

Figure 3-10: Comparison of Normalized PZ Volatility in CO_2 loaded 4.7-11.3 m PZ (2). ♦ Nguyen et al. (2010); ●: this work; dashed lines: Aspen Plus® Fawkes Model – 8 m PZ (Frailie et al., 2010). $x_{PZ} = \frac{\text{mol of total PZ}}{\text{mol of total PZ + mol of } H_2O}$.

3.3.4 Enthalpy of Vaporization

According to Equation XVIII.9 in Lewis and Randall (1923) and Equation IV.109 in Dodge (1944), the apparent enthalpy of vaporization of MEA and PZ was derived from empirical models Eq. 3-3 and 3-4, respectively.

$$\left(\frac{\partial ln f_1}{\partial T}\right)_{P,N} = \frac{H_1^* - \bar{H}_1}{RT^2}$$ Equation (XVIII.9), Lewis and Randall (1923)

Where f_1 is the fugacity of the constituent 1, $H_1^* - \bar{H}_1$ is the heat absorbed per mol when a small quantity of the constituent X_1 evaporates from the solution into a vacuum.

$$\frac{\partial ln \bar{f}_i}{\partial T} = -\frac{\bar{H}_i - \bar{H}_i^o}{RT^2}$$ Equation (IV.109), Dodge (1944)

Where $\bar{f}_i$ is the fugacity of the constituent i, $-(\bar{H}_i - \bar{H}_i^o)$ is the heat absorbed per mol when a small quantity of the constituent X_i evaporates from the solution into a vacuum.

Figure 3-11 presents the apparent enthalpy of vaporization of MEA and PZ predicted by Eq. 3-5 and 3-6, and $-\Delta H_{vap}$ from Aspen Plus® prediction by Hilliard MEA model (2008) and Fawkes model (Frailie et al., 2010).

$$\Delta H_{vap,MEA} = -R\frac{\partial \ln P_{MEA}}{\partial \frac{1}{T}} = -R*(-8153 - 2594\alpha^2) \quad (3\text{-}5)$$

$$\Delta H_{vap,PZ} = -R\frac{\partial \ln P_{PZ}}{\partial \frac{1}{T}} = -R*(-21.6T - 18174\alpha^2) \quad (3\text{-}6)$$

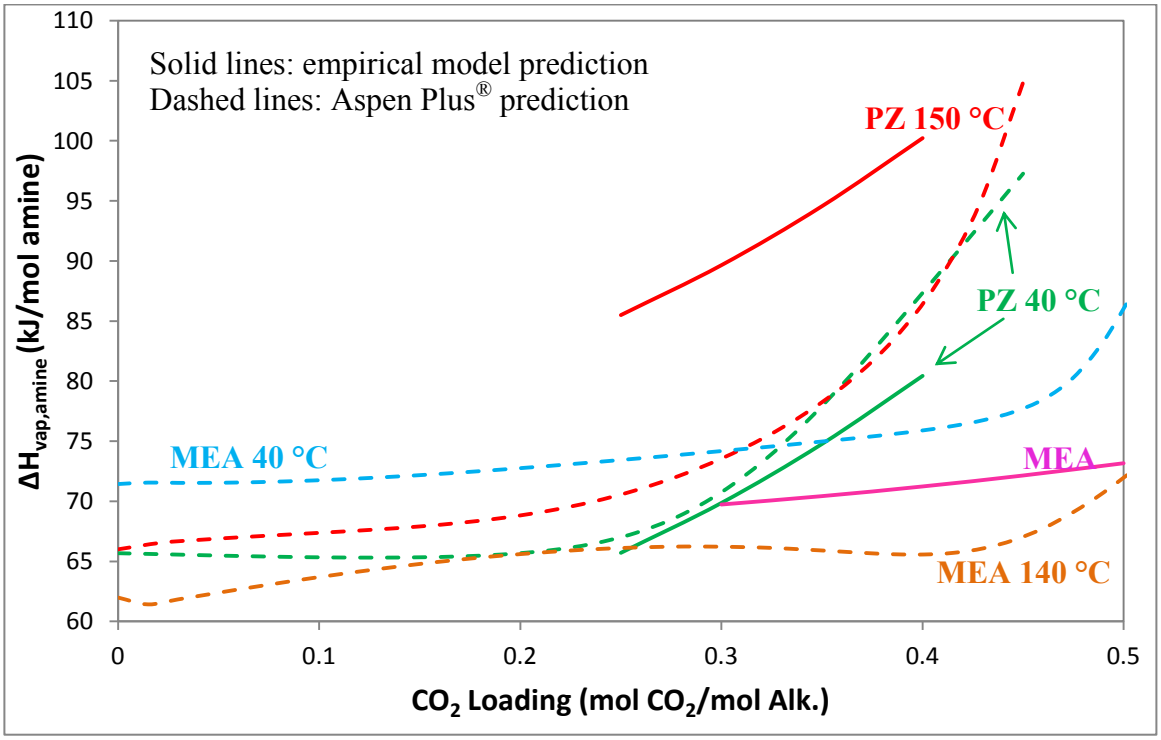

Figure 3-11: Enthalpy of Vaporization of 7 MEA and 8 mPZ. **Aspen Plus® Hilliard MEA model (2008) and Fawkes PZ model (Frailie et al., 2010) were used.**

$-\Delta H_{vap,MEA}$ does not depend on temperature, and is nearly constant over 0-0.45 CO_2 loading. $-\Delta H_{vap,PZ}$ is nearly constant below 0.25 loading, and beyond that point it increases as CO_2 loading increases. This may be because the reactions and speciation in PZ-CO_2-H_2O are more complex than that in MEA-CO_2-H_2O.

Over the practical range of CO_2 loading, there is always a significant concentration of free MEA. Therefore the heat of MEA absorption is essentially constant and corresponds to its value in MEA/H_2O.

Figure 3-12 shows the reaction stoichiometry for 8 m PZ at 40 ℃ using the Aspen Plus® Fawkes model (Frailie et al., 2010). It shows the mole change of different species when 1 mol PZ was absorbed into the solution. Figure 3-12 indicates the reactions taking place at different loading. At very lean loading (<0.1), there is significant free PZ, so its heat of vaporization is nearly constant. The stoichiometry of absorbing PZ is given by:

$$PZ(g) = PZ(aq) \quad (3\text{-}7)$$

As loading increases, more reactions take place. Starting from about 0.12 loading, the main apparent stoichiometry is:

$$PZ + HPZCOO \leftrightarrow PZH^+ + PZCOO^- \quad (3\text{-}8)$$

As CO_2 loading increases, according to Figure 3-12, one mole of HCO_3^- decrease corresponds to one mole increase in H_2O, and $PZCOO^-$ forms more than PZH^+. Therefore besides reaction 3-8, PZ starts to react with bicarbonate and $PZ(COO^-)_2$:

$$PZ + HCO_3^- \leftrightarrow H_2O + PZCOO^- \quad (3\text{-}9)$$

$$PZ + PZ(COO^-)_2 \leftrightarrow 2PZCOO^- \quad (3\text{-}10)$$

At the expected rich loading of 0.4 mol CO_2/equiv PZ and higher loading, in Figure 3-12, one mole of HCO_3^- decrease corresponds to one mole increase in H_2O and

$PZ(COO^-)_2$; $PZCOO^-$ generation is less than PZH^+. Thus besides reaction 3-8, another reaction is:

$$PZ + HPZCOO + HCO_3^- \leftrightarrow PZH^+ + H_2O + PZ(COO^-)_2 \quad (3\text{-}11)$$

Therefore the enthalpy of PZ absorption will be a function of CO_2 loading. These reactions have different temperature dependence and the changes in reactions and speciation contribute to temperature and loading effects on $-\Delta H_{vap,PZ}$.

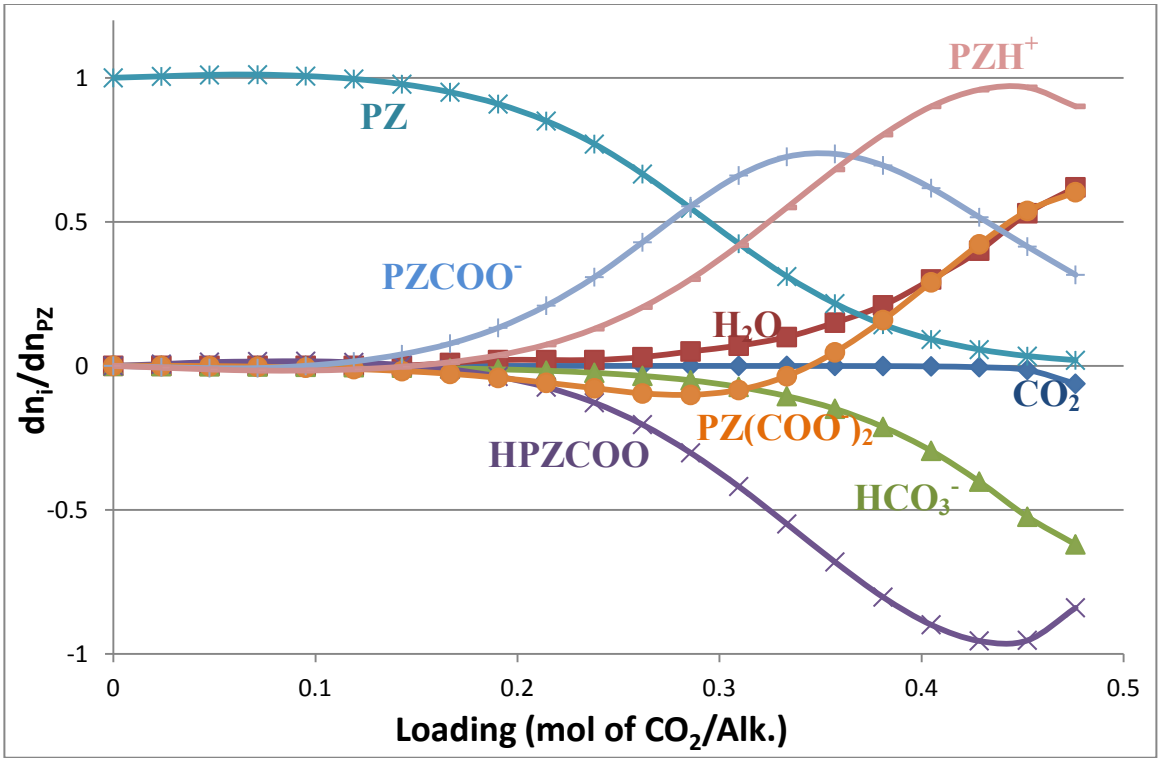

Figure 3-12: Reaction Stoichiometry for 8 m PZ at 40°C with Aspen Plus® Fawkes Model

3.4 SPECIFIC HEAT CAPACITY OF PZ-H_2O

3.4.1 Introduction

Specific heat capacity (C_p) can be used to calculate the temperature dependence of ΔH and in building the rigorous thermodynamic models. A differential scanning calorimetry (DSC) method has been previously used in the Rochelle group by Hilliard (2008) and Nguyen (Rochelle et al., 2009) for C_p measurements at 40-120°C with 3.5 and 7 m MEA-H_2O, 2 and 3.6 m PZ-H_2O, and 8-12 m PZ-CO_2-H_2O. Tables 1-6 and 1-7 give a brief literature review on specific heat capacity measurement for MEA and PZ solution.

In this work the DSC method was modified to measure C_p of 8 m PZ up to 150°C. Because of PZ solubility limits, the lower bound of temperature in this work is 70°C instead of 40°C. The higher bound is extended from 120 to 150 ℃ because in CO_2 capture process with concentrated PZ, the stripper temperature can be elevated up to 150°C. C_p of PZ-CO_2-H_2O cannot be measured at 150°C because the high total pressure exceeds the limit of the sample cells for the DSC, so C_p of unloaded 8 m PZ was measured in this work.

3.4.2 Experimental Method

This DSC method has been previously described in Hilliard (2008). It follows the ASTM E 1269-05 standard test method for determining specific heat capacity by DSC. Therefore the method will be briefly described here.

3.4.2.1 Sample Preparation

60 μL stainless steel sample pans with o-rings and lids from Perkin Elmer (#03190218) were used. PZ and DDI water were weighed and mixed to obtain the target concentration. Then the mixture was heated and stirred on a hot plate to make PZ

dissolve. After the solution got clear, an Eppendorf® pipette was used to transfer about 59.5 μL solution to the sample pan. To avoid precipitation of PZ solution in a cool pipette tip, part of the pipette tip was submerged in the heated PZ solution for a while. Then the 60 μL solution was carefully filled into the sample pan. An o-ring was placed inside the lid for sealing, and the sample pan and lid were joined together by a Perkin Elmer Quick Press (#0990-8467). All cells were sealed before going into the DSC. Figure 3-13 shows a cross view of a sample cell after sealing.

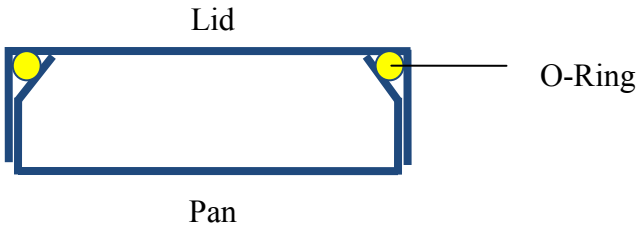

Figure 3-13: Cross View of a Sample Cell for the DSC Heat Capacity Method

3.4.2.2 Procedure

A DSC-Q100 calorimeter with a thermal analysis controller from TA Instruments was used. The equipment is located and maintained in the laboratory of Dr. Freeman's research group, the Department of Chemical Engineering at The University of Texas at Austin.

In each run, a cell containing the sample and a sealed empty reference cell were placed on the sample platforms inside the chamber of the DSC, and the heat flows to the two cells were measured. To obtain accurate results, before running the solution samples, a series of calibration runs with an empty cell, an indium sample, and an Al_2O_3 sample was performed to get the heat flow baseline, the cell constant, temperature calibration, and the sensitivity constant. The baseline was then subtracted from each sample heat profile using TA Analysis software.

The DSC program of this experiment was set up as: heat up and hold at 80°C for 5 min, cool down to 60°C and hold for 10 min, ramp the temperature up at 5°C/min to 155°C, then cool down to 40°C at the rate of 20°C/min. The heat flow from 60 to 155°C was recorded and used to get the C_p at each temperature. TA Instruments Universal Analysis 2000 was the software for analyzing the raw heat flow data.

For the 8 m PZ sample, three runs were carried out to determine the specific heat capacity.

3.4.3 Results

Table 3-4 presents the result from the specific heat capacity measurements. Figure 3-14 compares the measured C_p of 8 m PZ from this work with literature.

Table 3-4: Specific Heat Capacity of 8 m PZ

T	C_p	T	C_p	T	C_p
°C	(J/g*K)	°C	(J/g*K)	°C	(J/g*K)
70	3.43	100	3.58	130	3.71
75	3.47	105	3.60	135	3.73
80	3.49	110	3.63	140	3.76
85	3.52	115	3.65	145	3.78
90	3.54	120	3.67	150	3.81
95	3.56	125	3.69		

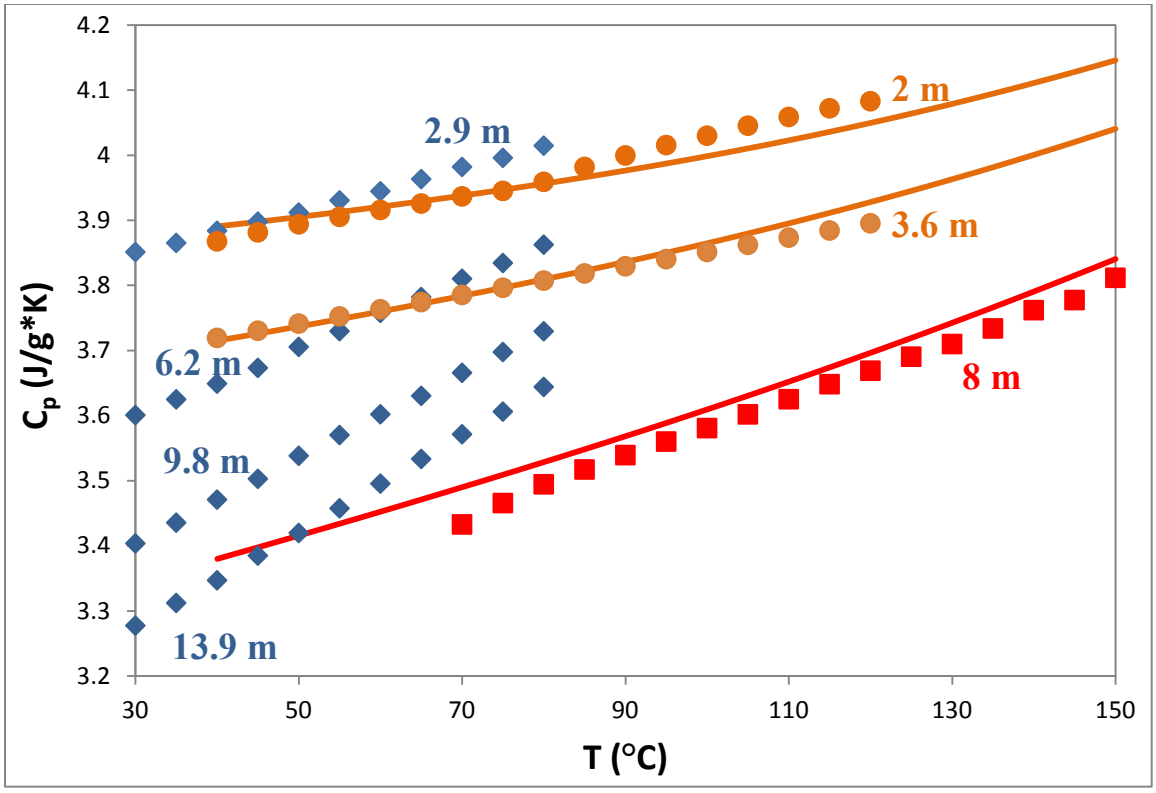

Figure 3-14: Comparison of Specific Heat Capacity of PZ-H_2O. ●: Hilliard (2008) 2 and 3.6 m PZ; ♦: Chen et al. (2010) 2.9, 6.2, 9.8, 13.9 m PZ; ■: this work 8 m PZ; solid lines: Aspen Plus® Fawkes Model 2, 3.6, 8 m PZ.

Data from Hilliard (2008) and this work have similar temperature dependence at different PZ concentration. Aspen Plus® Fawkes model generally predicts these UT data. C_p by Chen et al. (2010) has stronger temperature dependence and is higher than the UT data at the same PZ concentration. There may be some systematic error of either source of the data. Chen et al. mentioned that the PZ concentration was chosen as smaller or equal to 0.2 mol fraction (2.9-13.9 m) because of the PZ solubility limit, but according to Freeman's research (2011), at 30°C PZ is not soluble at 6.2-13.9 m concentration, and 2.9 m is on the limit of solid-liquid transition.

A small amount of water may vaporize as the temperature increases but the heat capacity measurements assume no vaporization. The water heat of vaporization was

counted in the total heat flow, thus the reported specific heat capacity of the solution may be higher than the true value. However this error can be neglected according to the following calculation.

Assume 10% of the sample cell volume is occupied by water vapor at 150°C, which is larger than the expected vapor volume. According to DIPPR (1998-Provo, BYU) water vapor pressure at 145 and 150°C is 414760 and 475090 Pa, respectively. Therefore the water in the vapor space is $60\mu L \cdot 10\% \cdot \frac{1m^3}{1e9^{\mu L}/_{m^3}} \cdot P_{H2O}(Pa)/8.314(\frac{J}{K.mol})/T(K)$, which is 7.158E-7 and 8.103E-7 mol at 145 and 150°C, respectively. Therefore, when the sample was heated from 145 to 150°C, (8.103E-7) - (7.158E-7) = 9.44E-8 mol of water was vaporized. The heat of vaporization of water is 3.8225E7 J/kmol at the average temperature 147.5°C, thus in this process $3.8225E7\frac{J}{kmol} \cdot \frac{1}{\frac{1000mol}{kmol}} \cdot (9.44E-8\,mol) = 3.61E-3\,J$ of heat was used in the vaporization of water and should be subtracted from the total heat. The average reported specific heat capacity at 145 and 150°C is 3.79 J/g·K, and the heat flow from 145 to 150°C is $3.79\frac{\text{J}}{\text{g.K}} \cdot 0.06\text{g} \cdot 5\text{K} = 1.138\,\text{J}$. Subtract the heat for vaporizing water and yield 1.134 J of heat. Therefore the more accurate heat capacity at 147.5°C is $\frac{1.134J}{0.06g \cdot 5K} = 3.78\frac{\text{J}}{\text{g.K}}$. The relative error of the reported heat capacity at 147.5°C is (3.79-3.78)/3.78=0.3%, which is very small and can be neglected.

3.5 CONCLUSIONS AND RECOMMENDATIONS

At 0-0.5 loading (α), 313-413 K, 3.5-11 m MEA (mol fraction x is 0.059-0.165), the empirical model of MEA volatility is $\ln(P_{MEA}/x_{MEA}) = 30.0\text{-}8153/T\text{-}2594\alpha^2/T$. In 7 m MEA with 0.2 and 0.5 loading, P_{MEA} is 920 and 230 Pa at 120 ℃. At 0.3-0.5 loading, the enthalpy of MEA vaporization, $-\Delta H_{vap,MEA}$, is about 70-73 kJ/mol MEA.

At 0.25-0.4 loading, 313-423 K, 4.7-11.3 m PZ (x is 0.078-0.169), the empirical model of PZ volatility is $\ln(P_{PZ}/x_{PZ}) = -123+21.6\ln T+20.2\alpha-18174\alpha^2/T$. In 8 m PZ with 0.3 and 0.4 loading, P_{PZ} is 400 and 120 Pa at 120 ℃, and 2620 and 980 Pa at 150 ℃. At 0.25-0.4 loading, $-\Delta H_{vap,PZ}$ is about 85-100 kJ/mol PZ at 150 ℃ and 66-80 kJ/mol PZ at 40 ℃.

$\Delta H_{vap,PZ}$ has a larger dependence on CO_2 loading than $\Delta H_{vap,MEA}$ in rich solution because of the more complex speciation/reactions in PZ at rich loading.

Specific heat capacity of 8 m PZ is 3.43-3.81 J/(g·K) at 70-150°C.

The liquid sampling method in the high temperature vapor-liquid equilibrium measurements needs to be modified. A better condensing system may help to reduce flashing; sampling into a vacuumed sample bomb, or sampling into a known amount of amine solution may help to get more representative samples.

Chapter 4: Thermodynamic Models of MEA-CO_2-H_2O System

This Chapter presents rigorous thermodynamic modeling of MEA-CO_2-H_2O with the Aspen Plus® electrolyte Non-Random Two Liquid (ENRTL) model. Based on the previous MEA model by Hilliard (2008) two new models were developed. One of the models includes a new species MEACOOH. Experimental CO_2 solubility, MEA volatility, total pressure, heat of absorption, specific heat capacity, and NMR speciation were compared with the model prediction. The results show that the model prediction improves by adding MEACOOH and related parameters. At high temperature or high CO_2 loading, the concentration of MEACOOH is above 1% in 7 m MEA. The sensitivity analysis shows that the heat of formation of MEACOOH has an effect on CO_2 partial pressure and heat of absorption at high temperature and high loading. Therefore MEACOOH may be considered an important species at high loading or high temperature. A profile for 11 m MEA with CO_2 solubility, MEA volatility, heat of absorption, speciation, and specific heat capacity was given by the model with MEACOOH. This work used Aspen Plus® Version 7.3.

4.1 ELECTROLYTE-NRTL MODEL

Electrolyte Non-Random Two Liquid (ENRTL) model was originally developed by Chen et al. (1979, 1982, 1986) for aqueous electrolyte systems. Mock et al. (1984, 1986) extended the model to mixed solvent electrolyte systems. It is a versatile model to count for liquid phase non-ideality over a full range of the electrolyte concentration, especially in aqueous or mixed solvent electrolyte systems. The ENRTL model was developed with the local composition concept, similar to the Non-Random Two Liquid

(NRTL) model by Renon and Prausnitz (1968). For non-electrolyte systems the ENRTL model reduces to the NRTL model.

4.1.1 ENRTL Model Framework in Aspen Plus®

4.1.1.1 ENRTL Parameters

Aspen Plus® has the built-in ENRTL model to calculate properties. The model uses interaction parameters to calculate the activity coefficients.

According to Chen et al. (1982) the excess Gibbs energy expression contains two contributions: the long-range ion-ion interactions and the local interactions. The long-range ion-ion interactions are represented by the unsymmetric Pitzer-Debye-Hückel model and the Born equation, while the local interactions are expressed by the NRTL theory. Equation (4-1) shows the excess Gibbs energy expression:

$$\frac{G_m^{*E}}{RT} = \frac{G_m^{*E,PDH}}{RT} + \frac{G_m^{*E,Born}}{RT} + \frac{G_m^{*E,lc}}{RT} \qquad (4\text{-}1)$$

Therefore

$$ln\gamma_i^* = ln\gamma_i^{*PDH} + ln\gamma_i^{*Born} + ln\gamma_i^{*lc} \qquad (4\text{-}2)$$

Where the superscript * means an unsymmetric reference state is used.

According to Aspen Plus® Help, the adjustable parameters for electrolyte NRTL model include the:

- Pure component dielectric constant coefficient of non-aqueous solvents
- Born radius of ionic species
- NRTL parameters for molecule-molecule, molecule-electrolyte, and electrolyte-electrolyte pairs

The NRTL parameters were adjusted in this work:

  - The molecule-molecule binary parameters:

$$\tau_{ij} = A_{ij} + \frac{B_{ij}}{T} + F_{ij} lnT + G_{ij} T \quad (4\text{-}3)$$

It can be used in the NRTL model as Equation 4-4 and Table 4-1 shows the corresponding parameters in Aspen Plus®:

$$ln\gamma_i = \frac{\sum_j x_j \tau_{ji} G_{ji}}{\sum_k x_k G_{ki}} + \sum_j \frac{x_j G_{ij}}{\sum_k x_k G_{kj}} \left(\tau_{ij} - \frac{\sum_m x_m \tau_{mj} G_{mj}}{\sum_k x_k G_{kj}} \right) \quad for\ T_{lower} \le T \le T_{upper} \quad (4\text{-}4)$$

Where

$$G_{ij} = \exp(-\alpha_{ij} \tau_{ij})$$

$$A_{ij} = C_{ij} + D_{ij}(T - 273.15K)$$

$$\tau_{ii} = 0$$

$$G_{ii} = 1$$

Table 4-1: Electrolyte NRTL Molecule-molecule Binary Parameters

Symbols in Eq. (4-3)	In Aspen Plus®	
	Parameters	**Default Values**
A_{ij}, A_{ji}	NRTL/1	0
B_{ij}, B_{ji}	NRTL/2	0
$\alpha_{ij} = \alpha_{ji}$	NRTL/3	0.3, 0.2, or 0.47*
-	NRTL/4	0
$F_{BB'}, F_{B'B}$	NRTL/5	0
$G_{BB'}, G_{B'B}$	NRTL/6	0

*: 0.3 for nonpolar substances; nonpolar with non-associated liquids; small deviations from ideality. 0.2 for saturated hydrocarbons with polar non-associated liquids and systems that exhibit liquid-liquid immiscibility. 0.47 for self-associated substances with nonpolar substances.

- Electrolyte-molecule pair parameters:

$$\tau_{ca,B} = C_{ca,B} + \frac{D_{ca,B}}{T} + E_{ca,B} \left[\frac{T_{ref} - T}{T} + ln\left(\frac{T}{T_{ref}} \right) \right] \quad (4\text{-}5)$$

$$\tau_{B,ca} = C_{B,ca} + \frac{D_{B,ca}}{T} + E_{B,ca}\left[\frac{T_{ref}-T}{T} + ln\left(\frac{T}{T_{ref}}\right)\right] \quad (4\text{-}6)$$

$$T_{ref} = 298.15K$$

Table 4-2 shows the corresponding parameters in Aspen Plus®.

Table 4-2: Electrolyte NRTL Electrolyte-molecule Binary Parameters

Symbols in Equation (4-5, 4-6)	In Aspen Plus®	
	Parameters	**Default Values**
$C_{ca,B}, C_{B,ca}$	GMELCC	8 and -4 for electrolyte/water pair, 10 and -2 for electrolyte/non-water solvent pair
$D_{ca,B}, D_{B,ca}$	GMELCD	0
$E_{ca,B}, E_{B,ca}$	GMELCE	0
$\alpha_{ca,B} = \alpha_{B,ca}$	GMELCN	0.2

4.1.1.2 Gibbs Free Energy and Enthalpy of Formation

Table 4-3: Parameters of Gibbs Free Energy and Enthalpy of Formation

Parameters	Description	Reference States
DGAQFM	Aqueous free energy of formation at infinite dilution, 25°C and 1 atm.	Infinite dilution in pure water at 25°C and 1 atm
DHAQFM	Aqueous heat of formation at infinite dilution.	Same as DGAQFM
DGFORM	Ideal gas Gibbs free energy of formation at 298.15 K.	The elements as ideal gases at 25°C and 1 atm
DHFORM	Ideal gas heat of formation at 298.15 K.	Same as DGFORM

4.1.1.3 Vapor Phase Calculation

The Redlich-Kwong equation-of-state is used for vapor phase calculation. The model is:

$$p = \frac{RT}{V_m - b} - \frac{a/T^{0.5}}{V_m(V_m + b)} \tag{4-7}$$

$$\sqrt{a} = \sum_i x_i \sqrt{a_i}$$

$$b = \sum_i x_i b_i$$

$$a_i = 0.42748023 R^2 T_{ci}^{2.5} / P_{ci}$$

$$b_i = 0.08664035 R T_{ci} / P_{ci}$$

4.1.1.4 Henry's Constant

The Henry's constant (H_{iA}) model is used when a dissolved gas i in solvent A is assumed a Henry's component.

$$ln \frac{H_i}{\gamma_i^{\infty}} = \sum_A w_A \, ln \frac{H_{iA}}{\gamma_{iA}^{\infty}} \tag{4-8}$$

Where w_A is a weighted average that relates to the critical volumes and mole fractions of solvents.

$$lnH_{iA}\left(T, P_A^{*,l}\right) = a_{iA} + \frac{b_{iA}}{T} + c_{iA} lnT + d_{iA} T + \frac{e_{iA}}{T^2} \quad for\ T_L \le T \le T_H \tag{4-9}$$

In this work, H_2O is the only solvent in the system. Therefore

$$ln \frac{H_i}{\gamma_i^{\infty}} = ln \frac{H_{iA}}{\gamma_{iA}^{\infty}} \tag{4-10}$$

Table 4-4: Henry's Parameters

Symbols in Equation (4-9)	In Aspen Plus®	
	Parameters	**Default Values**
a_{iA}	HENRY/1	-
b_{iA}	HENRY/2	0
c_{iA}	HENRY/3	0
d_{iA}	HENRY/4	0
T_L	HENRY/5	0
T_H	HENRY/6	2000
e_{iA}	HENRY/7	0

If a_{iA} is missing, $ln\frac{H_i}{\gamma_i^{\infty}}$ is set to zero and the weighting factor w_A is renormalized.

4.1.1.5 Ideal Gas Heat Capacity

Aspen ideal gas heat capacity calculation uses the following polynomial:

$$C_p^{*ig} = C_{1i} + C_{2i}T + C_{3i}T^2 + C_{4i}T^3 + C_{5i}T^4 + C_{6i}T^5 \quad C_{7i} \le T \le C_{8i} \qquad (4\text{-}11)$$

$$C_p^{*ig} = C_{9i} + C_{10i}T^{11} \quad for\ T < C_{7i} \qquad (4\text{-}12)$$

Table 4-5: Ideal Gas Heat Capacity Parameters

Symbols in Equation (4-11, 4-12)	In Aspen Plus®	
	Parameters	**Default Values**
C_{1i}	CPIG/1	-
$C_{2i}, \ldots, C_{6i}$	CPIG/2, …, 6	0
C_{7i}	CPIG/7	0
C_{8i}	CPIG/8	1000
C_{9i}, C_{10i}, C_{11i}	CPIG/9, 10, 11	-

4.1.1.6 Aqueous Infinite Dilution Heat Capacity

$$C_{p,i}^{\infty,aq} = C_{1i} + C_{2i}T + C_{3i}T^2 + \frac{C_{4i}}{T} + \frac{C_{5i}}{T^2} + \frac{C_{6i}}{\sqrt{T}} \quad for\ C_{7i} \le T \le C_{8i} \qquad (4\text{-}13)$$

For $T < C_{7i}\ or\ T > C_{8i}$, $C_{p,i}^{\infty,aq}$ is linearly extrapolated using the slope at C_{7i} or C_{8i}.

Table 4-6: Aqueous Infinite Dilution Heat Capacity Parameters

Symbol in Equation (4-13)	In Aspen Plus®	
	Parameters	**Default Values**
C_{1i}	CPAQ0/1	-
$C_{2i}, \ldots, C_{6i}$	CPAQ0/2,…,6	0
C_{7i}	CPAQ0/7	0
C_{8i}	CPAQ0/8	1000

4.1.1.7 Parameters for Zwitterions

Aspen Plus® has a special method to set up zwitterions. When a zwitterion is set up as a Henry's component, these parameters of the zwitterion are required: ideal gas heat capacity or aqueous infinite dilution heat capacity, molecular weight, charge (set to 0), Henry's constant, Antoine liquid vapor pressure coefficients (PLXANT), partial molal volume at infinite dilution (VLBROC), NRTL, and ENRTL parameters. HENRY/1 should be set to equal or less than -10 bar, and PLXANT/1 should be set to equal or less than -1.0E10 kPa, making the zwitterion non-volatile. NRTL and ENRTL parameters can be set to Aspen Plus® default values as in Tables 4-1 and 4-2. VLBROC can be set the same as a similar molecule for a reasonable approximation.

4.1.2 Prior Work on CO_2 Loaded Aqueous Amines

Aspen Plus® physical property databanks have included many interaction parameters and equilibrium constants regressed from previous experimental data. Better thermodynamic models can be achieved by adding new experimental data to the regressions, especially for the new solvents whose properties are not well built in Aspen Plus®.

Thermodynamic models of CO_2 loaded MEA and other amines have been studied by previous group members. Table 4-7 lists the relevant modeling work by previous researchers.

Table 4-7: Summary of Previous Thermodynamic Models for CO_2 Loaded Amines

Authors	Systems	Methods
Austgen (1991)	CO_2 and H_2S in MEA, MDEA, MDEA/MEA, MDEA/DEA	Aspen Plus® DRS
Freguia (2003)	CO_2 in MEA	Aspen Plus® DRS
Cullinane (2004)	CO_2 in PZ/K_2CO_3	Standalone FORTRAN model
Hilliard (2008)	CO_2 in MEA, PZ, K_2CO_3 and selected blends	Aspen Plus® DRS
Frailie et al. (2010)	5DeMayo (Cinco De Mayo) PZ model	Aspen Plus® DRS
Frailie et al. (2010)	Fawkes PZ/MDEA model	Aspen Plus® DRS
Plaza (2011)	Phoenix MEA model	Aspen Plus® DRS

A recent rigorous MEA model was developed by Hilliard (2008). As shown in Figures 2-6, 3-7, and 3-8, the Hilliard MEA thermodynamic model over-predicts P_{CO2} at high temperature, and misses MEA volatility data at high loading at 40-140 ℃. Some of the data incorporated in the Hilliard model were inconsistent, or may have systematic errors. There are also new literature data and high temperature data from this work on the MEA system. To achieve better predictions for the MEA-CO_2-H_2O system, in this work a series of new regressions in Aspen Plus® were done starting with the Hilliard (2008) model.

4.2 DATA REGRESSION OF MEA-H_2O SYSTEM

4.2.1 Model Development

The regression was more stable when data were regressed sequentially: pure component (amine, water), binary systems (amine-water), and then tertiary systems (amine-water-CO_2). The Hilliard MEA model (2008) was developed by this method. Since there is no new data for the pure component systems, the first step, pure MEA and water regression, was skipped in this work.

In the Hilliard (2008) MEA-H_2O model, total pressure, MEA volatility, specific heat capacity, and freezing point data were regressed. The new regression added the high temperature MEA volatility data presented in Chapter 3 and some new literature data. Table 4-8 shows the data that were used in the Hilliard (2008) model and the new model. Park and Lee (1997) data was not used in this work because of the high average absolute relative deviation (AARD) in Hilliard's MEA-H_2O model. All the data sets weighed equally in this regression. As stated in Chapter 3, the MEA volatility at low temperature by Hilliard (2008) is not consistent with other literature, thus the data below

46°C was not used in this regression. In this work MEA was defined as a Henry's component in Aspen Plus®.

Table 4-8: Data used in the MEA-H_2O Models

	Hilliard (2008)	**This work**
Total pressure, Nath and Bender (1983)	X	X
Total pressure, Tohara et al. (1982)	X	X
Vapor-liquid equilibrium, Park and Lee (1997)	X	
Vapor-liquid equilibrium, Tochigi et al. (1999)	X	X
Vapor-liquid equilibrium, Cai et al. (1996)	X	X
Specific heat capacity, Page et al. (1993)	X	X
Specific heat capacity, Chiu and Lee (1999)	X	X
Specific heat capacity, Weiland et al. (1997)	X	X
Specific heat capacity, Hilliard (2008)	X	X
Freezing point depression, Chang et al. (1993)	X	X
Vapor-liquid equilibrium, Kim et al. (2008)		X
Vapor-liquid equilibrium, this work		X
pK_a, Bates and Pinching (1951)	X	X
pK_a, Hamborg and Versteeg (2009)		X

4.2.2 MEA-H_2O Regression

Table 4-9 lists the regression results and standard deviation of the parameters. The other parameters CPIG/3, 4, 5, 6, NRTL/2, NRTL/6, and HENRY/4, 5, 6, were set to the default value 0.

Table 4-9: MEA-H_2O Regression Results

Parameter	Component i	Component j	Value (SI units)	Std. dev. (SI units)
CPIG/1	MEA		-171116	13222
CPIG/2	MEA		443	22
NRTL/1	MEA	H2O	-11.5	0.9
NRTL/3	H2O	MEA	0.2*	0
NRTL/5	MEA	H2O	1.8	0.2
HENRY/1	MEA	H2O	197	9
HENRY/2	MEA	H2O	-17102	458
HENRY/3	MEA	H2O	-24.2	1.3

*: set to default value 0.2.

The predicted pure MEA pressure matches the literature data as shown in Figure 4-1.

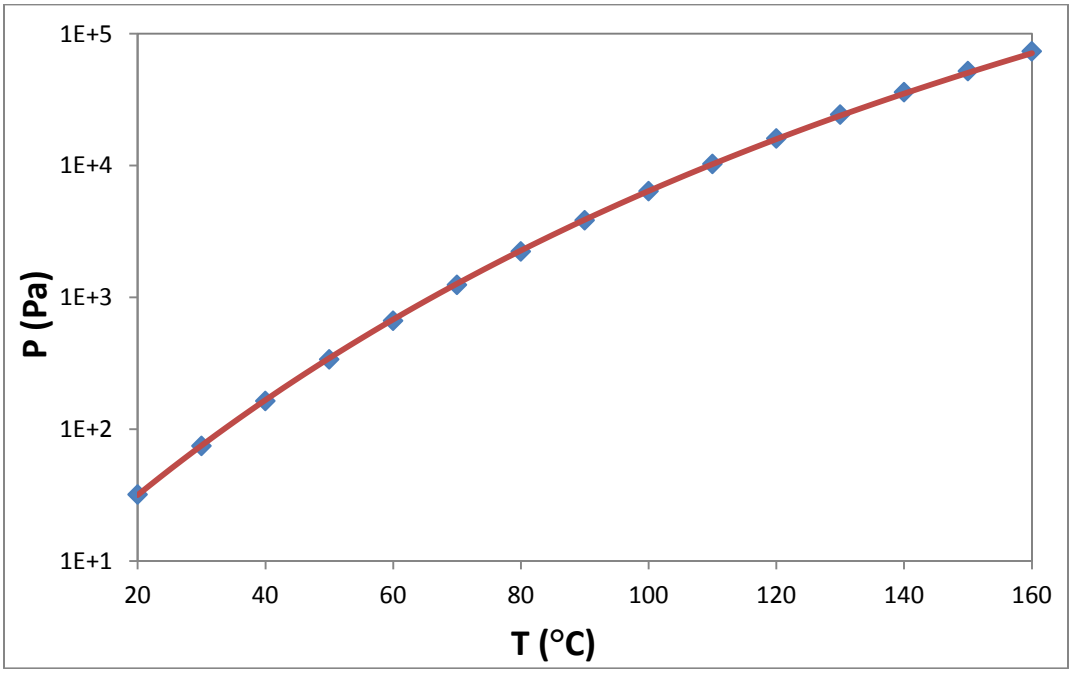

Figure 4-1: Pure MEA Vapor Pressure. **Points: experimental data from DIPPR; line: Aspen Plus® Model**

Figure 4-2 compares the new model prediction of normalized MEA volatility in 3.5-11 m MEA with the experimental data and the Hilliard's MEA model (2008).

Figure 4-3 presents the MEA volatility comparison in 7 m MEA. The major difference between the two models is at 40-60°C, because the low temperature Hilliard's MEA volatility was not used in this model. The new model fits the data and slope of the literature better than the Hilliard model at 40-70°C.

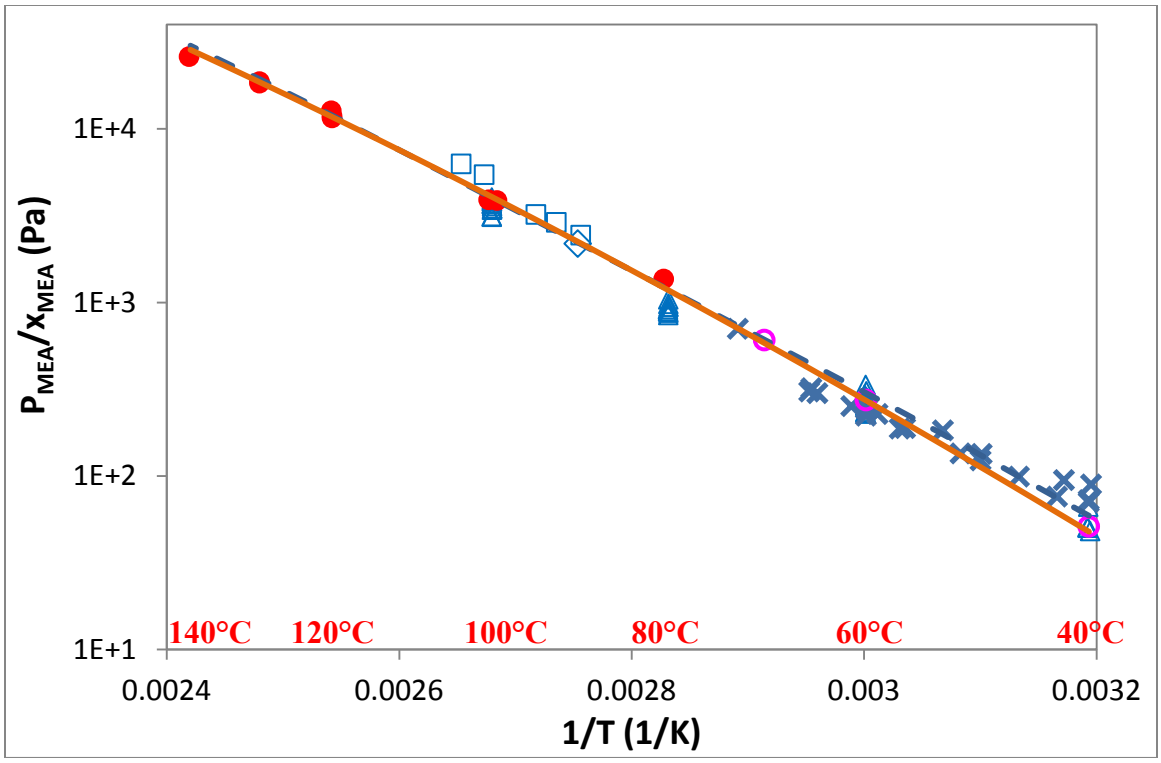

Figure 4-2: Comparison of Normalized MEA Volatility in 3.5-11 m MEA-H_2O. ○: Figure 3-20, *Gas Purification* (Kohl et al., 1997); Δ: Kim et al. (2008); □: Cai et al. (1996); ◊: Tochigi et al. (1999); X: Hilliard (2008); ●: this work; solid line: this work Aspen Plus® model – 7 m MEA; dashed line: Aspen Plus® Hilliard Model - 7 m MEA (2008); $x_{MEA} = \frac{\text{mol of MEA}}{\text{mol of MEA+mol of } H_2O}$.

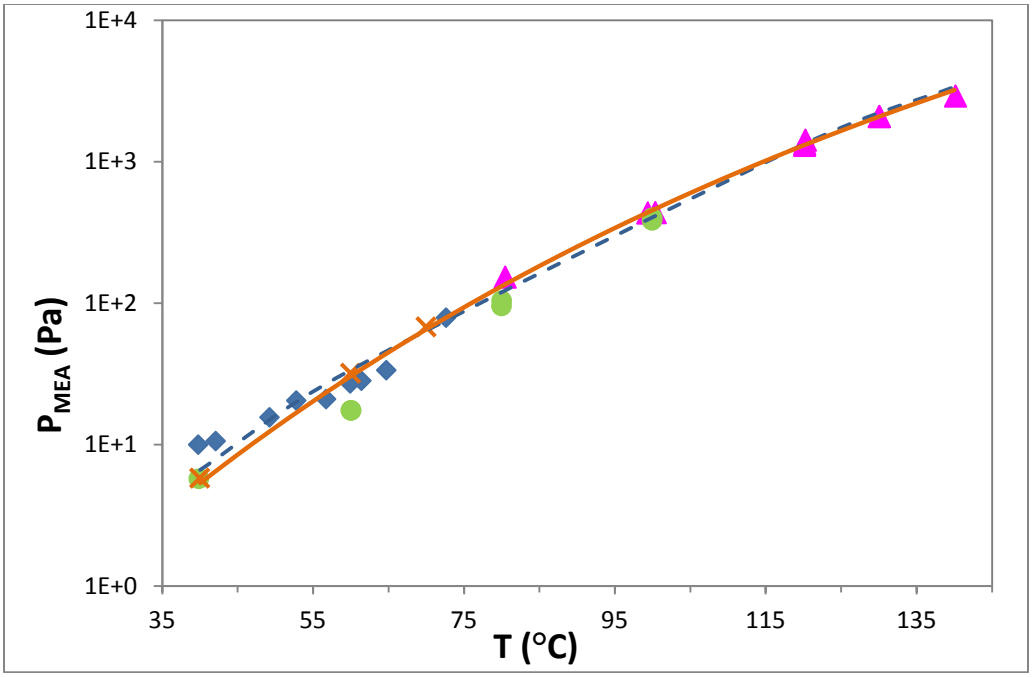

Figure 4-3: MEA Volatility in 7 m MEA. **♦: Hilliard (2008); ●: Kim et al. (2008); ▲: this work; X: Figure 3-20, *Gas Purification* (Kohl et al., 1997); solid line: Aspen Plus® model this work – 7 m MEA; dashed line: Aspen Plus® Hilliard Model – 7 m MEA (2008)**

Figure 4-4 shows the comparison of MEA partial pressure up to 31% MEA at 40-140°C. The new MEA model predicts the data well. It is better illustrated that Hilliard's MEA volatility at 40°C is inconsistent with other literature and the temperature dependence is smaller than the model prediction.

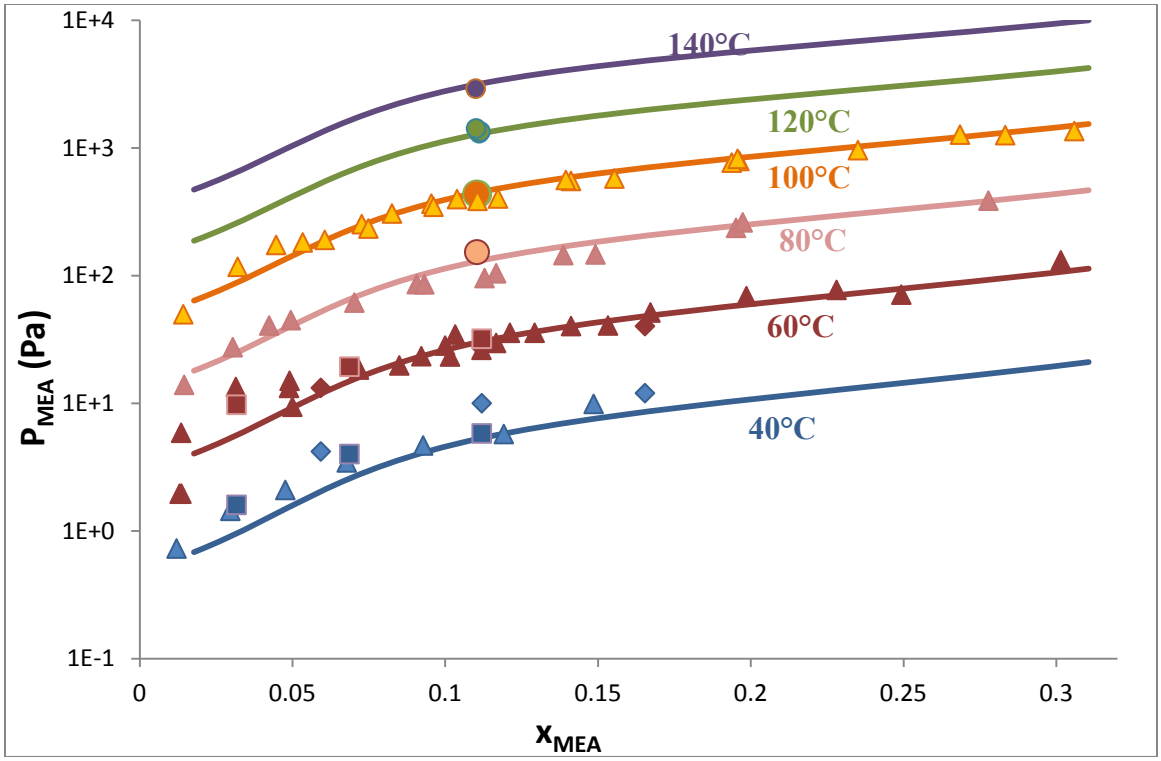

Figure 4-4: Volatility of MEA in MEA-H_2O. **♦: Hilliard (2008); ▲: Kim et al. (2008); ●: this work; ■: Figure 3-20, *Gas Purification* (Kohl et al., 1997); solid lines: Aspen Plus® model this work.**

Figure 4-5 gives the activity coefficients predicted by the new model. The reference state is pure water and infinite dilution of MEA. The activity coefficients decrease with temperature and increase with MEA.

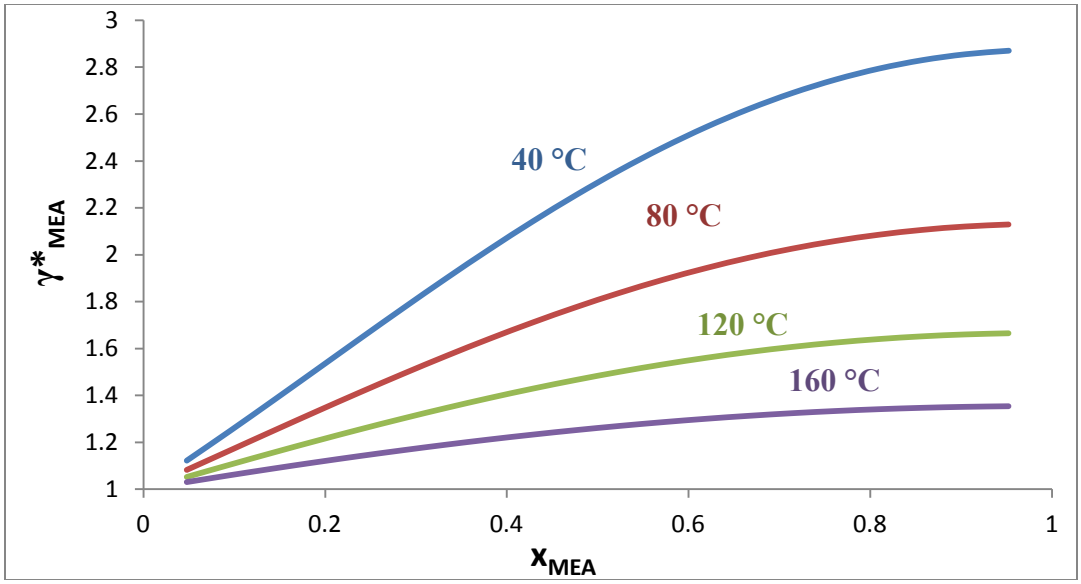

Figure 4-5: Asymmetric Activity Coefficients of MEA in MEA-H_2O

Figures 4-6 and 4-7 present the model prediction of the specific heat capacity of aqueous MEA over a wide range of temperature and MEA concentration. The model fairly predicts the data up to 40 m MEA and over 40-120°C.

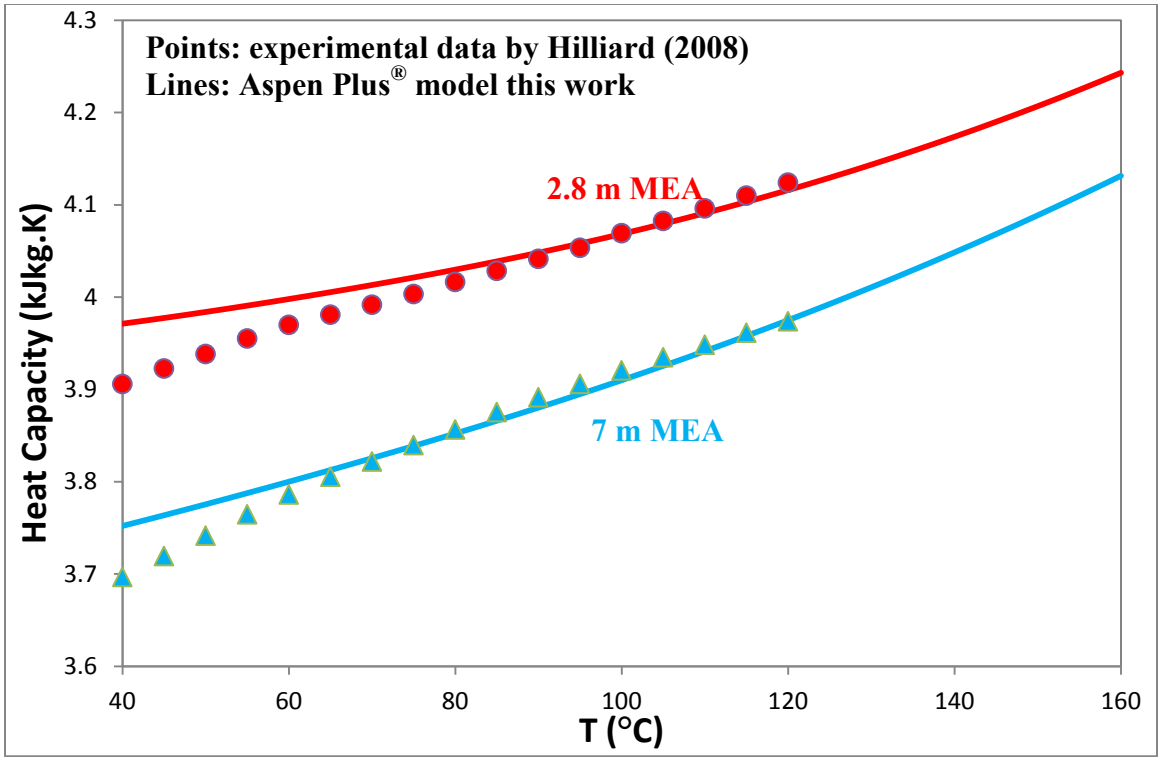

Figure 4-6: Specific Heat Capacity in MEA-H_2O

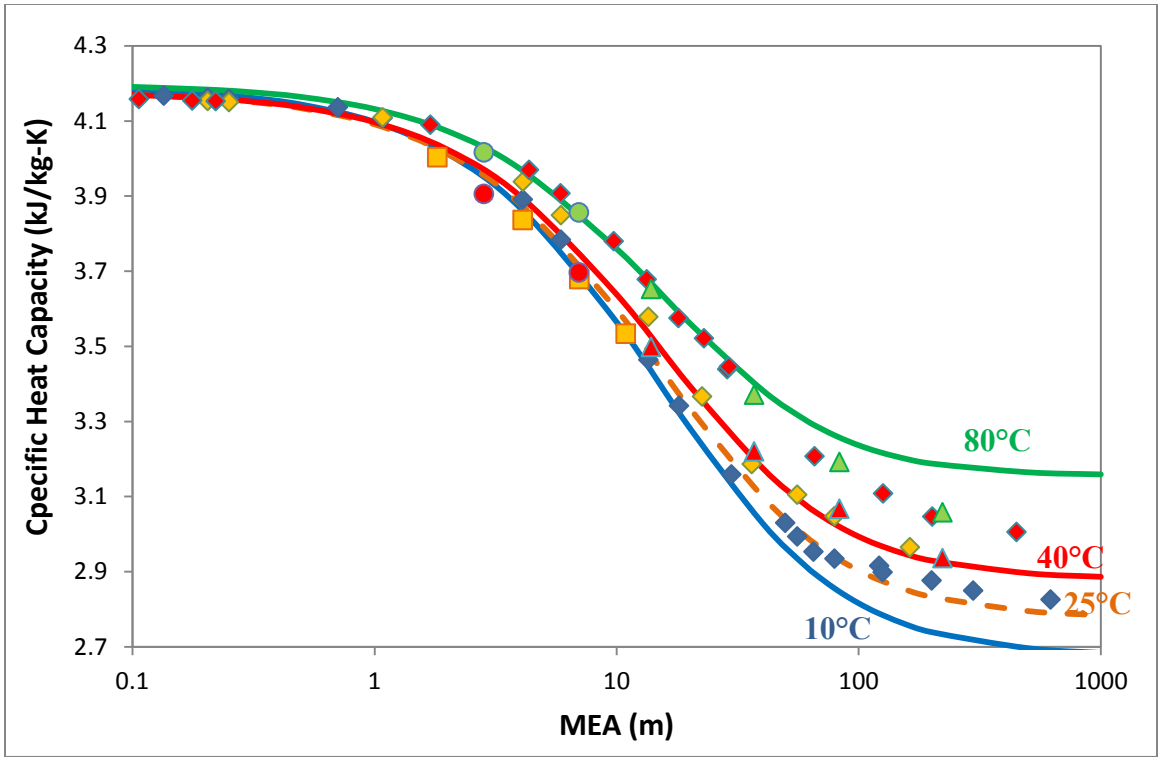

Figure 4-7: Comparison of Specific Heat Capacity of MEA-H_2O with Literature.
♦: Page et al. (1993); ■: Weiland et al. (1997); ▲: Chiu et al. (1999); ●: Hilliard (2008); Lines: Aspen Plus® Model this work

After matching the MEA volatility data and the specific heat capacity, DGAQFM and DHAQFM of $MEAH^+$ were adjusted manually to fit the pK_a of $MEAH^+$ in literature. Firstly DGAQFM was adjusted to match pK_a at 25°C, the reference temperature, then DHAQFM was adjusted to match the temperature dependence of pK_a. Figure 4-8 shows the pK_a comparison of the literature data and the model prediction. The temperature dependence fitting of this model is improved from Hilliard's MEA model (2008) because of the adding of the new high temperature experimental pK_a by Hamborg and Versteeg (2009).

$$MEA + H^+ \overset{K_a}{\leftrightarrow} MEAH^+ \tag{4-14}$$

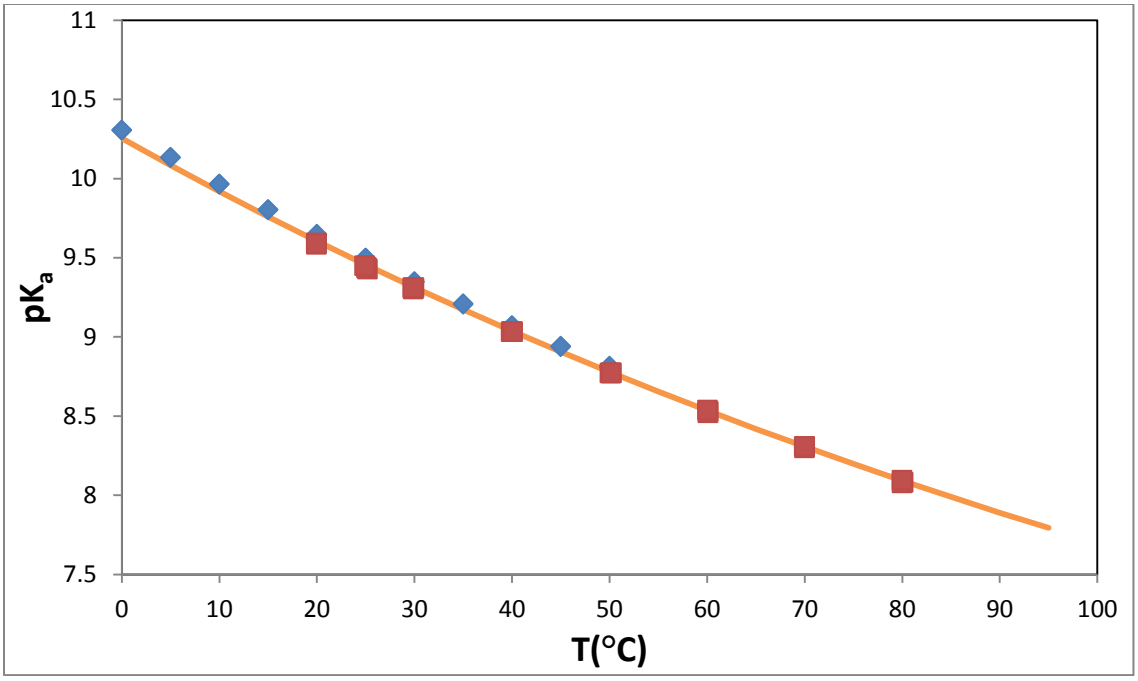

Figure 4-8: Comparison of pK_a of MEA, Molality Based, Asymmetric. ♦: Bates and Pinching (1951); ■: Hamborg and Versteeg (2009); line: Aspen Plus® model this work.

4.3 Data Regression of MEA-CO_2-H_2O without MEACOOH (Model A)

The regression of MEA-CO_2-H_2O was based on the MEA-H_2O regression in this work. To better predict all the experimental data, especially those for 7 m MEA, an additional species MEACOOH was considered for addition to the model. Therefore two different models were developed, one without MEACOOH (Model A) and one with MEACOOH (Model B). Model A will be discussed in this section and Model B will be discussed in 4.4.

4.3.1 Model A Development

In Hilliard's MEA-CO_2-H_2O model (2008), partial pressure of CO_2, MEA volatility, heat of absorption of CO_2, speciation, and specific heat capacity were regressed. However, the heat of absorption data may have systematic error as discussed in Chapter 2, MEA volatility data at below 45°C are suspicious as discussed in Chapter 3,

and there may be inconsistency among different data sets which makes the regression more difficult to converge. To reduce the complexity of the regression and reduce the inconsistency, selected data were incorporated in this work. Table 4-10 gives the data used in the three MEA models. P_{MEA} by Hilliard (2008) below 45°C was not used; P_{CO2} by Dugas et al. (2009) at 0.47 and higher loading was not used.

Table 4-10: Data used in the MEA-CO_2-H_2O Models

	Hilliard (2008)	**This work Model A**	**This work Model B**
P_{CO2}, Goldman and Leibush (1959)	X		
P_{CO2}, Lawson and Garst (1976)	X		
P_{CO2}, Lee et al. (1976), corrected	X	High loading	
P_{CO2}, Jou et al. (1995)	X	High loading	X
P_{CO2}, Ma'mun et al. (2005)	X		X
P_{CO2}, Hilliard (2008)	X	X	X
P_{MEA}, Hilliard (2008)	X	X	X
Specific heat capacity, Hilliard (2008)	X	X	X
Heat of absorption of CO_2, Kim et al. (2007)	X		
NMR speciation, Poplsteinova (2004)	X		
NMR speciation, Hilliard (2008)	X		
P_{CO2}, Dugas et al. (2009)		X	X
Total pressure, this work		X	X
P_{MEA}, this work		X	X
P_{CO2}, Aronu et al. (2011)			7 m MEA
pK_a of MEACOOH, McCann et al. (2009)			X

The data sets were assigned with different weights as in Table 4-11 to optimize the regression.

Table 4-11: Weights of the Data Sets in Model A

Data sets	Weight
Specific heat capacity in 7 m MEA, Hilliard (2008)	9
P_{CO2} in 7 and 11 m MEA, Hilliard (2008)	25
P_{CO2} in 3.5 m MEA, Hilliard (2008)	1
P_{MEA} in 7 and 11 m MEA, Hilliard (2008)	10
P_{MEA} in 3.5 m MEA, Hilliard (2008)	1
Total pressure, this work	18
P_{CO2}, Dugas et al. (2009)	8
P_{MEA}, this work	8
P_{MEA} at high loading, Hilliard (2008) and this work	18
P_{CO2} at high loading by Hilliard (2008), Lee et al. (1976) corrected, Jou et al. (1995)	10.5

Hilliard used five reactions in the model (2008):

$$H_2O \leftrightarrow H^+ + OH^- \quad (4\text{-}15)$$

$$CO_2 + H_2O \leftrightarrow H^+ + HCO_3^- \quad (4\text{-}16)$$

$$HCO_3^- \leftrightarrow H^+ + CO_3^{-2} \quad (4\text{-}17)$$

$$MEAH^+ \leftrightarrow MEA + H^+ \quad (4\text{-}18)$$

$$MEACOO^- + H_2O \leftrightarrow MEA + HCO_3^- \quad (4\text{-}19)$$

The carbonate and hydroxide concentration is very small over the whole loading range at the studied condition, thus the formation of hydroxide and carbonate (4-15) and (4-17) can be neglected. The chemical reactions were reduced to two main reactions for

easier convergence of the model. Reaction (4-20) and (4-21) are the main reactions at low and high CO_2 loading, respectively.

$$2MEA + CO_2 \leftrightarrow MEACOO^- + MEA^+ \quad (4\text{-}20)$$

$$MEA + H_2O + CO_2 \leftrightarrow MEA^+ + HCO_3^- \quad (4\text{-}21)$$

4.3.2 Model A Results

Table 4-12 lists the regression results and standard deviation of the parameters. Standard deviation 0 means the value was fixed in the final regression according to Aspen Plus® defaults or the results from a previous regression run. A very large standard deviation on the order of 1.0E11 means the value is on the regression bound or hits the limit in the data regression system in Aspen Plus®, but the value is still a good result.

Table 4-12: The Regressed Parameters of MEA-CO_2-H_2O System in Model A

#	Parameter	Component i	Component j	Value (SI units)	Standard deviation
1	DGAQFM/1	MEACOO-		-494,206,376	1,209,692
2	DHAQFM/1	MEACOO-		-731,086,866	1.13E+07
3	DHAQFM/1	MEA+		-338,000,000	12,138,474
4	CPAQ0/1	MEA+		183,474	926,721
5	CPAQ0/2	MEA+		18	526
6	CPAQ0/3	MEA+		0.47	6.83
7	CPAQ0/4	MEA+		0	0
8	CPAQ0/1	MEACOO-		-91,454	1,049,020
9	CPAQ0/2	MEACOO-		-2.7	75.5
10	CPAQ0/3	MEACOO-		0.8	7.9
11	CPAQ0/4	MEACOO-		0	0
12	GMELCC/1	H2O	(MEA+,MEACOO-)	9.42	0.80
13	GMELCD/1	H2O	(MEA+,MEACOO-)	0	0
14	GMELCE/1	H2O	(MEA+,MEACOO-)	0	0
15	GMELCC/1	(MEA+,MEACOO-)	H2O	-4.28	0.29
16	GMELCD/1	(MEA+,MEACOO-)	H2O	0	0
17	GMELCE/1	(MEA+,MEACOO-)	H2O	0	0
18	GMELCC/1	MEA	(MEA+,MEACOO-)	15.59	5.04

#	Parameter	Component i	Component j	Value (SI units)	Standard deviation
19	GMELCD/1	MEA	(MEA+,MEACOO-)	0	0
20	GMELCE/1	MEA	(MEA+,MEACOO-)	0	0
21	GMELCC/1	(MEA+,MEACOO-)	MEA	-9.23	0.58
22	GMELCD/1	(MEA+,MEACOO-)	MEA	0	0
23	GMELCE/1	(MEA+,MEACOO-)	MEA	0	0
24	GMELCC/1	H2O	(MEA+,HCO3-)	9.00	2.47
25	GMELCD/1	H2O	(MEA+,HCO3-)	0	0
26	GMELCE/1	H2O	(MEA+,HCO3-)	0	0
27	GMELCC/1	(MEA+,HCO3-)	H2O	-4.39	0.99
28	GMELCD/1	(MEA+,HCO3-)	H2O	0	0
29	GMELCE/1	(MEA+,HCO3-)	H2O	0	0
30	GMELCC/1	MEA	(MEA+,HCO3-)	12.34	9.39
31	GMELCD/1	MEA	(MEA+,HCO3-)	0	0
32	GMELCE/1	MEA	(MEA+,HCO3-)	0	0
33	GMELCC/1	(MEA+,HCO3-)	MEA	-3.47	8.81
34	GMELCD/1	(MEA+,HCO3-)	MEA	0	0
35	GMELCE/1	(MEA+,HCO3-)	MEA	0	0

Table 4-13 shows the correlation matrix of the Model A regression. The parameter number corresponds to the numbers in Table 4-12. Coefficients for non-regressed parameters are all zero and are not shown in Table 4-13.

Table 4-13: Parameter Correlation Matrix of Model A

	1	2	3	4	5	6	8	9	10	12	15	18	21	24	27	30	33
1	1.00																
2	0.04	1.00															
3	0.05	-0.95	1.00														
4	0.04	0.80	-0.84	1.00													
5	-0.08	0.14	-0.09	0.01	1.00												
6	0.00	-0.77	0.80	-0.97	-0.22	1.00											
8	-0.14	-0.69	0.68	-0.90	-0.14	0.91	1.00										
9	0.07	0.21	-0.28	0.41	-0.90	-0.21	-0.24	1.00									
10	0.14	0.60	-0.59	0.84	0.15	-0.87	-0.99	0.21	1.00								
12	0.74	-0.11	0.13	-0.13	-0.15	0.18	0.09	0.05	-0.09	1.00							
15	-0.46	0.14	-0.15	0.22	0.14	-0.26	-0.23	-0.02	0.23	-0.92	1.00						
18	-0.28	0.20	-0.24	0.07	0.03	-0.08	-0.01	0.00	0.01	-0.24	0.06	1.00					
21	-0.60	-0.01	0.04	0.03	0.09	-0.06	0.02	-0.07	-0.02	-0.71	0.62	-0.23	1.00				
24	-0.33	0.40	-0.43	0.30	0.06	-0.29	-0.25	0.06	0.24	-0.58	0.59	0.20	0.32	1.00			
27	0.23	-0.31	0.33	-0.25	-0.04	0.25	0.25	-0.05	-0.25	0.53	-0.59	-0.10	-0.31	-0.98	1.00		
30	-0.22	0.12	-0.17	-0.08	-0.04	0.08	0.06	0.02	-0.02	-0.12	0.05	0.23	-0.25	0.26	-0.24	1.00	
33	0.33	-0.40	0.45	-0.25	-0.11	0.26	0.14	-0.08	-0.08	0.31	-0.25	-0.19	0.08	-0.19	0.08	-0.49	1.00

Figure 4-9 gives the CO_2 solubility in 7 m MEA predicted by Model A. The model fits the data well up to 100°C. At 120 to 140°C low CO_2 loading and at 160°C the model over-predicts CO_2 partial pressure. This results in a high CO_2 heat of absorption at the high temperature. Figure 4-10 magnifies the high temperature / high loading part from Figure 4-9.

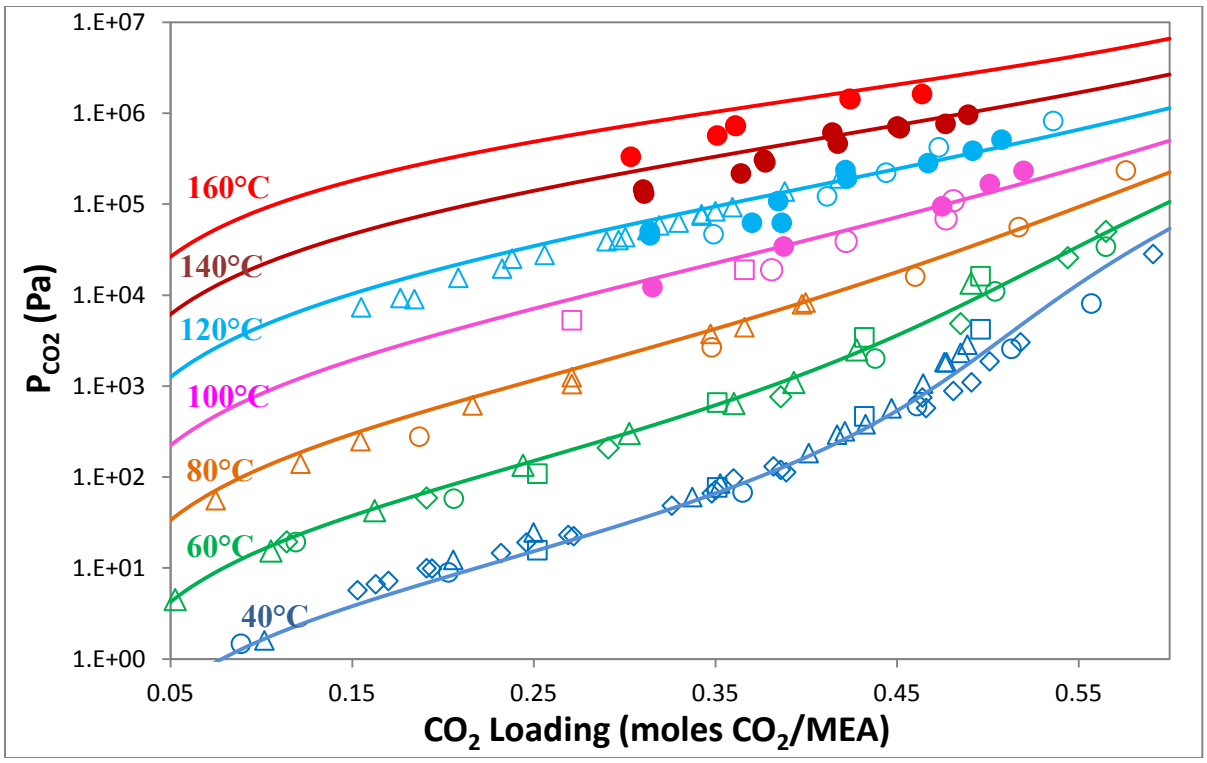

Figure 4-9: Prediction of CO_2 Solubility in 7 m MEA by Model A. **●: this work; ○: Jou et al. (1995); □: Dugas et al. (2009); ◊: Hilliard (2008); Δ: Ma'mun et al. (2005); solid lines: Model A for 7 m MEA.**

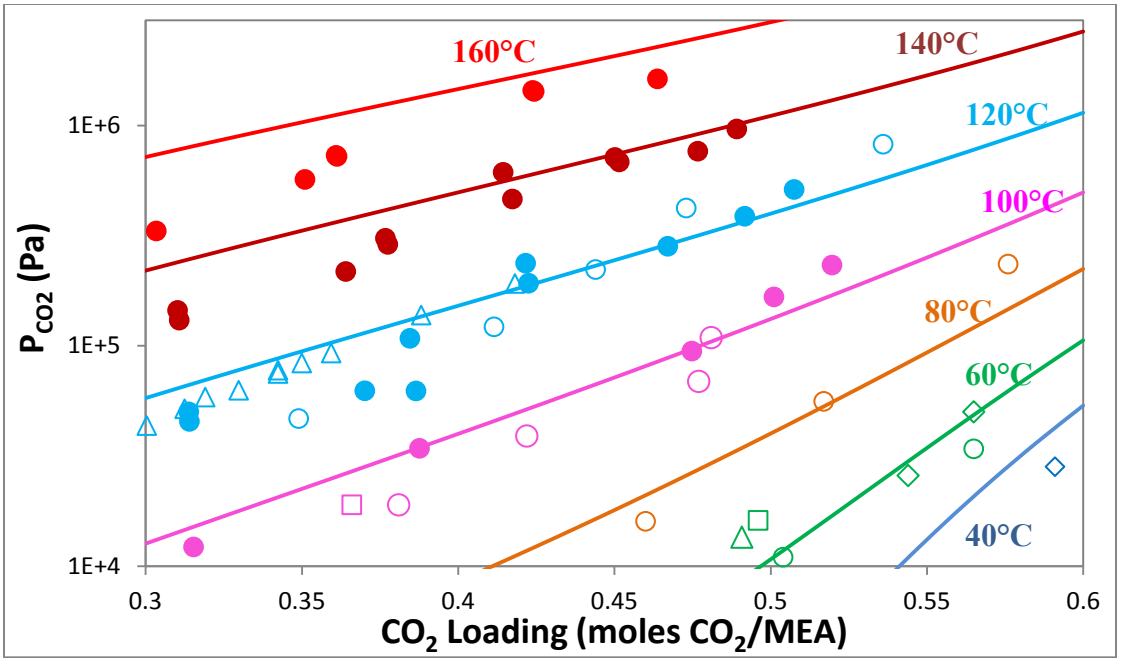

Figure 4-10: Prediction of CO_2 Solubility in 7 m MEA by Model A at High Temperature and High Loading. **●: this work; ○: Jou et al. (1995); □: Dugas et al. (2009); ◊: Hilliard (2008); Δ: Ma'mun et al. (2005); solid lines: Model A for 7 m MEA.**

Figure 4-11 compares the CO_2 heat of absorption prediction with the measured $-\Delta H_{abs}$ by Kim et al. (2007). The predicted heat of absorption was obtained by calculating P_{CO2} and the fugacity coefficient φ_{CO2} at T and T+dT in Aspen Plus® Analysis, then use the accurate form of Equation (2-12):

$$-\Delta H_{abs} = R\left(\frac{\partial ln f_{CO_2(g)}}{\partial \frac{1}{T}}\right)_{P,x} = R \cdot \frac{P_{CO2}(T+dT)\varphi_{CO2}(T+dT) - P_{CO2}(T)\varphi_{CO2}(T)}{\frac{1}{T+dT} - \frac{1}{T}}.$$

Therefore this is a differential ΔH_{abs}. The difference from the empirical derivation is that CO_2 fugacity instead of CO_2 partial pressure is used so this calculation is more accurate then the empirical model.

The predicted temperature dependence is unexpected, especially between 0.2 and 0.5 loading. The slope of $-\Delta H_{abs}$ at 120 and 160°C is too large at low loading, where -

ΔH_{abs} is expected to be relative constant. The absolute value of 40 and 80°C $-\Delta H_{abs}$ is too large compared with the measured $-\Delta H_{abs}$ by Kim et al. (2007) and the $-\Delta H_{abs}$ derived from CO_2 partial pressure in this work at lower than 0.5 loading, and is too small above 0.5 loading.

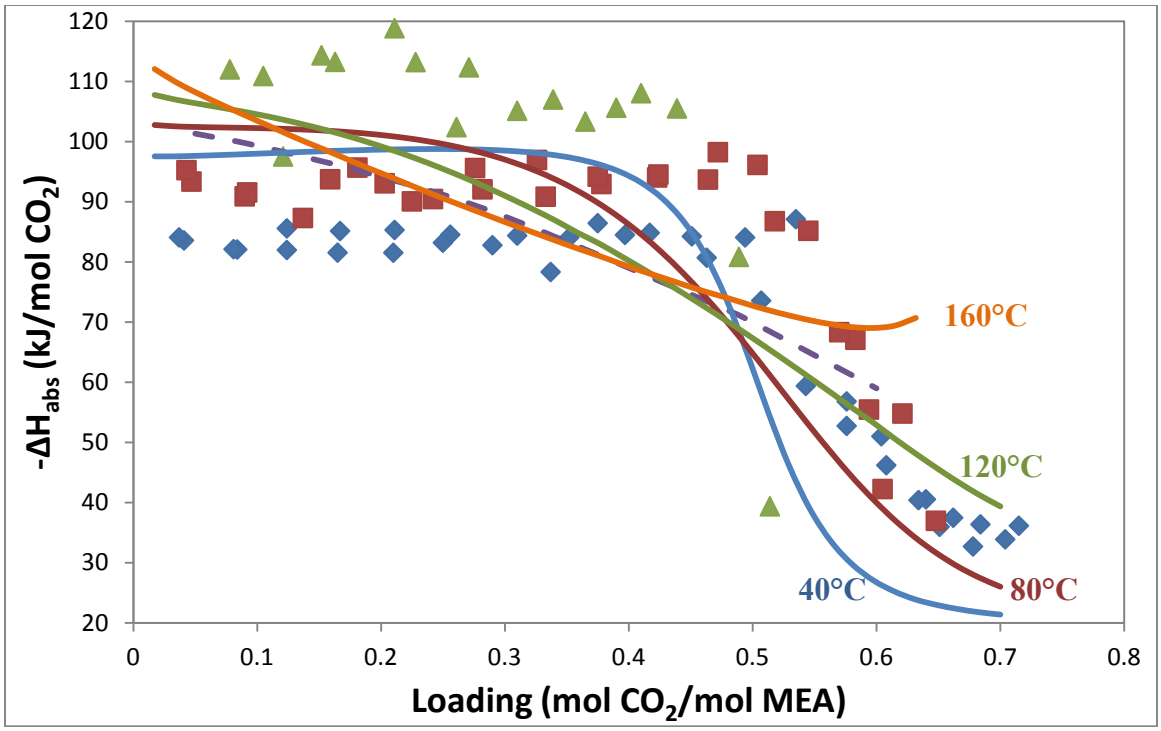

Figure 4-11: Comparison of Heat of Absorption of CO_2 in 7 m MEA with Model A.
Data points: Kim et al. (2007), ◊: 40°C, □: 80°C, Δ: 120°C; solid lines: Model A; dashed line: empirical model from this work

Figure 4-12 and Figure 4-13 show the prediction of the normalized MEA volatility by Model A. The same data sets are presented; Figure 4-13 uses CO_2 loading as the horizontal axis instead of P_{CO2}. Since the 40°C MEA volatility data were considered with error and not used in the regression, only the other temperature data were compared. Model A predicts data well at low CO_2 loading but over-predicts MEA volatility at high loading.

Figure 4-14 gives the MEA enthalpy of vaporization in 7 m MEA. $-\Delta H_{vap,MEA}$ was calculated in the same derivative method as $-\Delta H_{abs}$ of CO_2. Instead of P_{CO2} and φ_{CO2}, P_{MEA} and φ_{MEA} were obtained from Aspen Plus®. $-\Delta H_{vap,MEA}$ is larger than the value given by Hilliard's MEA model (Figure 3-11), probably because new MEA volatility data were included in Model A and previous data below 46°C were deleted from the regression. However the prediction at high CO_2 loading may not be reliable, because of the over-prediction of P_{MEA} at high loading.

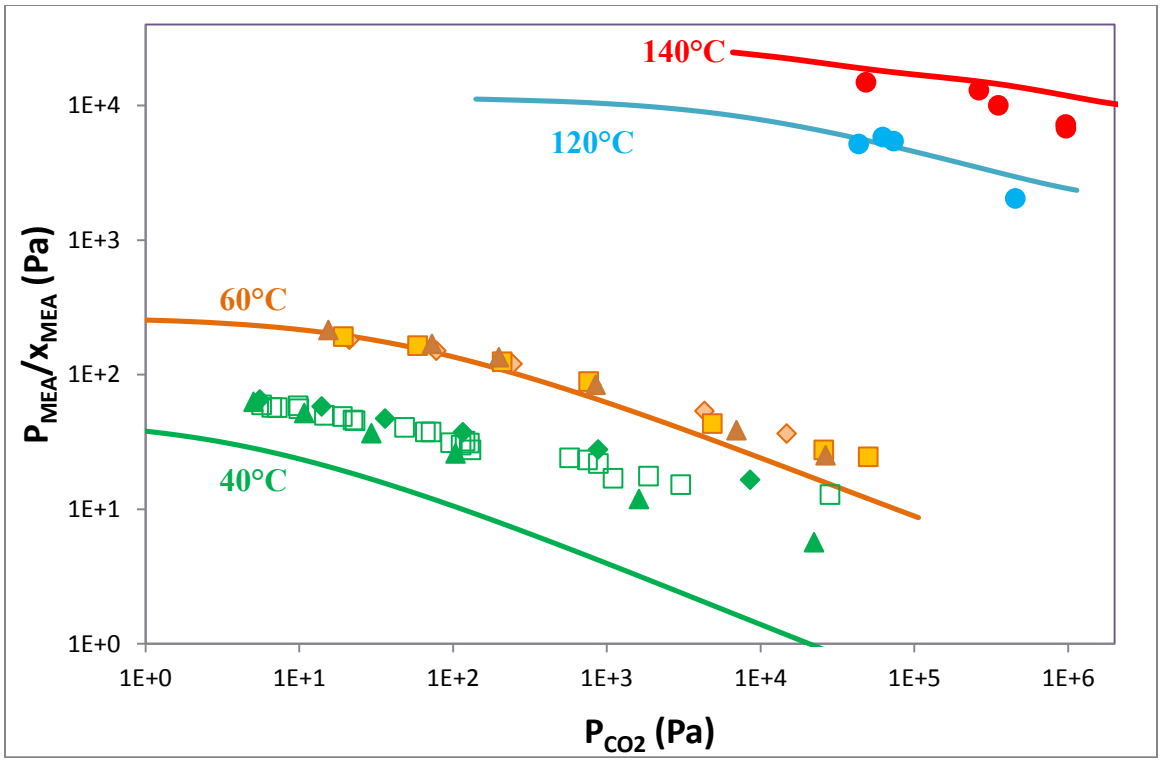

Figure 4-12: Prediction of Normalized MEA Partial Pressure over MEA-CO_2-H_2O (1) by Model A. **Hilliard (2008) MEA: ♦ 3.5 m, ■ 7 m, ▲ 11 m; ●: this work; solid lines: Model A - 7 m MEA.** $x_{MEA} = \frac{\text{mol of total MEA}}{\text{mol of total MEA + mol of } H_2O}$.

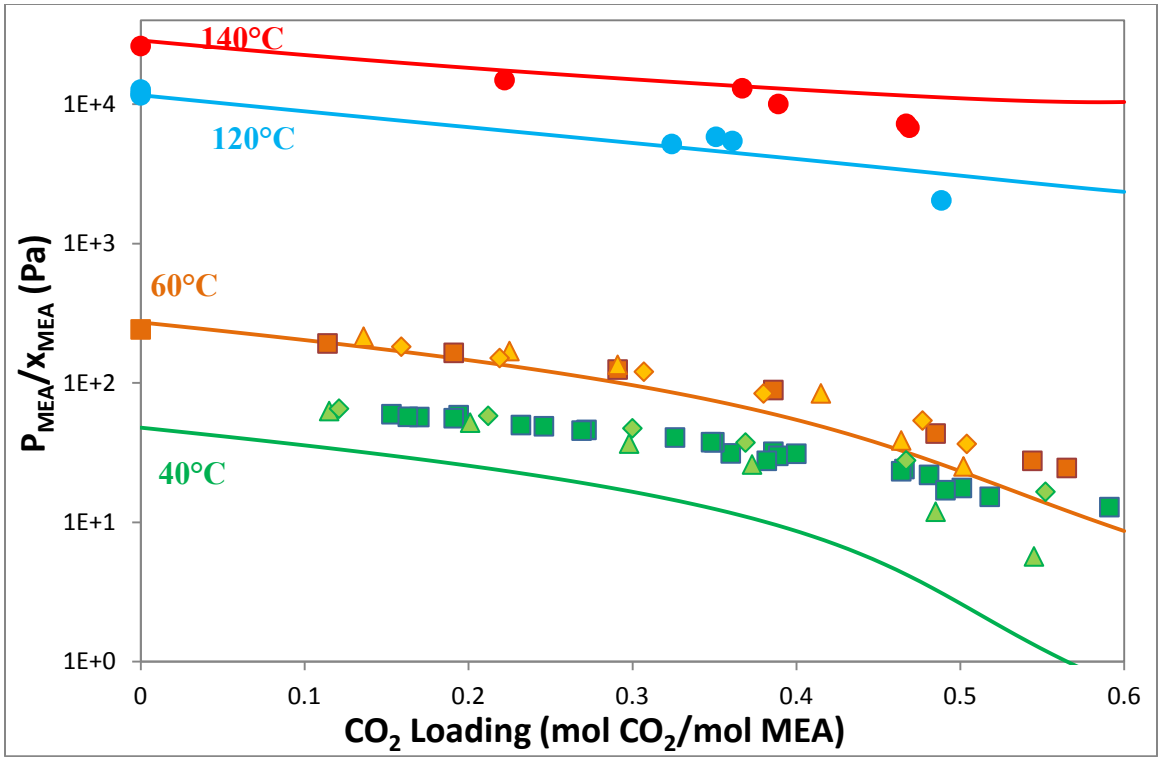

Figure 4-13: Prediction of Normalized MEA Partial Pressure over MEA-CO_2-H_2O (2) by Model A. Hilliard (2008) MEA: ♦ 3.5 m, ■ 7 m, ▲ 11 m; ●: this work; solid lines: Model A - 7 m MEA. $x_{MEA} = \frac{\text{mol of total MEA}}{\text{mol of total MEA + mol of } H_2O}$.

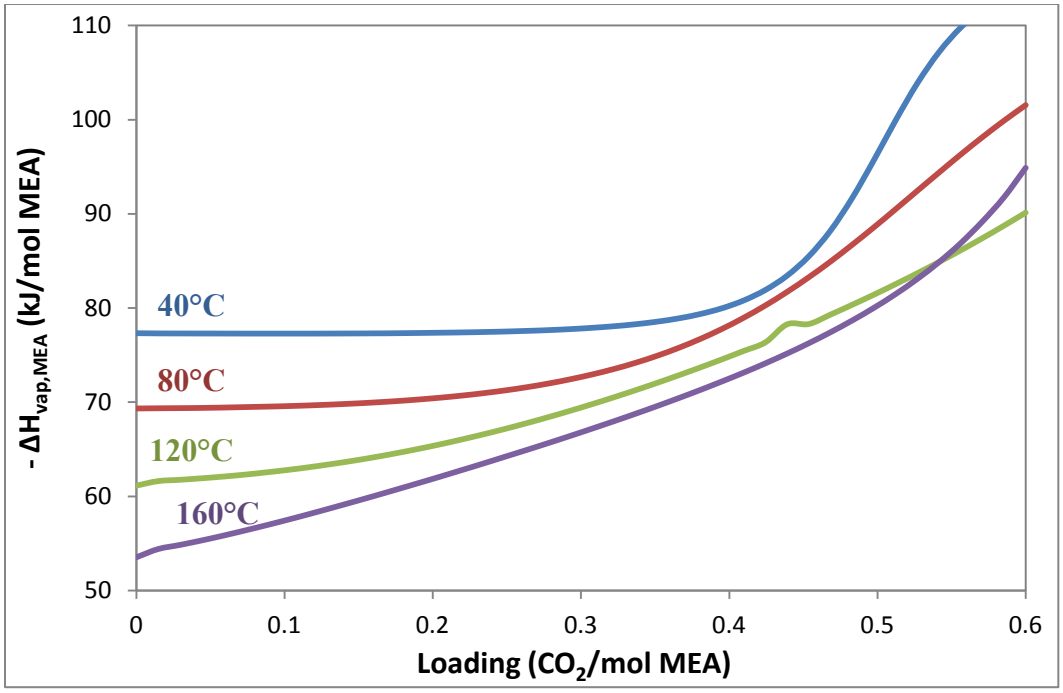

Figure 4-14: Enthalpy of Vaporization of MEA in 7 m MEA by Model A

Figure 4-15 gives the prediction of total pressure over CO_2 loaded 7 m MEA. The model predicts well at low CO_2 loading, but under-predicts the data at high loading. Considering Figure 4-9, Model A may over-predict P_{CO2} at low loading and under-predict P_{H2O} at high loading. The total pressure data by Aronu et al. (2011) was not incorporated in Model A, and there are some differences between the total pressure data by Aronu et al. (2011) and from this work as shown in Figure 4-15.

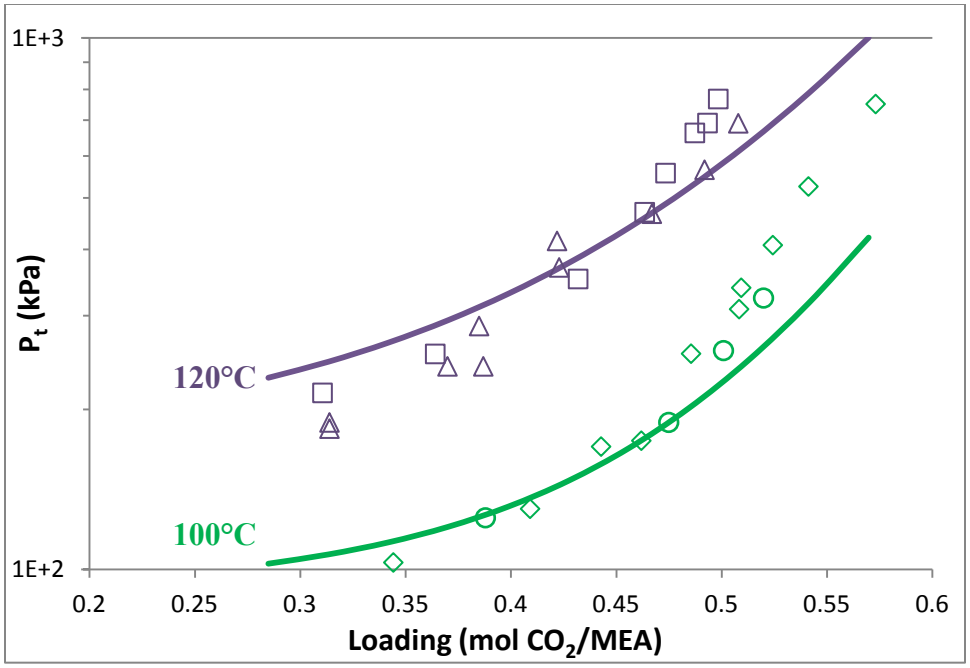

Figure 4-15: Prediction of Total Pressure in 7 m MEA by Model A. ○: 100°C this work; ◊: 100°C Aronu et al. (2011); Δ: 120°C this work; □: 120°C Aronu et al. (2011); Lines: Model A.

Figures 4-16 and 4-17 are the specific heat capacity comparison of Model A and experimental data. The model fairly predicts the data and the temperature dependence of the specific heat capacity.

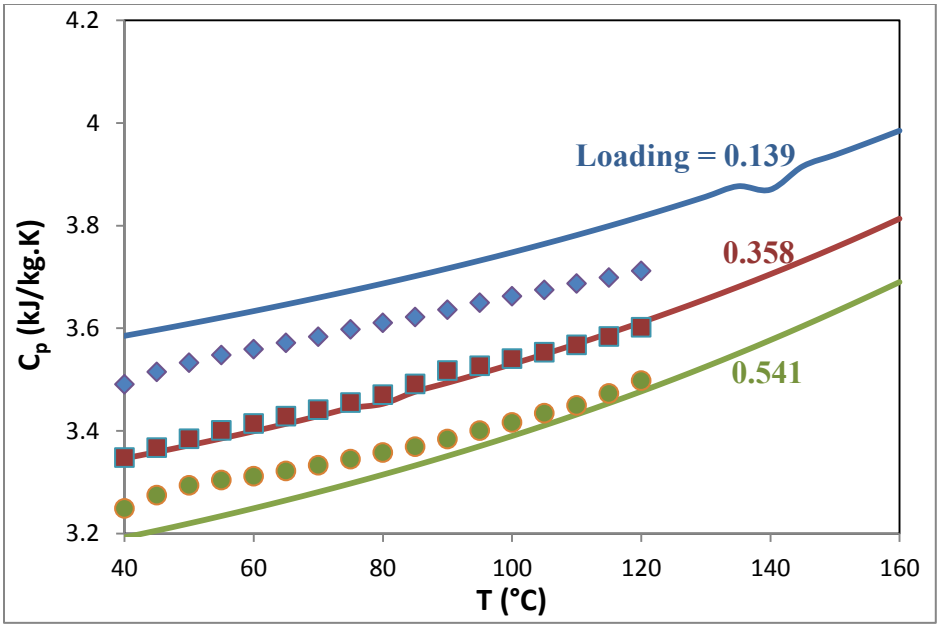

Figure 4-16: Prediction of Specific Heat Capacity of 7 m MEA by MEA-CO_2-H_2O Model A. Experimental data points (Hilliard 2008): ♦ 0.139 loading, ■ 0.358 loading, ● 0.541 loading; lines: Model A.

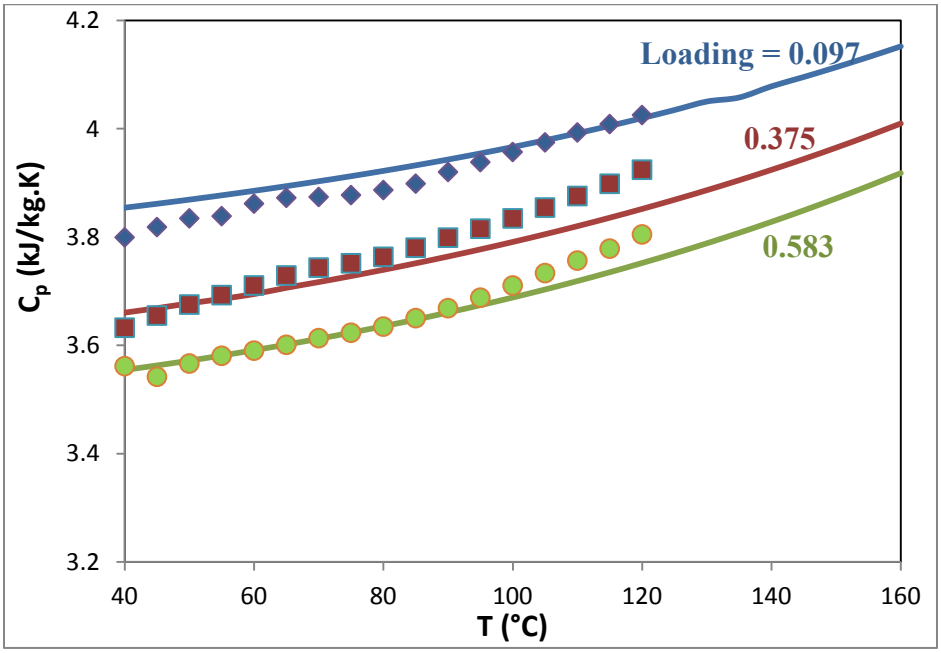

Figure 4-17: Prediction of Specific Heat Capacity of 3.5 m MEA by MEA-CO_2-H_2O Model A. Experimental data points (Hilliard 2008): ♦ 0.097 loading, ■ 0.375 loading, ● 0.583 loading; lines: Model A.

Figure 4-18 and 4-19 compare the predicted speciation by Model A and the experimental NMR data. Model A predicts the data well over the whole CO_2 loading range.

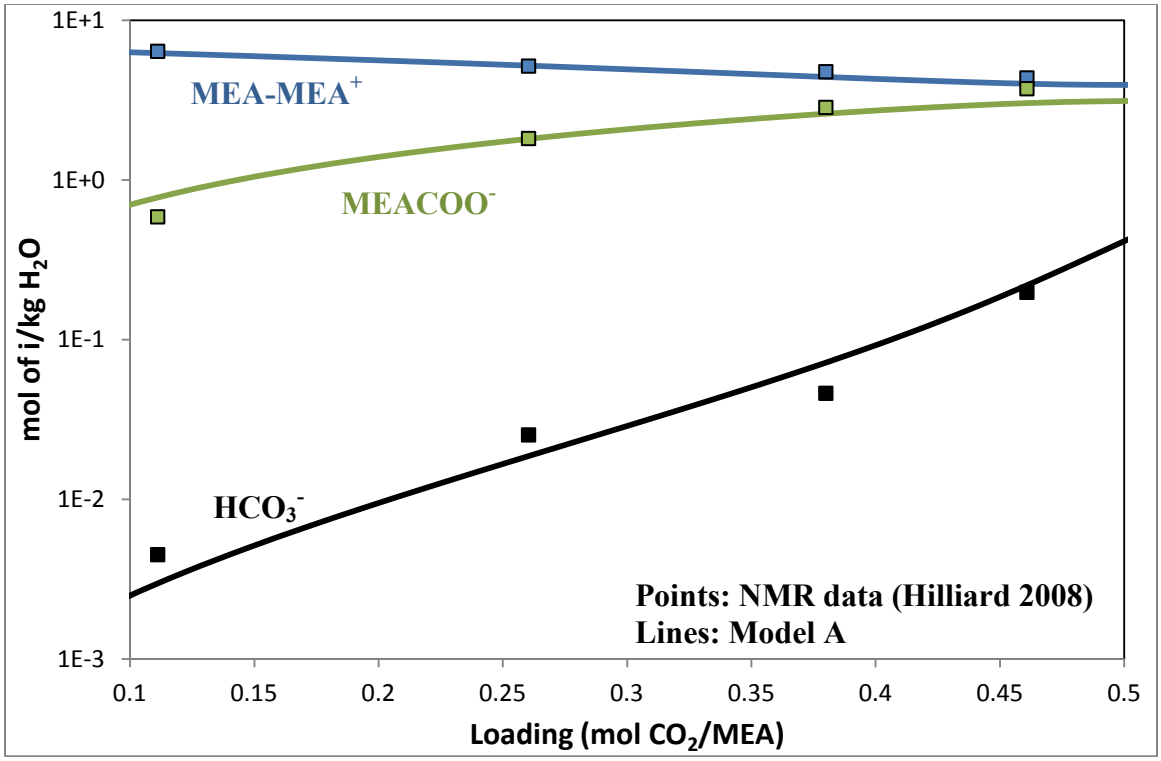

Figure 4-18: Speciation of 7 m MEA at 40 ℃ (1) by Model A

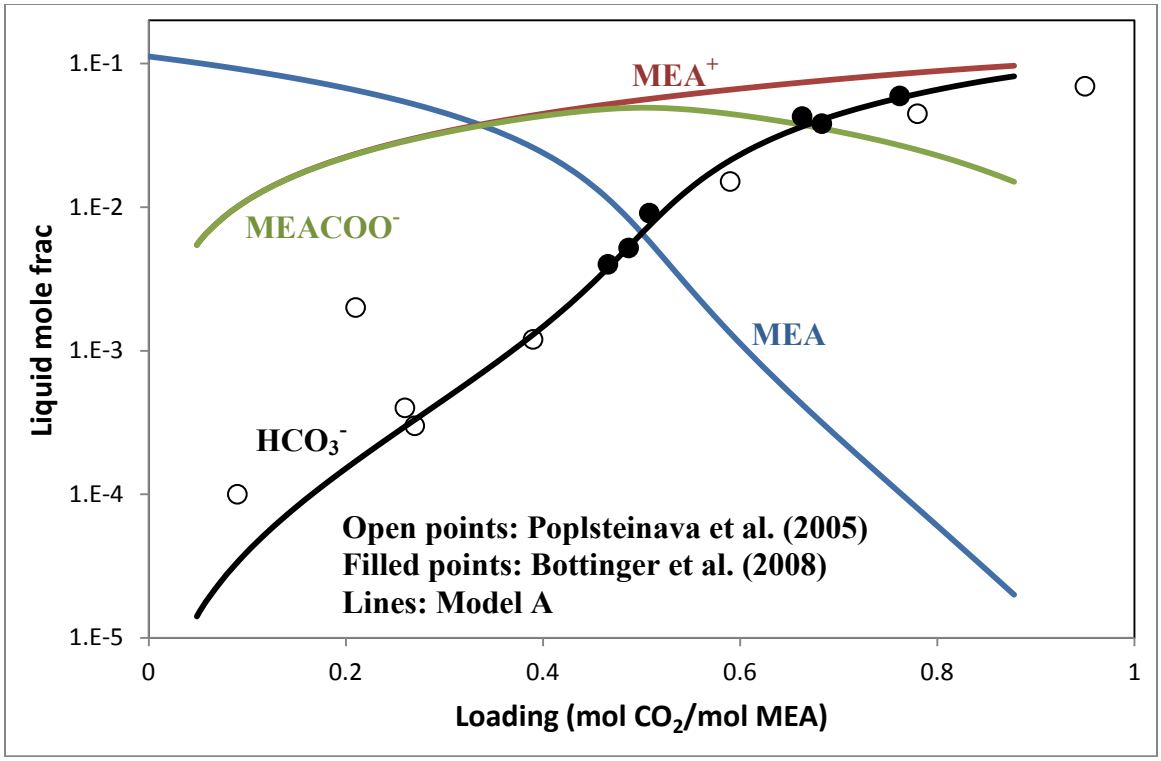

Figure 4-19: Speciation of 7 m MEA at 40 ℃ (2) by Model A

4.3.3 Model A Conclusions

For 7 m MEA, Model A predicts the CO_2 partial pressure up to 100°C, but over-predicts CO_2 partial pressure above 120°C at low CO_2 loading. Therefore as the temperature dependence of P_{CO2}, the CO_2 heat of absorption prediction by Model A is not accurate. P_{MEA} well predicted well except at high CO_2 loading. Enthalpy of vaporization of MEA is generally well-behaved but may not be accurate at high loading. Total pressure is under-predicted at 100 and 120°C at 0.48 and higher loading. Specific heat capacity at 40-120°C and speciation of CO_2 loaded MEA at 40°C are well predicted.

Therefore the major problems with Model A exist above 120°C and 0.48 CO_2 loading. To solve these problems, a new species MEACOOH was added and Model B was developed.

4.4 REGRESSION OF MEA-CO_2-H_2O WITH MEACOOH (MODEL B)

4.4.1 Model B Development

Caplow (1968) proposed the zwitterion mechanism for reactions of amines with CO_2. In this mechanism, the zwitterion MEACOOH serves as an intermediate as follows:

$$MEA + CO_2 \leftrightarrow MEACOOH \text{ (zwitterion)} \quad (4\text{-}22)$$

$$MEA + MEACOOH \leftrightarrow MEAH^+ + MEACOO^- \quad (4\text{-}23)$$

McCann et al. (2009) measured the equilibrium constants for the following reaction of zwitterion:

$$MEACOO^- + H^+ \overset{K}{\leftrightarrow} MEACOOH \quad (4\text{-}24)$$

Log K (M^{-1}) was reported as 7.49 at 30°C, which is the pK_a of MEACOOH.

Several experimental (Hikita et al. 1977 and 1979, Penny et al. 1983, Alper et al. 1990, Ali et al. 2005) and theoretical (da Silva et al. 2004, Arstad et al. 2007, Shim et al. 2009, Xie et al. 2010) studies have been done to the MEA reactions with CO_2. The other two mechanisms are:

$$MEA + CO_2 \leftrightarrow MEAH^+ + MEACOO^- \quad (4\text{-}25)$$

And

$$MEA + CO_2 \leftrightarrow MEACOOH \text{(carbamic acid)} \quad (4\text{-}26)$$

$$MEA + MEACOOH \leftrightarrow MEAH^+ + MEACOO^- \quad (4\text{-}27)$$

It was found that 2-oxazolidone was formed in the MEA thermal degradation (Polderman 1955, David 2009):

$$MEAH^+ + MEACOO^- \leftrightarrow MEA + H_2O + \quad (4\text{-}28)$$

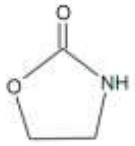

To better fit the data, a new species MEACOOH representing the above molecules zwitterion, carbamic acid, and 2-oxazolidone, was added to the MEA-CO_2-H_2O model and related parameters were added in the regression. To simplify the statement, this new species will be referred to as zwitterions or MEACOOH in this dissertation. Reaction (4-22) was added to the chemistry of the regression.

This model is referred to as Model B. The model was regressed to match the pK_a by McCann et al. (2009) as shown in Figure 4-20.

The data sets were assigned with different weights as in Table 4-14 to optimize the regression.

Table 4-14: Weights of the Data Sets in Model B

Data sets	Weight
Specific heat capacity in 7 m MEA, Hilliard (2008)	9
P_{CO2} in 7 and 11 m MEA, Hilliard (2008)	30
P_{CO2} in 3.5 m MEA, Hilliard (2008)	1
P_{MEA} in 7 and 11 m MEA, Hilliard (2008)	15
P_{MEA} in 3.5 m MEA, Hilliard (2008)	1
P_{CO2}, Jou et al. (1995)	3
P_{CO2}, Ma'mun et al. (2005)	5
Total pressure, this work	8
P_{CO2}, Dugas et al. (2009)	5
P_{CO2} in 7 m MEA, Aronu et al. (2011)	3
P_{MEA}, this work	8
P_{MEA} at high loading, Hilliard (2008) and this work	25

The following parameters of MEACOOH were set before the regression:

Molecular weight: 105.09 g/mol

Charge: 0

VLBROC: 0.0464 m^3/kmol (same as H_2O)

PLXANT/1: -1.0E20 kPa

HENRY/1 in H_2O: -10 bar

CPIG/1,2,3: 51338, -9.93, and 0.085 (same as CPAQ0/1,2,3 of $MEACOO^-$)

4.4.2 Model B Results

The regressed parameters are presented in Table 4-15. Standard deviation 0 means the parameter value was fixed in the final regression according to Aspen Plus® defaults or the results from a previous regression run. The standard deviation of DHFORM of MEACOOH was a large number on the order of 1.0E11, which means the value is on the regression bound or hits the limit in the data regression system in Aspen Plus®, but the value is still a good result. A sensitivity analysis will be performed to address the uncertainty in DHFORM of MEACOOH.

Table 4-15: Regressed Parameters in MEA-CO_2-H_2O Model B

#	Parameter	Component i	Component j	Value (SI units)	Standard deviation
1	DGAQFM/1	MEACOO-		-495,247,152	1,549,450
2	DHAQFM/1	MEACOO-		-721,181,462	31,069,098*
3	DHAQFM/1	MEA+		-339,000,000	29,274,874*
4	CPAQ0/1	MEA+		-469	4601
5	CPAQ0/2	MEA+		69	709
6	CPAQ0/3	MEA+		1.48	2.03
7	CPAQ0/4	MEA+		0	0
8	CPAQ0/1	MEACOO-		51,338	64675*
9	CPAQ0/2	MEACOO-		-9.93	114*
10	CPAQ0/3	MEACOO-		0.085	0.784*
11	CPAQ0/4	MEACOO-		0	0
12	CPIG/1	MEACOOH		51,338**	0

#	Parameter	Component i	Component j	Value (SI units)	Standard deviation
13	CPIG/2	MEACOOH		-9.93**	0
14	CPIG/3	MEACOOH		0.085**	0
15	CPIG/4	MEACOOH		0	0
16	CPIG/5	MEACOOH		0	0
17	CPIG/6	MEACOOH		0	0
18	CPIG/7	MEACOOH		0	0
19	DGFORM/1	MEACOOH		-505,389,210	6,643,988*
20	DHFORM/1	MEACOOH		-746,624,005	N/A
21	GMELCC/1	H2O	(MEA+,MEACOO-)	8.74	1.73
22	GMELCD/1	H2O	(MEA+,MEACOO-)	0	0
23	GMELCE/1	H2O	(MEA+,MEACOO-)	0	0
24	GMELCC/1	(MEA+,MEACOO-)	H2O	-4.19	0.58
25	GMELCD/1	(MEA+,MEACOO-)	H2O	0	0
26	GMELCE/1	(MEA+,MEACOO-)	H2O	0	0
27	GMELCC/1	MEA	(MEA+,MEACOO-)	6.36	2.71
28	GMELCD/1	MEA	(MEA+,MEACOO-)	0	0
29	GMELCE/1	MEA	(MEA+,MEACOO-)	0	0
30	GMELCC/1	(MEA+,MEACOO-)	MEA	-4.97	2.90
31	GMELCD/1	(MEA+,MEACOO-)	MEA	0	0
32	GMELCE/1	(MEA+,MEACOO-)	MEA	0	0
33	GMELCC/1	H2O	(MEA+,HCO3-)	10.28	1.64
34	GMELCD/1	H2O	(MEA+,HCO3-)	0	0
35	GMELCE/1	H2O	(MEA+,HCO3-)	0	0
36	GMELCC/1	(MEA+,HCO3-)	H2O	-4.73	0.75
37	GMELCD/1	(MEA+,HCO3-)	H2O	0	0
38	GMELCE/1	(MEA+,HCO3-)	H2O	0	0
39	GMELCC/1	MEA	(MEA+,HCO3-)	12.64	6.64
40	GMELCD/1	MEA	(MEA+,HCO3-)	0	0
41	GMELCE/1	MEA	(MEA+,HCO3-)	0	0
42	GMELCC/1	(MEA+,HCO3-)	MEA	0.27	2.91
43	GMELCD/1	(MEA+,HCO3-)	MEA	0	0
44	GMELCE/1	(MEA+,HCO3-)	MEA	0	0
45	GMELCC/1	MEACOOH	(MEA+,MEACOO-)	8	0
46	GMELCD/1	MEACOOH	(MEA+,MEACOO-)	0	0
47	GMELCE/1	MEACOOH	(MEA+,MEACOO-)	0	0
48	GMELCC/1	(MEA+,MEACOO-)	MEACOOH	-4	0
49	GMELCD/1	(MEA+,MEACOO-)	MEACOOH	0	0
50	GMELCE/1	(MEA+,MEACOO-)	MEACOOH	0	0

#	Parameter	Component i	Component j	Value (SI units)	Standard deviation
51	GMELCC/1	MEACOOH	(MEA+,HCO3-)	8	0
52	GMELCD/1	MEACOOH	(MEA+,HCO3-)	0	0
53	GMELCE/1	MEACOOH	(MEA+,HCO3-)	0	0
54	GMELCC/1	(MEA+,HCO3-)	MEACOOH	-4	0
55	GMELCD/1	(MEA+,HCO3-)	MEACOOH	0	0
56	GMELCE/1	(MEA+,HCO3-)	MEACOOH	0	0
57	NRTL/1	H2O	MEACOOH	0	0
58	NRTL/2	H2O	MEACOOH	0	0
59	NRTL/3	H2O	MEACOOH	0.2	0
60	NRTL/5	H2O	MEACOOH	0	0
61	NRTL/6	H2O	MEACOOH	0	0
62	NRTL/1	MEACOOH	H2O	0	0
63	NRTL/2	MEACOOH	H2O	0	0
64	NRTL/5	MEACOOH	H2O	0	0
65	NRTL/6	MEACOOH	H2O	0	0

*: The parameter was regressed in the last run with a small boundary, and the standard deviation in the last run was 0; the std. dev. in the table is from an earlier run in the progress of the regression. **: The values were set to be equal to CPAQ0/1,2,3 of $MEACOO^-$ in the last run.

Table 4-16 shows the correlation matrix of the Model B regression. The parameter number corresponds to the numbers in Table 4-15. Coefficients for non-regressed parameters are all zero and are not shown in Table 4-16.

Table 4-16: Parameter Correlation Matrix of Model B

	1	2*	3*	4	5	6	8*	9*	10*	19*	21	24	27	30	33	36	39	42
1	1.00																	
2*	-0.28	1.00																
3*	0.32	-0.99	1.00															
4	0.04	0.30	-0.24	1.00														
5	0.14	-0.37	0.31	-0.34	1.00													
6	-0.10	0.82	-0.82	0.31	-1.00	1.00												
8*	0.09	-0.88	0.87	-0.27	0.54	-0.11	1.00											
9*	0.08	0.00	0.00	-0.19	-0.45	0.75	0.25	1.00										
10*	-0.11	0.00	0.00	0.32	-0.25	-0.26	-0.89	-0.64	1.00									
19*	-0.12	-0.08	0.05	-0.49	0.36	0.14	0.05	0.00	0.00	1.00								
21	0.92	-0.25	0.27	0.02	0.14	-0.09	0.02	0.08	-0.05	-0.11	1.00							
24	-0.86	0.22	-0.24	-0.02	-0.14	0.09	-0.01	-0.08	0.04	0.11	-0.99	1.00						
27	-0.10	-0.34	0.35	-0.07	-0.06	0.06	-0.13	0.22	0.03	-0.04	0.09	-0.16	1.00					
30	0.05	0.32	-0.33	0.06	0.06	-0.06	0.13	-0.19	-0.05	0.02	-0.13	0.19	-0.99	1.00				
33	-0.41	0.39	-0.38	-0.05	-0.11	0.07	0.75	0.20	-0.68	-0.05	-0.60	0.65	-0.39	0.39	1.00			
36	0.27	-0.37	0.36	0.06	0.07	-0.04	-0.67	-0.20	0.60	0.15	0.49	-0.55	0.41	-0.41	-0.98	1.00		
39	0.11	0.52	-0.55	-0.05	0.06	-0.03	0.06	0.03	0.02	0.12	0.18	-0.20	0.43	-0.46	-0.26	0.16	1.00	
42	-0.17	-0.17	0.17	-0.62	-0.52	0.54	-0.03	0.06	-0.05	0.20	-0.15	0.14	0.11	-0.09	0.15	-0.12	-0.05	1.00

*: The coefficients of these parameters are earlier runs in the progress of the regression, not from the last run.

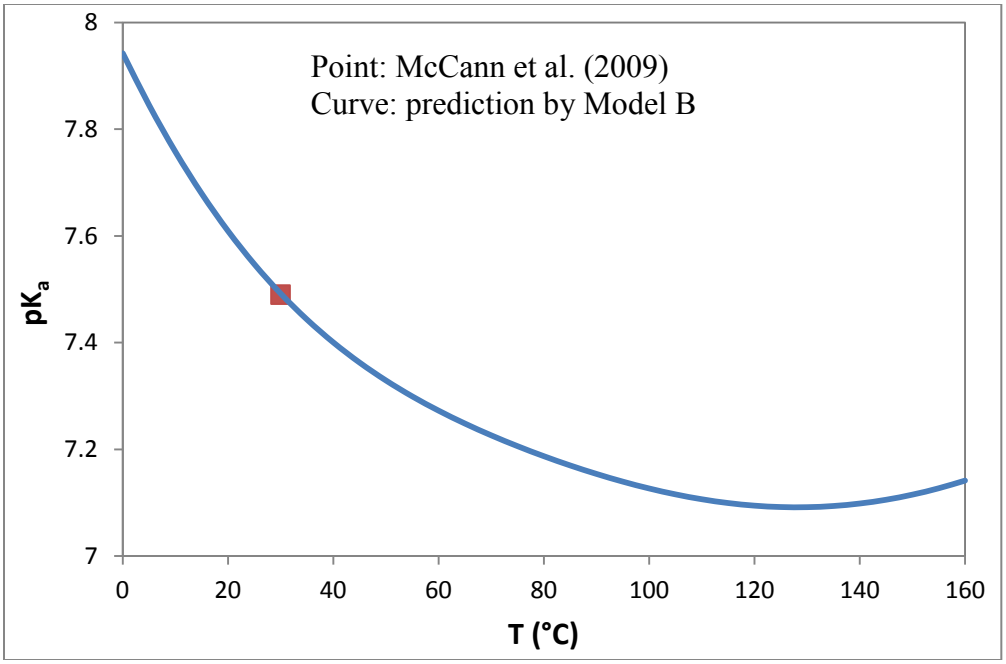

Figure 4-20: pK_a Fitting of MEACOOH, Molarity Based, Asymmetric

Figure 4-21 gives the comparison of CO_2 solubility in 7 m MEA predicted by Model A and B. Model B fits the data better than Model A at 40-160°C except a few outliers.

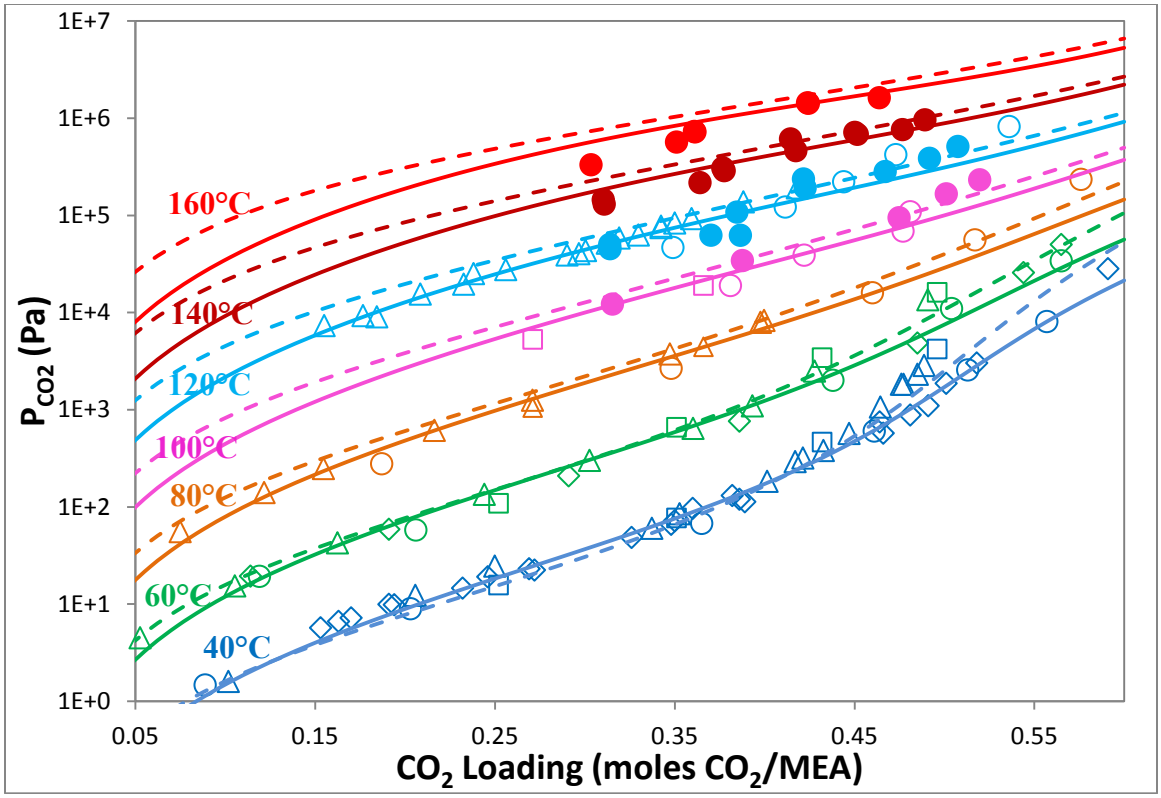

Figure 4-21: Prediction of CO_2 Solubility in 7 m MEA by Models A and B. ●: this work; ○: Jou et al. (1995); □: Dugas et al. (2009); ◊: Hilliard (2008); Δ: Ma'mun et al. (2005); solid lines: Model B for 7 m MEA; dashed lines: Model A for 7 m MEA.

Figure 4-22 compares the experimental data by Kim et al. (2007) and the prediction by Model B using the same derivative method as in Model A. The temperature dependence is reasonable; at low loading, ΔH_{abs} is relative constant. Figure 4-23 compares ΔH_{abs} from Model A, B, and the empirical model in Table 2-12. Generally, Model B predicts lower $-\Delta H_{abs}$ than Model A does below 0.5 loading, and predicts higher $-\Delta H_{abs}$ than Model A does above 0.5 loading. The temperature dependence of $-\Delta H_{abs}$ between 0.2 and 0.5 loading by Model B is more reasonable than that by Model A. The $-\Delta H_{abs}$ from the empirical model in Table 2-12 is close to the 160°C curves of Model A and B in 0.2-0.5 loading. A linear trend line of $-\Delta H_{abs}$ at 40°C in 0.2-0.5 loading from Model B will be very close to the empirical model prediction;

while a linear trend line of $-\Delta H_{abs}$ at 40°C in 0.2-0.5 loading from Model A will be higher than the empirical model prediction.

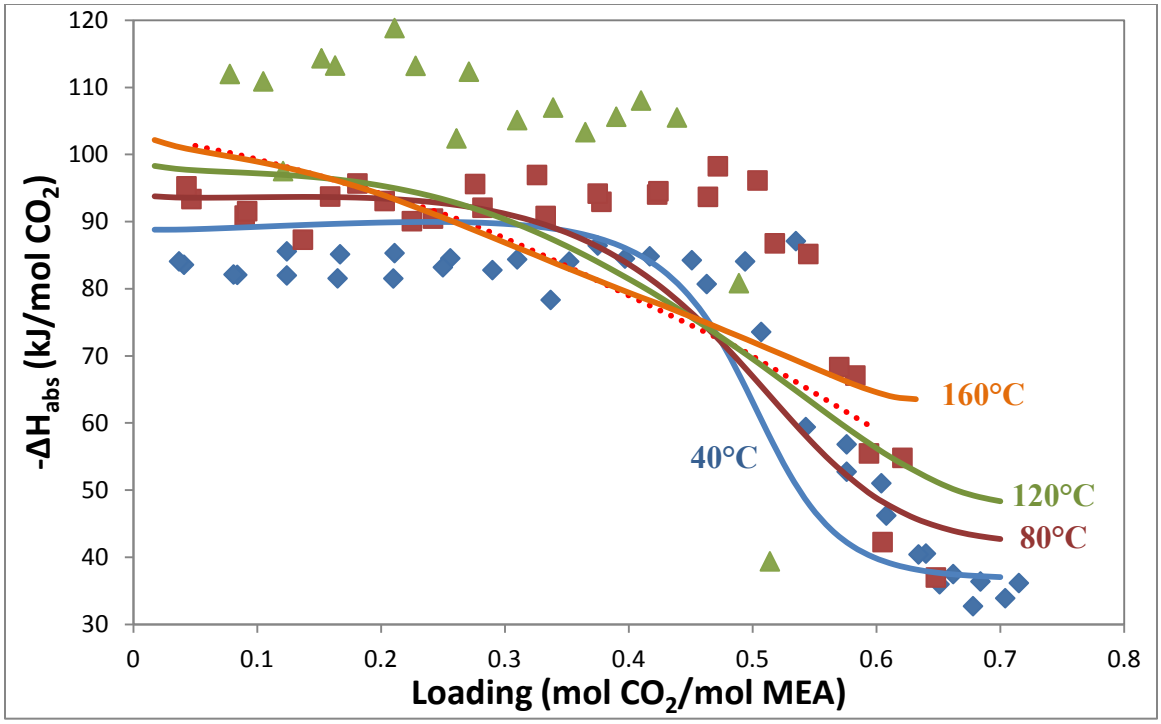

Figure 4-22: Comparison of Heat of Absorption of CO_2 in 7 m MEA by Model B.
Data points: Kim et al. (2007), ♦: 40°C, ■: 80°C, ▲: 120°C; solid lines: Model B; dotted line: empirical model from this work (Table 2-12).

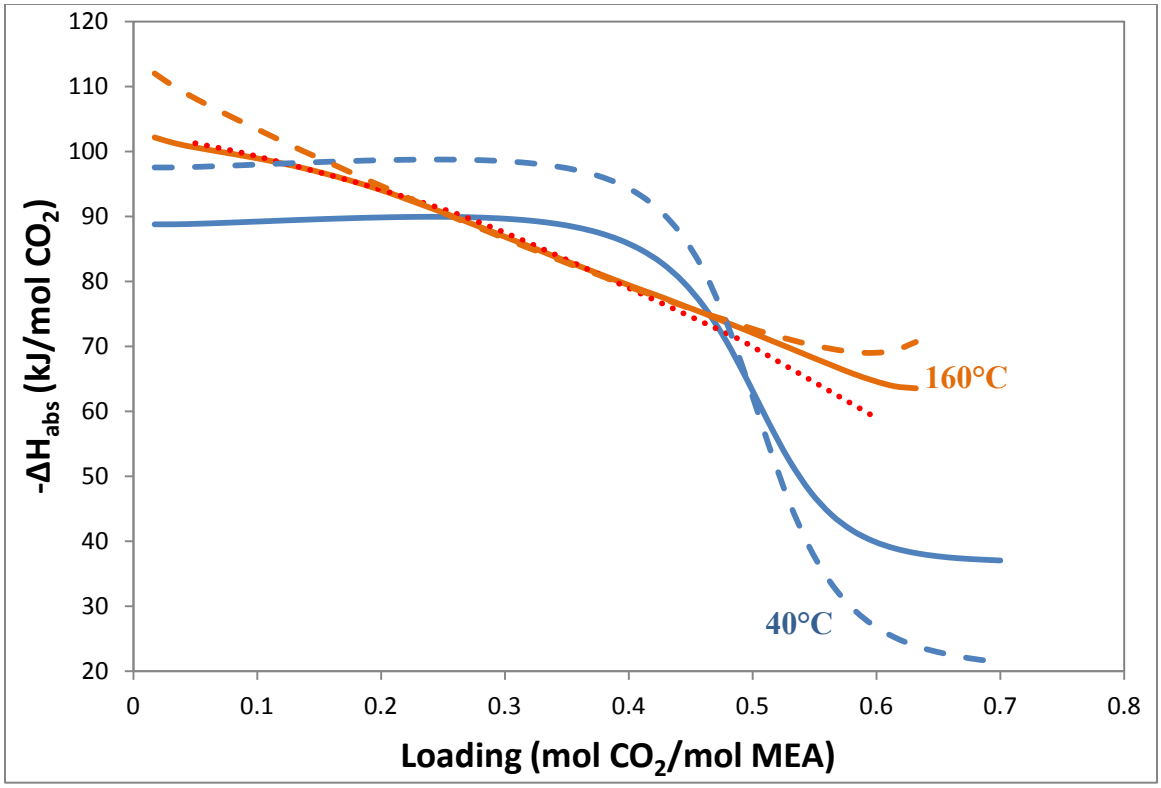

Figure 4-23: Comparison of Heat of Absorption of CO_2 in 7 m MEA. Solid lines: Model B; dashed lines: Model A; dotted line: empirical model from this work (Table 2-12).

Figures 4-24 and 4-25 compare the prediction of the normalized MEA volatility by Model A and B. The same data sets are presented; Figure 4-25 uses CO_2 loading as the horizontal axis instead of P_{CO2}. Since the 40°C MEA volatility data were considered with error and not used in the regression, only the other temperature data were compared. Model B predicts data well except a few outliers at 60 °C with high loading, where bigger experimental errors are expected. Generally Model B predicts better than Model A, compared with the experimental data. Figure 4-26 presented a favorable comparison of MEA volatility in 7 m MEA with Model B.

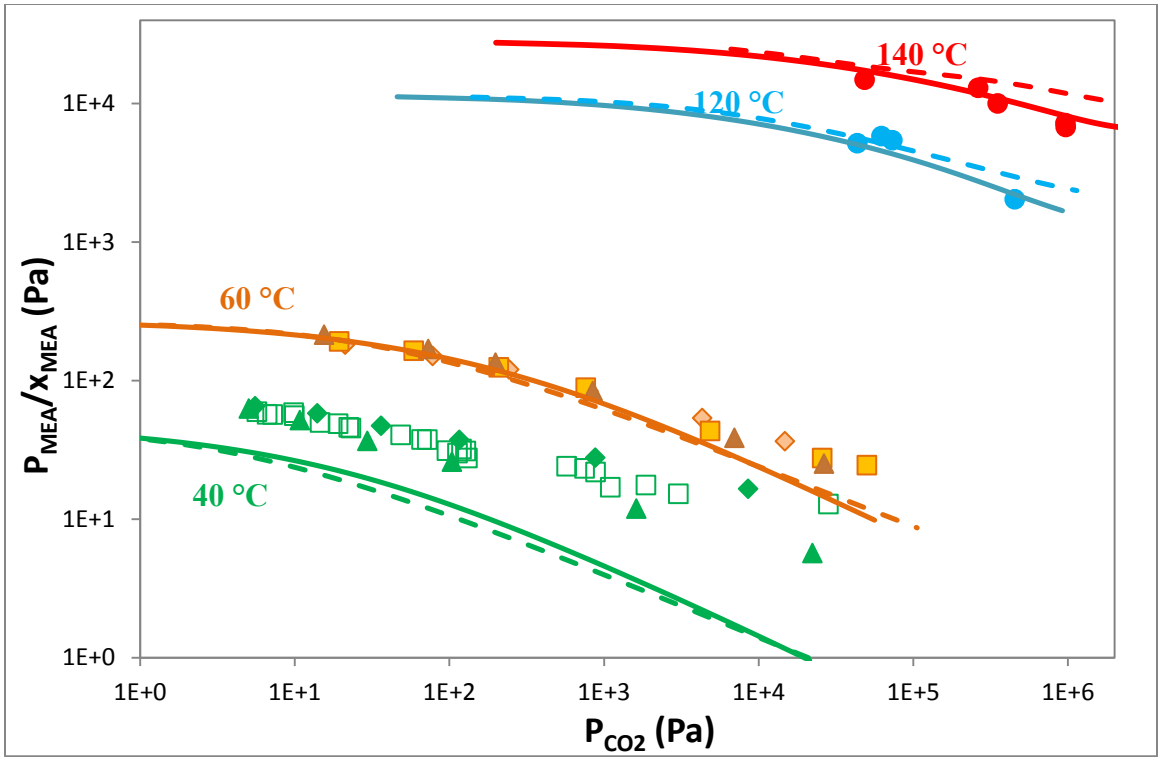

Figure 4-24: Prediction of Normalized MEA Partial Pressure over MEA-CO_2-H_2O (1) with Models A and B. Hilliard (2008) MEA: ♦ 3.5 m, ■ 7 m, ▲ 11 m; ●: this work; solid lines: Model B - 7 m MEA; dashed lines: Model A – 7 m MEA. $x_{MEA} = \frac{\text{mol of total MEA}}{\text{mol of total MEA + mol of } H_2O}$.

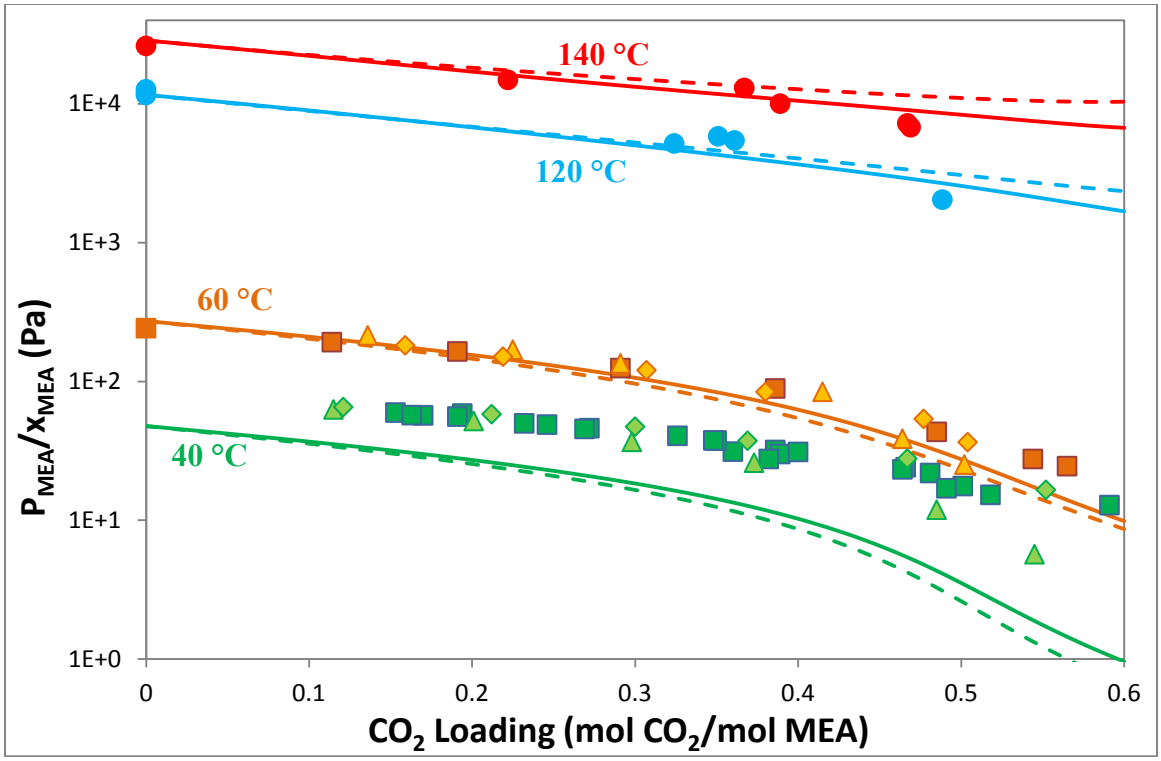

Figure 4-25: Prediction of Normalized MEA Partial Pressure over MEA-CO_2-H_2O (2) with Models A and B. Hilliard (2008) MEA: ♦ 3.5 m, ■ 7 m, ▲ 11 m; ●: this work; solid lines: Model B - 7 m MEA; dashed lines: Model A.

$$x_{MEA} = \frac{\text{mol of total MEA}}{\text{mol of total MEA + mol of } H_2O}.$$

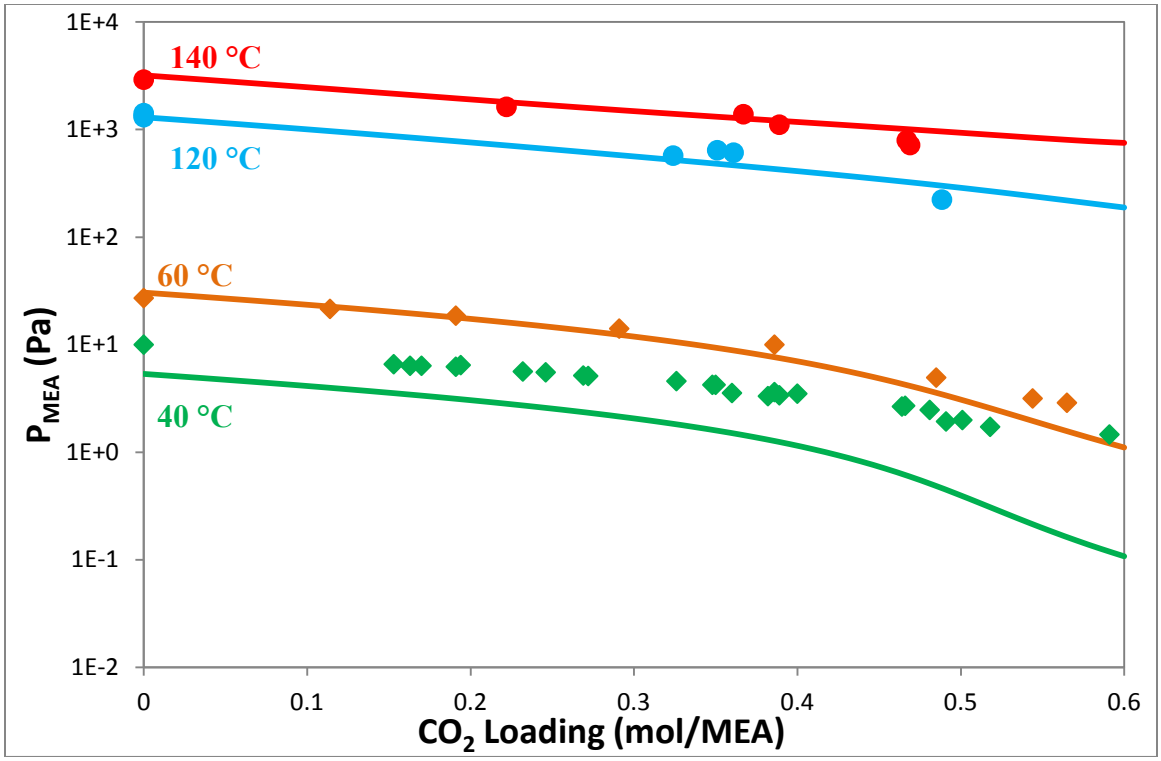

Figure 4-26: Prediction of MEA Partial Pressure over 7 m MEA by Model B. ♦: Hilliard (2008); ●: this work; lines: Model B.

Figure 4-27 gives a comparison of the MEA enthalpy of vaporization in 7 m MEA. $-\Delta H_{vap,MEA}$ was calculated using the same deferential method as in Model A. $-\Delta H_{vap,MEA}$ by Model B is larger than the value given by Hilliard's MEA model (Figure 3-11), probably because new MEA volatility data were included in Model B and previous data below 46°C were deleted from the regression. Comparing with Model A, Model B's prediction of $-\Delta H_{vap,MEA}$ is more constant at 80 to 160°C at low CO_2 loading, and is smaller within the whole studied temperature and loading range.

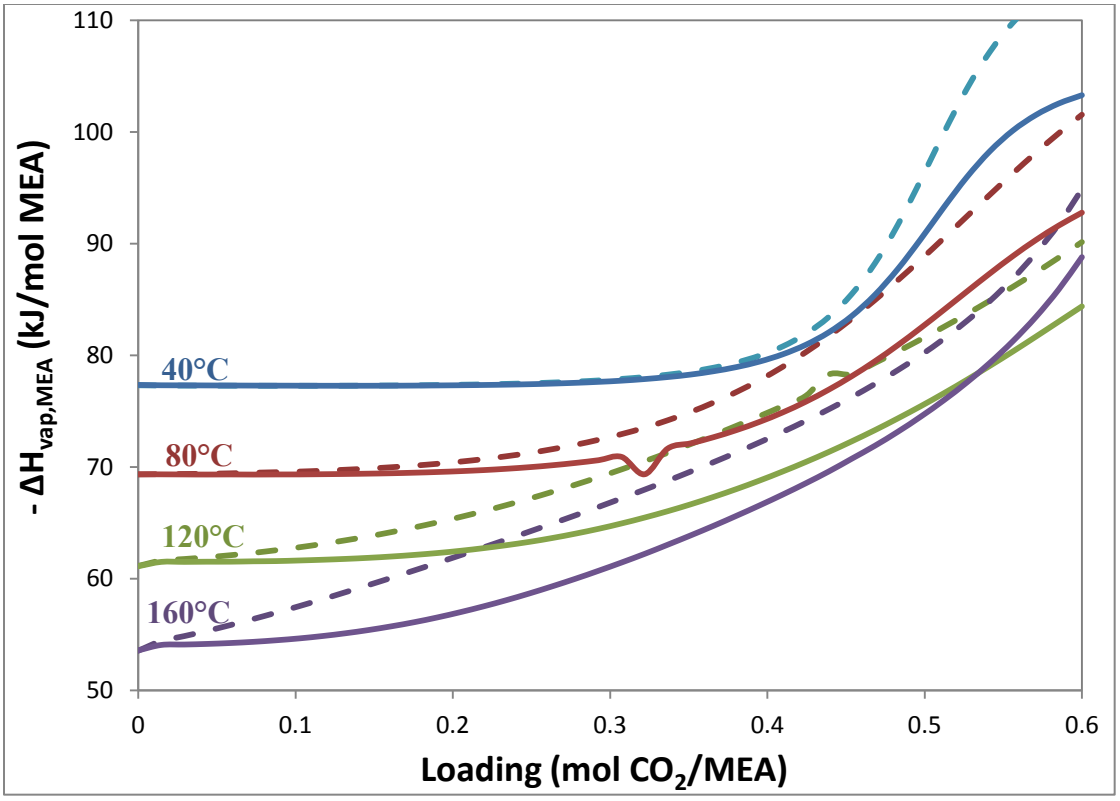

Figure 4-27: Comparison of Enthalpy of Vaporization of MEA in 7 m MEA with Models A and B. **Solid lines: Model B; dashed lines: Model A.**

Figure 4-28 gives the prediction of total pressure over CO_2 loaded 7 m MEA by Model A and B. Like Model A, Model B predicts well at low CO_2 loading, but under-predicts the data at high loading. Comparing with Figure 4-21, Model B may under-predict P_{CO2} at loading above 0.47 and at high temperature. The total pressure data by Aronu et al. (2011) was not incorporated in Model B, and there are some differences between the total pressure data by Aronu et al. (2011) and from this work as shown in Figure 4-28.

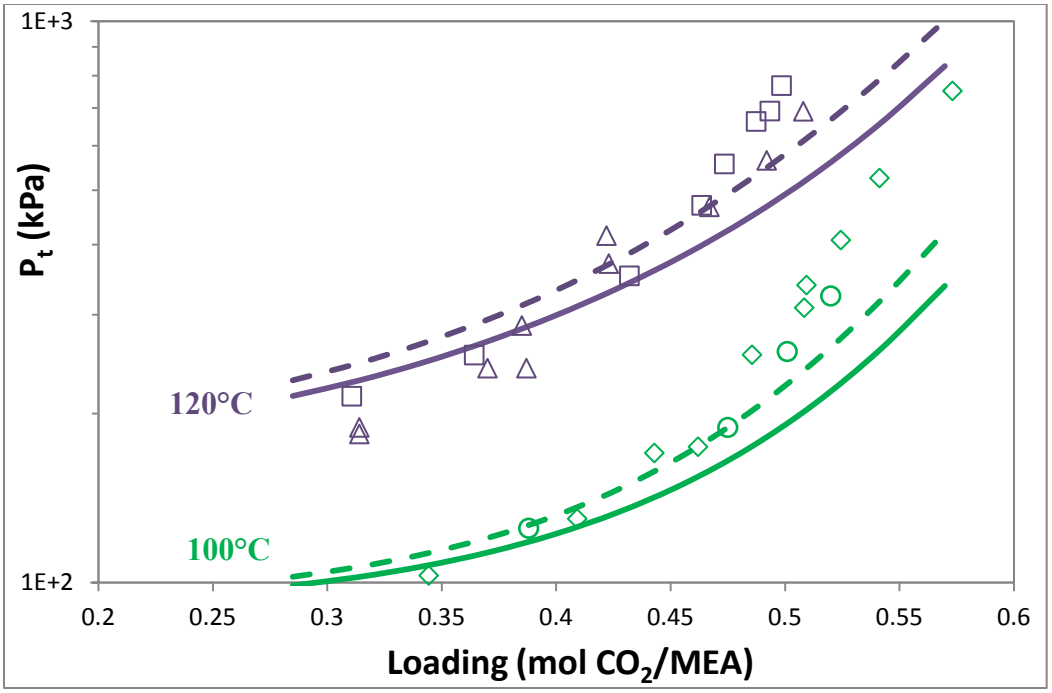

Figure 4-28: Comparison of Prediction of Total Pressure in 7 m MEA with Models A and B. **○: 100°C this work; ◊: 100°C Aronu et al. (2011); Δ: 120°C this work; □: 120°C Aronu et al. (2011); Lines: Model B.**

Figures 4-29 and 4-30 are the specific heat capacity comparison of Model A, Model B, and experimental data. Both the models fairly predict the data and the temperature dependence of the specific heat capacity.

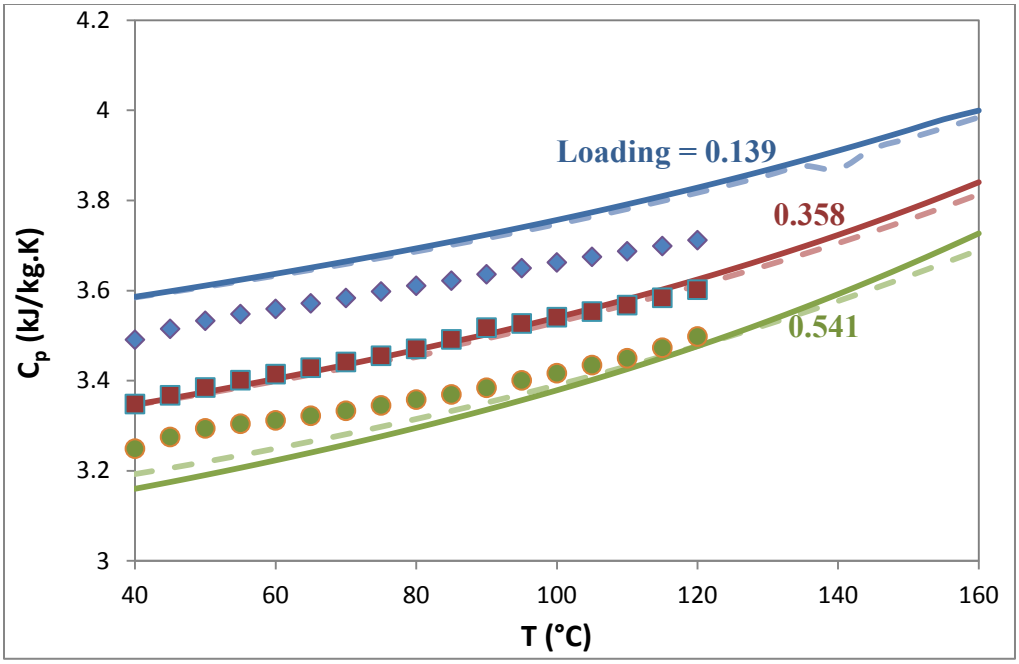

Figure 4-29: Prediction of Specific Heat Capacity in 7 m MEA by Models A and B.
Experimental data points (Hilliard 2008): ♦ 0.139 loading, ■ 0.358 loading, ● 0.541 loading; solid lines: Model B; dashed lines: Model A.

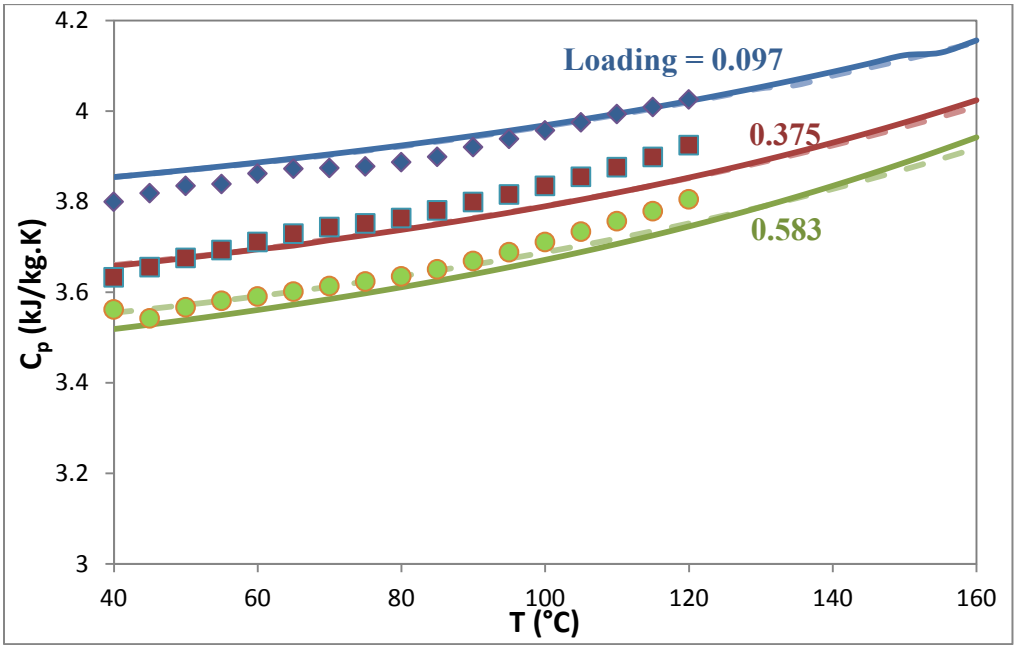

Figure 4-30: Prediction of Specific Heat Capacity in 3.5 m MEA by Models A and B.
Experimental data points (Hilliard 2008): ♦ 0.097 loading, ■ 0.375 loading, ● 0.583 loading; solid lines: Model B; dashed lines: Model A.

Figure 4-31 and 4-32 compares the predicted speciation by Model A, Model B and the experimental NMR data. Figure 4-32(b) is the enlarged high concentration and high loading part of Figure 4-32(a). The experimental data were by NMR, which cannot separate MEA from $MEAH^+$, or separate $MEACOO^-$ from MEACOOH, therefore the data reported were in concentration of MEA/$MEAH^+$, $MEACOO^-$, and HCO_3^-, and are compared with Model A and B prediction for MEA/$MEAH^+$, $MEACOO^-$/MEACOOH, and HCO_3^-, respectively. Both of the models well predict the data over the whole CO_2 loading range. Notice that the Model B predicted $MEACOO^-$/MEACOOH curve at high loading matches Poplsteinava et al. (2005) data well, and generally Model B predicts the Poplsteinava et al. (2005) data better and Model A predicts the Bottinger et al. (2008) data better. Model B under-predicts HCO_3^- concentration at low loading, but the concentration is less than 0.1% and the data scatter which reduces the importance.

Figure 4-33 shows the full speciation profile by Model B.

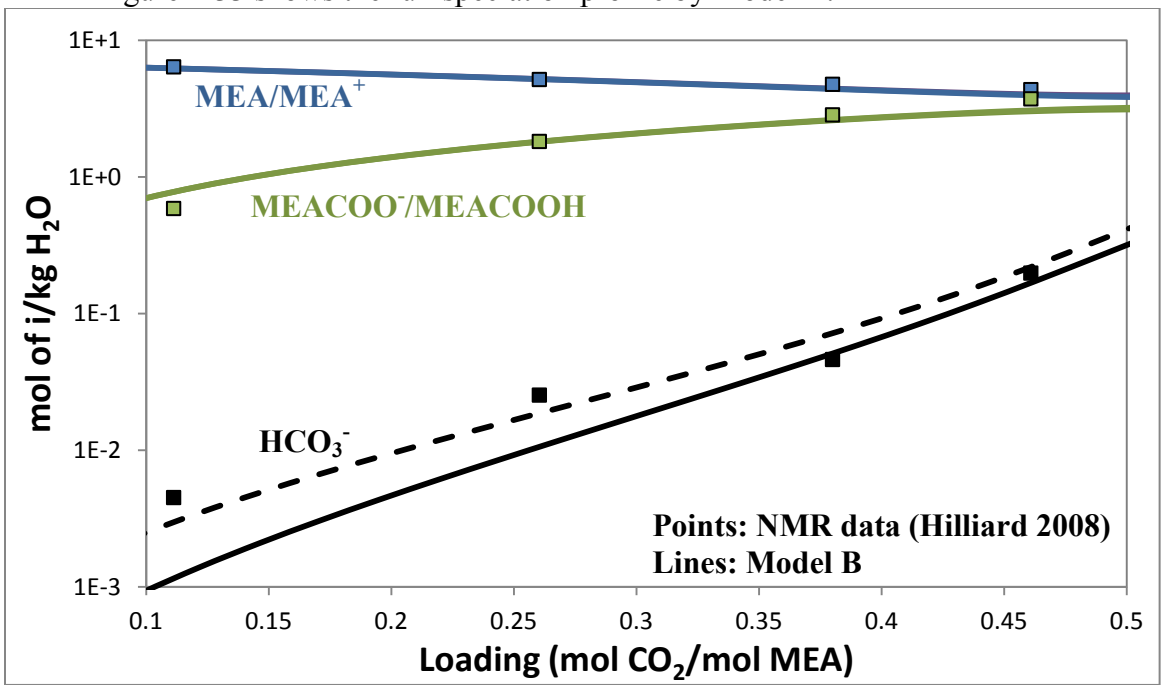

Figure 4-31: Comparison of Speciation in 7 m MEA at 40 ℃ (1) by Models A and B

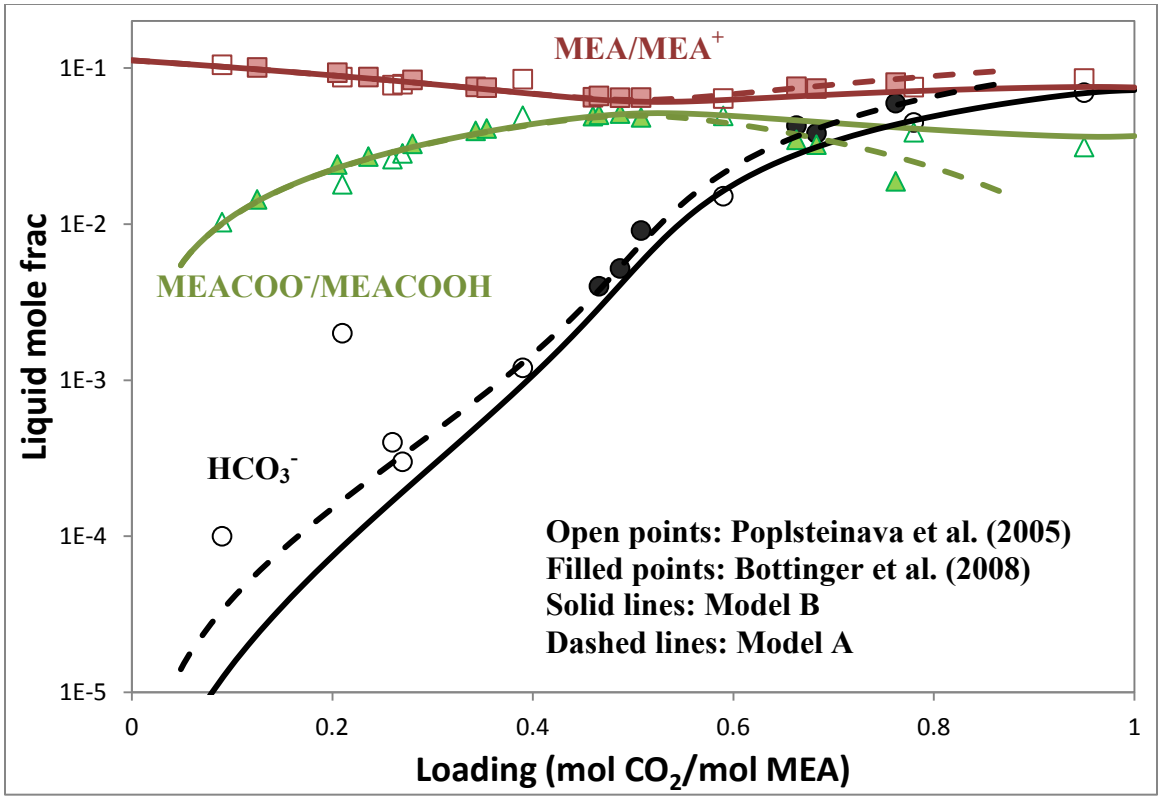

Figure 4-32 (a): Comparison of Speciation in 7 m MEA at 40 ℃ (2) with Models A and B

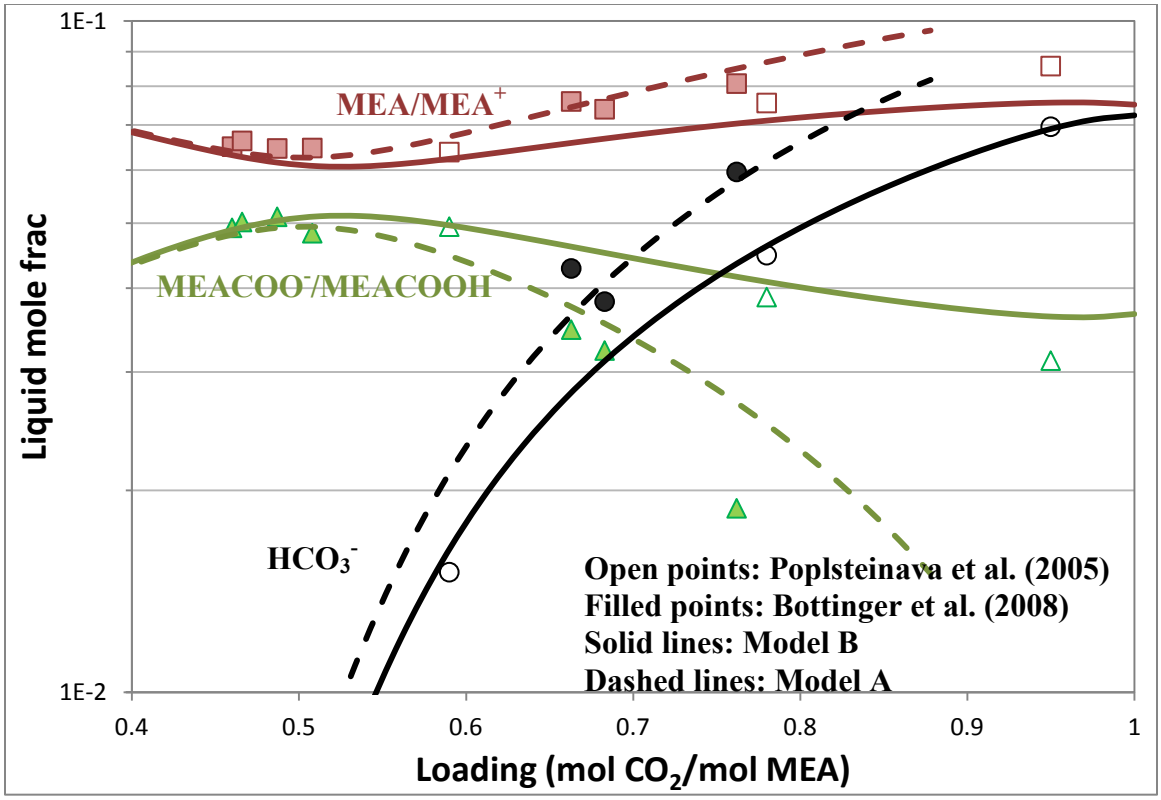

Figure 4-32 (b): Comparison of Speciation in 7 m MEA at 40 ℃ (2) with Models A and B

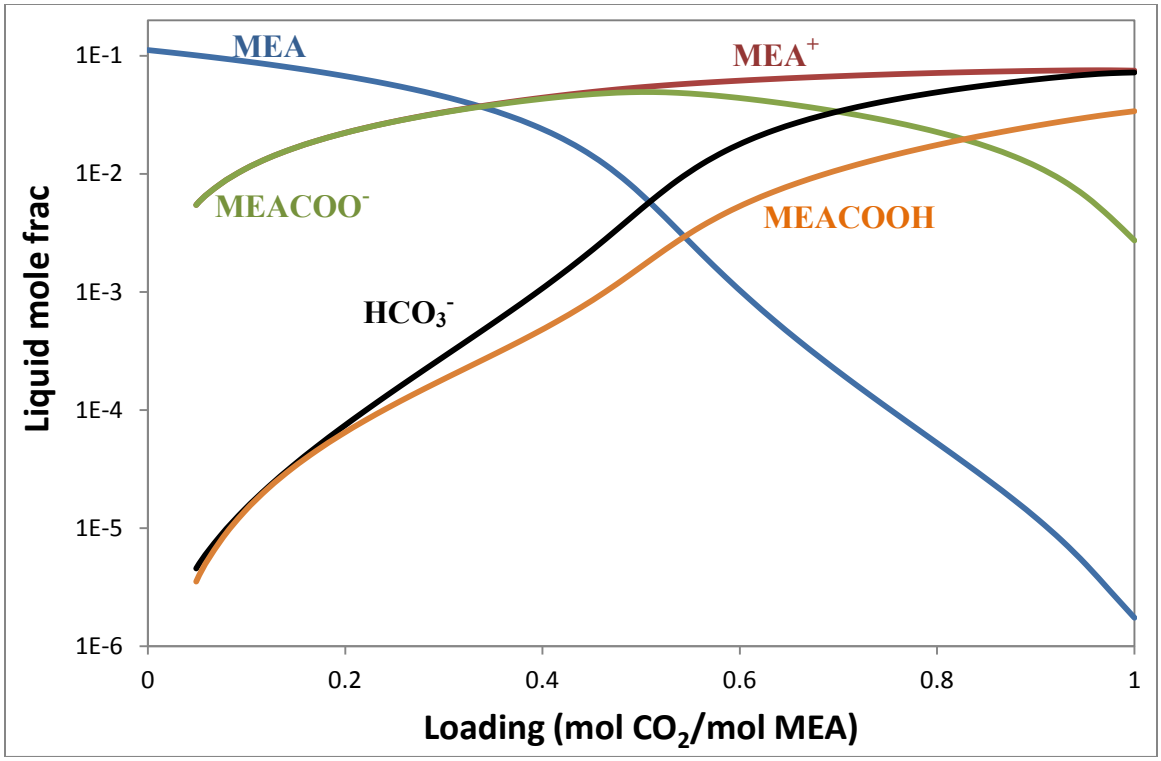

Figure 4-33: Speciation Prediction of 7 m MEA at 40 ℃ by Model B

Similarly, Figure 4-34 to 4-37 give the comparison of Model B speciation prediction and NMR experimental data. Model B predicts the data well, except for a few outliers.

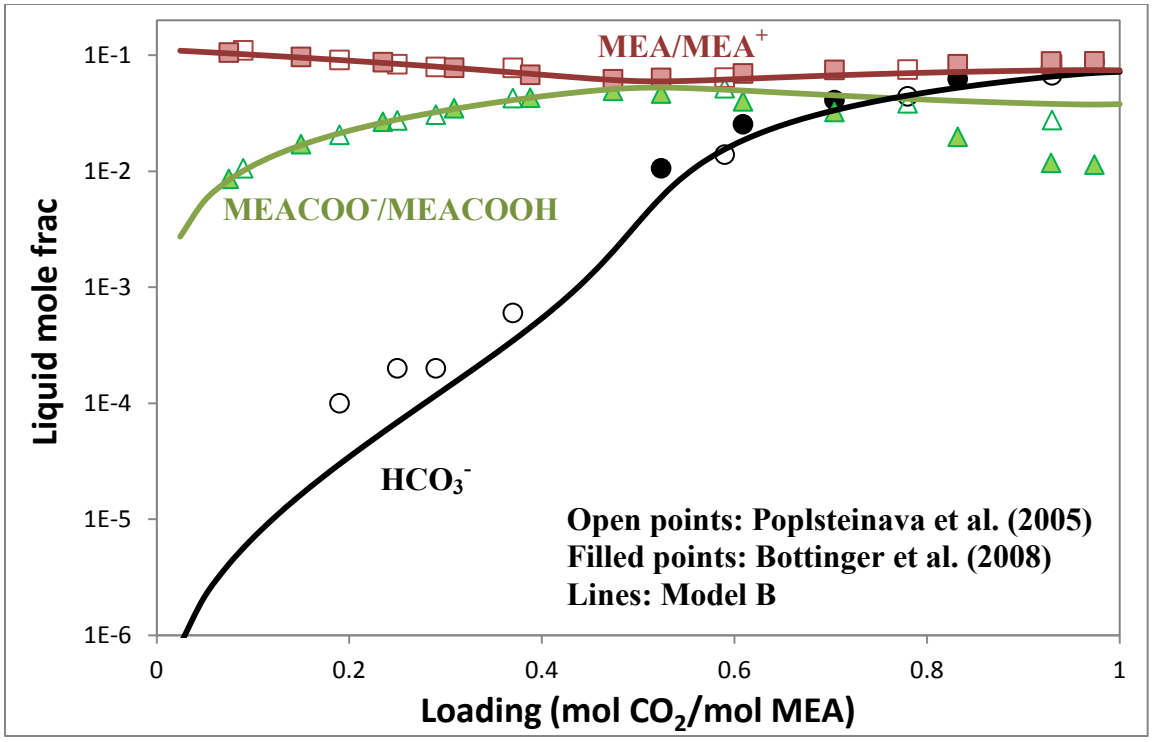

Figure 4-34: Comparison of Speciation of 7 m MEA at 20 ℃ with Model B

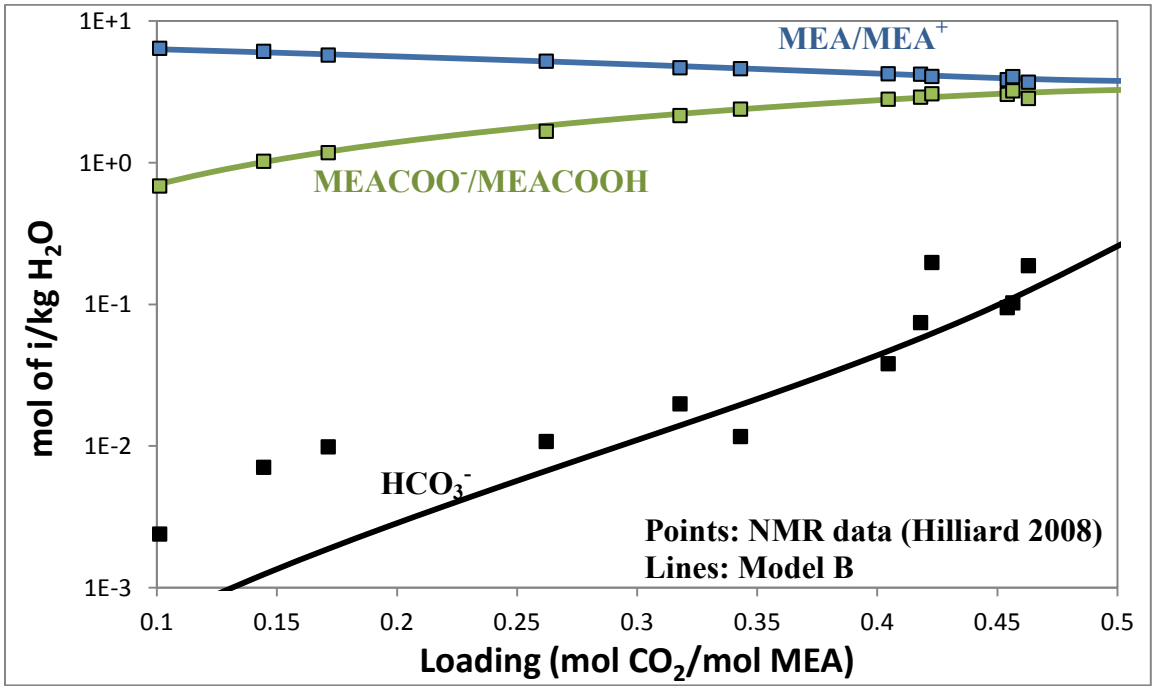

Figure 4-35: Comparison of Speciation of 7 m MEA at 27 ℃ with Model B

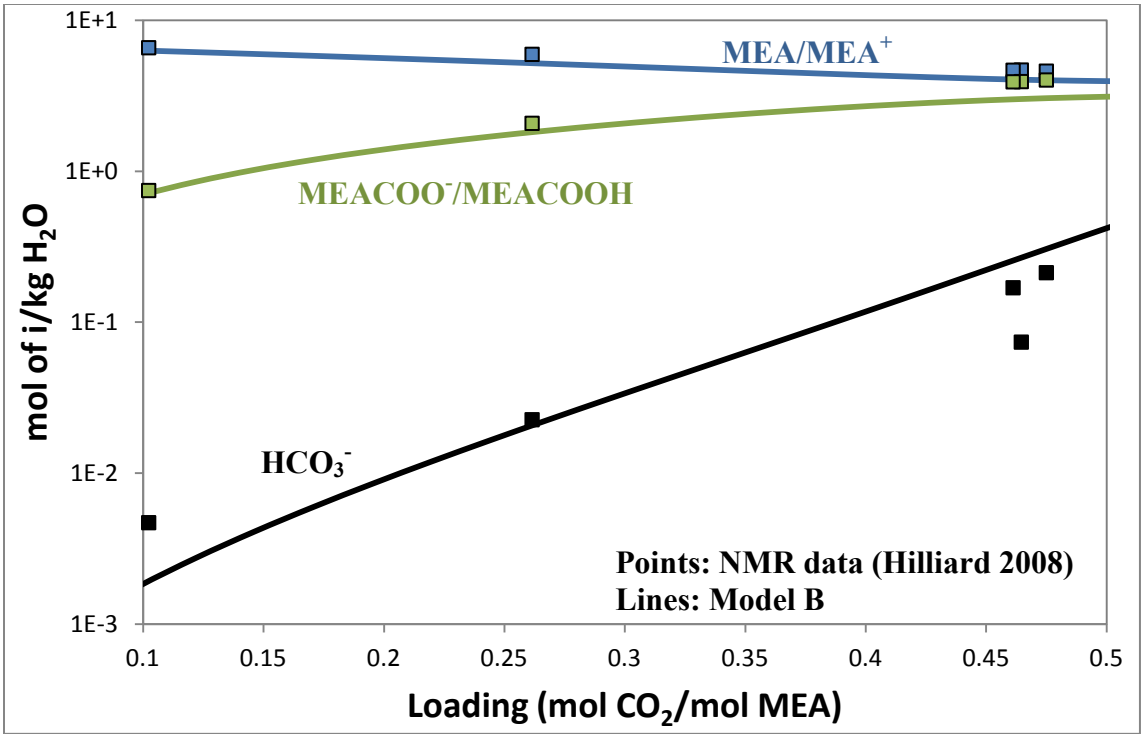

Figure 4-36: Comparison of Speciation of 7 m MEA at 60 ℃ (1) with Model B

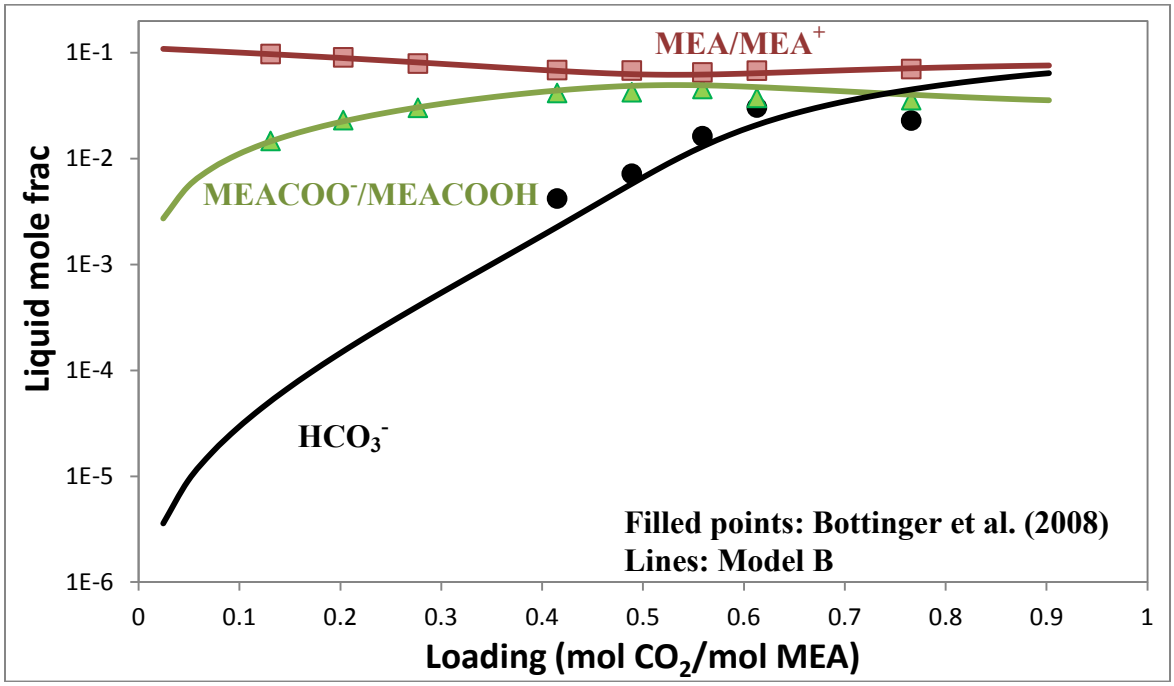

Figure 4-37: Comparison of Speciation of 7 m MEA at 60 ℃ (2) with Model B

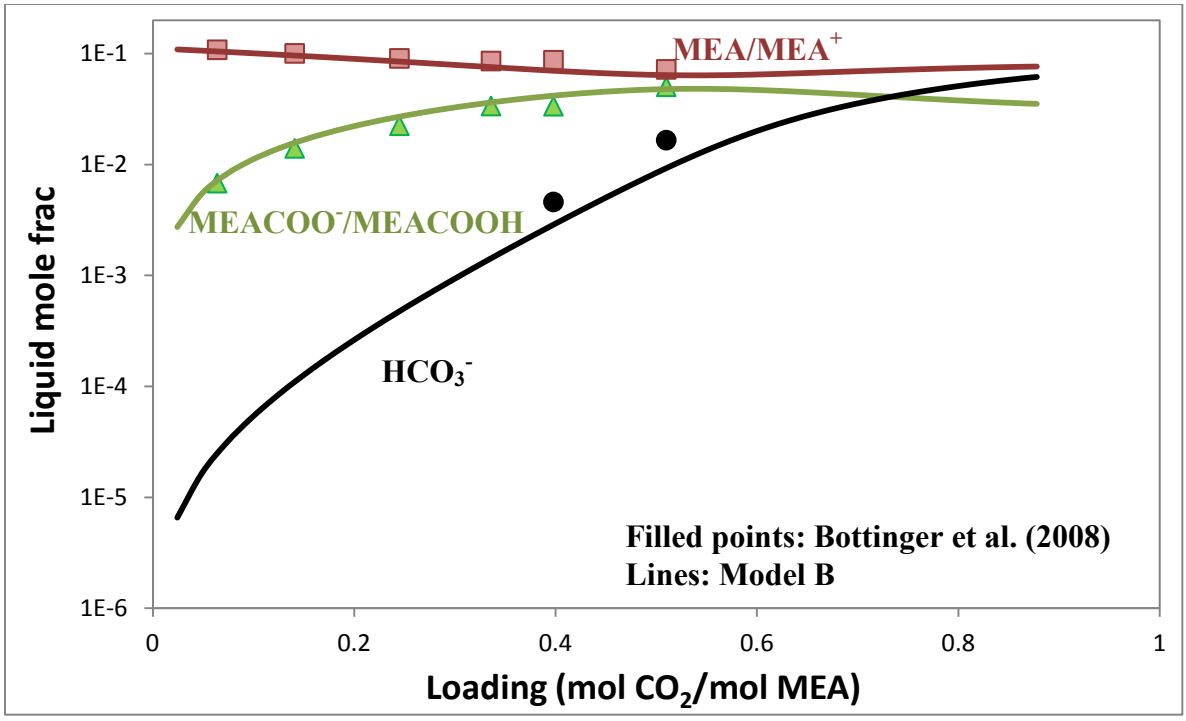

Figure 4-38: Comparison of Speciation of 7 m MEA at 80 ℃ with Model B

160°C speciation of 7 m MEA by Model B is shown in Figures 4-39 and 4-40. Comparing with 40°C speciation, less MEA reacts with CO_2 at 160°C; there is more HCO_3^- and MEACOOH at low loading and less at high loading at 160°C; there is more MEACOO- at low loading (<0.7) and less of it at high loading (>0.7) at 160°C. Therefore, in the practical rich loading range (0.45-0.55), there is more HCO_3^- and MEACOOH in the solution and this will affect other thermal properties. Figure 4-41 is the same as Figure 4-40 except for using a linear y-axis.

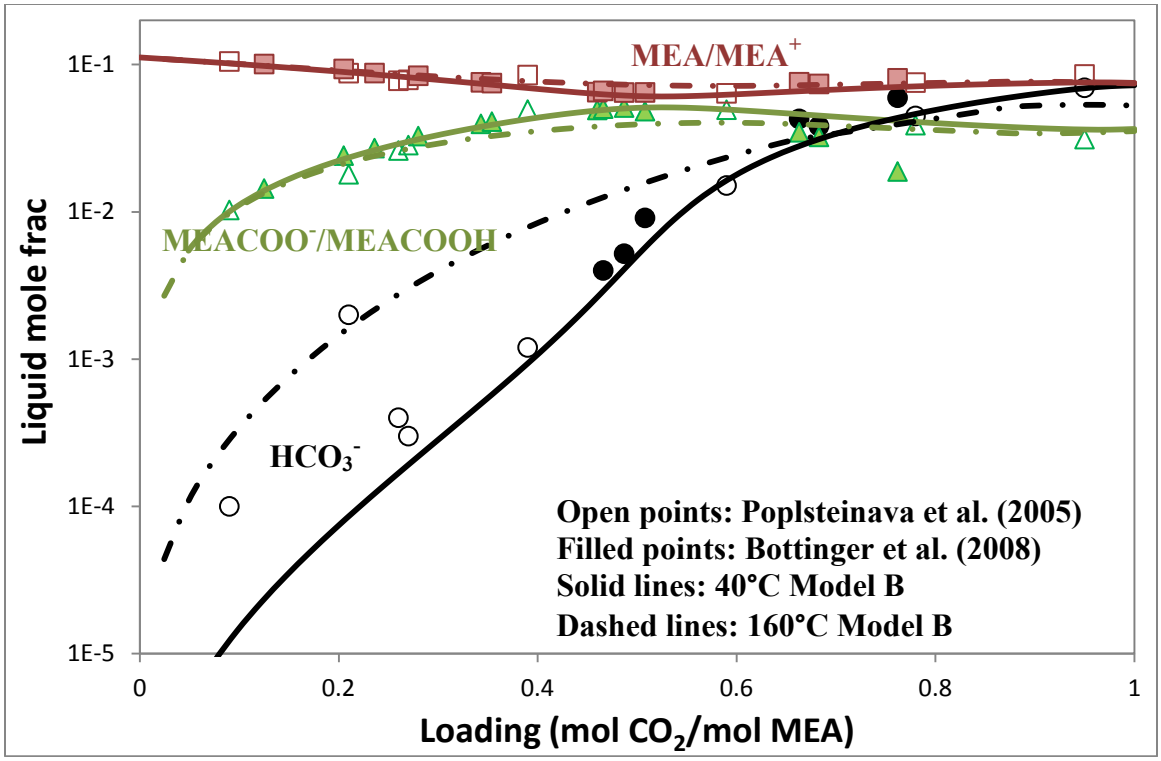

Figure 4-39: Comparison of Speciation of 7 m MEA at 40 and 160 ℃ (1) by Model B

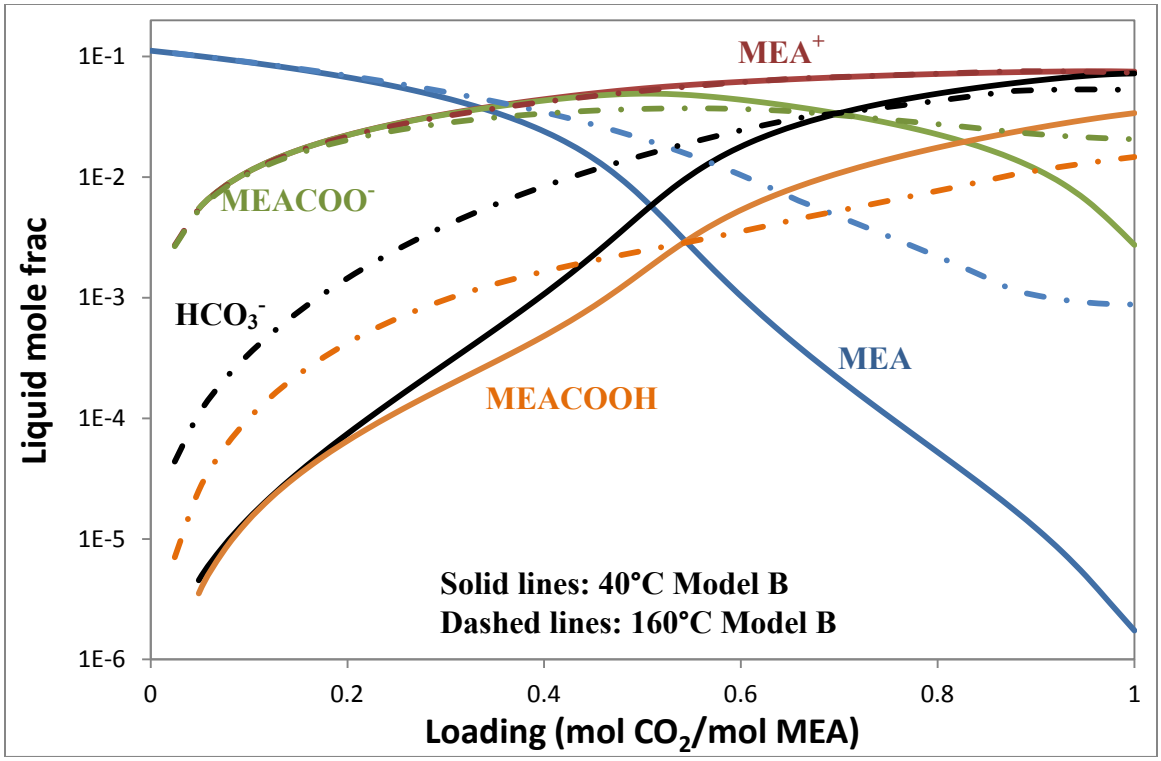

Figure 4-40: Comparison of Speciation of 7 m MEA at 40 and 160 ℃ (2) by Model B

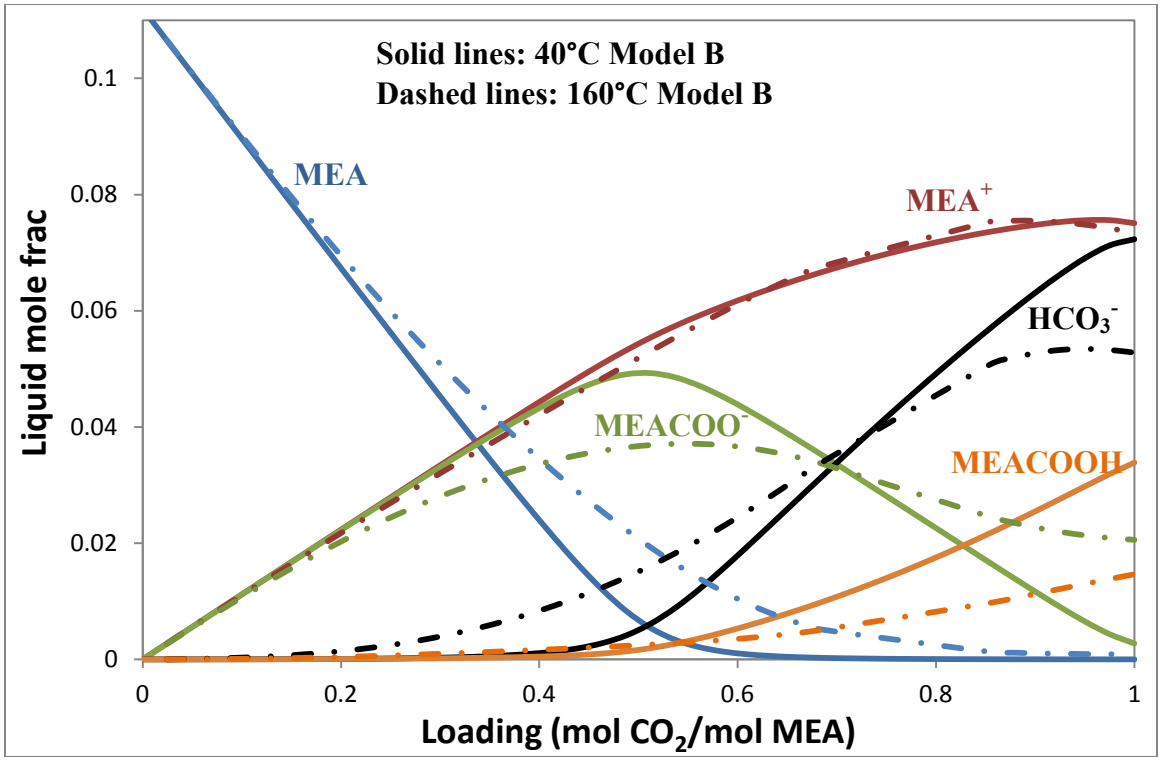

Figure 4-41: Comparison of Speciation of 7 m MEA at 40 and 160 ℃ (3) by Model B

4.4.3 Sensitivity Analysis

Because no effective standard deviation of the DHFORM of MEACOOH was given by Aspen Plus®, a sensitivity analysis was performed to the DHFORM of MEACOOH.

In Aspen Plus® Property Analysis, by changing the value of DHFORM of MEACOOH while fixing all the other parameters as in Model B, a new set of prediction can be obtained and compared with Model B and the measured data.

Table 4-17: Sensitivity Analysis of DHFORM of MEACOOH

	Value in Model B	Value in the Sensitivity Analysis	Difference
DHFORM (kJ/mol)	-746.6	-731.6	15.0

Figure 4-42 through 4-47 show the comparison of some properties between Model B and the sensitivity analysis. The new pK_a of MEACOOH at 30°C is 7.45, while it is 7.49 in Model B. And as shown in Figure 4-42, the temperature dependence of pK_a from the sensitivity analysis is larger than that in Model B. Figure 4-43 shows that after changing DHFORM of MEACOOH, the prediction curves deviate more from the experimental data, especially at high temperature and high CO_2 loading. Partial pressure of MEA changes very little in this analysis so the P_{MEA} is almost the same as in Figure 4-24 to 4-26.

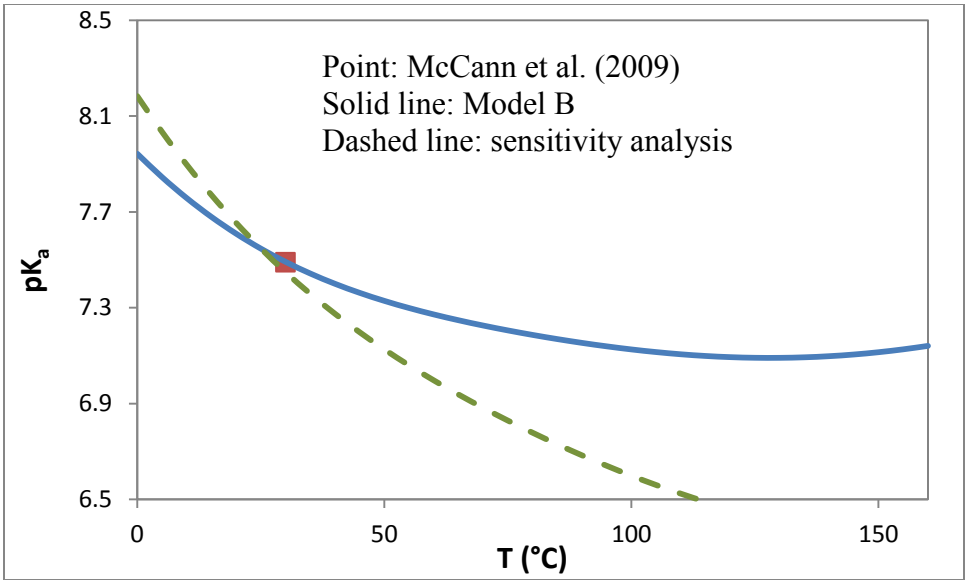

Figure 4-42 Sensitivity Analysis – pK_a of MEACOOH, Molarity Based, Asymmetric

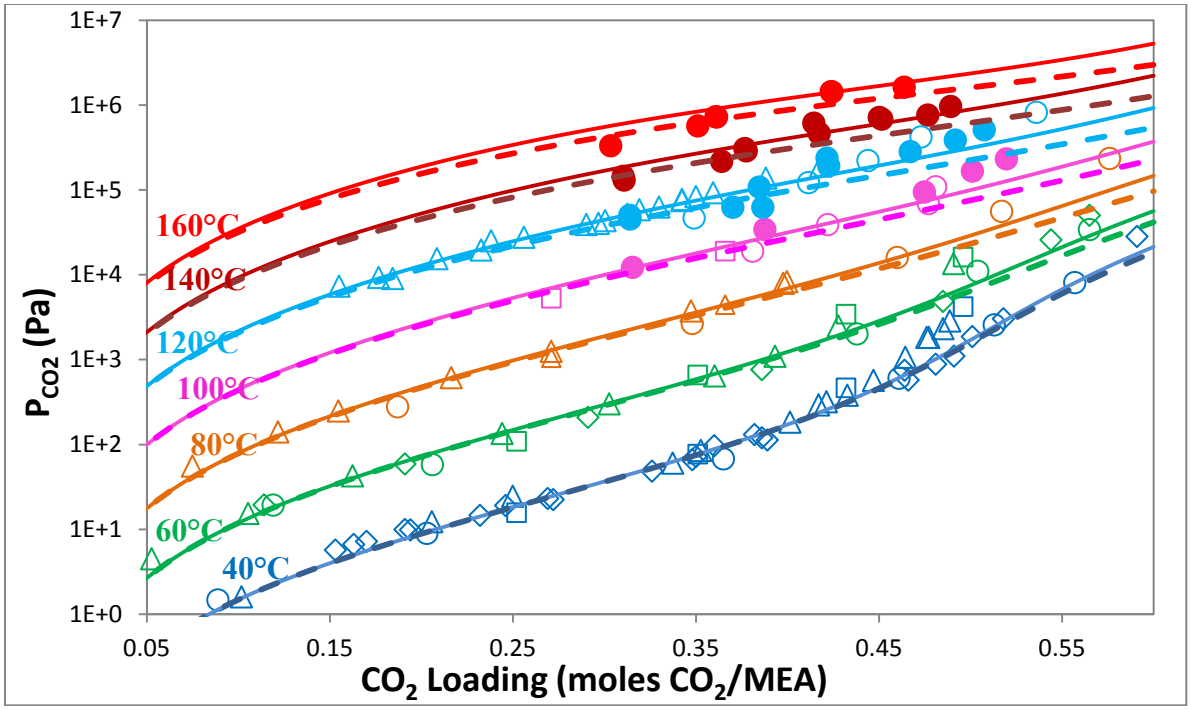

Figure 4-43: Sensitivity Analysis – CO_2 Solubility in 7 m MEA. **●: this work; ○: Jou et al. (1995); □: Dugas et al. (2009); ◊: Hilliard (2008); Δ: Ma'mun et al. (2005); solid lines: Model B for 7 m MEA; dashed lines: sensitivity analysis for 7 m MEA.**

Figure 4-44 presents the heat of absorption of CO_2 comparison. After reducing the absolute value of DHFORM of MEACOOH, $-\Delta H_{abs}$ decreases at 40 to 120°C, especially at 40 and 80°C with higher than 0.5 loading.

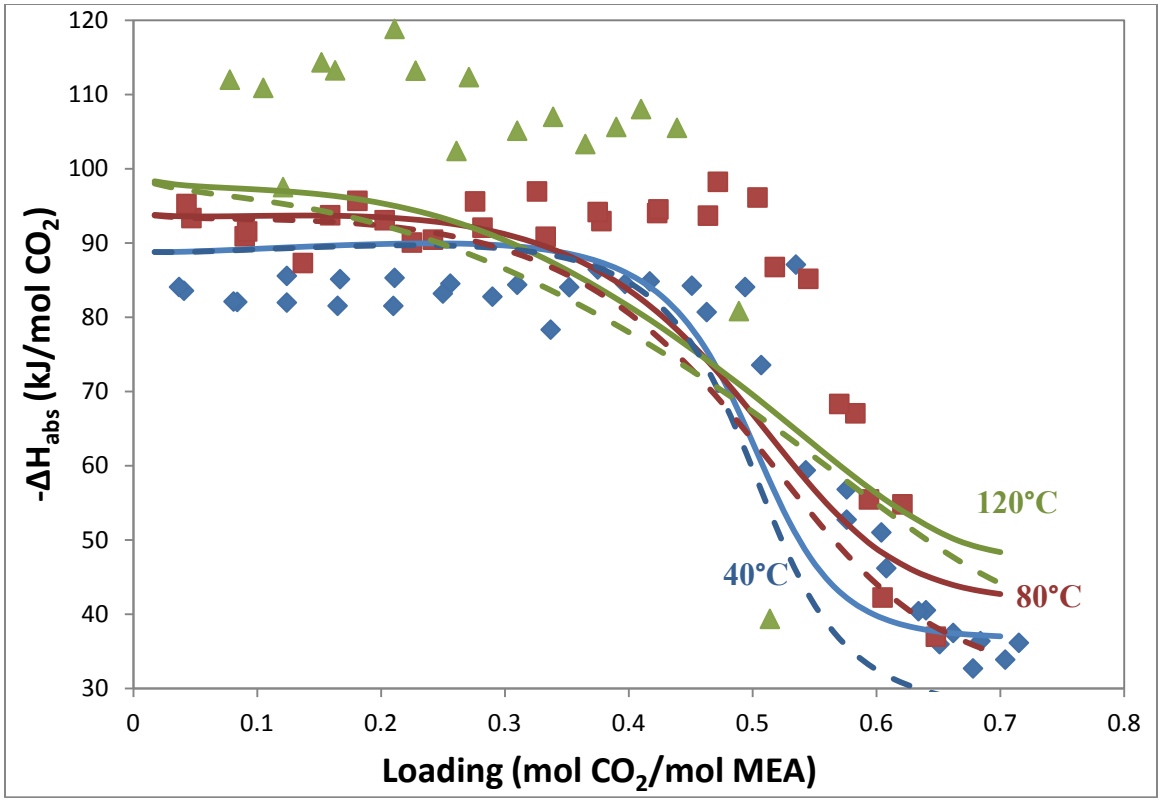

Figure 4-44: Sensitivity Analysis – Heat of Absorption of CO_2 in 7 m MEA. **Data points: Kim et al. (2007), ♦: 40°C, ■: 80°C, ▲: 120°C; solid lines: Model B; dashed line: sensitivity analysis.**

Figures 4-45 and 4-46 are the specific heat capacity analysis. C_p is further deviated from the data in the sensitivity analysis than in Model B at high temperature and high CO_2 loading.

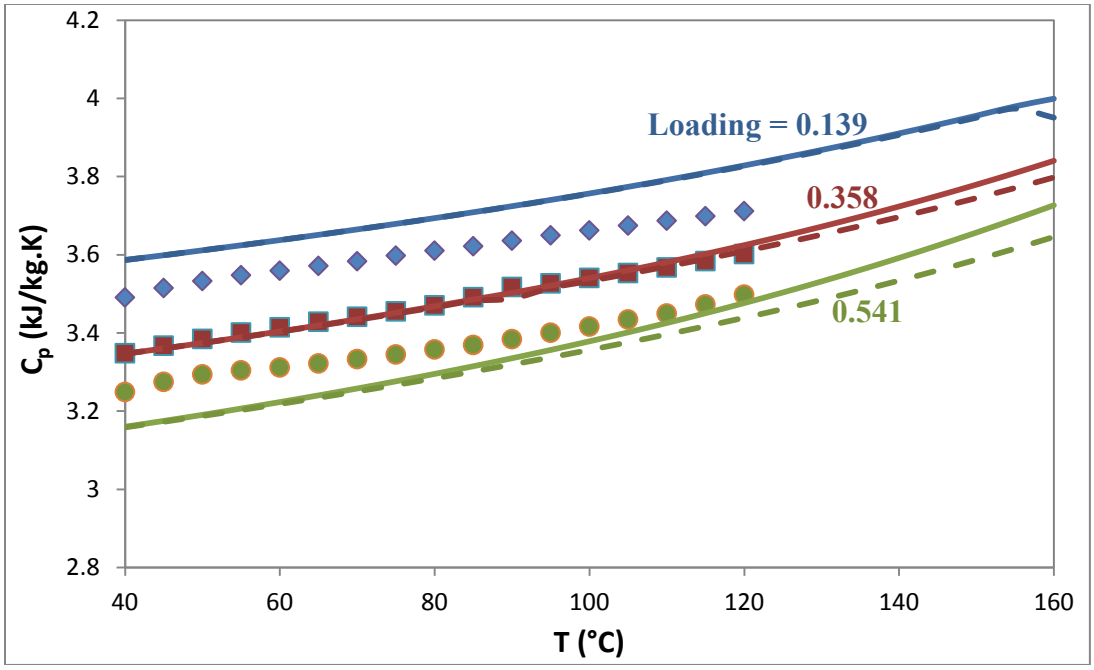

Figure 4-45: Sensitivity Analysis – Specific Heat Capacity of 7 m MEA.
Experimental data points (Hilliard 2008): ♦ 0.139 loading, ■ 0.358 loading, ● 0.541 loading; solid lines: Model B; dashed lines: sensitivity analysis.

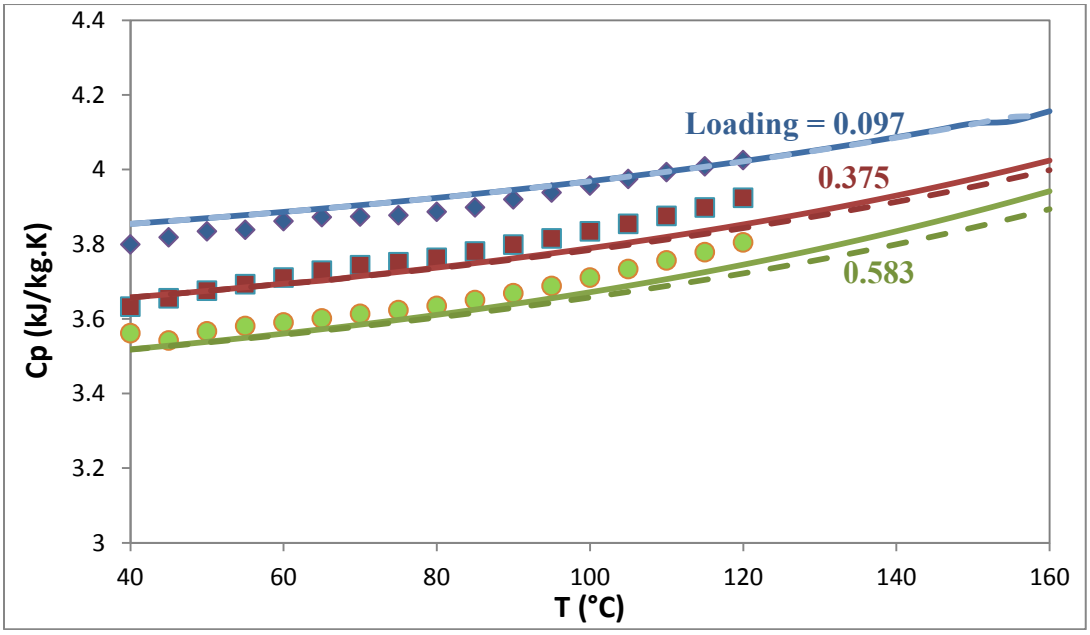

Figure 4-46: Sensitivity Analysis – Specific Heat Capacity of 3.5 m MEA.
Experimental data points (Hilliard 2008): ♦ 0.097 loading, ■ 0.375 loading, ● 0.583 loading; solid lines: Model B; dashed lines: sensitivity analysis.

Figure 4-47 is the sensitivity analysis for speciation in 7 m MEA. The differences between the results are very small, so the scale of y-axis is set to 0.01 - 0.2 to enlarge the difference on the plot. At higher than 0.6 loading, the prediction from sensitivity analysis deviates more from the experimental data and the Model B prediction.

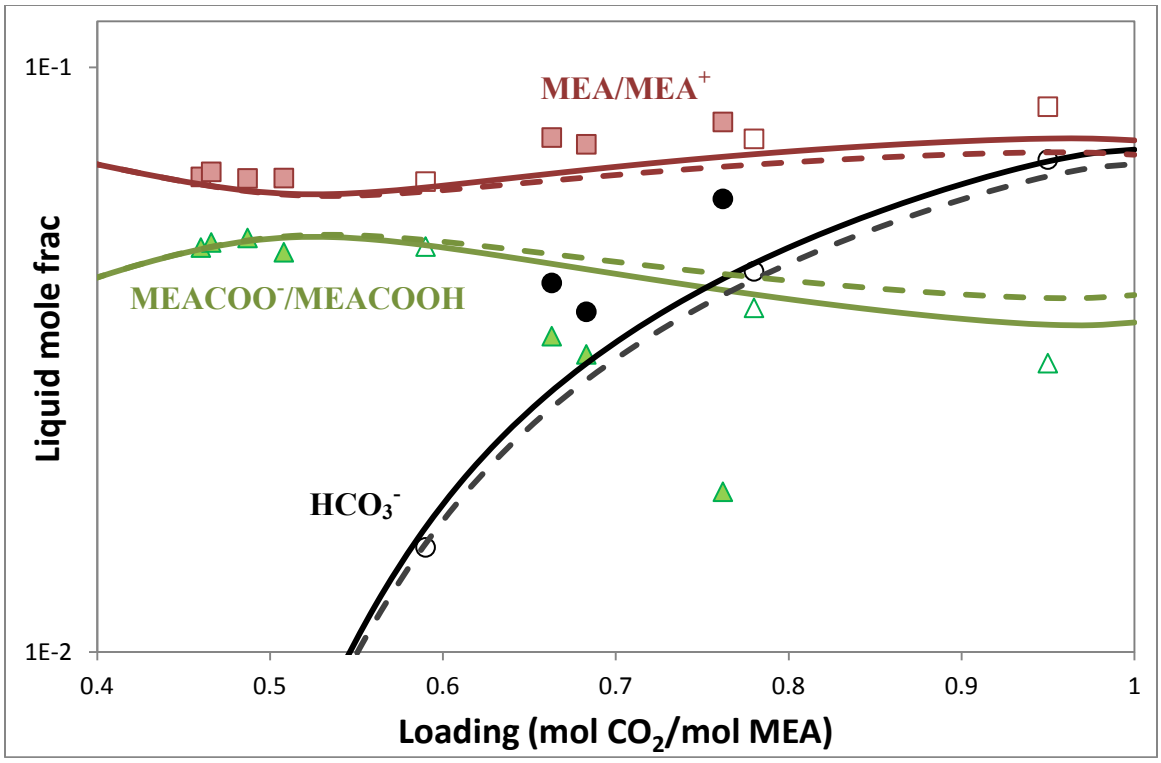

Figure 4-47: Sensitivity Analysis – Speciation in 7 m MEA at 40°C. **Open points: Poplsteinava et al. (2005); filled points: Bottinger et al. (2008); solid lines: Model B; dashed lines: sensitivity analysis.**

To conclude, after changing the value of DHFORM of MEACOOH by 15 kJ, CO_2 solubility and heat of absorption are affected more than the other properties and the prediction in the sensitivity analysis is not good to use, especially at high temperature and high loading.

4.4.4 Profile of 11 molal (40 wt%) MEA

11 m MEA or 40 wt% MEA has a high capacity, a fast reaction rate, and high heat of absorption. Assuming the lean and rich CO_2 loading corresponds to 0.5 and 5 kPa equilibrium P_{CO2} at 40°C, according to the empirical model for MEA in Table 2-11, the capacity of 7 and 11 m MEA are 0.50 and 0.66 mol CO_2 /kg (MEA+H_2O), respectively. If the stripping temperature increases from 120 to 140°C, the equivalent work of the CO_2 capture process can be reduced. The drawback of 11 m MEA is that the thermal degradation of MEA is high above 120°C. This may be solved by eliminating the residence time of high temperature processes. This section gives a profile of 11 m MEA by Model B for the design of CO_2 capture with high temperature stripping.

Figure 4-48 to 4-52 give the specific heat capacity, vapor-liquid equilibrium, heat of absorption, and speciation in 11 m MEA. In Figure 4-49 Model B prediction matches the CO_2 solubility data well except a few outliers at high loading 40 and 60°C. This may because the data incorporated in the regression in that range scatter and have two trends, as shown in Figure 4-21. Figure 4-50 presentes a favorable comparison of MEA volatility in 11 m MEA. Figure 4-51 indicates that the $-\Delta H_{abs}$ in 11 m MEA is a little larger than it is in 7 m MEA. According to Figure 4-52, in 11 m MEA, more MEACOOH is formed in the whole loading range, and it becomes an important species at high loading.

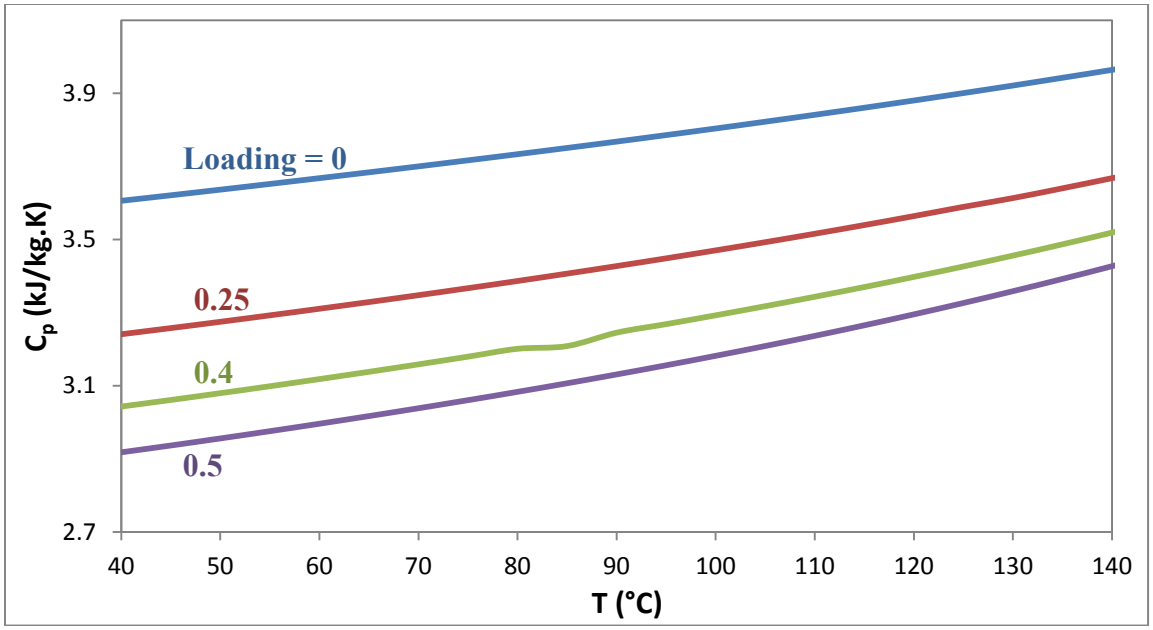

Figure 4-48: Specific Heat Capacity of 11 m MEA by Model B

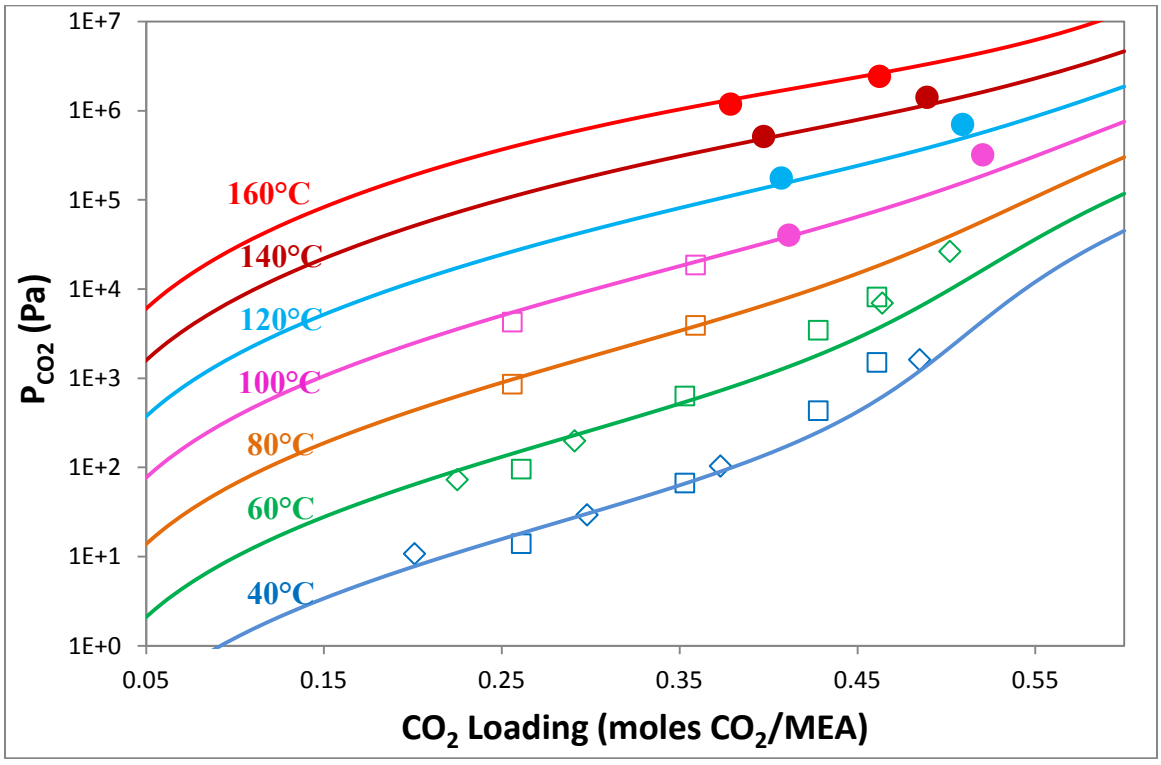

Figure 4-49: Prediction of CO_2 Solubility in 10.4-11 m MEA by Model B. ●: this work; □: Dugas et al. (2009); ◊: Hilliard (2008); lines: Model B for 11 m MEA.

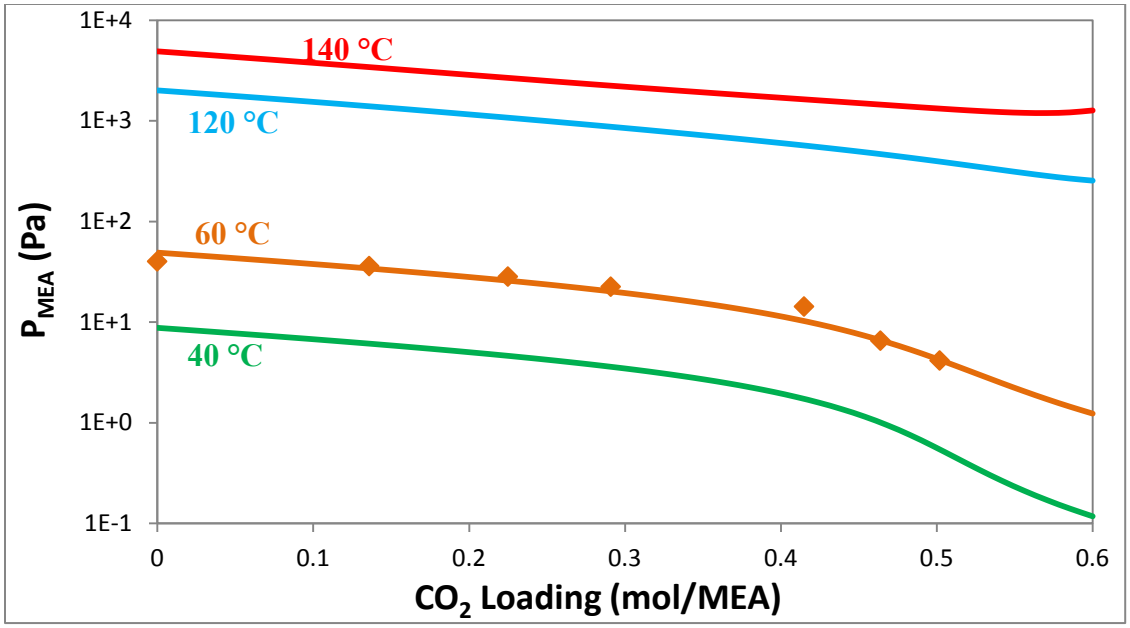

Figure 4-50: Prediction of MEA Partial Pressure over 11 m MEA by Model B.
Points: Hilliard (2008) 60°C 11 m MEA; lines: Model B - 11 m MEA.

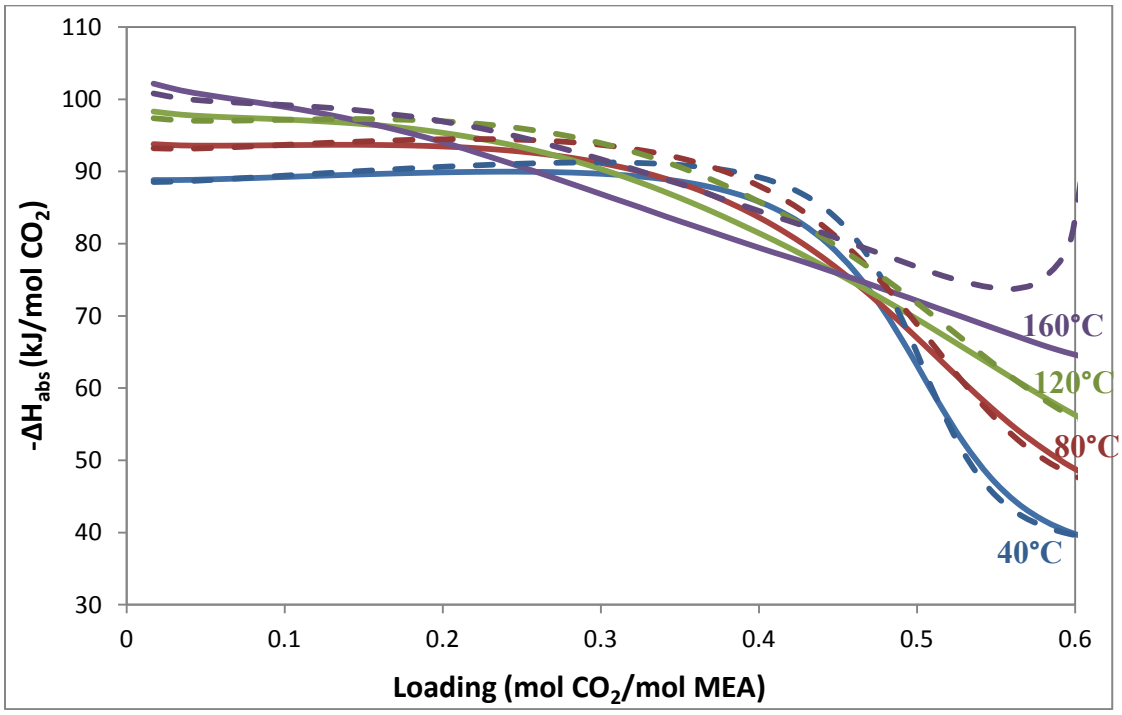

Figure 4-51: CO_2 Heat of Absorption in 7 and 11 m MEA by Model B. **Data points: Kim et al. (2007) 7 m MEA, ♦: 40°C, ■: 80°C, ▲: 120°C; solid lines: Model B - 7 m MEA; dashed lines: Model B - 11 m MEA.**

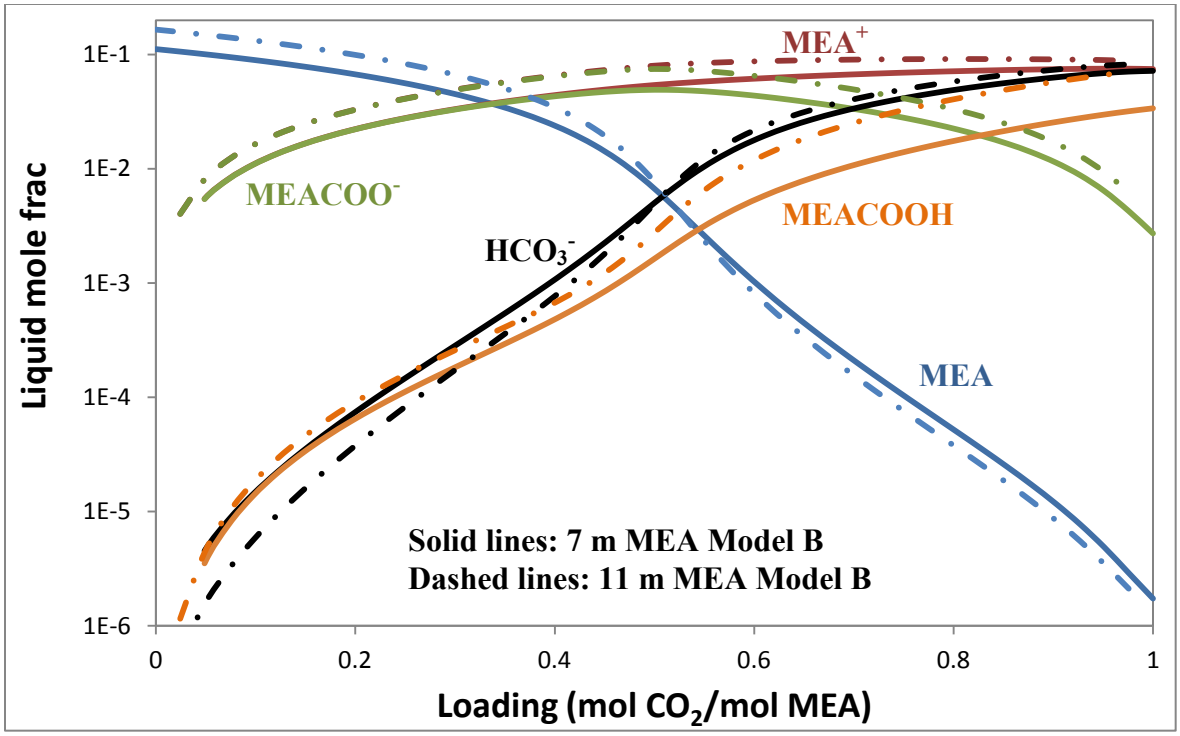

Figure 4-52: Speciation in 7 and 11 m MEA at 40°C by Model B

4.4.5 Model B Conclusions

For 7 m MEA, Model B well predicts CO_2 solubility except for a few outliers at high loading and high temperature; matches pK_a of MEACOOH; well predicts MEA volatility, specific heat capacity, and speciation. Reasonable CO_2 heat of absorption and enthalpy of MEA vaporization were obtained from Model B.

The speciation results show that at high temperature or high CO_2 loading, the concentration of MEACOOH is 0.1-3 % in 7 m MEA. The sensitivity analysis shows that the heat of formation of MEACOOH has an effect on CO_2 partial pressure and heat of absorption at high temperature and high loading. Therefore MEACOOH may be considered an important species at high loading or high temperature.

Model B also provides reasonable predictions of heat of absorption, speciation, and specific heat capacity for 11 m MEA.

4.5 CONCLUSIONS AND RECOMMENDATIONS

Two thermodynamic models in Aspen Plus® for the MEA-CO_2-H_2O system have been developed in this chapter: Model A without MEACOOH and Model B with MEACOOH. By comparing with experimental data of CO_2 solubility, MEA volatility, speciation, specific heat capacity, and total pressure, generally Model B gives a better prediction than Model A. Table 4-18 shows the result summary of Models A and B.

Table 4-18: Summary of Prediction by Models A and B

Experimental Data	Model A	Model B
P_{CO2}		Better
P_{MEA}		Better
$-\Delta H_{abs}$		Better
C_p	Similar	Similar
Speciation	Similar	Similar
P_t	Better	
pK_a of MEACOOH	-	Good

MEACOOH may be considered an important species at high temperature or high loading, when the concentration of MEACOOH is 0.1-3 % in 7 m MEA according to Model B. Model B prediction matches experimental pK_a of MEACOOH, and the measured concentration of MEACOO-/MEACOOH by NMR. The heat of formation of MEACOOH has effects on P_{CO2} and CO_2 heat of absorption, especially at high temperature and high loading. $-\Delta H_{abs}$ from Model B agrees with the $-\Delta H_{abs}$ from the empirical model developed in Chapter 2.

Although mostly developed from 7 m MEA data, Model B gives a good profile for 11 m (40 wt%) MEA.

Zwitterions may be considered to add into the thermodynamic models of other amine-CO_2-H_2O systems to get a better fitting of data at high temperature and CO_2 loading.

Chapter 5: Conclusions and Recommendations

This chapter summarizes the conclusions in total pressure experiments, high temperature vapor-liquid equilibrium experiments, and thermodynamic modeling in this work. Recommendations are made for future work.

5.1 TOTAL PRESSURE

Total pressure measurements at 100-160°C were performed with nine aqueous amine solvents: MEA, PZ, 8 m 1MPZ, 8 m 2MPZ, 4 m PZ/4 m 2MPZ, 3.75 m PZ/3.75 m 1MPZ/0.5 m DMPZ, DGA, 7 m MDEA/2 m PZ, and 5 m MDEA/5 m PZ. CO_2 partial pressure was derived from the total pressure data, and was correlated with a semi-empicial relationship: $\ln P_{CO_2}(\mathrm{Pa}) = a + b\frac{1}{T} + c\alpha + d\alpha^2 + e\frac{\alpha}{T} + f\frac{\alpha^2}{T}$, where α is the CO_2 loading (molCO_2/mol alkalinity).

For MEA and PZ, amine concentration does not have obvious effects on the CO_2 solubility when it is correlated as a function of CO_2 loading

Differential heat of absorption of CO_2 was derived from the semi-empirical models and is in the form of: $-\Delta H_{abs}(J/mol) = R(b + e\alpha + f\alpha^2)$. In this work $-\Delta H_{abs}$ varies from 66 kJ/mol for 4 m PZ/4 m 2MPZ and to 72, 72, and 73 kJ/mol for MEA, 7 m MDEA/2 m PZ, and DGA. Solvents with a higher heat of absorption may save more energy if stripping is at the same temperature.

The heat of absorption estimated from the total pressure data does not vary significantly with temperature. The temperature dependence of the heat of CO_2 absorption in MEA measured by Kim et al. (2007) is not consistent with either the total pressure CO_2 or the measured specific heat capacity.

Recommendations:

1. Increase the accuracy of total pressure measurements by the autoclave: use a platinum resistance thermometer instead of a thermocouple, keep a constant agitation rate, measure the weight of solution for each experimental run.
2. Find a more accurate way to calculate CO_2 partial pressure and to correct liquid loading: consider the non-ideality of N_2, water, amine, and CO_2 in the vapor phase.
3. Improve the semi-empirical models with more theoretical terms. This may capture a better CO_2 loading dependence of the heat of absorption at low to medium loading especially at low temperature.
4. Correlate CO_2 partial pressure with amine structures.

5.2 HIGH TEMPERATURE VAPOR-LIQUID EQUILIBRIUM

A high temperature vapor-liquid equilibrium method with online FTIR analysis was developed. Amine volatility was measured for MEA-H_2O at 80-140°C, MEA-CO_2-H_2O at 120 and 140°C, and PZ-CO_2-H_2O at 120 and 150°C.

At 0-0.5 loading (α), 313-413 K, 3.5-11 m MEA (mol fraction x is 0.059-0.165), the empirical model for MEA volatility (Pa) is $\ln(P_{MEA}/x_{MEA}) = 30.0\text{-}8153/T\text{-}2594\alpha^2/T$. In 7 m MEA with 0.2 and 0.5 loading, P_{MEA} is 920 and 230 Pa at 120 ℃. At 0.3-0.5 loading, the enthalpy of MEA vaporization, $-\Delta H_{vap,MEA}$, is 70 to 73 kJ/mol MEA.

At 0.25-0.4 loading, 313-423 K, 4.7-11.3 m PZ (x is 0.078-0.169), the empirical model of PZ volatility (Pa) is $\ln(P_{PZ}/x_{PZ}) = -123+21.6\ln T+20.2\alpha-18174\alpha^2/T$. In 8 m PZ with 0.3 and 0.4 loading, P_{PZ} is 400 and 120 Pa at 120 ℃, and 2620 and 980 Pa at 150 ℃. At 0.25-0.4 loading, $-\Delta H_{vap,PZ}$ is 85 to 100 kJ/mol PZ at 150 ℃ and 66 to 80 kJ/mol PZ at 40 ℃.

$\Delta H_{vap,PZ}$ has a larger dependence on CO_2 loading than $\Delta H_{vap,MEA}$ in rich solution because of the more complex speciation/reactions in PZ at rich loading.

The specific heat capacity of 8 m PZ is 3.43-3.81 J/(g·K) from 70 to 150°C.

Recommendations:

1. Add spargers to the gas inlet tube in each equilibrium cell to get smaller bubbles for better mass transfer.
2. The liquid sampling method needs to be modified. A better condensing system may help to reduce flashing; sampling into a vacuumed sample bomb, or sampling into a known amount of amine solution may help to get more representative samples.
3. Put better insulation to the connecting parts (the tube between the heated line and heating bath fluid) of the vapor sampling line to avoid condensing.
4. Use a better pressure controller instead of the regulator to control the feeding pressure.
5. Use a better thermometer instead of calibrating the temperature logger.
6. Redo or check the calibration of relative components in FTIR periodically.
7. Use an automatic bath fluid control system.
8. Optimize the vapor sample flow rate. It relates with temperature, pressure, and concentration of each component.
9. Measure MEA volatility in various MEA concentrations of MEA-H_2O and MEA-CO_2-H_2O.
10. Measure PZ volatility in various PZ concentrations of PZ-H_2O and PZ-CO_2-H_2O.
11. Perform the high temperature/pressure vapor-liquid equilibrium measurements with other aqueous amines.

5.3 MEA THERMODYNAMIC MODELING

Two new thermodynamic models of MEA-CO_2-H_2O were developed in Aspen Plus® starting with the Hilliard (2008) MEA model. One of them (Model B) includes a

new species MEACOOH and it gets a better prediction than the other (Model A) for CO_2 solubility, MEA volatility, speciation, heat of absorption, and other thermodynamic results. The major problems of Model A are at high temperature and high CO_2 loading.

The Model B prediction matches the experimental pK_a of MEACOOH, and measured concentration of MEACOO-/MEACOOH by NMR. In the prediction the concentration of MEACOOH is 0.1-3 % in 7 m MEA at high temperature or high loading, where the heat of formation of MEACOOH has effects on P_{CO2} and CO_2 heat of absorption. Model B solved the problems of Model A by adding MEACOOH and matched the experimental data of pK_a and speciation, therefore MEACOOH may be considered an important species at high temperature or high loading.

Although mostly developed from 7 m MEA data, Model B also gives a good profile for 11 m (40 wt%) MEA.

Recommendations:

1. Reduce the parameters in Model B regression by checking the correlation matrix and standard deviations of the parameters.
2. Find more experimental data for MEACOOH, and other related experimental data. Investigate more on the zwitterions and their effects on thermo properties of CO_2 loaded aqueous amines.
3. Zwitterions may be considered in other amine-CO_2-H_2O systems to get better thermodynamic models on a wider loading and temperature range.

Appendix A: Total Pressure Apparatus

A.1 VALIDYNE® DP15 TRANSDUCER CALIBRATION

A Validyne® DP15 transducer (±15 kPa accuracy) was calibrated by heating water and correlating the readings with known water vapor pressures from DIPPR (BYU, 1998- Provo, version 13.0). Separate calibrations were performed to the transducer with different equilibrium cells and different initial states.

A.1.1 Calorimeter

A.1.1.1 Calibration with Calorimeter - Vacuum

The following calibration was used for run MEA-1, PZ-1 and PZ-2. The vapor phase in the calorimeter was vacuumed before calibration and each experiment run, so no correction was conducted to the total pressure measured in these experiments.

Table A-1: Calibration with Calorimeter - Vacuum

Temperature (°C)	Transducer	Pressure (Pa)	Temperature (°C)	Transducer	Pressure (Pa)
100	0.005	101260	200	0.100	1551600
110	0.008	143120	190	0.080	1252500
120	0.012	198290	180	0.061	1000500
130	0.016	269710	170	0.048	790370
140	0.022	360750	160	0.038	616820
150	0.030	475090	150	0.031	475090
160	0.039	616820	140	0.022	360750
170	0.051	790370	130	0.017	269710
180	0.066	1000500	120	0.012	198290
190	0.085	1252500	110	0.009	143120
200	0.107	1551600	100	0.007	101260

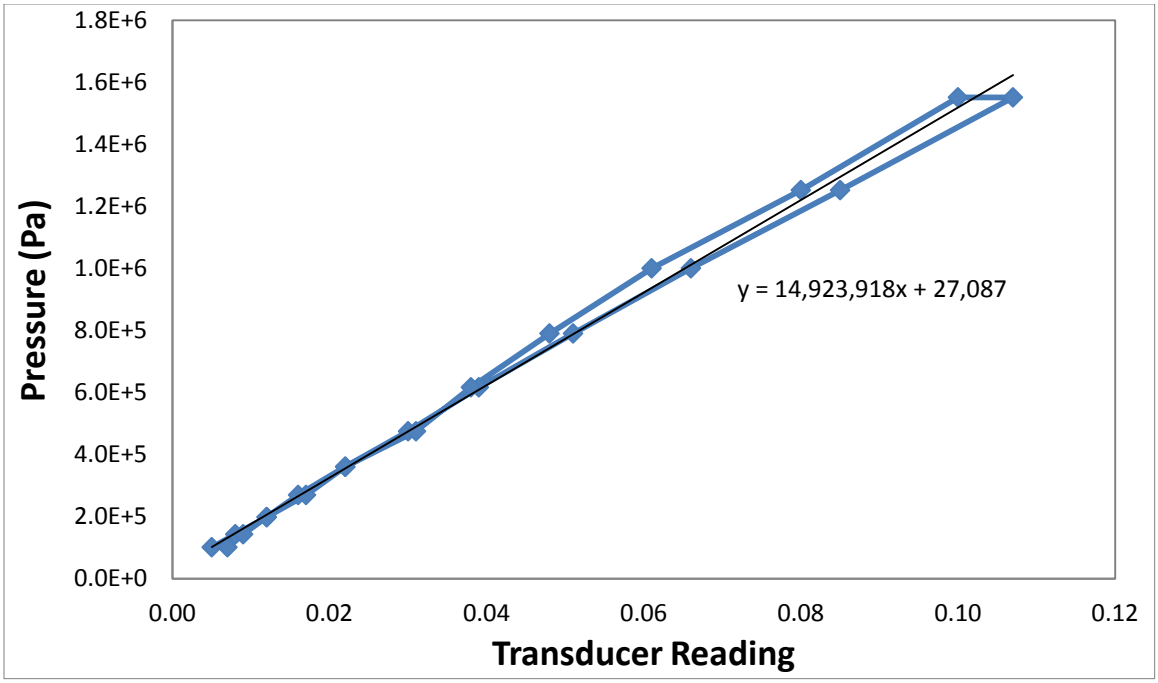

Figure A-1: Pressure Transducer Calibration with Calorimeter - Vacuum

A.1.1.2 Calibration with Calorimeter - Air

The following calibration was used for run PZ-3. 1 atm of air at room temperature was left in the cell during calibration and before the experiment run nitrogen was used to purge oxygen out. Thus corrections were made to the measured total pressure.

Table A-2: Calibration with Calorimeter - Air

T (°C)	Transducer Reading	P water (kPa)	P air (Pa)	P (Pa)	T (°C)	Transducer Reading	P water (kPa)	P air (Pa)	P (Pa)
19	0.038		101325	101325	170	0.668	790.37	153695.6	944065.6
100	0.14	101.26	129417.8	230677.8	180	0.847	1000.5	157163.9	1157664
110	0.176	143.12	132886.1	276006.1	190	1.053	1252.5	160632.1	1413132
120	0.223	198.29	136354.4	334644.4	200	1.31	1551.6	164100.4	1715700
130	0.277	269.71	139822.6	409532.6	200	1.256	1551.6	164100.4	1715700
140	0.354	360.75	143290.9	504040.9	190	1.005	1252.5	160632.1	1413132
152	0.476	501.11	147452.8	648562.8	180	0.804	1000.5	157163.9	1157664
160	0.539	616.82	150227.4	767047.4					

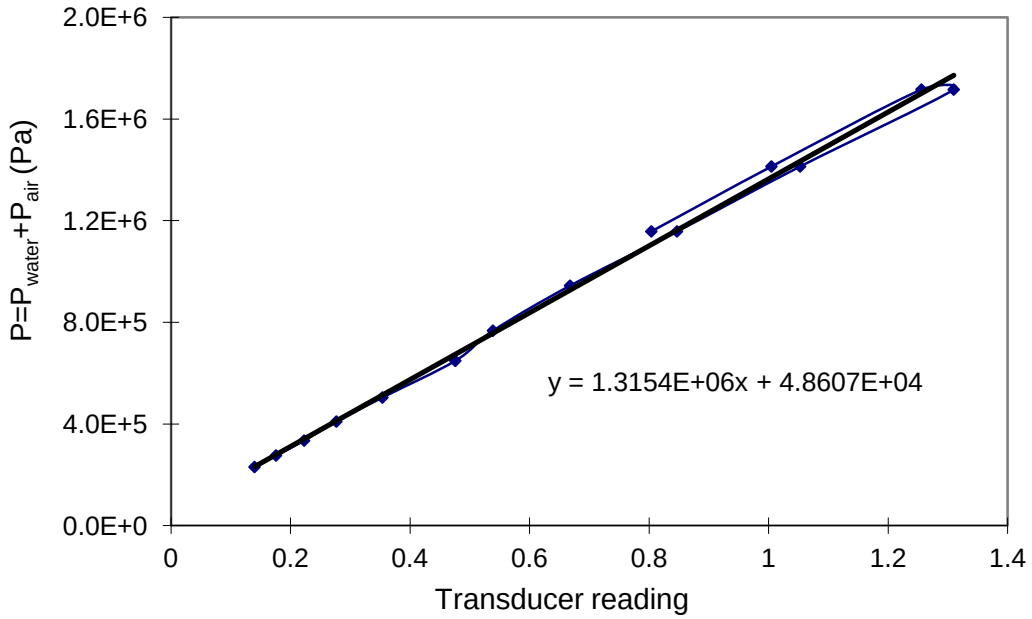

Figure A-2: Calibration with Calorimeter – Air

Calibration Calculation Example:

At 100 °C, the vapor pressure of water is 101260 kPa, the transducer reading is 0.14.

At 19 °C before calibration, the atmosphere has a reading of 0.038. Assume the air behaves as an ideal gas during calibration, according to PV=nRT, ignore the volume change, $P/P_i=T/T_i$, thus:

$$P_{air} = \frac{100 + 273.15(K)}{19 + 273.15(K)} \cdot 101325(Pa) = 129418(Pa)$$

The total pressure in the equilibrium cell at 100 °C:

$$P_{total} = P_{air} + P_{water} = 129418 + 101260 = 230678(Pa)$$

Then correlate the P_{total} with readings from the indicator and get the calibration curve in Figure A-2.

A.1.2 Autoclave

A.1.2.1 Calibration with Autoclave - Air

The following calibration was used for run MEA-2, PZ-4, and PZ-5. 1 atm of air at room temperature was left in the autoclave during calibration and before each experiment run nitrogen was used to purge oxygen out. Thus corrections were made to the measured total pressure.

Table A-3: Calibration with Autoclave - Air

T(°C)	Indicator reading	P water(Pa)	P air(Pa)	P(Pa)	T(°C)	Indicator reading	P water(Pa)	P air(Pa)	P(Pa)
28			102345	102345	190	1.047	1.25E+6	157400	1409900
102	0.175	108700	127493	236193	200	1.265	1.55E+6	160798	1712398
111	0.21	148000	130552	278552	200	1.273	1.55E+6	160798	1712398
121	0.248	204640	133950	338590	180	0.885	1.00E+6	154001	1154501
133	0.312	294800	138028	432828	159	0.59	601290	146864	748154
142	0.375	381620	141087	522707	139	0.398	350660	140067	490727
148	0.433	450160	143126	593286	121	0.276	204640	133950	338590
160	0.547	616820	147204	764024	100	0.2	101260	126813	228073
170	0.681	790370	150603	940973	190	1.079	1.25E+6	157400	1409900
159	0.55	601290	146864	748154	170	0.745	790370	150603	940973
171	0.704	809660	150942	960602	150	0.504	475090	143806	618896
170	0.681	790370	150603	940973	130	0.337	269710	137009	406719
178	0.82	955340	153321	1108661	110	0.236	143120	130212	273332
191	1.053	1.28E+6	157739	1437939					

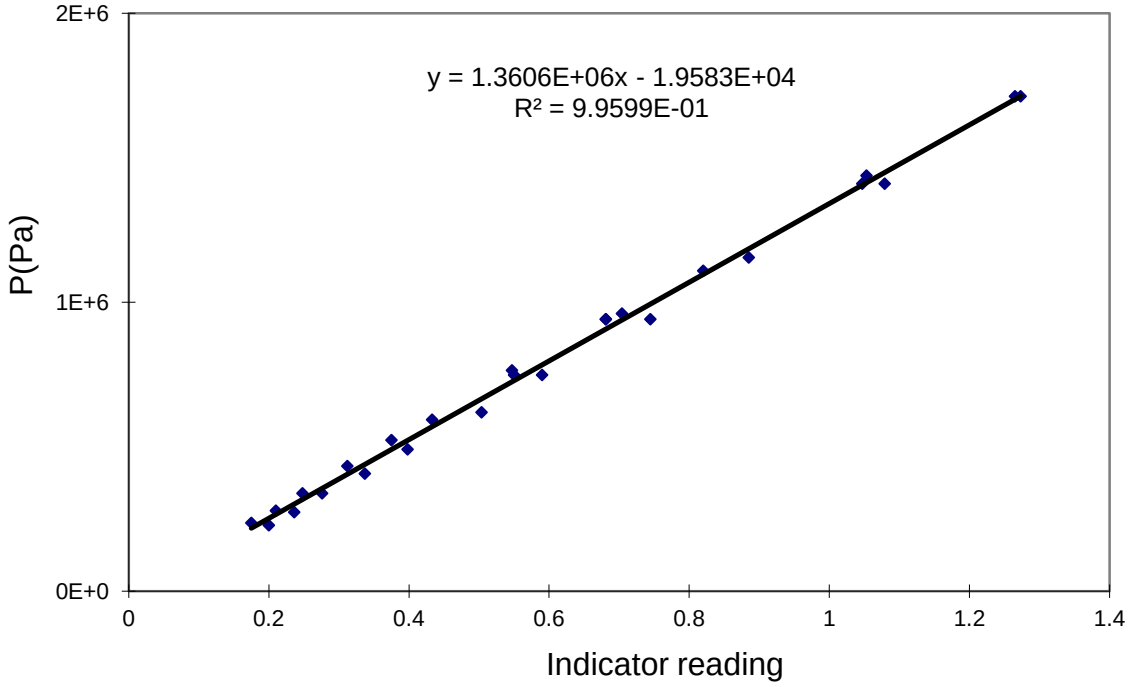

Figure A-3: Calibration with Autoclave – Air

Similar calculation was done as for the calorimeter to correct the calibration, except that the temperature is 298.15K for 1 atm air before calibration.

A.1.2.2 Calibration with Autoclave - Nitrogen

The following calibration was used for run MEA-3 and PZ-6. About 1 atm of nitrogen at room temperature was purged into the autoclave before calibration and before each experiment run. Thus corrections were made to the measured total pressure.

Table A-4: Calibration for Autoclave - Nitrogen

T(°C)	Indicator reading	P_{water} (kPa)	P_{N2}(Pa)	P(Pa)	T(°C)	Indicator reading	P_{water} (kPa)	P_{N2} (Pa)	P(Pa)
105	0.2225	120.7	128513	249213	200	1.357	1551.6	160798	1712398
110	0.242	143.12	130212	273332	190	1.131	1252.5	157400	1409900
121	0.295	204.64	133950	338590	180	0.942	1000.5	154001	1154501
131	0.351	277.88	137349	415229	169	0.769	771.45	150263	921713
140	0.417	360.75	140407	501157	160	0.6505	616.82	147204	764024

T(°C)	Indicator reading	P_{water} (kPa)	P_{N2}(Pa)	P(Pa)	T(°C)	Indicator reading	P_{water} (kPa)	P_{N2} (Pa)	P(Pa)
150	0.502	475.09	143806	618896	150	0.541	475.09	143806	618896
160	0.613	616.82	147204	764024	140	0.4505	360.75	140407	501157
171	0.7655	809.66	150942	960602	130	0.3795	269.71	137009	406719
180	0.923	1000.5	154001	1154501	120	0.322	198.29	133610	331900
190	1.1215	1252.5	157400	1409900	110	0.2775	143.12	130212	273332
200	1.364	1551.6	160798	1712398	99	0.239	97.702	126474	224176

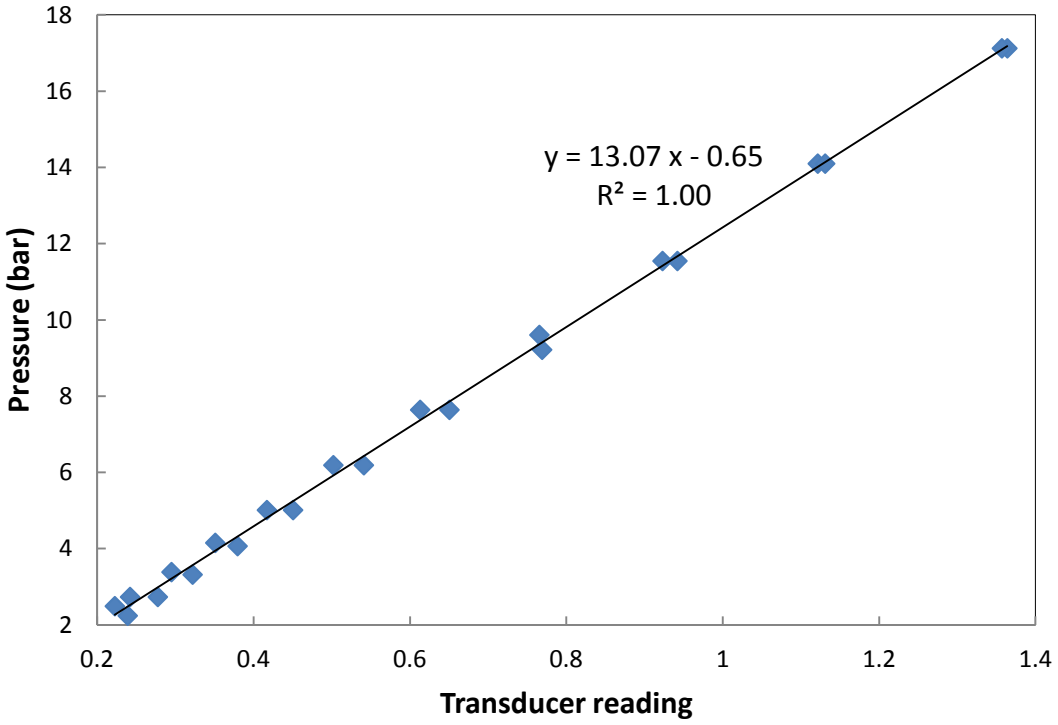

Figure A-4: Calibration with Autoclave – Nitrogen

Calibration Calculation Example:

At 105 °C, the vapor pressure of water is 120700 kPa, the transducer reading is 0.2225 (average value).

At 25 °C before calibration, the 1 atm nitrogen inside the vessel has a reading of 0.113. Assume the nitrogen behaves as an ideal gas during calibration, according to PV=nRT, ignore the volume change, $P/P_i=T/T_i$, thus:

$$P_{N_2} = \frac{105+273.15(K)}{25+273.15(K)} \cdot 101325(Pa) = 128513(Pa)$$

The total pressure in the equilibrium cell at 105 °C:

$$P_{total} = P_{N_2} + P_{water} = 128513 + 120700 = 249213(Pa)$$

Then correlate the P_{total} with readings from the indicator and get the calibration curve in Figure A-4.

A.1.2.3 Calibration with Autoclave - Vacuum

The following calibration was used for run MEA-4, MEA-5, and PZ 7-12. In the beginning of this calibration at about 110 ºC water vapor was released from a valve on top of the vessel directly to the back of hood until temperature dropped to 100 ºC. This was processed 3 times to purge all the air. So no correction was conducted to the total pressure measured in these experiments.

Table A-5: Calibration with Autoclave - Vacuum

Temperature (°C)	Transducer Reading	Pressure (kPa)
102.0	0.155	108.70
120.0	0.219	198.29
139.3	0.319	353.66
159.4	0.487	607.46
173.0	0.744	849.35
200.1	1.153	1554.90
220.8	1.719	2351.00
226.0	1.899	2593.40
209.1	1.378	1869.80
189.3	0.958	1233.40
171.2	0.659	813.56
150.6	0.434	482.78
130.9	0.292	277.05

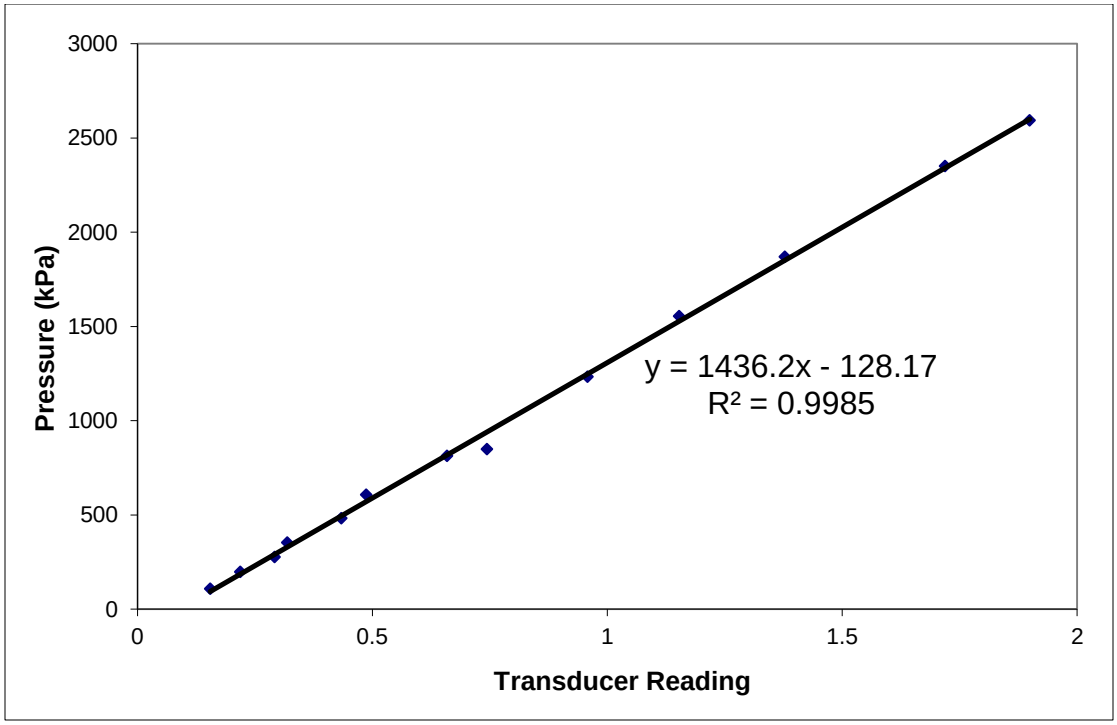

Figure A-5: Calibration with Autoclave – Vacuum

A.2 P AND T CALIBRATION WITH THE AUTOCLAVE AND LABVIEW® DATA LOGGER

The pressure transducer was calibrated with a dead weight tester. The calibration curve is shown in Figure A-6.

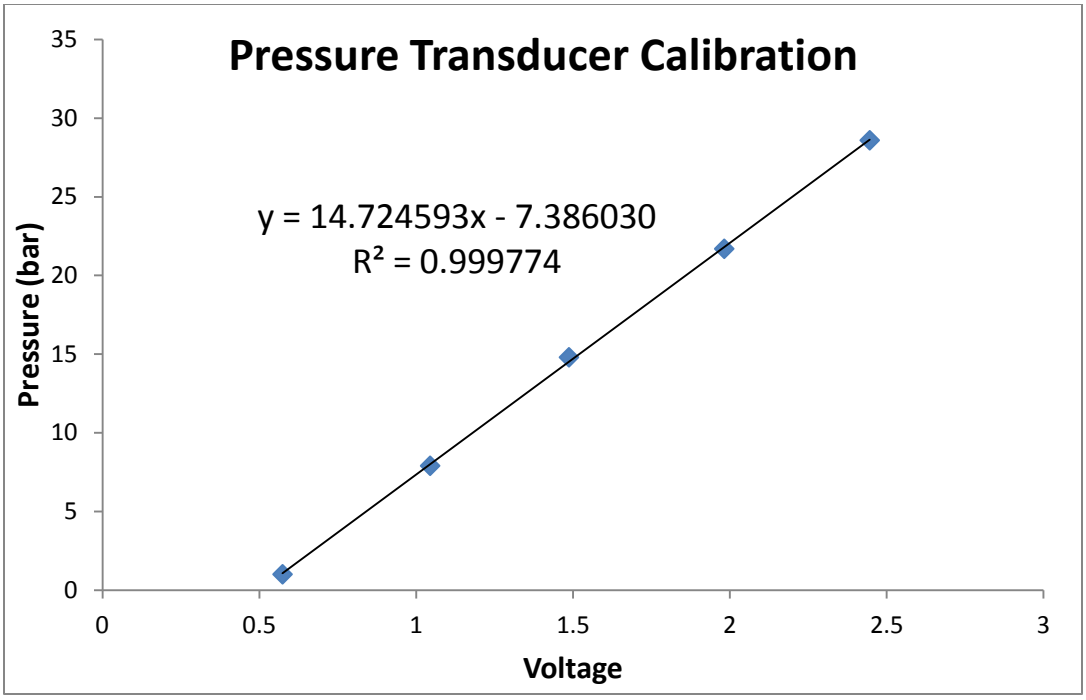

Figure A-6: Pressure Transducer Calibration with the Autoclave and LabView® Data Logger on 7/28/2009

LabView® SignalExpress® scales voltage to pressure data using the equation in Figure A.6 for the experiments before September 25th, 2009. After that an Omega® K type low noise thermocouple replaced the normal thermocouple and further pressure calibration associated with temperature measurement was performed. Pure water vapor pressure was measured at 100 to 204 °C and compared with literature data from DIPPR chemical databank. The correlation is shown in Figure A-7 below.

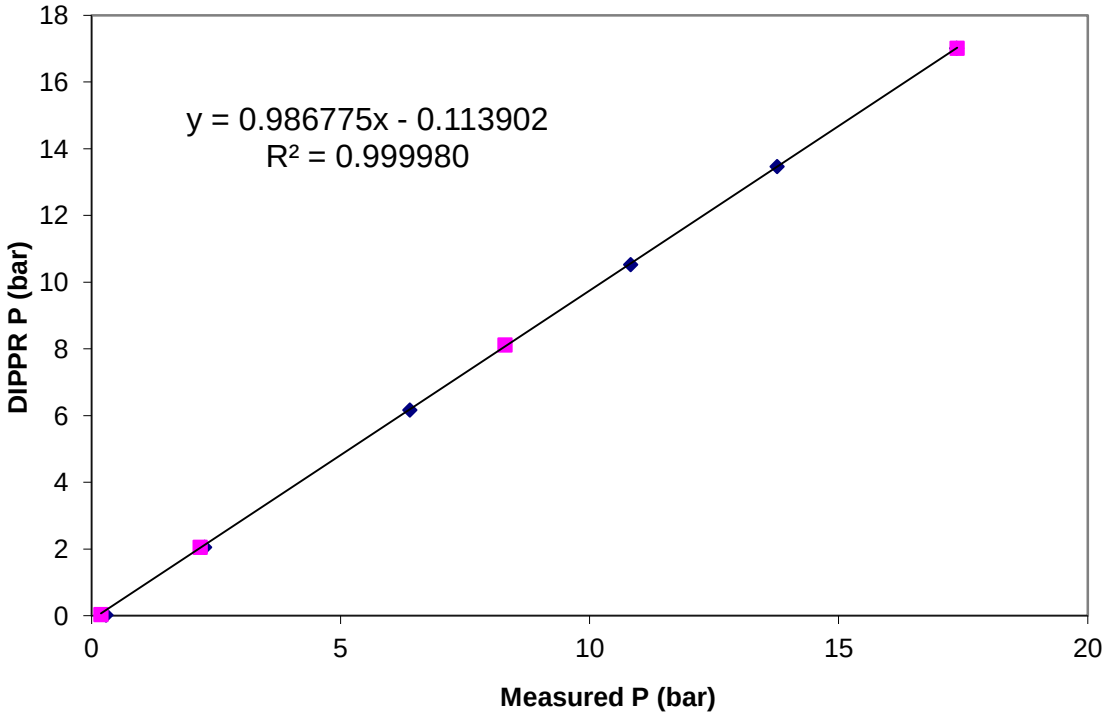

Figure A-7: Calibration of Pressure Transducer with the Thermocouple

For the experiments between September 25th 2009 and September 3rd 2010, a combination of the above two equations in Figures A-6 and A-7 was input into Signal Express® and used in total pressure experiments:

$$y = 14.529860x - 7.400745 \qquad \text{(A-1)}$$

y - pressure, bar.

x - voltage, V.

The pressure transducer calibration was repeated on September 3rd, 2010. Since then it was used in the total pressure experiments.

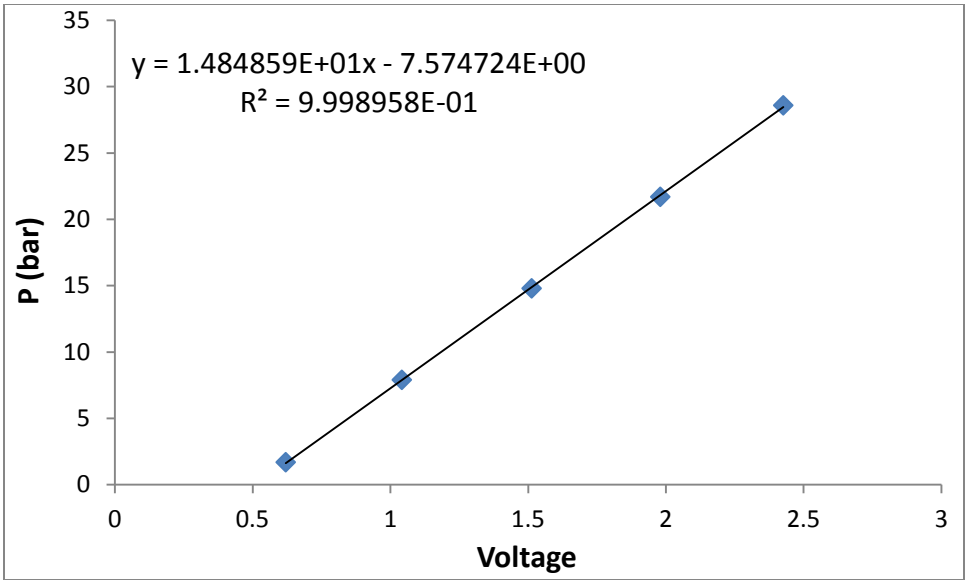

Figure A-8: Pressure Transducer Calibration with the Autoclave and LabView® Data Logger on 09/03/2010

Appendix B: High Temperature Pressure Vapor-Liquid Equilibrium Apparatus

B.1 Equilibrium Cells and Heads

Two 200 mL (i.d=1.5 in, inside depth=7 in) and one 600 mL (i.d=2.5 in, inside depth=8 in) stainless steel vessels (4752 and N4764-T-SS, Parr Instrument Co.) were used as equilibrium cells in series.

N4764-T-SS (600 mL) is a non-stirred vessel made of T316SS with the following features:

A. Head 818HC47 with only rupture disc assembly with 1000 psi rupture disc installed.
B. PTFE gasket with split ring.
C. MAWP is 3000 psi at 350 ℃.

The head 818HC47 has six openings. The openings are assigned for: gas feeding, gas sampling, rupture disc assembly, liquid sampling, thermocouple, pressure transducer and vent (share one opening by a "T" connector).

4752 general purpose vessel (200 mL) has the following features:

A. Head 428HC9 and cylinder made of T316SS.
B. PTFE flat gasket with split ring closure.
C. MAWP is 3000 psi at 350 ℃.

The head 428HC9 has two 1/8'' NPT ports. The openings are assigned for gas inlet and gas outlet, respectively.

The other tubes, valves, and fittings are from Swagelok®.

B.2 Oil Bath

DC 200 fluid 50 CS by Dow Corning was used in the oil bath (EX-35, Thermo Fisher Scientific). The bath is good for ambient +12 ℃ to 200 ℃ with a temperature

stability of ±0.01 ℃. The bath volume is 9.6 gallons, and a force/suction pump head circulates the bath fluid. Figure B-1 shows the dimensional diagram of the oil bath. The unit dimension is 52.4*28.9*64.5 (H*W*D) cm, and the bath W*L*D is 22.4*39.4*30.5 cm.

To avoid damaging the temperature control system of the bath, the level of the silicon oil (bath fluid) must be kept between the two slots in the stainless steel separating board in the oil bath. The oil expands as temperature increases, and because of the large quantity of the oil and the large temperature increase during an experiment, oil needs to be pumped in and out of the bath to maintain a good fluid level. Therefore, an oil reservoir and a peristaltic Masterflex pump (by Cole Parmer) between the bath and the reservoir were used.

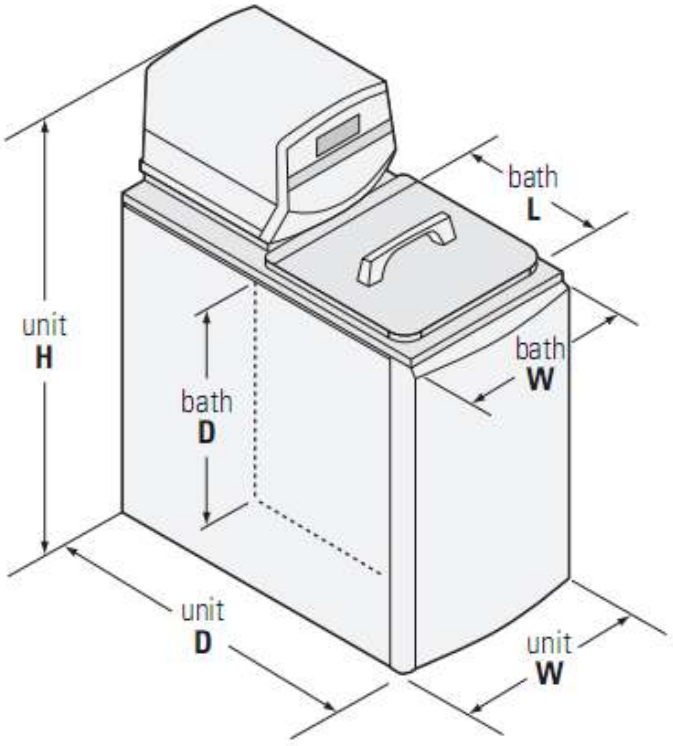

Figure B-1: NESLAB EX Dimensional Diagram (from Catalog of Thermo Scientific NESLAB™ RTE and EX Series Bath Circulators)

B.3 WIRING OF THE PRESSURE DAQ SYSTEM, CALIBRATION OF PRESSURE TRANSDUCER

A pressure transducer (Druck® PTX 611, 0–30 bar absolute) was connected to a signal converter and data logger NI USB 6009. LabView® SignalExpress® software was used for data recording. PTX611 gives signal in current. An in-house signal converter was built to convert current to voltage for data acquisition. The circuit of the data acquisition system is shown in Figure B-2.

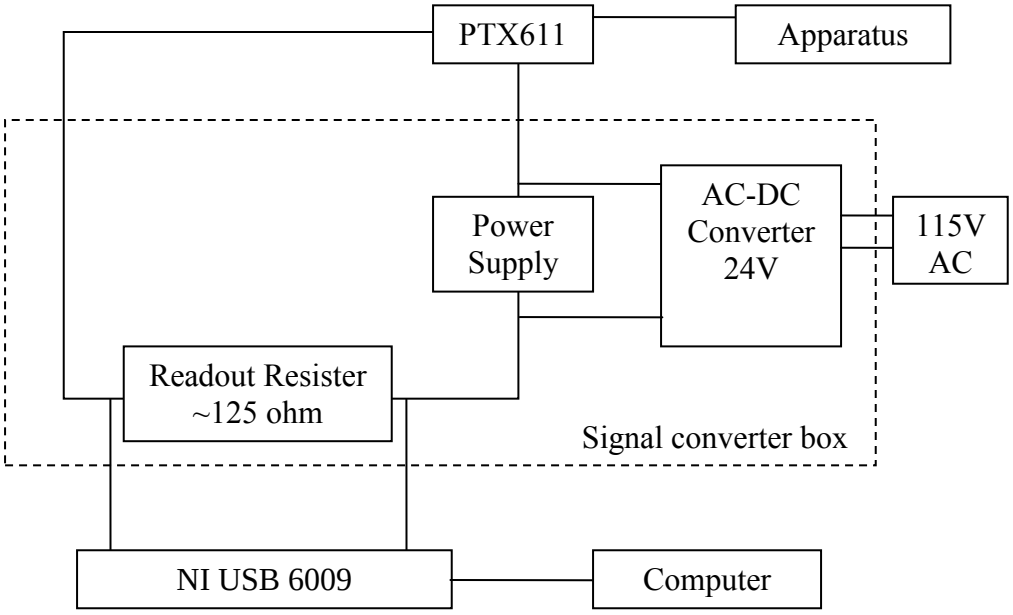

Figure B-2: Data Acquisition System of the Pressure Measurement

The pressure transducer was calibrated using a dead weight tester (S/N 19189/278, by Budenberg Volumetrics, Inc.), located and maintained in the fundamental laboratory in the Department of Chemical Engineering at The University of Texas at Austin. The transducer was connected to the dead weight tester, the pressure of which can be set by varying the weight loading. Figure B-3 is the calibration curve of the pressure and the voltage signal.

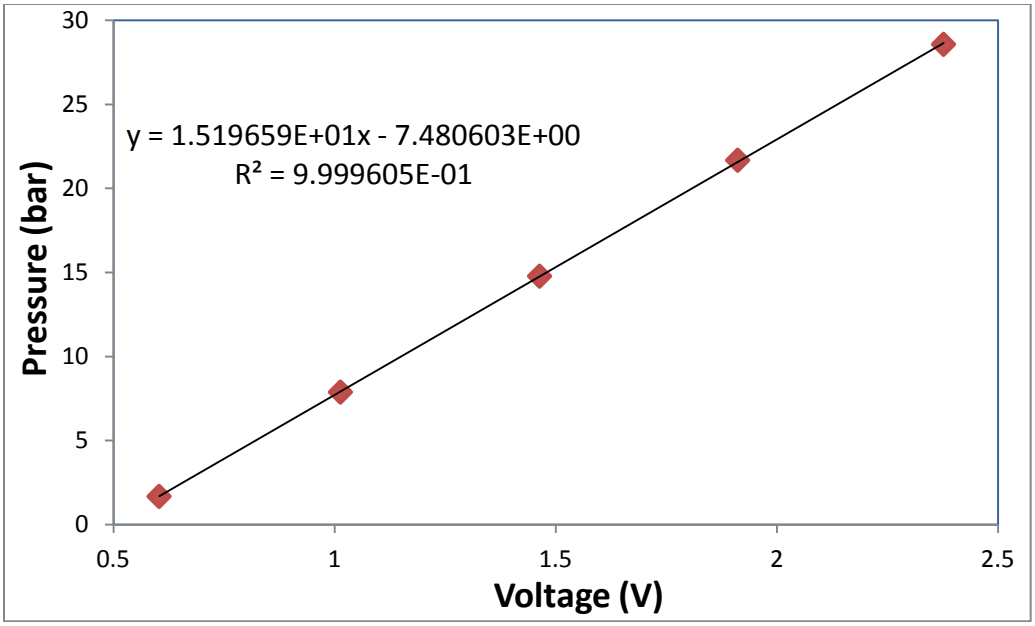

Figure B-3: Pressure Transducer Calibration on 8/17/2010

B.4 TEMPERATURE CALIBRATION

The HH506RA data logger from Omega® was found with a systematic error for temperature recording. Thus a temperature calibration was performed to the data logger.

Calibration was conducted with a Fuji Electric PXZ-4 temperature controller. Multiple thermocouples were held at the same position in the oil bath and multiple points were read by the temperature reader and the Fuji Electric PXZ-4 temperature controller. Readings from the two were correlated in Figure B-4, where the correlation equation was used in the following experiments with the HH506RA data logger.

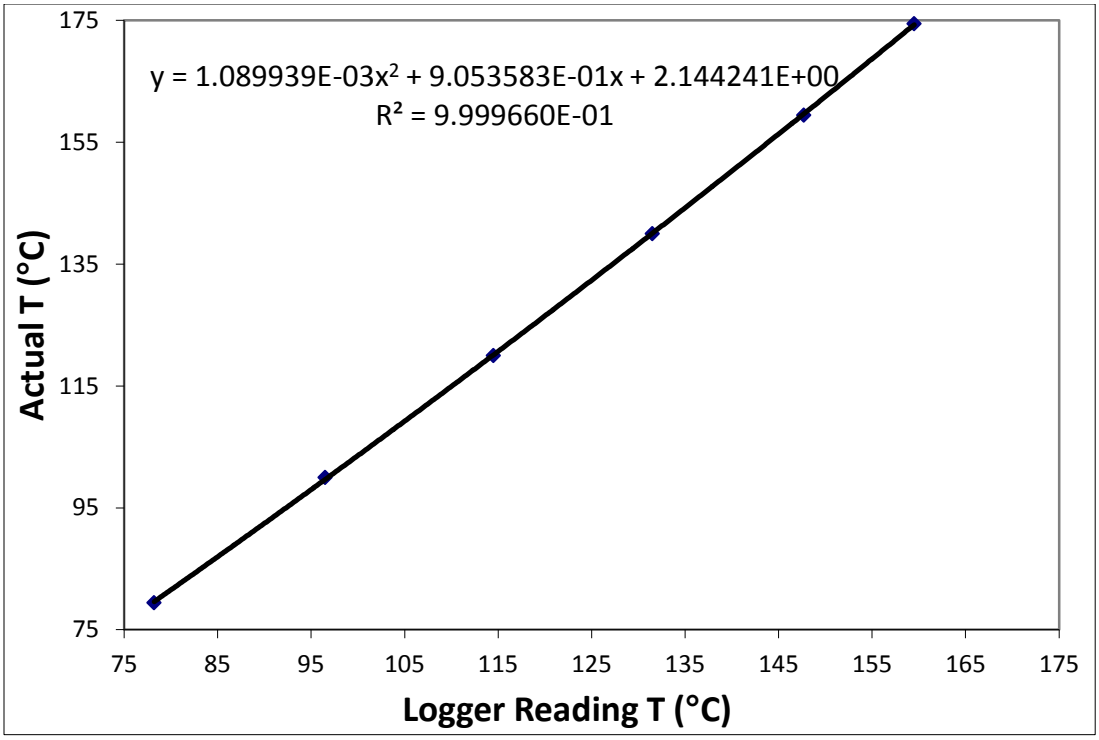

Figure B-4: Temperature Calibration for Data Logger Omega® HH506RA on 08/25/2010

B.5 Solution Charging, Starting up, Finishing, and Cleaning Procedures of the HTPVLE Experiment

B.5.1 Solution Charging and Starting of the HTPVLE Experiment

1. Pour certain amount of prepared solution into the three clean equilibrium cells. For high liquid level runs, about 170, 170, and 450 mL of the solution was added into the 200 mL, 200 mL, and 600 mL cells, respectively. For middle liquid level runs, about 100, 100, and 300 mL of the solution was added into the cells.
2. Assemble the clean covers onto the cells, make sure the o-rings are clean and in the right position, then for each cell put the two split rings on to hold the edges of the cover and the cell top, put three screws into the holes of each split ring and use a wrench to tighten the screws. This makes the sealing of the equilibrium cells.

3. Check the sealing. Close all the valves on the covers.
4. Connect N_2 to the first equilibrium cell and open the feeding valve. Let N_2 flow into the cells to increase the pressure to higher than 1 atm.
5. Close the feeding valve and disconnect N_2 line from the cells. Put the cells into the oil bath carefully. Hold the edges and 1/4'' tubes and avoid putting strength to connections of the fittings, especially the 1/8'' fittings. This process requires two people.
6. Pump silicon oil from the reservoir into the bath. As soon as the oil level reaches the lower slot in the separating board of the bath, stop pumping.
7. Turn on the bath; set the target temperature. As the temperature increases, the oil will expand; check the oil level every 20 min to make sure it is below the higher slot in the separating board of the bath. Pump oil out of the bath into the reservoir if necessary.
8. During the heating process, connect the gas line on the side of the hood to the feeding line of the first cell. Connect the FTIR heated lines to the vapor sampling line on the third equilibrium cell. Wrap insulation around the plastic tube that is not covered of the heated line.
9. After the temperature reaches the target and maintains for about 20 min, start the experiment procedure as in section 3.2.4.

B.5.2 Finishing and Cleaning Procedures of the HTPVLE Experiment

1. After one run, turn off the bath. Close all the valves.
2. When the system pressure is lower than 2 bar, for unloaded MEA solution, set the N_2O feeding pressure to be higher than the system pressure, open N_2O feeding and

keep the feeding valve open. For CO_2 loaded MEA, use N_2 or CO_2 instead of N_2O. For CO_2 loaded PZ, use N_2 instead of N_2O.

3. Leave the apparatus overnight for cooling down.
4. Close $N_2O/N_2/CO_2$ feeding, disconnect the FTIR heated lines and the feeding lines.
5. Hold the edges and ¼'' tubes of the apparatus to get it out of the bath. Put the cells in the special plastic pan for this apparatus. This process needs two people.
6. Loosen the screws of the split rings with a wrench and open up the cells. Put the covers of the cells upside down in a special plastic pan and put the pan aside.
7. Use a syringe to stir in the third equilibrium cell and collect a post-experiment liquid sample. Pour the rest solution into the waste container. Rinse each cell with running water and DI water until clean. Detergent and a brush may be used for cleaning if there is oil in the cell. The rinsing process needs two people.
8. Use paper towel and Kim Wipe to clean the inside of the covers. Use Kim Wipe to clean the edges on top of the equilibrium cells.

B.5.3 ATTENTION

1. Make sure the silicon oil level is between the two slots in the separating board of the bath when the bath is on. Low fluid level error may stop the bath from working.
2. Make sure all or the most of the vapor sampling lines are submerged under the silicon oil. This ensures the temperature control of the liquid sampling line and avoids condensing in the line.
3. Make sure the pressure in the equilibrium cells is above 1.5 atm to avoid oil leaking into the system when they are in the oil bath.

Appendix C: Raw Data

C.1 Total Pressure Experimental Data

The data here are from experiments with Validyne® DP15 transducer. The data from experiments with the PTX 611 transducer can be found directly in Chapter 2.

C.1.1 MEA-CO_2-H_2O Total P Data

MEA-4 failed so it is not listed here.

Table C-1: Raw Data for Run MEA-1

Temperature (°C)	Transducer	Pressure (Pa)	Temperature (°C)	Transducer	Pressure (Pa)
100	0.011	191250	140	0.051	788207
110	0.016	265870	130	0.034	534500
120	0.026	415109	120	0.023	370337
130	0.038	594196	110	0.015	250946
140	0.061	937446	100	0.010	176326
150	0.098	1489631			

Table C-2: Raw Data for Run MEA-2

T(°C)	Transducer	P (Pa)	$P_{corrcted}$ (Pa)	T(°C)	Transducer	P (Pa)	$P_{corrcted}$ (Pa)
101	0.257	330091	188823	160	1.593	2147173	1983628
111	0.344	448463	303420	166	1.765	2381876	2216066
121	0.467	615817	466998	161	1.615	2177106	2013184
130	0.634	843037	690820	149	1.171	1573680	1414288
140	0.870	1164139	1008146	139	0.887	1187269	1031654
150	1.191	1600211	1440443				

Table C-3: Raw Data for Run MEA-3

T(°C)	transducer reading	P_t(Pa)	T(°C)	transducer reading	P_t(Pa)	T(°C)	transducer reading	P_t(Pa)
101	0.2235	91477	160	1.15	1281241	129	0.4765	412044
111	0.275	155167	170	1.5535	1805101	120	0.378	286547
120	0.343	240791	170	1.5235	1765882	110	0.301	189520
131	0.4705	403473	160	1.156	1289085	100	0.249	125176
140	0.634	613945	150	0.878	929291			
150	0.8495	892032	140	0.6485	632901			

Table C-4: Raw Data for Run MEA-5

T(ºC)	transducer reading	P_t(Pa)	T(ºC)	transducer reading	P_t(Pa)	T(ºC)	transducer reading	P_t(Pa)
100.5	0.255	108340	150.2	0.64	644022	120.4	0.345	230689
111.3	0.291	156294	159.0	0.803	875068	109.0	0.293	159965
121.8	0.344	228767	152.0	0.671	687920	101.1	0.254	106695
131.9	0.417	330103	142.3	0.532	491656			
141.4	0.516	468989	129.9	0.409	319308			

C.1.2 PZ-CO_2-H_2O Total P Data

PZ-11 failed so it is not listed here.

Table C-5: Raw Data for Run PZ-1

Temperature (°C)	Transducer	Pressure (Pa)	Temperature (°C)	Transducer	Pressure (Pa)
100	0.011	191250	160	0.118	1788109
110	0.015	250946	150	0.084	1280696
120	0.024	385261	140	0.056	862826
130	0.032	504652	130	0.037	579272
140	0.054	832979	120	0.024	385261
150	0.086	1310544	110	0.015	250946

Table C-6: Raw Data for Run PZ-2

Temperature (°C)	Transducer	Pressure (Pa)	Corrected P (Pa)	Temperature (°C)	Transducer	Pressure (Pa)	Corrected P (Pa)
80	0.004	86783	36997	180	0.263	3952077	3888194
100	0.009	161402	108797	169	0.14	2116436	2054103
110	0.013	221098	167083	160	0.104	1579174	1518110
120	0.02	325565	270140	150	0.074	1131457	1071803
130	0.037	579272	522437	140	0.052	803131	744886
140	0.059	907598	849354	130	0.031	489728	432894
150	0.089	1355316	1295661	119	0.023	370337	315053
160	0.127	1922425	1861361	110	0.018	295718	241702
170	0.18	2713392	2650918	100	0.013	221098	168493

Table C-7: Raw Data for Run PZ-3

T(°C)	Transducer	P (Pa)	T(°C)	Transducer	P (Pa)
104	0.183	289325	160	1.460	1969091
111	0.227	347203	167	1.991	2667568
120	0.315	462958	161	1.429	1928314
130	0.452	643168	149	1.005	1370584
140	0.676	937817	139	0.670	929925
150	1.012	1379792	125	0.345	502420

Table C-8: Raw Data for Run PZ-4

T(°C)	Transducer	P_t (Pa)	Corrected P(Pa)	T(°C)	Transducer	P_t (Pa)	Corrected P(Pa)
110	0.246	315125	133868	170	1.5965	2152615	1942975
120	0.321	417170	231183	160	1.186	1594089	1389179
130	0.4275	562074	371356	150	0.842	1126042	925863
140	0.578	766844	571395	140	0.604	802219	606771
150	0.8055	1076380	876201	130	0.443	583163	392445
160	1.093	1467553	1262643	120	0.344	448463	262476
170	1.5295	2061455	1851814	110	0.267	343697	162441
174	1.774	2394121	2182589	100	0.224	285191	108666

Table C-9: Raw Data for Run PZ-5

T(°C)	Transducer reading	P_t(Pa)	P(Pa)	T(°C)	Transducer reading	P_t(Pa)	P(Pa)
81	0.2305	294035	136936	157	1.9265	2601613	2410800
89	0.287	370909	210261	150	1.6625	2242415	2054707
94	0.3335	434177	271311	139	1.2765	1717223	1534395
101	0.4075	534862	368890	130	1.0135	1359385	1180550
111	0.563	746435	576028	120	0.7715	1030120	855720
120	0.728	970934	796534	110	0.583	773647	603683
130	0.9795	1313125	1134289	100	0.4375	575680	410152
140	1.2945	1741714	1558442	90	0.3225	419211	258119
146	1.4925	2011113	1825179	82	0.256	328731	171188
150	1.6675	2249218	2061510				

Table C-10: Raw Data for Run PZ-6

T(ºC)	Transducer reading	P_t(Pa)	T(ºC)	Transducer reading	P_t(Pa)	T(ºC)	Transducer reading	P_t(Pa)
100	0.251	262580	151	1.4605	1843641	130	0.8415	1034471
110	0.3615	407013	160	1.932	2460012	120	0.625	751464
120	0.523	618119	160	1.9115	2433213	110	0.467	544933
134	0.807	989360	150	1.5205	1922081	100	0.3335	370432
140	0.9905	1229235	140	1.122	1401145			

Table C-11: Raw Data for Run PZ-7

T(ºC)	Transducer reading	P_t(Pa)	T(ºC)	Transducer reading	P_t(Pa)	T(ºC)	Transducer reading	P_t(Pa)
121	0.538	482894	161	1.863	2369457	129	0.7875	837945
137	0.9375	1050095	163	1.9655	2515848	119	0.5895	557678
146	1.239	1479419	150	1.4155	1731268	110	0.441	348092
152	1.469	1807285	139	1.048	1207975			

Table C-12: Raw Data for Run PZ-8

T(ºC)	Transducer reading	P_t(Pa)	T(ºC)	Transducer reading	P_t(Pa)	T(ºC)	Transducer reading	P_t(Pa)
100.3	0.22	74518.1	163.4	0.875	1035847	159.8	0.815	954906
110.1	0.251	139819	171.9	1.12	1388487	149.5	0.612	662796
118.5	0.288	193348	180.5	1.437	1843775	141.1	0.493	491536
129.9	0.359	294670	191.8	1.98	2623128	131.1	0.39	343991
140.9	0.466	448507	182.9	1.564	2029640			
151.5	0.62	669834	173.2	1.193	1497001			

Table C-13: Raw Data for Run PZ-9

T(ºC)	Transducer reading	P_t(Pa)	T(ºC)	Transducer reading	P_t(Pa)	T(ºC)	Transducer reading	P_t(Pa)
100.0	0.705	799937	140.6	1.720	2248496	117.8	1.006	1228207
110.0	0.850	1005924	146.7	1.954	2583187	112.2	0.864	1025533
120.0	1.090	1348350	140.5	1.701	2221231	100.6	0.626	686342
129.4	1.363	1738306	128.3	1.299	1646638			

Table C-14: Raw Data for Run PZ-10

T(ºC)	Transducer reading	P_t(Pa)	T(ºC)	Transducer reading	P_t(Pa)	T(ºC)	Transducer reading	P_t(Pa)
101.1	0.222	100211	169.4	1.125	1380592	140.0	0.512	507307
110.6	0.275	174033	180.0	1.495	1909424	130.0	0.403	353178
121.1	0.320	236125	191.1	1.988	2614787	120.0	0.324	242135
131.1	0.393	338550	180.6	1.535	1966727	108.9	0.263	157210
138.9	0.488	473104	170.0	1.164	1436458	100.6	0.232	114694
150.0	0.654	708830	160.6	0.881	1032286			
159.4	0.862	1005288	150.0	0.670	731810			

Table C-15: Raw Data for Run PZ-12

T(ºC)	Transducer reading	P_t(Pa)	T(ºC)	Transducer reading	P_t(Pa)	T(ºC)	Transducer reading	P_t(Pa)
100.0	0.279	168981	160.0	1.367	1714917	140.0	0.822	937738
109.4	0.350	268343	170.0	1.751	2263643	130.6	0.632	667468
120.0	0.461	424820	175.0	1.981	2592581	120.6	0.484	457686
130.0	0.610	636038	170.6	1.788	2316616	110.0	0.373	301209
140.0	0.802	909014	160.6	1.405	1769326	100.6	0.299	197539
150.0	1.056	1271034	148.3	1.034	1239909			

C.2 HIGH T P VAPOR-LIQUID EQUILIBRIUM RAW DATA

Table C-16: Raw Data for MEA Volatility in MEA-H_2O

Date	T(℃)	MEA	P_{MEA}	P_{H2O}	P_t
		m	Pa	kPa	kPa
20110311	99.4	6.91	434	95	95
20110311	120.2	6.94	1305	183	184
20110316	120.2	6.97	1345	207	208
20110316	130.1	7.00	2085	261	263
20110601	80.5	6.89	153	44	44
20110601	100.4	6.88	437	93	93
20110601	120.3	6.87	1421	202	203
20110602	130.1	6.86	2090	272	274
20110602	140.2	6.86	2914	362	365

Table C-17: Raw Data for MEA Volatility in MEA-CO_2-H_2O

Run #	Date	T	MEA	CO_2 Loading		P_{MEA}	P_{CO2}	P_{H2O}	P_t
		℃	m	Analyzed	Est. from P_{CO2}	Pa	kPa	kPa	kPa
MEA-S2	20110614	119.9	6.90	0.249	0.324	573	43	155	199
MEA-S2-2	20110615	119.9	6.87	0.345	0.351	642	62	167	230
MEA-S2-2	20110615	120.3	6.82	0.464	0.489	223	454	180	634
MEA-S3	20110627	139.9	6.81	0.210	0.222	1627	49	326	376
MEA-S3	20110627	140.0	6.63	0.335	0.367	1389	263	314	578
MEA-S3-2	20110628	139.9	6.57	0.427	0.469	718	969	316	1286
MEA-S4	20110701	140.3	6.86	0.486	0.467	795	966	317	1283
MEA-S4	20110701	140.2	6.90	0.408	0.389	1110	352	324	677
MEA-S4-2	20110705	120.4	7.00	0.368	0.361	610	73	169	243

Table C-18: Raw Data for PZ Volatility in PZ-CO_2-H_2O

Run #	Date	T	PZ	CO_2 Loading		P_{PZ}	P_{CO2}	P_{H2O}	P_t
		℃	m	Analyzed	Est. from P_{CO2}	Pa	kPa	kPa	kPa
PZ-F1	20101117	120.0	7.74	0.390	0.391	106	535	161	696
PZ-F1	20101117	119.5	8.17	0.290	0.291	482	91	166	257
PZ-F1	20101118	149.7	8.22	0.359	0.391	1269	2064	478	2543
PZ-F1	20101118	149.5	8.76	0.251	0.261	3139	287	397	687
PZ-F2	20101123	149.9	7.66	0.312	0.39	1164	2033	474	2508
PZ-F2	20101123	149.4	8.29	0.241	0.267	2851	309	395	707
PZ-F2	20101124	119.8	8.08	0.339	0.391	191	528	163	691
PZ-F2	20101124	118.6	8.70	0.303	0.302	523	104	154	259
PZ-F3	20101129	149.8	5.91	0.348	0.391	840	2051	493	2545
PZ-F3	20101129	149.7	6.11	0.228	0.239	2078	212	419	633
PZ-F3	20101129	149.0	6.11	0.228	0.258	2042	268	406	675
PZ-F3	20101130	120.1	6.14	0.336	0.391	130	530	178	708
PZ-F3	20101130	119.6	6.48	0.275	0.289	338	89	170	259
PZ-F4	20101202	149.8	4.73	0.340	0.389	615	2004	519	2523
PZ-F4	20101202	149.7	4.91	0.230	0.243	1742	223	428	653
PZ-F4	20101206	120.1	4.89	0.368	0.391	67	532	183	715
PZ-F4	20101206	119.8	5.08	0.284	0.28	232	77	179	256
PZ-F5	20101216	150.0	9.54	0.331	0.392	1261	2112	443	2557
PZ-F5	20101216	149.4	10.21	0.233	0.259	4533	275	403	683
PZ-F5	20101217	120.4	9.86	0.344	0.397	139	599	159	759
PZ-SP1	20110124	120.6	10.40	0.347	0.396	142	599	158	757

Run #	Date	T	PZ	CO_2 Loading		P_{PZ}	P_{CO2}	P_{H2O}	P_t
		℃	m	Analyzed	Est. from P_{CO2}	Pa	kPa	kPa	kPa
PZ-SP1	20110124	119.3	10.65	0.296	0.305	554	113	150	264
PZ-SP1	20110126	149	10.75	0.329	0.398	1623	2234	444	2679
PZ-SP1	20110126	148.6	11.30	0.234	0.273	4720	324	356	685
PZ-S1	20110707	120.2	7.81	0.382	0.385	169	485	160	645
PZ-S1-2	20110708	120.3	8.02	0.322	0.327	228	174	171	344
PZ-S2	20110712	149	7.5	0.245	0.32	1730	667	381	1049
PZ-S2	20110712	149	7.69	0.282	0.305	1820	533	372	907
PZ-S2	20110712	149.2	7.80	0.258	0.278	2859	363	382	748
PZ-S2	20110712	149	7.83	0.235	0.253	3617	250	363	617
PZ-S3	20110718	149.9	7.65	0.408	0.393	1188	2140	452	2593
PZ-S3	20110718	149.8	7.75	0.368	0.369	1459	1452	417	1871
PZ-S3	20110718	149.8	7.86	0.273	0.295	2879	474	367	844
PZ-S3	20110718	149.5	7.92	0.236	0.249	3397	242	377	623
PZ-S3-2	20110719	120.4	7.72	0.390	0.392	80	552	156	709
PZ-S3-2	20110719	120	7.69	0.316	0.325	176	166	158	325

References

Addicks J., Owren G., Tangvik K. Solubility of Carbon Dioxide and Methane in Aqueous Alkanolamine Solutions. *Proceedings of the International Gas Research Conference*, Amsterdam, November 2001.

Addicks, J. Solubility of Carbon Dioxide and Methane in Aqueous N-Methyldiethanolamine Solutions at Pressures between 100 and 200 bar. Norwegian University of Science and Technology, Department of Refrigeration and Air Conditioning, Trondheim, Norway. Ph.D. thesis. 2002.

Ali S.H. Kinetics of the Reaction of Carbon Dioxide with Blends of Amines in Amines in Aqueous Media Using the stopped-Flow Technique. *International Journal of Chemical Kinetics*. 2005, 37 (7), 391-405.

Alper E. Reaction Mechanism and Kinetics of Aqueous Solutions of 2-Amino-2-methyl-1-propanol and Carbon Dioxide. *Ind. Eng. Chem. Res.*, 1990, *29* (8), 1725-1728.

Anoufrikov Y., Kamps A.P-S., Rumpf B., Smirnova N.A., Maurer G. Solubility of H_2S in H_2O+N-Methyldiethanolamine+(H_2SO_4 or Na_2SO_4). *Ind. Eng. Chem. Res.* 2002, 41, 2571-2578.

Aronu U.E., Ghondal S., Hessen E.T., Haug-Warberg T., Hartono A., Hoff K.A., Svendsen H.F. Equilibrium in the H_2O-MEA-CO_2 System: New Data and Modeling. *Chemical Engineering Science*. Accepted.

Arstad B., Blom R., Swang O. CO_2 Absorption in Aqueous Solutions of Alkanolamines: Mechanistic Insight from Quantum Chemical Calculations. *J. Phys. Chem. A*, 2007, *111* (7), 1222-1228.

Austgen D.M., Rochelle G.T., Peng X., Chen C.C. Model of Vapor-Liquid Equilibria for Aqueous Acid Gas-Alkanolamine Systems Using the Electrolyte-NRTL Equation. *Ind. Eng. Chem. Res*. 1989, 28, 1060-1073.

Autoclave Engineers®, Zipperclave® 500&1000 mL stirred reactor, http://www.autoclaveengineers.com/ae_pdfs/SR_500_1000_Zip.pdf

Bates R.G., Pinching G.D. Acidic Dissociation Constant and Related Thermodynamic Quantities for Monoethanolammonium Ion in Water from 0 to 50°C. *Journal of Research of the National Bureau of Standards*. 1951, 46 (5), 349352.

Bishnoi S., Rochelle G.T. Absorption of Carbon Dioxide into Aqueous Piperazine: Reaction Kinetics, Mass Transfer, and Solubility. *Chemical Engineering Science.* 2000, 55, 5531-5543.

Bishnoi S. Carbon Dioxide Absorption and Solution Equilibrium in Piperazine Activated Methyldiethanolamine. The University of Texas at Austin. Ph.D. Dissertation. 2000.

Bottger A., Ermatchkov V., Maurer G. Solubility of Carbon Dioxide in Aqueous Solutions of N-Methyldiethanolamine and Piperazine in the High Gas Loading Region. *J. Chem. Eng. Data*. 2009, 54 (6), 1905-1909.

Böttinger W., Maiwald M., Hasse H. Online NMR Spectroscopic Study of Species Distribution in MEA–H_2O–CO_2 and DEA–H_2O–CO_2. *Fluid Phase Equilibria*. 2008, Vol 263, Iss 2., 131-143.

Cai ZY., Xie RJ., Wu ZL. Binary Isobaric Vapor-Liquid Equilibria of Ethanolamines + Water. *J. Chem. Eng. Data*, 1996, 41, 1101-1103.

Caplow M. Kinetics of carbamate formation and breakdown. *J. Am. Chem. Soc.* 1968, 90(24), 6795-6803.

Carson J.K., Marsh K.N., Mather A.E. Enthalpy of Solution of Carbon Dioxide in (Water + Ethanolamine, or Diethanolamine, or N-Methyldiethanolamine) at T = 298.15 K. *Journal of Chemical Thermodynamics.* 2000, 32, 1285-1296.

Chang H.T., Posey M., Rochelle G.T. Thermodynamics of Alkanolamine-Water Solutions from Freezing Point Measurements. *Ind. Eng. Chem. Res*. 1993, 32, (10), 2324-2335.

Chen C.C., Britt H.I., Boston J.F., Evans L.B. Extension and Application of the Pitzer Equation for Vapor-Liquid Equilibrium of Aqueous Electrolyte Systems with Molecular Solutes. *AIChE J*. 1979, 25, 820-831.

Chen C.C., Britt H.I., Boston J.F., Evans L.B. Local Composition Model for Excess Gibbs Energy of Electrolyte Solutions. Part 1: Single Solvent, Single Completely Dissociated Electrolyte Systems. *AIChE J.* 1982, 28, (4), 588-596.

Chen C.C. Evans L.B. A Local Composition Model for the Excess Gibbs Energy of Aqueous Electrolyte Systems. *AIChE J*. 1986, 32, (3), 444-454.

Chen X., Closmann, F., Rochelle GT. Accurate Screening of amines by the Wetted Wall Column. *GHGT-10*, 2010.

Chen X., Rochelle GT. Aqueous Piperazine Derivatives for CO_2 Capture: Accurate Screening by a Wetted Wall Column. *Chem. Eng. Res. Des*. 2011, Vol 89 (9), 1693-1710.

Chen Y-R**.,** Caparanga A.R., Soriano A.N., Li M.H. Liquid Heat Capacity of the Solvent System (Piperazine + N-Methyldiethanolamine + Water). *J. Chem. Thermodynamics*, 2010, Vol 42 (1), 54-59.

Chiu L.F., Li M.H. Heat Capacity of Alkanolamine Aqueous Solutions. *J. Chem. Eng. Data*, 1999a, 44 (6), 1396-1401.

Chiu L.F., Liu H.F., Li M.H. Heat Capacity of Alkanolamines by Differential Scanning Calorimetry. *J. Chem. Eng. Data*, 1999b, 44 (4), 631-636.

Cullinane, J.T. Thermodynamics and Kinetics of Aqueous Piperazine with Potassium Carbonate for Carbon Dioxide Absorption. The University of Texas at Austin. Ph.D. Dissertation. 2005.

da Silva E.F., Svendsen H.F. Ab Initio Study of the Reaction of Carbamate Formation from CO_2 and Alkanolamines. *Ind. Eng. Chem. Res.*, 2004, *43* (13), 3413-3418.

Dang, H. Absorption Rate and Solubility in Monoethanolamine/Piperazine/Water. The University of Texas at Austin. M.S.E. Thesis. 2000.

Davis J.D. Thermal Degradation of Aqueous Amines Used for Carbon Dioxide Capture. The University of Texas at Austin. Ph.D. Dissertation. 2009.

de Koeijer G., Solbraa E. High Pressure Gas Sweetening with Amines for Reducing CO_2 Emissions. Proceedings from IEA GHGT-7 Vancouver. 2004.

Derks P.W.J., Dijkstra H.B.S., Hogendoorn J.A., Versteeg G.F. Solubility of Carbon Dioxide in Aqueous Piperazine Solutions. *AIChE J.* August 2005, Vol 51, No. 8, 2311-2327.

Dingman J.C., Jackson J.L., Moore T.F., Branson J.A. Equilibrium Data for the H_2S-CO_2-Dyglycolamine® Agent-Water System, presented to the 62nd Annual Gas Process Association Convention, San Francisco, Mar. 14-16, 1983.

DIPPR, 1998-Provo, UT: BYU DIPPR, Thermophysical Properties Laboratory, 1998-Version 13.0.

Dodge B.F. *Chemical Engineering Thermodynamics, Chemical Engineering Series*. First Edition, McGraw-Hill Book Company, Inc. New York and London, 1944.

Dugas R.E., Rochelle G.T. Absorption and Desorption Rates of Carbon Dioxide with Monoethanolamine and Piperazine. *Energy Procedia.* 2009. Vol. 1, 1, 1163-1169.

EPA (US Environmental Protection Agency). The Experience with Emissions Control Policies in the United States. 2007. http://www.epa.gov/airmarkets/international/china/JES_USexperience.pdf

Ermatchkov V., Kamps A. P-S., Speyer D. and Maurer G. Solubility of carbon dioxide in aqueous solutions of piperazine in the low gas loading region. *J. Chem. Eng. Data*, 2006, 51 (5), 1788-1796.

Frailie P.T., Plaza J.M., Van Wagener D.H., Rochelle G.T. Modeling Piperazine Thermodynamics. *GHGT-10*. 2010.

Freeman S.A. Thermal Degradation and Oxidation of Aqueous Piperazine for Carbon Dioxide Capture. The University of Texas at Austin. Ph.D. Dissertation. 2011.

Freguia, S. Modeling of CO_2 Removal from Flue Gasses with Monoethanolamine. The University of Texas at Austin. M.S.E. Thesis. 2002.

Goff G.S. Oxidative Degradation of Aqueous Monoethanolamine in CO_2 Capture Processes: Iron and Copper Catalysts, Inhibition, and O_2 Mass Transfer. The University of Texas at Austin. Ph.D. Dissertation. 2005.

Goldman A.M., Leibush A.G. Study of the Equilibrium of Carbon Dioxide Desorption of Monoethanolamine Solutions in the Temperature Rage 75-140°C. *Tr. Gos. Nauchno-Issled. Proektn. Inst. Azotn. Promsti*. 1959, 10, 54-82.

Hamborg E.S., Versteeg G.F. Dissociation constants and thermodynamic properties of alkanolamines. *Energy Procedia*. *GHGT-9*. 2009. Vol 1, Iss 1. 1213-1218.

Hikita H., Asai S., Ishikawa H., Honda M. The Kinetics of Reactions of Carbon Dioxide with Monoethanolamine, Diethanolamine and Triethanolamine by A Rapid Mixing Method. *Chem. Eng. J*. 1977, 13 (1), 7-12.

Hikita H., Asai S., Katsu Y., Ikuno S. Absorption of Carbon Dioxide into Aqueous Monoethanolamine Solutions. *AIChE J.* 1979, 25, 793-800.

Hilliard M.D. A Predictive Thermodynamic Model for an Aqueous Blend of Potassium Carbonate, Piperazine and Monoethanolamine for CO_2 Capture from Flue Gas. The University of Texas at Austin. Ph.D. Dissertation. 2008.

Huttenhuis P.J.G., Agrawal N.J., Hogendoorn J.A., Versteeg G.F. Gas solubility of H_2S and CO_2 in aqueous solutions of N-methyldiethanolamine. *Journal of Petroleum Science and Engineering.* 2007, 55, 122-134.

International Energy Agency, CO_2 emissions from fuel combustion highlights (2009 edition), 2009.

IPCC (the Intergovernmental Panel on Climate Change). Fourth Assessment Report – Climate Change 2007. http://www.ipcc.ch/publications_and_data/publications_ipcc_fourth_assessment_report_synthesis_report.htm

Jenab M.H., Abdi M.A., Najibi S.H., Vahidi M., Matin N.S. Solubility of Carbon Dioxide in Aqueous Mixtures of N-Methyldiethanolamine + Piperazine + Sulfolane. *J. Chem. Eng. Data*. 2005, 50, 583-586.

Jenab M.H., Vahidi M., Mehrabi M. Solubility of Carbon Dioxide in Aqueous Mixtures of DIPA+MDEA and DIPA+PZ Solutions. *Journal of the Chinese Chemical Society*, 2006, 53, 283-286.

Jones J.H., Froning H.R., Claytor Jr. E.E. Solubility of Acidic Gases in Aqueous Monoethanolamine. *J. of Chem. Eng. Data*. 1959 Vol 4, No. 1, 85-92.

Jou F-Y., Mather A.E., Otto F.D. Solubility of H_2S and CO_2 in Aqueous Methyldiethanolamine Solutions. *Ind. Eng. Chem. Process Des. Dev.* 1982, 21, 539-544.

Jou F-Y., Otto F.D., Mather A.E. Vapor-Liquid Equilibrium of CO_2 in Aqueous Mixture of Monoethanolamine and Methyldiethanolamine. *Ind. Eng. Chem. Res.* 1994, 33, 2002-2005.

Jou F-Y., Mather A. E.; Otto, F. D., The Solubility of CO_2 in a 30 Mass Percent Monoethanolamine Solution. *The Canadian Journal of Chemical Engineering*, 1995, 73, 140-146.

Kadiwala S., Rayer A.V., Henni A. High Pressure Solubility of Carbon Dioxide (CO_2) in Aqueous Piperazine Solutions. *Fluid Phase Equilibria*. 2010, 292, 20-28.

Kamps A. PS., Xia J., Maurer G. Solubility of CO_2 in (H_2O + Piperazine) and in (H_2O + MDEA+ Piperazine). *AIChE Journal*. 2003, 49(10), 2662-2670.

Kim I., Svendsen H.F. Heat of Absorption of Carbon Dioxide (CO_2) in Monoethanolamine (MEA) and 2-(Aminoethyl)ethanolamine (AEEA) Solutions. *Ind. Eng. Chem. Res*. 2007, 46, 5803-5809.

Kim I., Svendsen H.F., Borresen E. Ebulliometric Determination of Vapor-Liquid Equilibria for Pure Water, Monoethanolamine, N-Methyldiethanolamine, 3-(Methylamino)-propylamine, and Their Binary and Ternary Solutions. *J. Chem. Eng. Data*, 2008, 53, 2521-2531.

Kohl AL., Nielsen RB. *Gas Purification*. Fifth Edition. Houston, Gulf Publishing Company. 1997, pp 231.

Lawson, J. D., Garst, A. W.. Gas Sweetening Data: Equilibrium Solubility of Hydrogen Sulfide and Carbon Dioxide in Aqueous Monoethanolamine and Aqueous Diethanolamine Solutions. *J. Chem. Eng. Data.* 1976, 21, (1), 20-30.

Lee J.I., Otto F.D., Mather A.E. Equilibrium between Carbon Dioxide and Aqueous Monoethanolamine Solutions. *J. Applied Chemistry and Biotechnology*. 1976, 26, 541-549.

Lee J. I., Otto F.D., Mather A.E. The Measurement and Prediction of the Solubility of Mixtures of Carbon Dioxide and Hydrogen Sulphide in a 2.5 N Monoethanolamine Solution. *The Canadian Journal of Chemical Engineering*. 1976, Vol 54, Iss. 3, 214-219.

Lewis G.N., Randall M. *Thermodynamics and the Free Energy of Chemical Substances.* First Edition, McGraw-Hill Book Company, Inc. New York and London, 1923.

Li M.-H., Chang B.-C. Solubilities of Carbon Dioxide in Water + Monoethanolamine +2-Amino-2-methyl-1-propanol. *J. Chem. Eng. Data*. 1994, 39, 448-452.

Li M.-H., Chang B.-C. Solubility of Mixtures of Carbon Dioxide and Hydrogen Sulfide in Water + Monoethanolamine + 2-Amino-2-methyl-1-propano. *J. Chem. Eng. Data.* 1995,40, 328-331.

Liu H.B., Zhang C.F., Xu G.W. A Study on Equilibrium Solubility for Carbon Dioxide in Methyldiethanolamine-Piperazine-Water Solution. *Ind. Eng. Chem. Res*. 1999, 38, 4032-4036.

Lyudkovskaya M.A., Leibush A.G. Solubility of Carbon Dioxide in Solutions of Ethanolamines under Pressure. *Zh. Prikl. Khim*. 1949, 22, 558-567.

Maddox R.N., Bhairi A.H., Deirs J.R., Thomas P.A. *Equilibrium Solubility of Carbon Dioxide or Hydrogen Sulfide in Aqueous Solutions of Monoethanolamine, Diglycolamine, Diethanolamine and Methyldiethanolamine*. GPA Research Report RR-104. Mar. 1987.

Ma'mun S., Nilsen R., Svendsen HF., Juliussen O. Solubility f Carbon Dioxide in 30 mass% Monoethanolamine and 50 mass% Methyldiethanolamine Solutions. *J. Chem. Eng. Data.* 2005, 50, 630-634.

Martin J.L., Otto F.D., Mather A.E. Solubility of Hydrogen Sulfide and Carbon Dioxide in a Diglycolamine Solution. *J. Chem. Eng. Data*, 1978, Vol. 23, No. 2, 163-164.

Mathonat C., Majer V., Mather A.E., Grolier J-P.E. Use of Flow Calorimetry for Determining Enthalpies of Absorption and the Solubility of CO_2 in Aqueous Monoethanolamine Solutions. *Ind. Eng. Chem. Res*. 1998, 37 (10), 4136-4141.

McCann N., Phan D., Wang X., Conway W., Burns R., Attalla M., Puxty G., and Maeder M. Kinetics and Mechanism of Carbamate Formation from CO_2(aq), Carbonate Species, and Monoethanolamine in Aqueous Solution. *J. Phys. Chem. A*. 2009, 113, 5022-5029.

Mock B., Evans L.B., Chen C.C. Phase Equilibria in Multiple-Solvent Electrolyte Systems: A New Thermodynamic Model. *Proceedings of the 1984 Summer Computer Simulation Conference*. pp. 558.

Mock B., Evans L.B., Chen C.C. Thermodynamic Representation of Phase Equilibria of Mixed-Solvent Electrolyte Systems. *AIChE J.* 1986, 32 (10), 1655-1664.

Muhlbauer H.G., Monaghan P.R. *Equilibrium Data for H_2S-CO_2-Monoethanolamine*. Jefferson Chemical Co, Austin, TX. 1957.

Murrieta-Guevara F., Romero-Martinez A, Trejo A. Solubilities of Carbon Dioxide and Hydrogen Sulfide in Propylene Carbonate, *N*-methylpyrrolidone and Sulfolane. *Fluid Phase Equilibria*. 1998, Vol 44, Iss. 1, 105-115.

Murrieta-Guevara F., Rebolledo-Libreros E., Trejo A. Solubility of Carbon Dioxide in Binary Mixtures of N-Methylpyrrolidone with Alkanolamines. *J. Chem. Eng. Data*. 1992, 37, 4-7.

Murrieta-Guevara F., Rebolledo-Libreros E., Trejo A. Gas Solubility of Carbon Dioxide and Hydrogen Sulfide in Mixtures of Sulfolane with Monoethanolamine. *Fluid Phase Equilibria*. 1993, Vol 86, 225-231.

Murrieta-Guevara F., Rebolledo-Libreros E., Romero-Martinez A., Trejo A. Solubility of CO_2 in Aqueous Mixtures of Diethanolamine with 2-Methyldiethanolamine and 2-Amino-2-methyl-1-propanol. *Fluid Phase Equilibria*. 1998, 150-151, pp 721-729.

Nath A., Bender E. Isothermal Vapor-Liquid Equilibria of Binary and Ternary Mixtures Containing Alcohol, Alkanolamine, and Water with a New Static Device. *J. Chem. Eng. Data*, 1983, 28, 370-375.

Nguyen T, Hilliard M.D., Rochelle G.T. Amine volatility in CO_2 capture. *International Journal of Greenhouse Gas Control*. 2010, 4, 707–715.

Page M., Huot J.Y., Jolicoeur C.A. A Comprehensive Thermodynamic Investigation of Water- ethanolamine Mixtures at 10, 25, and 40 ℃. *Can. J. Chem*. Vol. 71, 1993, 1064-1072.

Park S. B., Lee H. Vapor-Liquid Equilibria for the Binary Monoethanolamine + Water and Monoethanolamine + Ethanol Systems. *Korean Journal of Chemical Engineering*, 1997, 14, (2), 146-148.

Penny D.E., Ritter T.J. Kinetic Study of the Reaction between Carbon Dioxide and Primary Amines. *J. Chem. Soc., Faraday Trans.1*. 1983, 79, 2103.

Polderman L.D., Dillon C.P., Steele A.B. Why MEA Solution Breaks Down in Gas-Treating Service. *Oil & Gas Journal*. 1955, 54: 180-183.

Poplsteinava J., Krane J., Svendsen H.F. Liquid-Phase Composition Determination in CO_2-H_2O-Alkanolamine Systems: An NMR Study. *Ind. Eng. Chem. Res*. 2005, 44, 9894-9903.

Posey M.L. Thermodynamic Model for Acid Gas Loaded Aqueous Alkanolamine Solutions. The University of Texas at Austin. Ph.D. Dissertation. 1996.

Puxty G., Allport A., Attalla M. Vapor Liquid Equilibria Data for a Range of New Carbon Dioxide Absorbents. *Energy Procedia. GHGT-9*. 2009, 1. 941-947.

Reed R.M., Wood W.R. Recent Design Developments in Amine Gas Purification Plants. *Transactions of American Institute of Chemical Engineers*. 1941, Vol. 37, June 25, 363-383.

Renon H., Prausnitz J.M. Local Compositions in Thermodynamic Excess Functions for Liquid Mixtures. *AIChE J.* 1968, Vol. 14, No. 1, 135-144.

Robinson, D. B. *Vapor-Liquid Equilibrium Studies: GRI Project −Acid Gas Absorption*; University of Oklahoma: Norman, OK, 1993.

Rochelle GT et al. CO_2 Capture by Aqueous Absorption, First Quarterly Progress Report 2009. Luminant Carbon Management Program. The University of Texas at Austin. 2009.

Rochelle GT et al. CO_2 Capture by Aqueous Absorption, Fourth Quarterly Progress Report 2009. Luminant Carbon Management Program. The University of Texas at Austin. 2010.

Sartori G., Savage D.W. Sterically Hindered Amines for CO_2 Removal from Gases. *Ind. Eng. Chem. Fundam*. 1983, 22, 239-249.

Sexton A.J. Amine Oxidation in CO_2 Capture Processes. The University of Texas at Austin. Ph.D. Dissertation. 2008.

Shen K.P., Li M.H. Solubility of Carbon Dioxide in Aqueous Mixtures of Monoethanolamine with Methyldiethanolamine. *J. Chem. Eng. Data*. 1992, 37 (1), 96-100.

Shim J-G., Kim J-H., Jhon Y.H., Kim J., Cho K-H. DFT Calculations on the Role of Base in the Reaction between CO_2 and Monoethanolamine. *Ind. Eng. Chem. Res.*, 2009, *48* (4), 2172-2178.

Teng T-J.T., Mather A.E. Solubility of H_2S, CO_2 and Their Mixtures in an AMP Solution. *The Canadian Journal of Chemical Engineering*. 1989, Vol 67, 846-850.

Teng T-J.T., Mather A.E. Solubility of CO_2 in an AMP Solution. *J. Chem. Eng. Data*. 1990, 35, 410-411.

Tochigi K., Akimoto K., Ochi K., Liu F., Rawase Y. Isothermal Vapor-Liquid Equilibria for Water + 2-Aminoethanol + Dimethyl Sulfoxide and Its Constituent Three Binary Systems. *J. Chem. Eng. Data*. 1999, 44, (3), 588-590.

Tontiwachwuthikul P., Meisen A., Lim C.J. Solubility of CO_2 in 2-Amino-2-methyl-1-propanol Solutions. *J. Chem. Eng. Data*. 1991, 36 (1), 130-133.

Touhara H., Okazaki S., Okino F., Tanaka H., Ikari K., Nakanishi K. Thermodynamic Properties of Aqueous Mixtures of Hydrophilic Compounds 2 Aminoethanol and Its Methyl Derivatives. *J. Chem. Thermodynamics*. 1982, 14, 145-156.

Van Wagener D.H. Stripper Modeling for CO_2 Removal Using Monoethanolamine and Piperazine Solvents. The University of Texas at Austin. Ph.D. Dissertation. 2011.

Weiland R.H., Dingman J.C., Cronin D.B. Heat Capacity of Aqueous Monoethanolamine, Diethanolamine, N-Methyldiethanolamine, and N-Methyldiethanolamine Based Blends with Carbon Dioxide. *J. Chem. Eng. Data*. 1997, 42, 1004-1006.

Wilson H.L., Wilding W.V. Vapor-Liquid and Liquid-Liquid Equilibrium Measurements on Twenty Two Binary Mixtures. Experimental Results for DIPPR 1990-91 Projects on Phase Equilibria and Pure Component Properties: 1994; 63-115.

Xia J.Z., P-S Kamps A., Maurer G. Solubility of H_2S in (H_2O + Piperazine) and in (H_2O + MDEA + Piperazine). *Fluid Phase Equilibria*. 2003, 207, 23-34.

Xie H-B., Zhou Y., Zhang Y., Johnson J.K. Reaction Mechanism of Monoethanolamine with CO_2 in Aqueous Solution from Molecular Modeling. *J. Phys. Chem. A*. 2010, 114, 11844-11852.

Xu G.-W., Zhang C.-F., Qin S.-J., Guo W.-H., Liu H.-B. Gas-Liquid Equilibrium in a CO_2-MDEA-H_2O System and the Effect of Piperazine on It. *Ind. Eng. Chem. Res.* 1998, 37, 1473-1477.

Vita

Qing Xu was born in Xi'an, China. She graduated from the High School attached to the Northwestern Polytechnical University in 2002 and was admitted to Tsinghua University in Beijing without college entrance exam to study chemical engineering. She received a Bachelor of Engineering in chemical engineering from Tsinghua University in July 2006. In September 2006 she joined Dr. Rochelle's group as a Ph.D. student in the Department of Chemical Engineering at The University of Texas at Austin. In December 2008 she received an M.S.E degree in chemical engineering for the research on solvent reclaiming by crystallization of K_2SO_4. Qing has accepted full-time employment with UOP in Des Plaines, IL.

Permanent email address: qing.xu06@gmail.com

This dissertation was typed by the author.